THE UNIVERSITY *of* EDINBURGH

Investigating the genetic and molecular basis of age-related macular degeneration

Chloe M. Stanton

Thesis submitted for the degree of Doctor of Philosophy

The University of Edinburgh

2011

Declaration

I declare that this thesis is composed of original research undertaken by myself. The contributions of others to the work are clearly indicated.

Chloe Stanton

August 2011

Acknowledgments

Firstly, I would like to thank Professor Alan Wright, for giving me the opportunity to work on this project, and for his ideas, help and guidance throughout my PhD. I am also extremely grateful to Dr. Kevin Chalmers and Dr. Caroline Hayward for their tremendous help with the day-to-day aspects of the project – in particular, thanks to Kevin, for sharing his expertise on all things protein, and to Caroline, for her guidance in statistics. Thanks to Susan Campbell for all the DNA plates, plasma samples and genotyping help. Thanks to all the members of the lab for being so helpful - Alan Lennon, Dr. Milica Gakovic, Dr. Xinhua Shu and special thanks to Brian Tulloch for his support during the ELISA "trouble-shooting" period! It has been such a pleasure to work with you all!

Also at the Human Genetics Unit, thanks to Dr. Shalini Jadeja, Emma Hall, Peter Budd, Dr. Martin Reijns, Dr. Mark Handley, Dr. Fiona Semple, Dr. Kirsty Tyrrell and Dr. Morad Ansari for providing reagents, cells or advice. Thanks to HGU Technical Services for performing the sequencing, Computing Services for all the software updates and to Craig Nicol for his help with graphics.

Collaborators in Edinburgh and further afield contributed greatly to this project. Key results were obtained through collaboration with Professor Marius Ueffing, who was kind enough to host my visit to the Helmholtz Zentrum in Munich. This enabled me to perform the yeast two-hybrid screen with Dr. Elod Kortvely. Thanks also to Dr. Karsten Boldt for performing mass spectrometry, to Dr. Johannes Gloeckner for the empty TAP vectors, and to Dr. Steffanie Hauck for helpful discussions.

Genotyping information, DNA or plasma from AMD case-control cohorts were kindly provided by Dr. John Yates, Dr. Tony Moore, Professor Baljean Dhillon, Dr. Anand Swaroop, Dr. Dwight Stambolian, Dr. Johanna Seddon and Dr. Anneke den Hollander. Plasma samples from the SOCCs series were shared by Professor Malcolm Dunlop and Marion Walker. Dr. Osamu Onodera contributed serum samples obtained from CARASIL patients and Japanese controls. Thanks to the patients and controls who contributed to these series, and to the clinicians and researchers who co-ordinated the collections. Thanks to Dr. Jeremy Chien for providing antibodies and technical suggestions for optimising the HTRA1 ELISA. Dr. Michael Ehrmann kindly provided an antibody raised against HTRA1 which became a useful tool. Professor Brian Walker, Lynne Ramage, Roland Stimpson and Lee Murphy shared data from a microarray they had performed in adipose tissue, and DNA from the same individuals to allow genotyping. Professor Bob Sim made useful suggestions regarding development of assays to investigate complement activity and Cat Graham provided helpful discussion regarding statistics for ELISA analysis.

Finally, thank you to my friends (near and far) and loved ones – especially James - for your support, encouragement and for the fun times! Most of all, thank you to my amazing family. I couldn't have done it without you - this book is for you.

Table of contents

Abstract

Age-related macular degeneration (AMD) is the leading cause of blindness worldwide, affecting an estimated 50 million individuals aged over 65 years. Environmental and genetic risk-factors contribute to the development of AMD. An AMD-risk locus on chromosome 10q26 spans two genes, *ARMS2* and *HTRA1*, and controversy exists as to which variants are responsible for increased risk of disease. Recent work suggests that HTRA1 expression levels are significantly increased in carriers of the risk haplotype associated with AMD. However, relatively little is known about the interactions, substrate specificity and roles in disease played by this secreted serine protease.

This thesis aims to elucidate the potential role played by HTRA1 in AMD pathogenesis. A combination of tandem affinity purification (TAP) and yeast two-hybrid techniques was used to identify interacting partners of HTRA1. A number of proteins, with diverse roles in the alternative complement pathway, cell signaling, cell-matrix interactions, inflammation, angiogenesis and fibrosis, were identified. These are attractive candidates for further study as such processes are disturbed in AMD, implicating HTRA1 and its binding partners in disease development.

One interacting partner, Complement Factor D (CFD), is a key activator in the alternative complement pathway. CFD, a 24 kDa serine protease, is expressed as an inactive zymogen, from which a signal peptide and activation peptide are cleaved before release of the mature, active protein into the circulation. *In vitro* studies show that CFD interacts with, and can be a substrate for, HTRA1. The interacting domain between the two proteins is localised to a region of 30 amino acids at the N-terminal end of proCFD. The 5 amino acid pro-peptide of CFD appears to be both necessary and sufficient for proteolysis of CFD by HTRA1.

Investigation of the functional relevance of the interaction between HTRA1 and CFD shows that proCFD is cleaved by HTRA1, whilst mature CFD is not subjected to proteolysis. HTRA1-mediated cleavage of CFD forms an active protease, leading to activation of factor B in the alternative complement pathway in *in vitro* assays. Furthermore, a normal complement response is restored to CFD-depleted serum by addition of proCFD activated by HTRA1. Thus, an HTRA1-

mediated increase in alternative complement pathway activity may explain a proportion of the AMD-risk attributed to the chr10q26 locus.

Genetic and protein-based approaches were used to study the potential role of CFD in AMD pathogenesis, independent of an interaction with HTRA1. An intronic SNP, rs3826945, was significantly associated with increased risk of AMD in two British case-control cohorts, and in a combined meta-analysis with 4 additional cohorts from North America and Europe (*p*-value = 0.032, Odds Ratio = 1.112 in 4765 cases and 2693 controls). Assessment of copy number variation and sequencing of CFD did not identify any functional variants which may explain the association with disease. However, plasma levels of CFD were measured by ELISA in 751 AMD cases and 474 controls, and were found to be significantly elevated in AMD cases compared to controls (*p*-value = 0.00025). This further implicates complement activation in AMD pathogenesis, and makes CFD an attractive candidate for therapeutic intervention. An alteration in the level of activated CFD, possibly mediated via an interaction with HTRA1, either at the systemic or local tissue level, may play a role in disease development and progression.

Abbreviations

[S]	Substrate concentration
√3	Cube root
°C	Degree Celsius
A	Adenine (DNA)
A	Alanine (amino acid)
A2E	N-retinylidene-N-retinylethanolamine
A69S	Alanine to serine at position 69 in ARMS2
ABCA1	ATP-binding cassette, sub-family A, member 1
ACTBL2	Beta-actin-like protein 2
AD	GAL4 transcription factor activation domain
ADE2	Adenylosuccinate synthetase
AGE	Advanced glycation end product
AMC	7-amino-4-methyl coumarin
AMD	Age-related macular degeneration
AP2α	Activator protein 2 alpha transcription factor
AREDS	Age-Related Eye Disease Study
ARM	Age-related maculopathy
ARMS2	Age-related maculopathy susceptibility protein 2
Asp	Aspartic acid (amino acid)
Ba	Activation fragment of complement factor B
Bb	Activation fragment of complement factor B
BBS	Borate Buffered saline
BlamD	Basal laminar deposits
BLAST	Basic Local Alignment Search Tool
BlinD	Basal linear deposits
BM	Bruch's membrane
bm choroid	Basement membranes of the choroid
bm RPE	Basement membranes of the RPE
BMI	Body mass index
BMP	Bone mophogenic protein
BMP-2	Bone morphogenetic protein 2
Bmp4	Bone morphogenetic protein 4 (mouse)
bp	Base pair
BSA	Bovine serum albumin
C.I .	Confidence interval
C2	Complement component 2
C3	Complement component 3
C3a	Anaphylotoxin produced by cleavage of C3
C3aR	Complement component 3a Receptor
C3b	Activation product of C3 cleavage
C3bBb	C3-convertase
C3bBbC3b	C5-convertase
C3d	Breakdown product of C3b
C3f	C3b is catabolised to inactive products
C5	Complement component C5
C5a	Anaphylotoxin produced by cleavage of C5
C5aR	Complement component 5a Receptor

cAMP	Cyclic adenosine monophosphate
CARASIL	Cerebral autosomal recessive arteriopathy with subcortical infarcts and leukoencephalopathy
CARMS	Clinical Age-Related Maculopathy Grading System
CATT	Comparison of Age-Related Macular Degeneration Treatments Trials
CCL2	Chemokine, CC motif, ligand 2
CCR2	Chemokine receptor 2
CD35	Complement receptor type 1
CD46	Complement regulators membrane co-factor
CD46	Membrane cofactor protein
CD55	Decay accelerating factor
cDNA	Complementary DNA
CEP	Carboxyethylpyrrole
CEPH	Centre d'Etude du Polymorphisme Humain
CETP	Cholesteryl ester transfer protein
CFB	Complement Factor B
CFD	Complement factor D
CFD_Y2H	Synthetic peptide corresponding to region of complement factor D isolated in yeast two-hybrid screening
CFH	Complement Factor H
CFHR1	Complement factor H-related 1
CFHR3	Complement factor H-related 3
CFI	Complement Factor I
Cl_2MD	Dichloromethylene diphosphonate
cm^2	Centimetre
CNBr	Cyanogen bromide
CNV	Choroidal neovascularisation
CO2	Carbon dioxide
COL10A1	Collagen, type 10A1
COL1A1	Collagen, type 1A1
COL12A1	Collagen, type 12A1
COL3A1	Collagen, type 3A1
COL5A2	Collagen, type 5A2
COL8A1	Collagen, type 8A1
CR1	Complement receptor 1
CRALBP	Cellular retinoid binding protein
CRP	C-reactive protein
CSH1	Chorionic somatomammotropin hormone 1
CST3	Cystatin C
C_T	Threshold cycle
CTAP	C-terminal tandem affinity purification tag
CTGF	Connective tissue growth factor
CV	Coefficient of variation
CVF	Cobra Venom Factor
CX3CR1	Chemokine, CX3C motif, receptor 1
D	Aspartic acid (amino acid)

D'	Statistical measure of linkage disequilibrium between two SNPs
DAF	Decay accelerating factor
DBD	GAL4 transcription factor DNA-binding domain.
DEFA1	Alpha-defensin 1
DEST	Destination vector of Gateway cloning system
DGVB-MgEGTA	Glucose-Gelatin Veronal Buffer containing Magnesium and EGTA
dH_2O	Deionised water
DMEM	Dulbecco's modified Eagle's medium
DMSO	Dimethyl sulfoxide
DNA	Deoxyribonucleic acid
dNTPs	Deoxyribonucleotide triphosphates
DSVLA-MCA	Synthetic peptide (Asp-Ser-Val-Leu-Ala-MCA)
DTT	Dithiothreitol
E	Glutamate (amino acid)
E. coli	*Escherichia coli*
E2	Electrode buffer
ECL	Enhanced Chemiluminescence
ECM	Extracellular matrix
EDTA	Ethylenediaminetetraacetic acid
EFEMP1	Fibulin-3 gene
EGF	Epidermal growth factor-like domain
EGFCA	Calcium-binding EGF-like domain
EGTA	Ethylene glycol-bis(2-aminoethylether)-N,N,N,N'-tetraacetic acid
EL	Elastin layer
ELISA	Enzyme-linked immunosorbent assay
ER	Endoplasmic reticulum
ERAD	ER-associated degradation
EV	Empty vector
F-12	Nutrient Mixture F-12
FAM	Fluorescent dye
FBLN1	Fibulin-1
FCFD4514S	Anti-complement factor D antibody fragment
FCS	Fetal calf serum
FT	Flow-through
g	G-force
g	gram
GA	Geographic atrophy
GDF	Growth differentiation factor
GFP	Green fluorescent protein
Glu	Glutamic acid
GRP78	78 kDa glucose regulated protein
GST	Glutathione S-transferase
H	Histidine (amino acid)
HEK	Human embryonic kidney
HEMICENTIN-1	Fibulin-6

HEPES	4-(2-hydroxyethyl)-1-piperazineethanesulfonic acid
HF	High-Fidelilty buffer for Phusion polymerase
HGU	Human Genetics Unit
HIS3	Imidazoleglycerol-phosphate dehydratase gene
His_6	Hexa-histidine tag
HPLC	High Performance Liquid Chromotography
hprd	Human Protein Reference Database
HRP	Horseradish peroxidase
HSPA1A	Heat shock 70 kDa protein 1
HSPA8	Heat shock cognate 71 kDa protein
HSPG	Heparin sulphate proteoglycans
hTERT-RPE1	Human Telomerase Reverse Rranscriptase-immortalised Retinal Pigment Epithelial 1 cell-line
HTRA1	High temperature requirement A1 serine protease
HTRA1**	Polyclonal detection antibody for HTRA1 ELISA
HWE	Hardy-Weinberg equilibrium
I	Isoleucine (amino acid)
iC3b	Breakdown product of C3b
ICL	Inner collagenous layer
IGF	Insulin growth factor
IGFBP	Insulin-like Growth Factor Binding Protein
IGFBP8	Insulin-like growth factor-binding protein 8
Ig	Immunoglobulin
indel	Insertion/deletion in 3' UTR of ARMS2
IPTG	Isopropyl β-D thiogalactoside
IRBP	Interphotoreceptor Retinoid Binding Protein
K	Lysine (amino acid)
kb	Kilobase
kDa	Kilo Dalton
K_m	Michaelis constant
KPRP	Keratinocyte proline-rich protein
L	Leucine (amino acid)
LacZ	Reporter gene encoding β-galactosidase
L-AMP	Agar containing 100 µg/ml ampicillin
LAP	Latency associated peptide
LB	Luria-Bertani
LC-MS/MS	Liquid chromatography coupled with tandem mass spectrometry
LD	Linkage disequilibrium
LDL	Low-density lipoprotein
LDS	Lithium dodecyl sulfate
LIPC	Hepatic triglyceride lipase
LOC387715	Hypothetical locus 387715
LOD	Log of Odds
LPS	Lipopolysaccharide
LRP6	Low-density lipoprotein receptor-related protein 6
LTBP	TGF-β–binding protein
M	Molar

MAb	Mouse monoclonal capture antibody for HTRA1 ELISA
MAC	Membrane attack complex
MAF	Minor allele frequencies
Masp1	Mannose-binding lectin-associated serine protease-1
MBL	Mannose-binding lectin
MCA	Methyl coumaric acid
MCP-1	Monocyte chemoattractant protein -1
MEL1	Alpha-galactosidase
MES	2-(N-morpholino)ethanesulfonic acid
MGB	Minor groove binder
MHC	Major histocompatibility complex
µg	Microgram
µl	Microlitre
ml	Millilitre
mM	Millimolar
MMP	Matrix metalloproteinase
MMP2	Matrix metalloproteinase 2
MMP9	Matrix metalloproteinase 9
MOPS	3-(N-morpholino)propanesulfonic acid
MP-100	Microporator-100
MPGN II	Membranoproliferative glomerulonephritis type II
mRNA	Messenger RNA
ms	Milliseconds
MTT	3-(4,5-Dimethylthiazol-2-yl)-2,5-diphenyltetrazolium bromide
MW	Molecular weight
N	Number
NCBI	National Center for Biotechnology Information
NEB	New England Biolabs
NFDM	Non-fat dried milk
ng	Nanograms
NIH	National Institutes of Health
Ni-NTA	Ni^{2+}-nitrilotriacetate
nm	Nanometers
nM	Nanomolar
NP40	Nondet P-40
OCL	Outer collagenous layer
OD	Optical density
ONL	Outer nuclear layer
OR	Odds ratio
ORF	Open reading frame
OS	Rod outer segments
p	Probability
P1	Internal control plasma sample 1
P2	Internal control plasma sample 2
P3	Internal control plasma sample 3
P8	Internal control plasma sample 8
P9	Internal control plasma sample 9
PAGE	Polyacrylamide gel electrophoresis

PBS	Phosphate buffered saline
PBST	Phosphate Buffered Saline 0.05% Tween-20
PCR	Polymerase Chain Reaction
PDZ	Domain found in Post synaptic density protein, Drosophila disc large tumor suppressor, and Zonula occludens-1 protein
PEDF	Pigment epithelium derived factor
PJ69-4A	*Saccharomyces cerevisiae* strain
PJ69-4α	*Saccharomyces cerevisiae* strain
PLEKHA1	Pleckstrin homology domain-containing protein, Family A, Member 1
PMA	Phorbol myristate acetate
PPRGR-MCA	Synthetic peptide (Pro-Pro-Arg-Cly-Arg-MCA)
PRSS11	Protease, serine 1
PVDF	Polyvinylidene Difluoride
Q	Glutamine (amino acid)
qPCR	Quantitative real-time PCR
R^2	Squared correlation coefficient
R	Arginine (amino acid)
RBC	Red blood cell
Rfu	Relative fluorescent units
RNA	Ribonucleic acid
RNAseP	Ribonuclease P
ROS	Reactive oxidant species
RPE	Retinal pigment epithelium
RPE1	Telomerase-immortalised Retinal Pigment Epithelial 1 cell-line
rpm	Revolutions per minute
RPMI	Roswell Park Memorial Institute Media
rs	Reference SNP
RT	Reverse Transcriptase
RT-PCR	Reverse transcription polymerase chain reaction
S	Serine (amino acid)
s.e.m	Standard error of mean
S/F	Arginine-80-to Glycine mutation in complement C3
SD	Standard deviation
SDS	Sodium dodecyl sulphate
SD-WL	Minimal media lacking tryptophan and leucine
SNP	Single nucleotide polymorphism
SOC	Super Optimal broth with Catabolite repression
SOCCS	Scottish general population controls
SPARC	Secreted protein, acidic and rich in cysteine
SRF	Serum response factor
STE	Buffer contining Tris-HCl, NaCl, EDTA, DTT
TAP	Tandem affinity purification
TAPP1	Tandem-PH-domain-containing protein-1
TBE	Tris, Borate, EDTA
TBS	Tris buffered saline
TBST	Tris buffered saline containing 0.05% Tween-20

TE	Tris, EDTA
TEN150	Buffer containing Tris-HCl, NaCl
TGF-β	Transforming growth factor β
THBS1	Thrombospondin-1
THP-1	Human acute monocytic leukemia cell line
TIMP3	Tissue inhibitor of metalloproteases 3
TLR	Toll-like receptor
TMB	Tetramethylbenzidine chromagen
TNF-α	Tumor necrosis factor alpha
TSP1	Thrombospondin type 1 repeats
TUBA1A	Tubulin alpha-1A chain
U	Unit
UK1	Scottish AMD case-control cohort
UK2	AMD case-control cohort from Cambridge, England
USA1	AMD case-control cohort from Michigan, USA
USA2	AMD case-control cohort from NIH, USA
USA3	AMD case-control cohort from Tufts University, USA
UTR	Untranslated region
V	Valine (amino acid)
V	Volts
V	Reaction rate
VBS	Veronal buffered saline
VEGF	Vascular endothelial growth factor
VEGFR2	Vascular endothelial growth factor receptor 2
VIC	Fluorescent dye
V_{max}	Maximum rate achieved at saturating substrate concentration
vWF	von Willebrand factor
W	Tryptophan (amino acid)
-WLH	Triple dropout medium (-tryptophan, leucine, histidine)
-WLHA	Medium lacking tryptophan, leucine, histidine and adenine
WT	Wild-type
WTCCC	Wellcome Trust Case-Control Consortium
X	Stop codon
Y	Tyrosine (amino acid)
ΔC	C-terminal domains deleted
ΔN	N-terminal domains deleted

List of Figures

List of Tables

1: Chapter 1

Introduction

1.1 Age-related macular degeneration (AMD)

Age-related macular degeneration (AMD) is the leading cause of blindness in people aged over 65 years in developed countries (VanNewkirk et al. 2000; Friedman et al. 2004). AMD leads to the progressive impairment of central vision as the macula degenerates over time. Loss of central vision has profound consequences on an individual, affecting the ability to perform tasks such as reading and writing. As life expectancy increases, the burden placed by AMD upon individuals, their carers and society will increase. Due to the increasing number of affected individuals worldwide and the current lack of treatment options, a comprehensive understanding of this disease is very important.

1.1.1 Global prevalence of AMD

In the UK, it has been estimated that 3.7% of people aged over 75 years suffer from visual impairment as a consequence of AMD (Evans et al. 2004). This proportion rises steeply to affect 14.4% of individuals aged over 90 years (Evans et al. 2004). Similar studies in the USA have found that 30% of people aged over 75 years show signs of maculopathy, with 6-8% affected by advanced AMD (Klein et al. 1992; Friedman et al. 2004).

This suggests that in the UK and the USA, more than 2 million people aged over 75 years are afflicted by visual impairment as a result of severe AMD, with many millions more affected by early stages of age-related maculopathy (ARM). As the elderly population in developed countries continues to grow, the prevalence of AMD can be expected to rise.

1.1.2 The eye

The major features of the human eye are shown schematically in cross-section in Figure 1.1. Maintenance of homeostasis in the eye and correct functioning of the cellular phototransduction pathway requires a highly ordered tissue structure and normal cell-cell relationships. In AMD, retinal pigment epithelial cell dysfunction leads to photoreceptor cell death, and the disruption of tissue structure.

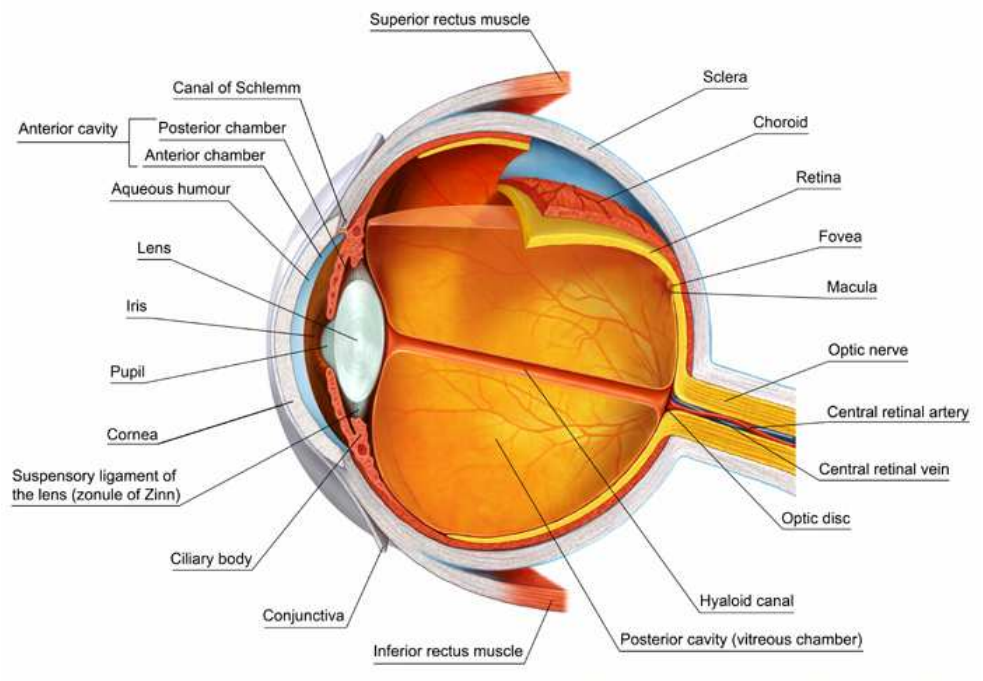

Figure 1.1 A cross-section of the human eye.
The eye is made up of three layers, enclosing the aqueous humour, the vitreous and the lens. The cornea and sclera form the outermost layer, overlying the iris, ciliary body and the choroid. The retina is the innermost layer. The photoreceptor cells of the neural retina are separated from the blood supply in the choroid by the retinal pigment epithelium (RPE), resting on the collagen-rich Bruch's membrane. The macula is a region of the retina approximately 6 mm in diameter that contains a high concentration of photoreceptor cells responsible for visual acuity.

Source: www.virtualmedicalcentre.com/anatomy.asp?sid=28&title=The-Eye-and-Vision

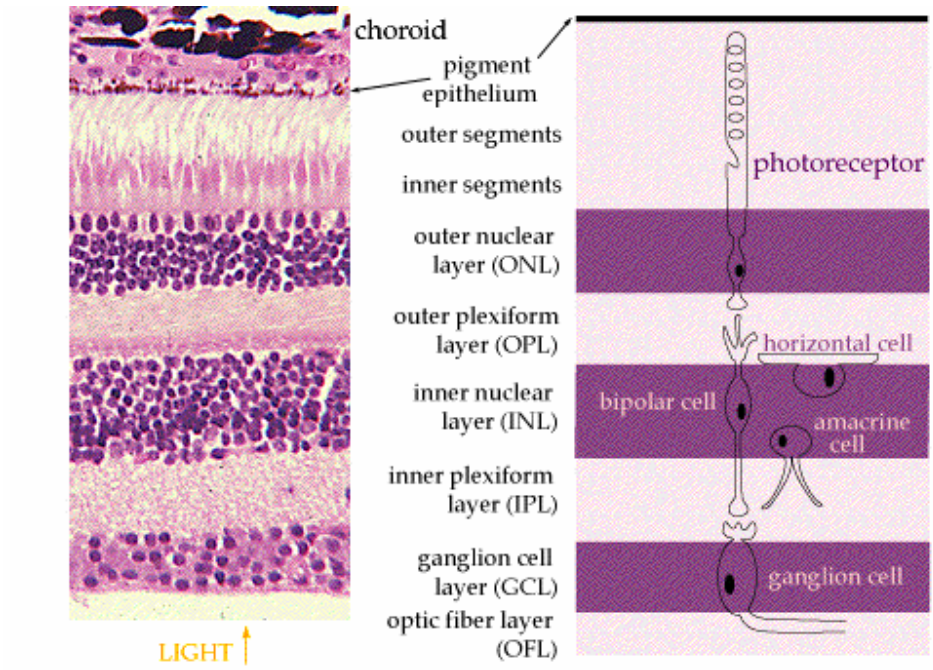

Figure 1.2 Structure of the vertebrate retina.
Light enters the eye through the lens. Light must then travel through several layers of cells in the retina to reach the light-senstive photoreceptors. In the photoreceptors, photosensitive pigments including rhodopsin are activated, and signal transduction from the photoreceptor cells to the bipolar cells and ganglion cells is induced. Ganglion cell axons in the optic nerve transmit the impulse to the brain where the image is formed.

Source: http://thalamus.wustl.edu/course/eye3.gif

1.1.2.1 The retina

As shown in Figure 1.1, the retina lines the majority of the back of the eye. The retina is a multilayered neural structure (Figure 1.2), and processes light which enters the eye. Axons transmit nerve impulses initiated in the retinal photoreceptors to the brain via the optic nerve, except at the "blind spot" where the optic nerve enters the eye. Directly behind the lens at the posterior pole of the eye, the macula is a region of the retina approximately 6 mm in diameter that has a high concentration of densely packed photoreceptor cells known as cones (Figure 1.1). The fovea is the central region of the macula, and contains only cones. These specialised neurons receive visual stimuli, initiate phototransduction and are responsible for visual acuity (McIlwain, 1996).

As shown in Figure 1.1 and 1.2, the photoreceptor cells of the retina are separated from their blood supply in the choroid by the retinal pigment epithelium (RPE), resting on the collagen-rich Bruch's membrane in the extracellular matrix (ECM).

1.1.2.1.1 Photoreceptor cells

The photoreceptor cells of the retina (rods and cones) contain light-sensitive pigments which allow the absorption of light and transduction of nerve impulses in response. Cones are responsible for colour vision, and contain several different pigments derived from vitamin A and opsins, each detecting distinct wavelengths of light. Rods contain the pigment rhodopsin (11-*cis* retinaldehyde and opsin), and this is important in night vision. Light must pass through several layers of cells before reaching the photoreceptors (Figure 1.2). At the fovea, the anterior retinal layers are thinner than at the periphery, allowing more light to reach the cones at this location.

Vertebrate photoreceptors have a specialised cilium known as the outer segment which consists of large numbers of disc-like lamellae (Figure 1.2). These contain the photo-sensitive pigments of the rods and cones. The outer segment is connected to the inner segment by the ciliary stalk or connecting cilium. The inner segment guides light photons to the pigments in the outer segment, and also contains the numerous mitochondria required to meet the metabolic demands of the

photoreceptor. The inner segment is connected to the cell body in the outer nuclear layer (ONL), and from here to the synaptic terminal from which impulses are transmitted, through bipolar cells in the inner nuclear layer and ganglion cells in the ganglion cell layer (Figure 1.2). Ganglion cells transmit the nerve impulse to the brain in the optic nerve (McIlwain 1996).

1.1.2.1.2 Retinal pigment epithelium (RPE)

RPE cells are pigmented cells which form a monolayer, separating the neural retina from the blood supply in the choroid (Figure 1.2). Outer segments of photoreceptor cells interdigitate with apical microvilli of the RPE. The basolateral RPE plasma membrane forms one of the five layers of the Bruch's membrane.

RPE cells have a crucial role in maintaining the blood-retinal barrier (Strauss 2005). Furthermore, the RPE maintains exchange of oxygen and nutrients from the choroid to the photoreceptors, phagocytoses shed photoreceptor outer segments, and re-isomerises all-*trans*-retinal into 11-*cis*-retinal (Figure 1.3). The metabolic support of the RPE cells is vital to photoreceptors. Dysfunctional RPE may lead to the development of drusen deposits between the monolayer RPE and the underlying Bruch's membrane, a hallmark of AMD (Penfold et al. 2001). Accumulation of waste products and debris in drusen over time may lead to inflammation (Hageman et al. 2001).

1.1.2.1.3 Bruch's membrane

The pentalaminar Bruch's membrane (BM) separates the RPE cells from the choroid (Figure 1.1, 1.2), and is involved in the exchange of biomolecules between these tissues. BM also has roles in adhesion of RPE cells via integrin cell-surface receptors and anchoring plaques (Marshall et al. 1992; Del Priore and Tezel 1998) and in restricting migration of cells in the RPE and choroid.

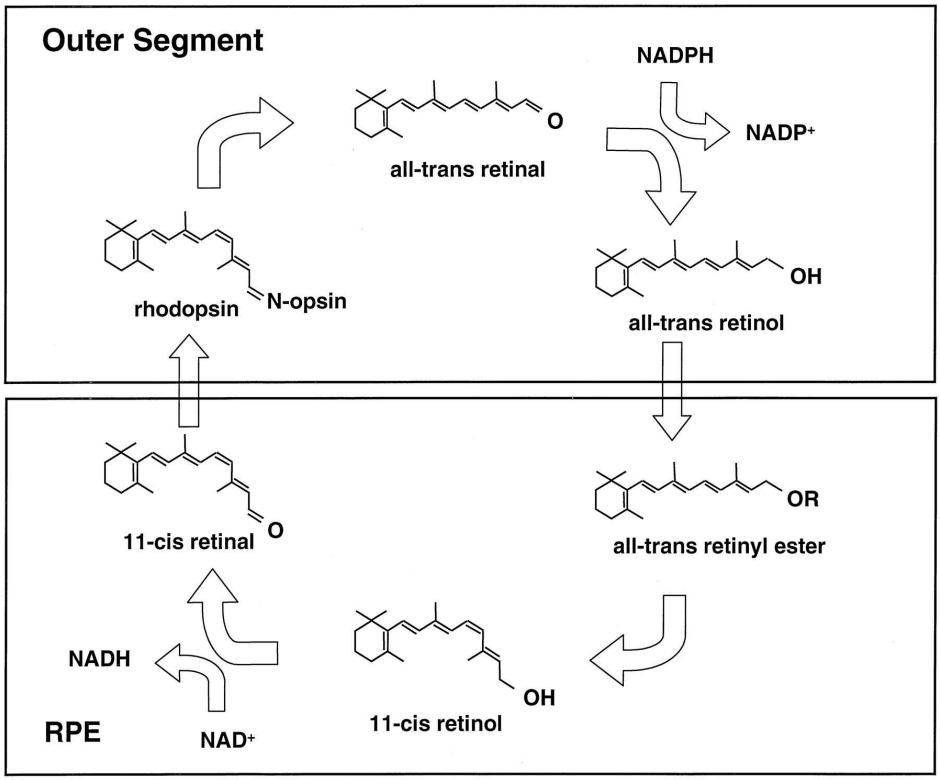

Figure 1.3 The visual cycle.
The visual cycle involves cycling of retinoids between the rod outer segments (OS; upper panel) and the RPE (lower panel). The visual cycle begins in the outer segment. Light activates rhodopsin, causing the release of all-*trans* retinal and initiating signal transduction. All-trans retinol is transported across the sub-retinal space by the carrier protein IRBP, and enters the RPE. All-*trans*-retinol is converted to all-*trans*-retinyl ester, then into 11-*cis*-retinol and finally into11-*cis*-retinal. The regenerated chromophore is transported back to the photoreceptors for further use. Source: (Rattner et al. 2000).

1.1.2.1.3.1 The layers of Bruch's membrane

The five layers of BM are the basement membrane of the RPE, the inner collagenous layer (ICL), the elastin layer (EL), the outer collagenous layer (OCL) and the basement membrane of the choriocapillaris. The different components of these layers, indicated in Figure 1.4, are thought to be expressed mainly by the RPE and choroidal cells (van Soest et al. 2007; Booij et al. 2009).

The basement membrane of both the RPE and choroid are rich in collagens type IV, fibronectin (FN)(Pauleikhoff et al. 1992), laminin (Aisenbrey et al. 2006) and heparin sulphate proteoglycans (HSPG (Hewitt et al. 1989)). The basement membrane of the choriocapillaris also contains collagens type V and VI. These are thought to play a role in platelet aggregation and epithelial cell migration (Narayanan and Page 1983) and in attaching BM to the choroidal endothelium (Marshall et al. 1994) respectively.

The ICL and the OCL are multi-layered grids, consisting of collagens type I, III and V. These layers of BM also contain glycosaminoglycans (Hewitt et al. 1989) and complement and coagulation proteins.

The elastin layer is rich in elastin fibres, forming a layered sheet with perforations of approximately 1 µm forming between the elastin fibres. Collagen type VI is also present, along with collagen fibres extending from the collagenous layers to either side. TIMP3 (tissue inhibitor of metalloproteases 3) has also been identified in the EL (Booij et al. 2009). In a recent study of 121 donor eyes, the EL in the macular region was found to be up to six times thinner than the EL at the periphery in human eyes from all ages (Chong et al. 2005). This does not appear to correlate with topographical differences in expression of the elastin gene (although other components are expressed at a lower level in the macular region; van Soest et al. 2007), which suggests that BM may have regional differences in structure, function and turnover of components.

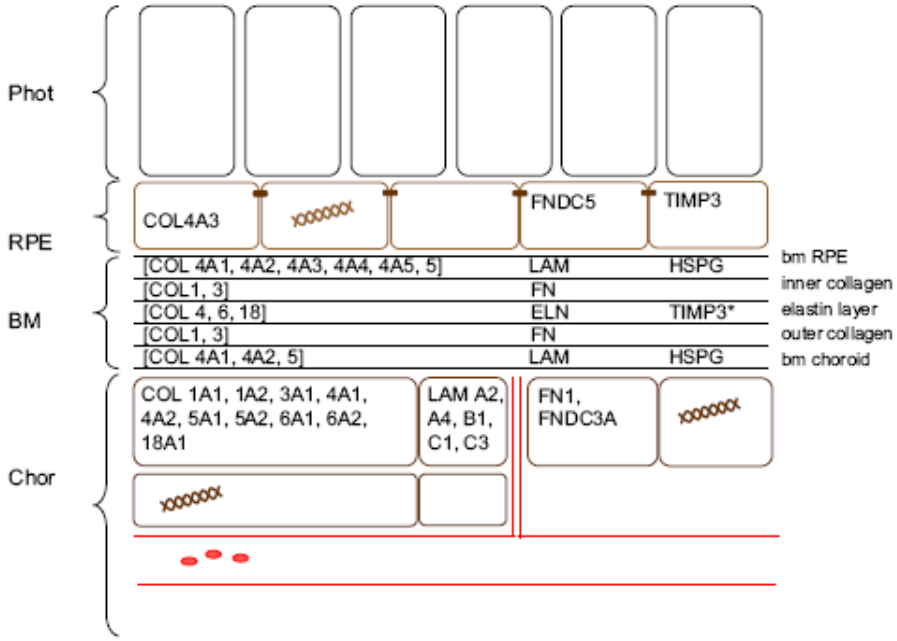

Figure 1.4 Bruch's membrane structure and composition.
A schematic drawing of the layered Bruch's membrane (BM), indicating the major proteins in each layer and the corresponding genes expressed in RPE and choroidal cells. The DNA encoding these genes in the RPE and choroidal cells is shown as a double helix shape. The basement membranes of the RPE and choroid are abbreviated as bm RPE and bm choroid respectively.
Source: Booij et al. (2010).

1.1.2.1.3.2 Diffusion of molecules across Bruch's membrane

Biomolecules such as oxygen, vitamin A and serum components move from the choroid to the RPE, and oxidised lipids and waste products are removed from the RPE across the BM. This is a largely passive process (Strauss 2005). Diffusion of these components is dependent on the pore size of BM layers, upon hydrostatic pressure and binding to BM components. This is influenced by the structure and composition of BM, and is further altered during ageing (Huang et al. 2007).

1.1.2.1.3.3 Changes to the Bruch's membrane during normal ageing

The structure and composition of BM changes during normal ageing. There is an increase in thickness of BM (van der Schaft et al. 1992; Ramrattan et al. 1994). This is partly due to more collagen cross-linking and differential turnover of proteoglycans such as heparan sulphate and chondroitin sulphate (Hewitt et al. 1989; Inatani and Tanihara 2002). This also has implications for regulating inflammation, as heparan sulphate may have anti-inflammatory properties through its interaction with Complement Factor H (CFH; (Meri and Pangburn 1994). BM is further modified by deposition of calcium (van der Schaft et al. 1992), iron (Hahn et al. 2003) and zinc (Lengyel et al. 2007) during ageing. Advanced glycation end products (AGEs) - chemically modified oxidised and glycosylated proteins and fats - accumulate on structural proteins in BM, causing age-related damage (Gugliucci et al. 2007). Lipids, including cholesterol, also accumulate in BM with age (Huang et al. 2007) and may build up preferentially in the macular region compared to the periphery (Holz et al. 1994), although there is substantial variability between individuals.

As a consequence of BM thickening, the elasticity and permeability of the BM are compromised. This can lead to the accumulation of waste material between the BM and the RPE. These are called drusen deposits, and are classified by location, size and shape (de Jong 2006). Soft, confluent drusen are a major risk factor for AMD. Thus, normal age-related changes in the BM may contribute to AMD pathology (Figure 1.5).

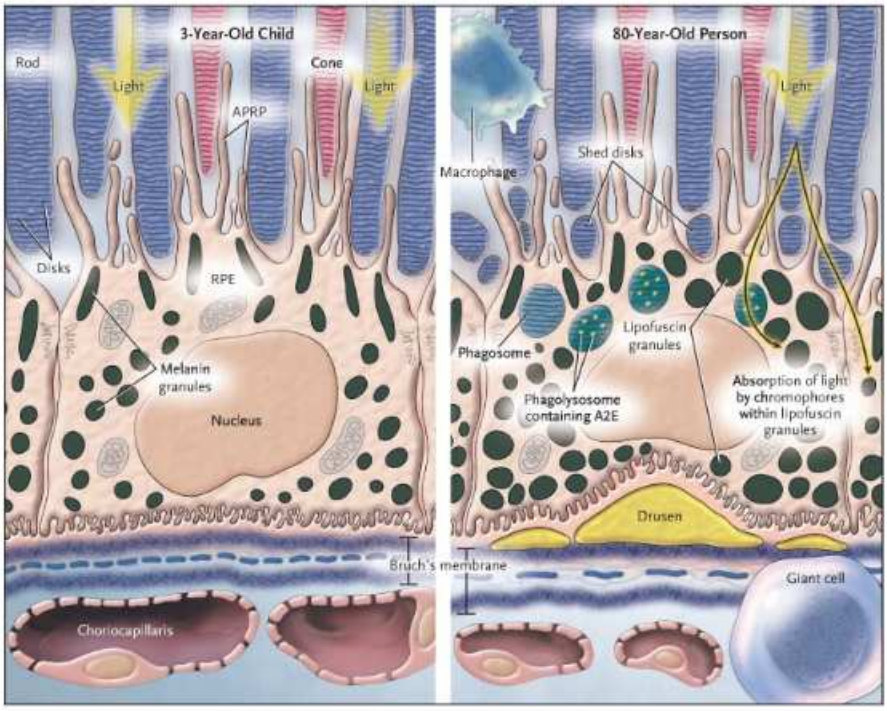

Figure 1.5 Age-related changes in the retina.
A comparison of the retina of a 3 year old child (left panel) and an 80 year old person (right panel) shows that there is an increase in thickness of the Bruch's membrane, development of lipofuscin granules and accumulation of waste material in drusen between the BM and the RPE. In some individuals, these changes contribute to the development of AMD, by causing RPE and photoreceptor cell dysfunction and death. Source: de Jong (2006).

1.1.3 Clinical features of AMD

Early or intermediate forms of macular degeneration, clinically defined by small numbers of drusen deposits and pigment abnormalities, are considered as age-related maculopathy (ARM). These individuals often maintain normal visual acuity. AMD refers to more advanced cases of the disease, in which large confluent drusen, geographic atrophy (GA) or neovascularisation are observed (Figure 1.6).

1.1.3.1 Dry AMD

Over 80% of AMD cases are "dry" or atrophic, with progressive degeneration of RPE and photoreceptor cells causing central geographic atrophy (GA). GA is characterized by hypopigmentation as a result of RPE cell death. Overlying photoreceptor cells die as a result of the loss of metabolic support provided by the RPE. This leads to blurring and gradual loss of central vision. Disease progression involves formation of sub-RPE drusen deposits, inflammation and lipofuscin accumulation (involving oxidative stress), as shown in Figure 1.5. Dry AMD may progress to exudative AMD in which neovascularisation occurs.

1.1.3.1.1 Changes in the Bruch's membrane

During normal ageing, the Bruch's membrane thickens, becomes less permeable and sub-RPE deposits are formed. The changes observed during normal ageing can contribute towards AMD pathology in a variety of ways (Figure 1.5). Genetics and environmental factors can further contribute to these changes.

Increased BM thickness affects the diffusion of biomolecules from the RPE and choroid, and leads to sub-RPE drusen deposits forming. Accumulation of AGEs may promote AMD (Yamada et al. 2006), whilst collagen cross-linking reduces turnover of BM components by decreasing the access of proteases to the pentalaminar structure (Ramrattan et al. 1994). This creates further thickening of the BM, exacerbating the restrictions in metabolite exchange and causing further drusen deposition. An increase in the proportion of heparan sulphate relative to other proteoglycans may alter the local regulation of inflammation (Meri and Pangburn

1994). Calcification of the BM has been correlated with AMD (Spraul et al. 1999), and has been proposed to make the EL brittle and susceptible to breaking, which may aid neovascularisation. Retinal degeneration can be induced by oxidative stress caused by iron accumulation (Kurz et al. 2007). Furthermore, both iron and zinc may be involved in oligomerisation of CFH (Nan et al. 2008), a key regulator of the alternative complement pathway with a known role in AMD pathogenesis.

1.1.3.1.2 Drusen

In early stages of AMD, basal laminar deposits (BlamD) and basal linear deposits (BlinD) develop (Green and Enger 1993). BlamD are diffuse deposits between the plasma membrane and basal lamina of the RPE, whilst BlinD develop within the ICL of Bruch's membrane (Curcio and Millican 1999). The composition of these deposits differs; BlamD are composed of collagenous material and basement membranes, and BlinD are composed of vesicular matter. BlinD develop after BlamD, and are markers for AMD progression (Curcio and Millican 1999; Sarks et al. 2007). The third class of sub-RPE deposit characteristic of AMD are drusen. Drusen are focal deposits, positioned between the basement membrane of the RPE and the Bruch's membrane (Figures 1.5 and 1.6).

The characteristics of drusen vary, although they tend to develop in the macular region, and can be classified based on size, shape and colour as either hard or soft. Hard drusen are clinically defined as small, yellow punctate deposits that are <63 μm in diameter. Small numbers of hard drusen are not a risk factor for AMD, and appear to increase in number during normal ageing (Fine et al. 2000). Soft drusen are larger (≤125 μm) amorphous deposits with less defined edges than hard drusen (Figure 1.6). Soft drusen are a significant risk factor for advanced AMD, especially if accompanied by alterations in pigmentation in the macular region (Klein et al. 2002).

Drusen are considered the hallmark of AMD. Although the exact role of drusen in disease pathogenesis remains unclear, these deposits are likely to disrupt RPE and photoreceptor cells directly, and also by the activation of inflammatory responses (Anderson et al. 2002). The molecular composition of drusen has been

analysed by proteomic and immunohistochemical approaches, with more than 100 proteins identified (Mullins et al. 2000; Russell et al. 2000; Hageman et al. 2001; Anderson et al. 2002; Crabb et al. 2002; Johnson et al. 2002). These proteins include components of the complement pathway, acute-phase inflammatory molecules, fibronectin, lipids, apolipoproteins B and E, glycoproteins and amyloid β (Crabb et al. 2002; Johnson et al. 2002). As many as 65% of the proteins identified are common to drusen from AMD and disease-free aged eyes, and many components are found in both hard and soft drusen (Mullins et al. 2000; Anderson et al. 2002; Crabb et al. 2002; Johnson et al. 2002; Nozaki et al. 2006a). Dendritic cell processes have been identified in drusen deposits (Hageman et al. 2001). High levels of zinc have been detected in drusen deposits, and have been suggested to have a role in the accumulation and aggregation of deposits, such as has been observed in Alzheimer's disease and Parkinson's disease (Lengyel et al. 2007).

Constituents of drusen appear to be produced by photoreceptor cells, RPE cells, choroidal cells and from the serum (Booij et al. 2009). Components of the complement pathway, including CFH and the membrane attack complex (MAC), are present in drusen. This implicates the alternative complement pathway and the innate immune response in the formation of drusen, disruption of the BM, and degeneration of RPE and photoreceptor cells observed in AMD (Anderson et al. 2002). This has been subsequently confirmed using genetic approaches.

1.1.3.1.3 Lipofuscin deposits

The development of lipofuscin deposits is thought to arise as a consequence of age-related RPE cell dysfunction (Figure 1.5; (Feeney-Burns et al. 1984)). This prevents the transport of vitamin A derivatives required for the visual cycle (Figure 1.3) and the phagocytosis of shed rod outer segments (Strauss 2005). Lipofuscin deposits are composed of oxidised lipids and proteins from photoreceptors, phagosomes and lysosomes. Oxidation of these proteins, including the cellular retinoid binding protein CRALBP, occurs as a result of exposure to high oxygen levels in the eye and to UVA and visible light (Sparrow and Boulton 2005; Warburton et al. 2005).

Lipofuscin contains the bisretinoid fluorophore A2E (N-retinylidene-N-retinylethanolamine), a remnant of photoreceptor outer segments. A2E is a potent inducer of reactive oxidant species (ROS) and has cytotoxic properties, damaging proteins, lipids and DNA (Sparrow and Boulton 2005). A2E inhibits degradation of proteins by the lysosome in cultured RPE cells, consistent with lipofuscin generation as a result of incomplete digestion of rod outer segments.

1.1.3.2 Choroidal neovascularisation in wet AMD

In more severe cases of "wet" or exudative AMD, shown in Figure 1.6, neovascularisation occurs in the choroid of the sub-macular region. The adult retina has a high metabolic rate, and the highest relative oxygen requirement in the body. To meet these requirements the retina is provided with oxygen and nutrients from two circulatory systems, arising from the retina (supplying the inner 2/3 of the retina) and the choroid. Under normal conditions, the outer third of the retina contains no blood vessels, but obtains metabolites and oxygen from the choroidal vessels (Figure 1.1). However, when there is a pathogenic increase in pro-angiogenic signalling (involving the balance of pro-angiogenic vascular endothelial growth factor (VEGF) to anti-angiogenic pigment epithelium derived factor (PEDF)) in the sub-retinal region, choroidal neovascularisation (CNV) can occur (Figure 1.6). New blood vessels originate from the choroid, penetrate the BM and spread into the subretinal space. Local inflammation may promote CNV formation in AMD, promoting secretion of VEGF by the RPE and injuring the BM. Bleeding through the fragile neovascular membrane leads to irreversible loss of central vision and fibrovascular scarring (Fine et al. 2000). Interestingly, wet AMD is more prevalent in Asian populations, often arising without any of the characteristic features of dry AMD, such as drusen (Klein et al. 2006).

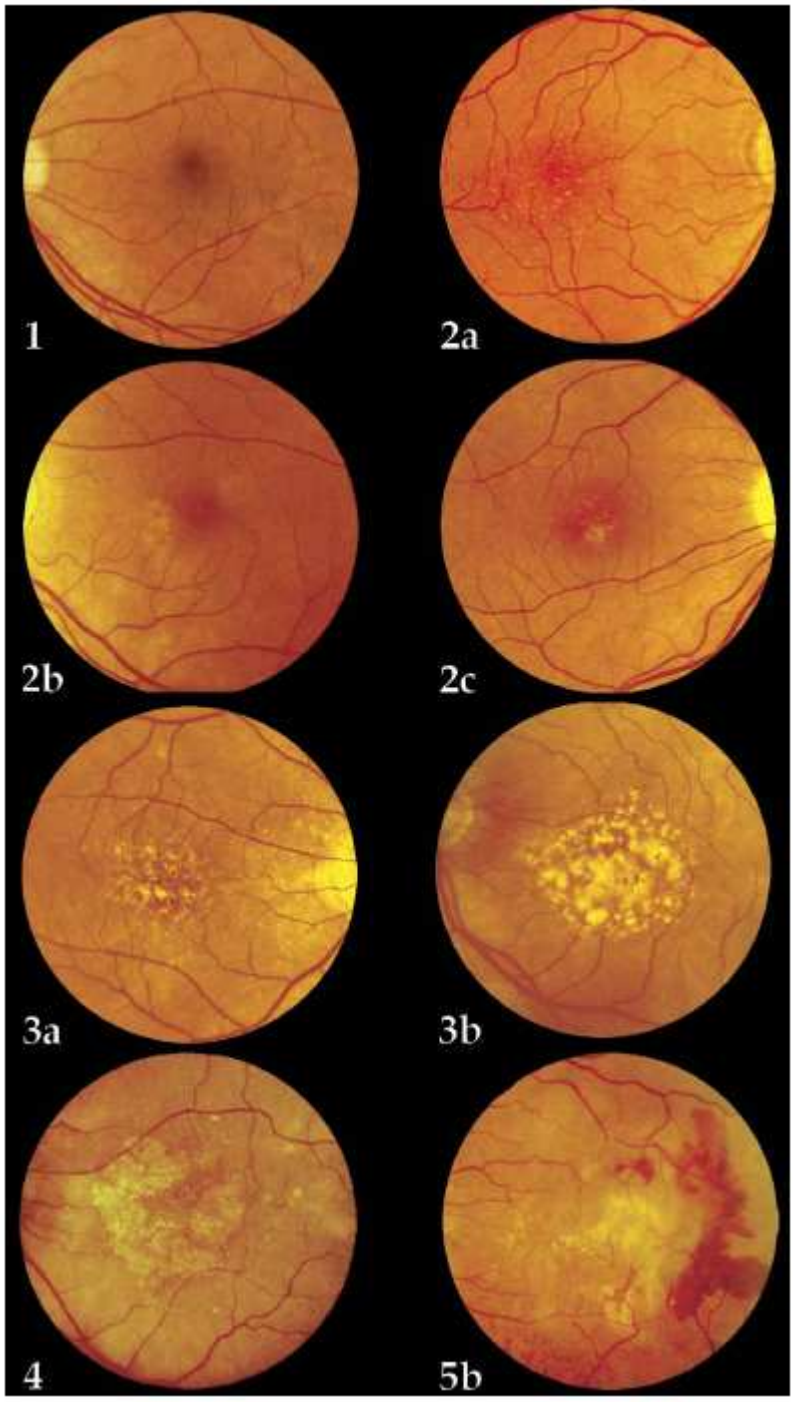

Figure 1.6 Clinical characteristics of age-related macular degeneration.

A five stage grading criterion is often used for characterising age-related maculopathy (ARM) and age-related macular degeneration (AMD). (1) A healthy retina with no drusen. ARM is characterised by (2a) several small drusen (yellow spots) and no RPE changes; (2b) RPE alteration, but no drusen; (2c) both small drusen and RPE changes; (3a) several intermediate-size and large drusen; (3b) drusenoid RPE detachment. Late-stage AMD is characterised by (4) geographic atrophy or (5b) choroidal neovascularisation.
Source: (Seddon et al. 2006b).

1.1.4 Therapeutic options for treatment of AMD

At the present time, effective treatments for dry AMD are lacking. High doses of antioxidant and zinc supplements slowed AMD progression in a 5 year study involving 3640 AMD cases (OR 0.72, 99% C.I. 0.52-0.98; (Age-Related Eye Disease Study Research 2001)). Recently, high dietary intake of zinc and other anti-oxidants was found to reduce the hazard ratio of AMD for individuals with high genetic susceptibility (Ho et al. 2011).

Therapeutic options for wet AMD, including anti-angiogenic agents such as VEGF inhibitors, and photodynamic therapy, are aimed at preventing further loss of sight rather than reversing the course of the disease. VEGF-inhibitors are now the most commonly used therapy. Lucentis and Avastin (monoclonal antibodies against full-length VEGF, and a fragment of VEGF, respectively) have very similar beneficial responses in a recent clinical trial (CATT 2011).

An increased understanding of the biological mechanisms behind AMD may provide new therapeutic targets, whilst identification of genetic risk-factors may aid in the early identification of at-risk individuals, allowing therapeutic intervention before photoreceptor death occurs.

1.1.5 Underlying mechanisms of disease

During the course of normal ageing, changes occur in the eye. These affect the metabolic activity and function of the RPE, photoreceptor survival, Bruch's membrane structure and permeability and development of basal deposits and drusen. In some individuals, these changes contribute to the development of AMD pathology. Although the switch from normal ageing to disease processes is multi-factorial, the underlying mechanisms of AMD which result in RPE dysfunction and photoreceptor cell death appear to be shared.

1.1.5.1 Oxidative damage

The combination of constant light exposure, high oxygen consumption and photoreactive compounds in the visual cycle means the retina is exposed to

substantial oxidative stress. Outer segments of photoreceptors are constantly phagocytosed by RPE cells (Tate et al. 1995). The retina is somewhat protected from oxidative damage by anti-oxidant enzymes including superoxide dismutase and glutathione peroxidase (Tate et al. 1995; Frank et al. 1999; Beatty et al. 2000). However, both the photoreceptors and RPE are highly susceptible to oxidative damage of DNA, proteins and lipids. This can cause cell death and has significant consequences on the structure and function of the retina, contributing to the pathogenesis of AMD.

1.1.5.2 Mitochondrial dysfunction

Mitochondria have been implicated in AMD and other age-related neurodegenerative diseases, such as Alzheimer's disease (Lin and Beal 2006). Impaired energy metabolism and generation of reactive oxygen species is observed in dysfunctional mitochondria during aging, with a decrease in number of mitochondria seen in AMD retinas compared to controls (Feher et al. 2006). Deletions in the mitochondrial genome accumulate in the retina with age (Barron et al. 2001) and mutations in mitochondrial proteins are known to play a role in neurodegenerative eye diseases, including AMD (Carelli et al. 2004; Canter et al. 2008). Defective mitochondrial function may lead to apoptosis (Liang and Godley 2003) of RPE cells, and cause photoreceptor cell death as a result of diminished metabolic support (Wallace 2005).

1.1.5.3 Inflammation

The innate immune system has been implicated in the pathogenesis of AMD for many years (Penfold et al. 1985; Hageman et al. 2001). Characterisation of the constituents of drusen showed that many proteins involved in the immune response were localised to these deposits, including immunoglobulins (IgG), complement component C5 and the terminal component of the complement pathway, the MAC (Crabb et al. 2002). Based on the high level of IgG detected in the eyes of AMD cases, drusen formation was suggested to occur as a consequence of an immune response against antigens derived from the RPE (Johnson et al. 2000). The identification of acute-phase proteins such as C-reactive protein (CRP) and

vitronectin, activators of the complement pathway (C5, C5b-9, C3b and C3d) and the complement regulators membrane co-factor (CD46) and complement receptor 1 (CR1), in drusen further implicated local inflammation (Hageman et al. 2001; Anderson et al. 2002). In addition to the immune-reactivity of drusen, the study by Anderson and colleagues of 400 AMD eyes also showed that some RPE cells had a build up of CRP and C5 in the cytoplasm, and that this corresponded to dying cells (Anderson et al. 2002).

These findings led to the hypothesis that RPE cell dysfunction is the primary event in AMD pathology, causing the accumulation of cellular debris. This acts as a trigger for pro-inflammatory signalling, inducing local expression of pro-inflammatory molecules, recruitment of inflammatory cells, and activation of the alternative complement pathway. During this process, such molecules are deposited alongside the cellular debris to form drusen (Hageman et al. 2001, Anderson et al. 2002). However, the exact mechanism of drusen biogenesis remains undetermined.

Subsequent work has identified a number of molecules derived from the RPE that are antigenic. A2E, a component of lipofuscin, is recognised as a non-self molecule (Zhou et al. 2006) and activates the complement cascade. Likewise, amyloid β co-localises with activated components of the complement pathway in drusen, and can trigger a local immune response through an interaction with Complement Factor I (Johnson et al. 2002; Wang et al. 2008). Carboxyethylpyrrole (CEP), an oxidatively modified fragment of the polyunsaturated fatty acid docosahexaenoic acid, can also promote a local immune response (Hollyfield et al. 2008). Together, this suggests activation of the innate immune response as a result of complement-activating components of drusen may exacerbate RPE cell dysfunction by inducing bystander damage and leading to AMD.

1.1.5.4 Phagocytes in AMD

Phagocytes including macrophages, microglia and dendritic cells are present in the healthy adult retina. Resident microglial cells contribute to neuronal homeostasis and immunoregulation (Langmann 2007). These cells are present in the retina since embryological development. Injury and degeneration of the retina activates the

microglia and leads to proliferation. The activated cells secrete pro-inflammatory molecules, migrate to sites of injury and phagocytose debris (Langmann 2007). These cells are involved in the clearance of sub-RPE debris (Chen et al. 2002) and are detected in macular lesions in AMD eyes (Gupta et al. 2003).

1.1.5.4.1 Macrophages in AMD

Macrophages are recruited from the blood supply in the choroid to clear the sub-retinal deposits in the AMD eye (Forrester 2003). These cells have been localised to deposits in AMD eyes using electron microscopy (Killingsworth et al. 1990). Macrophages have also been identified near sites of RPE atrophy, CNV and in areas of Bruch's membrane damage in AMD eyes (Penfold et al. 1985; Lopez et al. 1993; Dastgheib and Green 1994; Green 1999; Penfold et al. 2001; Grossniklaus et al. 2002; Coleman et al. 2008) using histopathology.

The role of macrophages in CNV remains to be clarified. It seems that some macrophages combat CNV. Interleukin-10 deficient mice show decreased susceptibility to laser-induced CNV as a result of increased recruitment of macrophages to the site of injury (Apte et al. 2006). However, other macrophages appear to have a causative role in CNV (Espinosa-Heidmann et al. 2003; Sakurai et al. 2003). The uptake of dichloromethylene diphosphonate (Cl_2MD)-containing liposomes causes macrophage death in mice. These mice show impaired macrophage recruitment to sites of laser injury on the retina, and this correlates with less severe CNV at these lesions.

These contradictory findings are consistent with macrophages existing as two subtypes: pro-inflammatory M1 macrophages, and anti-inflammatory M2 macrophages (Mantovani et al. 2004). M2 macrophages have been suggested to perform scavenging and tissue-remodelling, and may be recruited beneficially to clear drusen. Recruitment of M1 macrophages may be to the detriment of the tissue, inducing and worsening inflammation by expression of pro-inflammatory cytokines and promoting development of CNV (Mantovani et al. 2004).

1.1.5.5 Tissue metalloproteases and other proteases

The balance between pro-angiogenic and anti-angiogenic signals is crucial to maintaining the appropriate vasculature for a healthy tissue. Over-expression of pro-angiogenic VEGF is necessary, but not sufficient, to induce neovascularisation from the choroid into the subretinal space. Additional injury to the Bruch's membrane appears to be required (Schwesinger et al. 2001). Matrix metalloproteinases (MMPs) are known to degrade components of the extracellular matrix (ECM), and appear to be required during angiogenesis.

MMPs and the tissue inhibitor of metalloproteinases-3 enzyme (TIMP3) have been implicated in pathological processes underlying AMD (Guo et al. 1999; Kamei and Hollyfield 1999). Drusen deposits are lacking in MMP activity, suggesting proteolytic degradation of drusen may be compromised in AMD individuals (Leu et al. 2002). However, MMP9 has been reported to be elevated in plasma from 33 AMD cases compared to 17 controls (Chau et al. 2007). In experimental models of laser-induced CNV, metalloproteinases MMP2 and MMP9 influence the severity of choroidal neovascularisation (Lambert et al. 2002; Lambert et al. 2003). A microsatellite polymorphism in the promoter of *MMP9 w*as identified as a potential susceptibility factor for wet AMD (Fiotti et al. 2005). However, this study was small (107 cases and 223 controls) and the association has not been replicated.

Mutations in the gene encoding TIMP-3 cause Sorsby's fundus dystrophy. This is a rare inherited form of macular degeneration associated with deposits in the Bruch's membrane and sub-retinal neovascularisation (Weber et al. 1994). Large genome-wide association studies have identified an AMD-susceptibility locus near *TIMP3* (Chen et al. 2010; Yu et al. 2011). The precise mechanism by which these proteases may be involved in AMD remains to be determined, although degradation of the ECM and the Bruch's membrane may be important.

1.2 Risk factors for AMD

AMD is a disease with complex etiology, arising through the interaction of genetic and environmental factors.

1.2.1 Epidemiological risk factors

Epidemiological studies have identified advanced age, smoking, ocular pigmentation, race, high blood pressure and diet as risk factors, along with family history (Klein et al. 2004). Increasing age undoubtedly has a substantial influence upon risk of developing AMD (Klein et al. 1997; Friedman et al. 2004). Cigarette smoking also greatly increases the risk of developing the disease (Christen et al. 1996; Seddon et al. 1996; Tomany et al. 2004). Caucasians are more susceptible to AMD, especially wet AMD, than Hispanic or black populations (Sommer et al. 1991; Cruickshanks et al. 1997). Obesity and high fat diets are both associated with increased risk of AMD (Mares-Perlman et al. 1995; Cho et al. 2001; Seddon et al. 2003b). Conversely, dietary factors such as antioxidants and omega-3-fatty acids, are protective (Seddon et al. 1994; Age-Related Eye Disease Study Research 2001; Seddon et al. 2003c). The contribution of other risk factors such as hypertension, high cholesterol levels, and sunlight exposure remains unclear.

The combination of environmental risk factors acting to induce oxidative stress, or inflammation, over a lifetime is likely to contribute to the age-associated increase in AMD-risk.

1.2.2 Genetic risk factors

Familial aggregation studies indicate that as much as 25% of AMD cases have a genetic contribution (Klaver et al. 1998). First degree relatives of AMD cases have a 50% risk of AMD, compared to 12% for relatives of disease-free controls (Klaver et al. 1998). A combination of linkage and association studies has elucidated the contribution of several genes to AMD.

1.2.2.1 Linkage studies

Linkage analysis performed in multiple families and sibling-pairs suggest that susceptibility loci for AMD may be found on most chromosomes in the human genome. However, only two genomic regions have been strongly replicated in such studies - a region on chromosome 1q25-31 (Majewski et al. 2003; Iyengar et al. 2004) and another on chromosome 10q26 (Kenealy et al. 2004 ; Jakobsdottir et al. 2005). Meta-analysis performed by Fisher et al. (2005) further implicated risk loci on chromosome 1q and chromosome 10q. Chromosomes 2p, 3p, 4q, 12q and 16q also showed evidence for linkage with AMD (Fisher et al. 2005).

1.2.2.2 Association studies

Recent advances in AMD genetics have been made using population-based association studies, utilising unrelated AMD cases and disease-free control subjects to identify causative alleles of genetic markers (such as single nucleotide polymorphisms, SNPs) or variants in linkage disequilibrium (LD) with disease-causing alleles. A Manhattan plot summarising the peaks of association identified in the most recent genome-wide association scan for AMD in shown in Figure 1.7.

1.2.3 Complement Factor H *(CFH)*

Complement Factor H (*CFH*) on chromosome 1q31 was proposed as a candidate gene based on such analyses. Klein et al. (2005) performed a genome-wide association scan of 96 cases and 50 controls for polymorphisms associated with AMD. An intronic variant (rs380390) with a *p*-value less than 10^{-7}, that increased the likelihood of developing AMD by a factor of 7.4 in homozygotes (95% confidence interval (C.I.) 2.9 -19) was identified. Re-sequencing of the *CFH* gene identified a T-C transition in exon 9 that was in linkage disequilibrium (LD) with rs380390, and results in a tyrosine to histidine change at position 402 of CFH. This region of the protein binds heparin and C-reactive protein (CRP) and controls the activity of CFH in regulation of the complement system (Klein et al. 2005). The association between AMD and the Y402H polymorphism in *CFH* was replicated in independent studies, all attributing a significantly increased risk of AMD to this

variant in heterozygotes (Edwards et al. 2005; Hageman et al. 2005; Haines et al. 2005). Y402H is estimated to account for as much as 50% of the population-attributable risk for AMD (Edwards et al. 2005).

Hageman et al. (2005) also found an association between increased AMD susceptibility and I62V (rs800292) in *CFH* in two independent cohorts from North America ($p=1.1 \times 10^{-4}$ and $p=3.2 \times 10^{-7}$). The I62V variant is located in an exon splice enhancer (Wang et al. 2004). Li et al. (2006) found that 20 polymorphisms in and around *CFH* were more strongly associated with AMD than the Y402H variant in their cohort of 726 AMD cases and 286 controls. No single polymorphism was responsible for the increase in susceptibility; rather, haplotypes, including non-coding variants, were formed which influenced risk (Li et al. 2006). The common, noncoding variant rs1410996 in *CFH* was also found to be associated with AMD (Maller et al. 2006). Thus it appears that there are several AMD-susceptibility alleles in and around the CFH gene on chromosome 1, including non-coding variants (Figure 1.8). Interestingly, allele frequencies of these variants in *CFH* differ substantially in Asian populations, and do not appear to confer the same risk of AMD (Gotoh et al. 2006).

Membranoproliferative glomerulonephritis type II (MPGN II) is a disease with ocular manifestations identical to those observed in AMD (Mullins et al. 2001). In their analysis of *CFH* in 900 AMD cases and 400 controls, Hageman et al. (2005) also identified several common SNPs as risk factors associated with both AMD and MPGN II. Protective haplotypes for both diseases were also identified. Furthermore, CFH was detected in the macula and in drusen, providing evidence for a role for CFH in AMD pathogenesis (Hageman et al. 2005). Additional studies subsequently confirmed a role for CFH in AMD development (Conley et al. 2005; Magnusson et al. 2005; Zareparsi et al. 2005a).

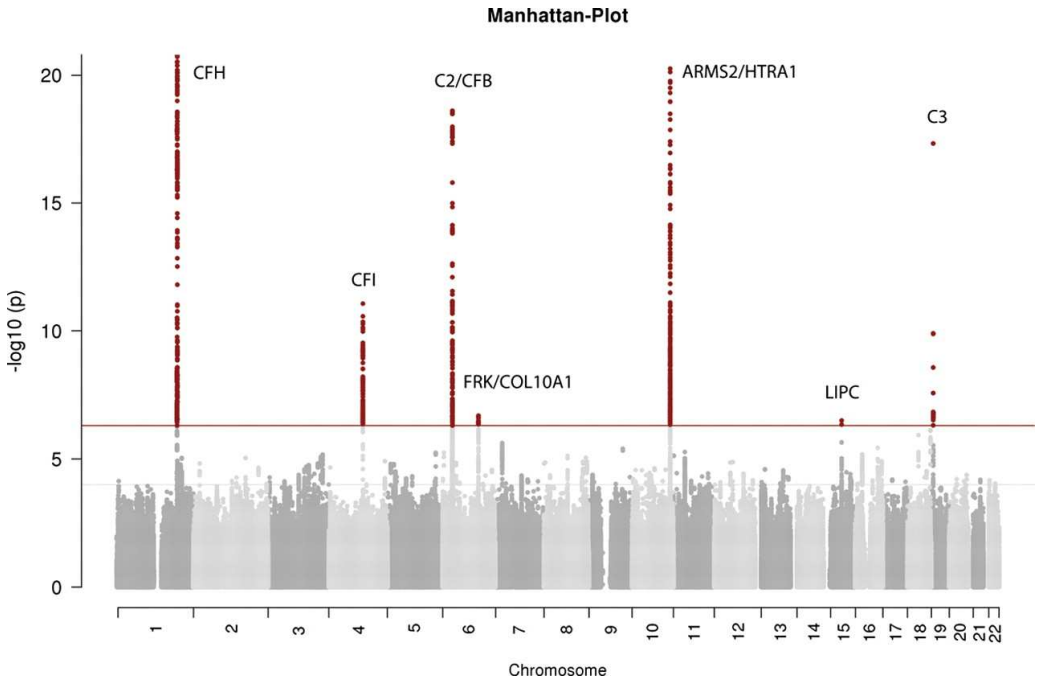

Figure 1.7 Major susceptibility loci for AMD identified in association studies.

Genetic loci that substantially alter AMD-risk have been identified by linkage and association studies. Recently, genome-wide association scans performed in thousands of AMD cases and controls have confirmed previously reported loci in *CFH, CFI, CFB, C3* and *ARMS2/HTRA1*, and have identified new susceptibility loci near *COL10A1, COL8A1, TIMP3, LIPC* and *VEGF*. In the Manhattan Plot shown above, SNPs showing a genome-wide significant association (threshold p-value shown by red line) with AMD are highlighted in red. Chromosomal position is indicated on the x-axis.
Source: Yu et al. (2011).

1.2.4 Genetic association of additional complement genes with AMD

As a result of the identification of a major susceptibility factor in *CFH*, inflammation is considered to play an important role in the degeneration of the macula and in AMD pathogenesis. Several other components of the complement pathway (Figure 1.10) have subsequently been implicated in AMD, providing further evidence for the damage caused by aberrant regulation of inflammatory processes in the eye.

1.2.4.1 *CFHR1* and *CFHR3*

CFHR1 and *CFHR3* genes, which are homologous to and located adjacent to *CFH* on chromosome 1q23, are deleted in a common protective haplotype (Figure 1.8). This results in a loss of detectable protein in the serum of homozygous carriers of the risk haplotype (Hughes et al. 2006); the functional consequence of this remains unclear. The protective effect of *CFHR1* and *CFHR3* deletion is independent of genotype at *CFH* Y402H (Hughes et al. 2006; Schmid-Kubista et al. 2009), but is slightly reduced by genotype at the intronic *CFH* SNP rs10737680 (Raychaudhuri et al. 2010), as shown in Figure 1.8.

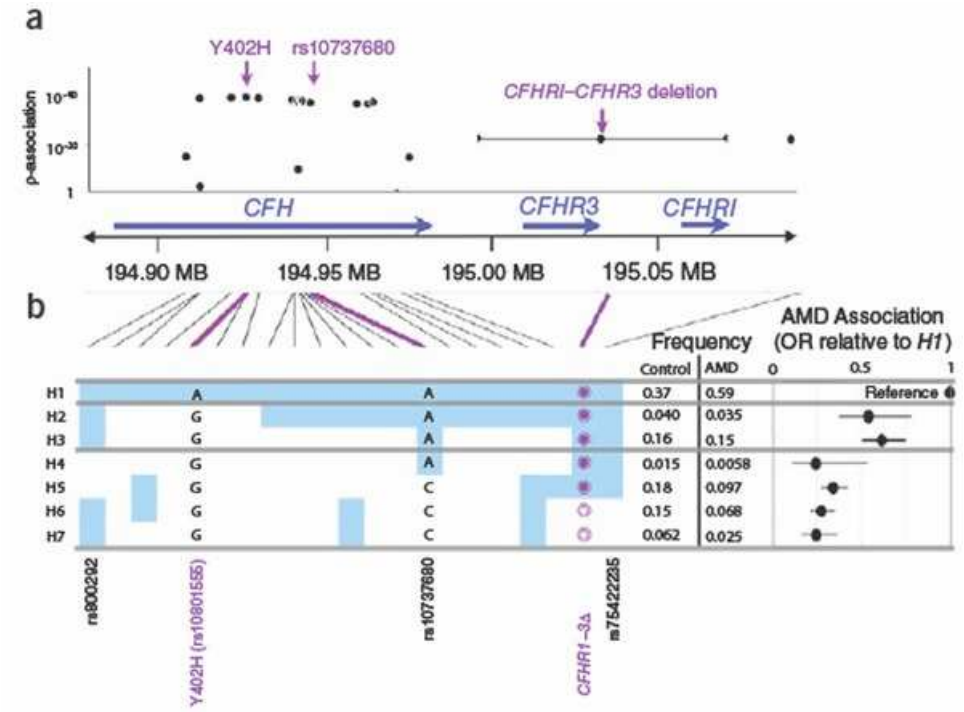

Figure 1.8 *CFH, CFHR1* and *CFHR3* are associated with AMD susceptibility.

CFHR1 and *CFHR3* genes are homologous to, and located adjacent to, *CFH* on chromosome 1q23. (**a**) Variants in *CFH*, including Y402H and rs10737680, are significantly associated with AMD, and *CFHR1* and *CFHR3* are deleted in a common protective haplotype. (**b**) Raychaudhuri et al (2010) identified 7 haplotypes with frequencies >1%. Haplotypes are composed of the *CFH* Y402H proxy rs10801555, *CFH* rs10737680, deletion status of *CFHR1–CFHR3* (empty circle, deleted; filled circle, not deleted), rs7542235 and rs800292 (CFH I62V). H1 is presented as the reference haplotype. SNP genotypes shaded in blue are the same as in H1, SNP genotypes different from H1 are shaded white. The observed frequency in controls and affected individuals and the odds ratio of disease for each haplotype relative to that of the most common haplotype, *H1* is shown to the right.
Source: Raychaudhuri et al. (2010).

1.2.4.2 Complement Factor B and C2

The genes encoding Complement Factor B (*BF/CFB)* and complement component 2 (*C2*) are located 500 bp apart on chromosome 6p21 in the major histocompatibility complex (MHC) class III region. In a study of 898 affected individuals and 389 controls from two independent cohorts, two variants in each gene were significantly associated with AMD (Gold et al. 2006). The L9H variant in *CFB* and the E318D variant in *C2* are located on the same protective haplotype for AMD ($p=3.4 \times 10^{-6}$, OR = 0.36 (95% confidence interval (C.I.) = 0.23–0.56)). A second highly protective haplotype consists of the R32Q allele in *CFB* and rs547154 in intron 10 of *C2* and ($p=2.1 \times 10^{-7}$, OR = 0.45 (95% C.I. = 0.33–0.61)). A common risk haplotype was also identified (p=0.0013, OR = 1.32). High LD in this region makes it difficult to separate the relative contribution of the SNPs on these haplotypes, and to identify the gene responsible for increased risk. However, functional studies of some of the coding changes in factor B show decreased enzyme activity, ability to form the convertase and activity in assays of complement activity for the protective variants (Lokki and Koskimies 1991; Montes et al. 2009).

1.2.4.3 Complement component C3 (*C3*)

A variant in the complement C3 gene was recently associated with risk of developing AMD (Yates et al. 2007). In a study of 847 AMD cases and 701 unaffected controls, heterozygotes for the S/F variant (Arg102Gly) in the *C3* gene had a 70% increased risk for AMD, whilst individuals homozygous for the F variant are at more than twice the risk of developing AMD. This may be responsible for an estimated 22% of population-attributable risk for the disease. Interestingly, like polymorphisms in *CFH* (Hageman et al. 2005; Montes et al. 2008), this variant has also been associated with MPGN II (Finn and Mathieson 1993). Functional studies have shown that the 102G variant activates the alternative complement pathway more efficiently than R102 (Heurich et al. 2011).

1.2.4.4 Complement Factor I (*CFI*)

A variant 2781 bp downstream of the 3' UTR of the gene encoding Complement Factor I (CFI) has also shown association with AMD. Located within a linkage peak on chromosome 4 (Fisher et al. 2005), the non-coding SNP rs10033900 was first significantly associated with AMD in a study of 1228 AMD cases and 825 controls ($p=9.11 \times 10-8$; (Fagerness et al. 2009). Subsequent studies have replicated the association between rs10033900 and AMD in smaller groups of Caucasian (Ennis et al. 2009) and Japanese (Kondo et al. 2010) cases and controls. The causal variant in CFI has yet to be identified.

1.2.5 The chromosome 10q26 risk locus

Chromosome 10q26 has been shown by numerous groups to contain AMD risk loci with an equivalent impact on AMD risk as CFH (Majewski et al. 2003; Seddon et al. 2003d; Weeks et al. 2004; Fisher et al. 2005; Jakobsdottir et al. 2005). Three genes, *PLEKHA1*, *LOC387715* (*ARMS2*) and *HTRA1* (also known as *PRSS11*) lie in a 200 kb region of strong linkage disequilibrium, shown in Figure 1.9. Identification of the variant(s) influencing susceptibility to AMD in this region has proved difficult and controversial.

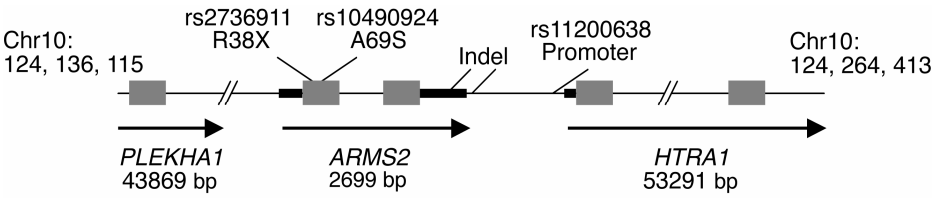

Figure 1.9 The chromosome 10q26 locus.
Location of variants on chromosome 10 which are associated with AMD susceptibility in relation to candidate genes (not drawn to scale). Coding sequences of candidate genes are shaded in grey; untranslated regions are shown in black. Nucleotide positions and distances along chromosome 10 are derived from the NCBI Entrez Gene database. Figure adapted from (Allikmets and Dean 2008).

1.2.5.1 *PLEKHA1*

Jakobsdottir et al. (2005) genotyped numerous SNPs in a region of chromosome 10 spanning *PLEKHA1, LOC387715* (*ARMS2*) and *HTRA1* (Figure 1.9). SNP analysis in 612 AMD cases, 184 unrelated controls and 323 families suggested that variants in *PLEKHA1*, encoding TAPP1, a protein which may act in local lymphocyte activation, were responsible for increased susceptibility to AMD (Jakobsdottir et al. 2005).

1.2.5.2 *ARMS2/LOC387715*

Rivera et al. (2005) studied the same region of chromosome 10q in two independent cohorts of AMD case-controls, and found that the strongest association with AMD ($p= 10^{-34}$) arose from rs10490924, a coding change from alanine to serine at position 69 (A69S) in the hypothetical locus *LOC387715* (Figure 1.9). The A69S variant in *LOC387715* was subsequently reported as a second major susceptibility allele for AMD following multi-variate analyses performed using A69S, smoking and the Y402H variant of *CFH* to test gene-gene and gene-environment interactions (Schmidt et al. 2006). However, no plausible role in AMD pathogenesis was proposed as there was an absence of any functional information for *LOC387715* (Rivera et al. 2005). The lack of functional information, together with the subsequent removal of *LOC387715* from the GenBank database, led to the strong association on chromosome 10q26 being attributed to promoter variants in *HTRA1*, which are in complete LD with risk variants in *LOC387715* and which may affect gene expression (Dewan et al. 2006).

1.2.5.3 *HTRA1*

Wet AMD is more prevalent in Asian populations than Caucasian, where approximately 10% of AMD cases have this more aggressive form of the disease. Dewan et al. (2006) performed a whole genome association scan of 96 wet AMD cases and 130 age-matched controls in a Chinese population to identify variants that increased susceptibility to the wet AMD phenotype. A single A-to-G SNP,

rs11200638, in complete LD with the SNP in *LOC387715* previously associated with AMD, was identified (Rivera et al. 2005; Dewan et al. 2006). This variant, associated with a 10-fold increased risk for wet AMD in individuals homozygous for the A allele, lies in the promoter region of *HTRA1* (Figure 1.9), in putative binding sites for transcription factor AP2α and serum response factor (SRF). Transcription of *HTRA1* was shown to be upregulated by the AA genotype, suggesting that the increased susceptibility to AMD arises as a result of increased HTRA1 expression and activity (Dewan et al. 2006). This theory gained support when increased *HTRA1* mRNA and protein were detected in RPE from 4 AMD-affected individuals carrying the AA risk allele (Yang et al. 2006).

Yang et al. (2006) found that the promoter polymorphism in *HTRA1* was also associated with AMD in Caucasians, causing an estimated 49.3% population-attributable risk for AMD. Furthermore, this variant also increases risk of developing dry AMD, and HTRA1 has been detected in drusen deposits in AMD-affected eyes. Carrying a risk allele in either *CFH* or chromosome 10q26 accounts for an estimated 71.4% population-attributable risk of AMD, whilst possessing risk alleles in both *HTRA1* and *CFH* increases the susceptibility to developing AMD by 40-fold (Yang et al. 2006; Cameron et al. 2007).

1.2.5.4 The contribution of *LOC387715/ARMS2* to association at chromosome 10q26

As reported by Dewan et al. (2006), *LOC387715* was removed from the GenBank database, leading to a shift in focus to variants in *HTRA1* which were associated with AMD. However, *LOC387715* has subsequently been reinstated to the database, using the symbol *ARMS2* (age-related maculopathy susceptibility 2).

1.2.5.4.1 The SNP rs10490924

Variants in *LOC387715/ARMS2* have recently been gaining support as the true risk alleles for AMD on chromosome 10q26. Kanda et al. (2007) provided contradictory evidence to that of Dewan et al. (2006) as to the up-regulation of HTRA1 expression in individuals homozygous for the A allele at rs11200638. The region surrounding

rs11200638 was also shown not to bind the transcription factor AP2α, as hypothesised by Dewan et al. (2006). Furthermore, using logistic regression analysis to evaluate the contribution of multiple SNPs across a 220 kb region spanning *PLEKHA1*, *LOC387715* (*ARMS2*) and *HTRA1* to the strong association with AMD, Kanda and colleagues find that when rs10490924, the A69S variant in *ARMS2*, was included, no other SNPs showed evidence of significant association to the disease. This led to the suggestion that a single variant (rs10490924 or an ungenotyped variant in complete LD) is responsible for the large effect on disease susceptibility on chromosome 10q26 (Kanda et al. 2007).

1.2.5.4.2 The *ARMS2* 3' UTR indel

A recent discovery of a combination of a 372 base pair deletion and a 54 base pair insertion in the 3' UTR of the *ARMS2* gene, which is significantly associated with AMD in 760 AMD cases and 549 controls ($p = 4.1 \times 10^{-29}$), adds further weight to the argument for *ARMS2* playing a role in AMD risk (Fritsche et al. 2008). This variant (in/del in Figure 1.9) is tightly linked to rs10490924 and several other SNPs, forming a risk haplotype with an 8.1-fold increased risk of AMD for homozygous individuals. The deletion removes a polyadenylation signal, whilst the insertion of an AU-rich element appears to lead to rapid mRNA decay in individuals with the indel polymorphism. As a consequence, expression of *ARMS2* is not detected in homozygous carriers of the indel variant in some studies (Fritsche et al. 2008; Yang et al. 2010).

Yang et al. (2010) also showed that a second coding change in *ARMS2* – R38X – results in reduced *ARMS2* mRNA and protein. This mutation is weakly protective for AMD, suggesting that loss of ARMS2 protein may be necessary but not sufficient to cause AMD.

Wang et al. (2010) showed that the 3' UTR indel consists of two adjacent indels, 17 base pairs apart. The indel was in strong LD with rs10490924 (D' 0.99). As in previous reports, the indel was strongly associated with AMD ($p=10^{-13}$). However, in this study the stability of the *ARMS2* transcript did not appear to be affected by the indel. Furthermore, the indel was not associated with lower levels of

ARMS2 mRNA in retina or white blood cells. This led to further speculation that A69S is the causal variant at the chromosome 10q26 locus, although the functional consequences remain unknown. Mechanisms by which the proteins encoded by *ARMS2* and *HTRA1* may affect processes leading to AMD are outlined in Section 1.4.

1.2.6 Additional genetic risk factors remain to be found

In addition to the major risk loci in *CFH* and *ARMS2/HTRA1*, other loci which convey smaller risk effects have shown association or linkage with AMD. Such loci include *VEGF*, Fibulin 5, *CST3, CX3CR1*, *TLR4*, *LRP6* and *MMP9* genes (Stone et al. 2004; Tuo et al. 2004; Fiotti et al. 2005; Goverdhan et al. 2005; Zareparsi et al. 2005b; Churchill et al. 2006; Haines et al. 2006). Most of these associations have not been replicated in subsequent (larger) studies. For example, TLR4, and other members of the toll-like receptor family, are unlikely to be involved in AMD susceptibility (Edwards et al. 2008). In the last year, genome-wide association scans performed in highly powered case-control cohorts comprising several thousand individuals have not found association with common variants in these genes. However, these large studies have identified association between AMD and variants in or near *TIMP3*, *COL10A1*, *COL8A1*, *CETP*, *LIPC*, *LDL* and *ABCA1* (Chen et al. 2010; Yu et al. 2011). The proteins encoded by these genes have roles in the ECM (structural or degradation) and in lipid metabolism. Although replication of such associations has proved difficult, these and other unidentified susceptibility loci may play roles in drusen formation, neovascularisation and angiogenesis or in the inflammatory process.

1.3 The Complement Systems

The complement system is part of the innate immune system, providing protection against bacterial infection, clearing inflammatory debris and “complementing” adaptive immunity (Walport 2001). More than 30 plasma and cell surface proteins are involved in the three pathways of Complement (Figure 1.10). Activation of the classical pathway, the alternative pathway and the mannose-binding lectin (MBL)

pathway induces an enzymatic cascade, cleaving C3, and leading to the formation of inflammatory mediators and the membrane attack complex (MAC). These processes result in cell lysis, inflammation and phagocytosis. Under normal conditions, complement pathways are tightly regulated to target invading microorganisms, whilst minimising deposition of complement on normal cells. Dysregulation of the complement pathways can have detrimental effects, as seen in the alternative complement pathway in AMD.

1.3.1 Activation of the alternative complement pathway

The alternative complement pathway is activated in response to bacteria, viruses, fungi and tumour cells. In plasma, C3 is spontaneously cleaved at low levels to form C3b. C3b contains an activated thioester bond which binds to hydroxyl groups on proteins and carbohydrates on target surfaces. This identifies surfaces as foreign, leading to further recruitment of C3b to the surface (Walport 2001, Figure 1.10). When C3b is deposited on the foreign surface, it can bind factor B, forming the C3bB pro-C3 convertase. When Factor B is bound to C3b, Factor D (CFD) binds this complex and cleaves factor B to Bb and Ba. The Ba fragment is released. The Bb fragment remains associated with C3b to form the unstable C3bBb complex (Xu et al. 2001). Properdin stabilises this complex (Walport 2001). This is the C3 convertase of the alternative complement pathway which results in an amplification loop of C3b formation, and deposition on the foreign surface. The C5-convertase (C3bBbC3b) is subsequently formed, triggering formation of the MAC and cell lysis.

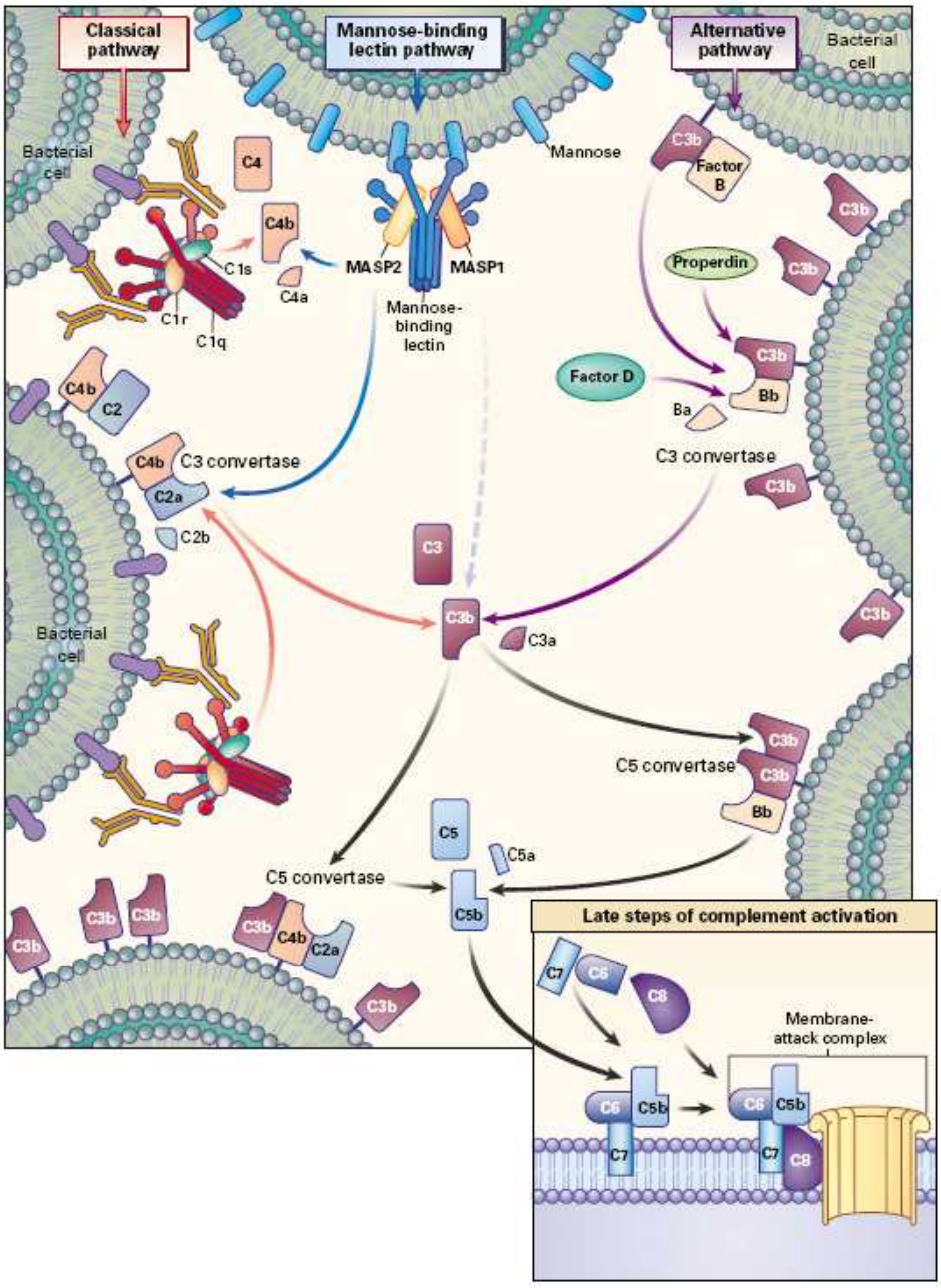

Figure 1.10 The Complement Pathway.

The Complement pathway is part of the innate immune system, and comprises of three pathways. Activation of the classical pathway, the alternative pathway and the mannose-binding lectin (MBL) pathway induces an enzymatic cascade, cleaving C3, and leading to the formation of inflammatory mediators and the membrane attack complex (MAC). Components of the alternative pathway, including Factor H, C3 and Factor B, have been implicated in AMD. Source: Walport (2001).

1.3.2 Regulation of the alternative complement pathway

Dependent on the glycoproteins in the surrounding environment, immobilised C3b may bind to the plasma protein CFH rather than factor B. This is a crucial step in recognition of self, rather than foreign membranes, and in regulating complement activation (Pangburn et al. 2000). Host cell membranes contain polyanions such as sialic acid, which enables CFH to bind C3b with a higher affinity than factor B. Microorganisms do not have polyanions on their surface, and so factor B has higher affinity for C3b (Pangburn et al. 2000). When bound C3b interacts with CFH, C3b is catabolised to inactive products (iC3b and C3f) by factor I. Factor I is a regulatory protease which requires CFH as a co-factor. The cell membrane proteins complement receptor type 1 (CD35), and membrane cofactor protein (CD46) are also involved in decay of C3b (Riley-Vargas et al. 2004). Decay accelerating factor (DAF; CD55) dissociates the convertase complex (Kim and Song 2006).

CFH is the only fluid-phase regulator of the alternative complement pathway, and is vital for the appropriate regulation of the pathway. CFH not only binds and inactivates C3b, but also immobilises complement cascade triggers, including CRP (Rodríguez de Córdoba et al. 2004). Thus, CFH modulates complement activation, dampening the inflammatory response. This reduces chronic inflammation that can cause tissue damage. CFH deficiency leads to MPGN II and hemolytic-uremic syndrome (Levy et al. 1986).

1.3.3 Dysregulation of alternative complement pathway in AMD

The strong genetic association of alternative complement pathway genes, together with the identification of complement proteins in drusen by immunohistochemistry and proteomic approaches, clearly implicates this pathway in disease development. More recent studies have shown that alternative complement pathway components in plasma are also altered, consistent with activation of the pathway in AMD cases (Hakobyan et al. 2008; Scholl et al. 2008; Reynolds et al. 2009; Hecker et al. 2010).

AMD risk-associated coding variants in *CFH* affect protein function. The 402H risk variant appears to influence binding to surfaces containing sialic acid (Herbert et al. 2007; Prosser et al. 2007). The protective CFH 62I variant binds C3b

more strongly than the V variant, and promotes inactivation by factor I (Tortajada et al. 2009). A protective variant in factor B, 32Q, forms the C3 convertase with C3b less efficiently than the wild-type protein, resulting in less activation of complement (Tortajada et al. 2009). The C3b fragment generated from the AMD-risk variant in C3 (102G) binds CFH less strongly than the non-risk 102R form of the protein, decreasing catabolism by factor I and enhancing C3 convertase activity by extending the lifetime of the convertase (Heurich et al. 2011).

The role of non-coding variants, and the deletion of *CFHR1* and *CFHR3*, is less clear, although these are likely to affect gene expression.

1.3.4 Animal models of AMD involving complement and inflammation

Although mice lack a macula, the structure of the retina and function of the RPE cells is highly conserved between mouse and man. The use of mouse models in studying AMD is complicated by the shorter life-span of mice, and the differences in the immune systems of mice and humans. Another complication is that common polymorphisms associated with AMD in humans tend not to result in a complete loss of gene function, such as is studied in knock-out mice. Furthermore, AMD is a multi-factorial disorder, and replicating genetic haplotypes and environmental risk factors is difficult. Despite this, mice have been used to study the role of genetic variants in AMD. A variety of such models have been reported to reproduce pathological features of AMD, implicating inflammation, oxidative stress and lipid metabolism in the disease (Zeiss 2010), although many of these findings are controversial.

1.3.4.1 The *Cfh*$^{-/-}$ mouse

In humans, a total deficiency of CFH causes systemic activation of the alternative complement pathway. This causes MPGN II (Levy et al. 1986). This phenotype is replicated in the *Cfh*$^{-/-}$mouse. These animals have significantly reduced systemic C3 levels, develop glomerulonephritis and die by age of 12 - 15 months (Pickering et al. 2002). Systemic C3 depletion caused by the loss of Cfh can be prevented by introduction of a second mutation in factor B (Pickering et al. 2002). Aged *Cfh*$^{-/-}$

mice (2 years) have been reported to have elevated levels of complement C3 deposition in the photoreceptor layer. This was proposed to contribute to oxidative stress, photoreceptor loss and reduced rod photoreceptor function (Coffey et al. 2007). In contrast to the characteristic Bruch's membrane thickening and drusen observed in human AMD, the *Cfh*$^{-/-}$ mice have reduced Bruch's membrane thickness and reduced sub-RPE deposits, indicating that this is not a true AMD-like phenotype.

1.3.4.2 *C3aR1*$^{-/-}$ and *C5aR1*$^{-/-}$ mice

Anderson et al. (2002) identified the complement pathway activation products of C3 and C5 cleavage (C3a and C5a) in drusen in AMD eyes. These fragments are anaphylatoxins, and promote inflammation, chemotaxis, cytotoxic oxygen radical production and secretion of VEGF. The receptors C3aR and C5aR are crucial to mediating the biological effects of C3a and C5a. Mice deficient in these receptors show a reduction in chemotactic recruitment of leukocytes and lowered *VEGF* expression (Nozaki et al. 2006a). No AMD-like features arise spontaneously in these mice. Following laser-induced injury to the *C3aR1*$^{-/-}$ or *C5aR1*$^{-/-}$ mice, choroidal neovascularisation was reported to be less severe than in wild-type mice. Small molecule antagonists of the receptors or neutralising antibodies against C3a or C5a reproduced the protective effects of genetic ablation of the receptors (Nozaki et al. 2006). Variants in these receptors have not been implicated in altering AMD-risk in humans. Inflammatory processes resulting from complement C3a and C5a deposition in drusen may contribute to AMD progression.

1.3.4.3 Inflammatory cytokine models

Migration of leukocytes during inflammation is directed by cytokines called chemokines. The CXC and CC subfamilies of chemokines (named according to the arrangement of the first two of four conserved cysteine residues) mediate chemotaxis via binding to G protein–coupled receptors (Graves and Jiang 1995).

Macrophages are recruited from the circulation to remove complement components from sites of complement deposition, by the combined action of CCL2 (chemokine, CC motif, ligand 2) and its receptor CCR2.

Macrophages in *Cc12*$^{-/-}$ or *Ccr2*$^{-/-}$ mice show defects in chemotaxis. *Cc12*$^{-/-}$ or *Ccr2*$^{-/-}$mice aged over 16 months have been reported to exhibit pathology similar to that seen in AMD, including deposits in the BM and RPE (containing C3a, C5a and A2E), RPE and photoreceptor atrophy and CNV (Ambati et al. 2003). More recently, the drusen-like deposits reported in *Cc12*$^{-/-}$ mice were shown to be sub-retinal, rather than sub-RPE, and to result from the accelerated, normal age-related accumulation of lipofuscin-containing macrophages (Luhmann et al. 2009).

Leukocytes such as microglia and macrophages possess the G protein–coupled receptor CX3CR1 (chemokine, CX3C motif, receptor 1). Upon binding of the ligand CX3CL1, the receptor mediates adhesion and migration of leukocytes to inflamed tissues. Indeed, CX3CR1-positive cells detected in drusen are microglia (Chan et al. 2008). Variants in *CX3CR1* have been associated with increased susceptibility to AMD (Tuo et al. 2004; Combadière et al. 2007) although replication has not been achieved in larger genome-wide studies (Chen et al. 2010; Yu et al. 2011). Aged *Cx3cr1*$^{-/-}$ mice reportedly show subretinal accumulation of microglia, drusen-like deposits, photoreceptor degeneration and CNV after laser injury (Combadière et al. 2007). However, subretinal accumulation of autofluorescent microglia occurs during normal ageing, and could be confused with drusen-like deposits (Xu et al. 2008).

Double mutant *Cc12*$^{-/-}$/*Cx3cr1*$^{-/-}$ mice have been reported to develop AMD-like pathology, including drusen-like deposits, BM thickening, atrophy of RPE and photoreceptors (Ross et al. 2008). These changes are apparent after only 6 weeks, compared to 16-18 months for the single knock-out animals (Tuo et al. 2007; Chan et al. 2008). However, it seems likely that the drusen-like deposits reported in these animals are subretinal accumulations of autofluoresent macrophages and microglia, rather than drusen. These are unlikely to be informative models of AMD, as these cells accumulate during normal ageing in the eyes of healthy wildtype mice.

1.4 Proposed mechanisms of disease for the candidates on chromosome 10

Understanding the pathogenic mechanisms by which *ARMS2/HTRA1* are involved in AMD development is an ongoing process. As discussed in Section 1.2.5.4, it is not

clear whether variants in *ARMS2* or those in *HTRA1* are responsible for an increased susceptibility to AMD. Due to the strong linkage disequilibrium in this locus on chromosome 10q26, it is not possible to identify the causative variant by allele frequency differences. It is therefore important to understand the functional role played by both proteins, and to investigate whether either protein (or both) contributes to the pathophysiology of AMD.

1.4.1 ARMS2

ARMS2 is a 12 kDa protein of unknown function, containing no known domains, and no sequence homology to other proteins. *ARMS2* is conserved only in higher primates (Kanda et al. 2007), and has proved difficult to study. Both Kanda et al. (2007) and Fritsche et al. (2008) used immunostaining to show that ARMS2 is localised to mitochondria, with intense staining in the photoreceptor layer of the retina. Mitochondrial dysfunction has been implicated in AMD (Barron et al. 2001; Feher et al. 2006; Carelli et al. 2004; Canter et al. 2008). A role for ARMS2 in mitochondrial homeostasis, modulating oxidative stress and apoptosis, was proposed (Fritsche et al. 2008) However, recent work identified ARMS2 as a secreted protein, present at high levels in the choroid (Kortvely et al. 2010). *ARMS2* expression was reported to be restricted to only the placenta and the retina (Jakobsdottir et al. 2005; Fritsche et al. 2008), but ubiquitous expression of *ARMS2* in 18 human tissues screened by RT-PCR has now been reported (Wang et al. 2010b). This merely highlights the current controversy and lack of understanding regarding the true roles of ARMS2 in AMD susceptibility.

1.4.2 HTRA1

HTRA1 is a member of the mammalian HtrA (high temperature requirement A) serine protease family, first identified in *Escherichia coli* as a heat shock protein required for survival at high temperatures (Clausen et al. 2002). Four members of this highly conserved family of peptidases have been described in humans. Each member of the family has a characteristic trypsin-like catalytic domain paired with one or more C-terminal PDZ domains (Hu et al. 1998; Gray et al. 2000; Clausen et

al. 2002; Nie et al. 2003). Additionally, HTRA1 also has an N-terminal secretory signal sequence, an insulin-like growth factor or Mac25 domain, followed by a Kazal-type serine protease inhibitor domain (Zumbrunn and Trueb 1996). PDZ domains mediate protein-protein interactions by binding to 4-6 amino acid motifs, generally found at the C-terminus of target proteins (Hung and Sheng 2002). Peptidase activity of HTRA1 is regulated by ligand binding to the PDZ domain for some substrates (Murwantoko et al. 2004) but not all (Truebestein et al. 2011). Auto-activation of HTRA1 may occur via N-terminal cleavage of the Kazal inhibitory domain (Hu et al. 1998; Chien et al. 2006). The domain structure of HTRA1 is shown in Figure 1.11.

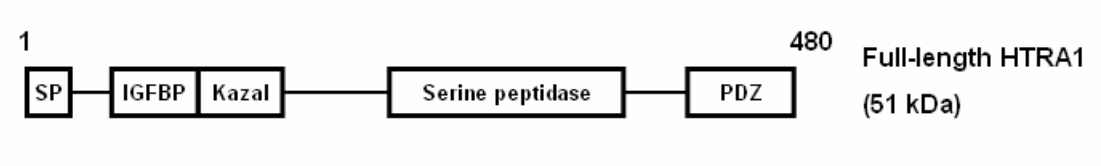

Figure 1.11 Domain structure of HTRA1.
HTRA1 is a member of the highly conserved mammalian HtrA (high temperature requirement A) serine protease family. HTRA1 has an N-terminal secretory signal sequence (SP), an insulin-like growth factor binding domain (IGFBP), a Kazal-type serine protease inhibitor domain (which may be involved in self-regulation), a characteristic trypsin-like catalytic domain and a C-terminal PDZ domain.

1.4.2.1 Expression of HTRA1

HTRA1 is a secreted protein, widely expressed in a range of human tissues (Zumbrunn and Trueb 1996; De Luca et al. 2003). The highest expression levels have been reported in the placenta (particularly during the third trimester), mature layers of epidermis, liver and in kidney tubules (De Luca et al. 2003).

1.4.2.2 Function of HTRA1

Ingenuity pathway analysis performed by Gilicze et al. (2007) found that HTRA1 was involved in two gene networks, one pertaining to genes involved in cell death and cancer, and the other to genes involved in the development and function of bones, muscles and connective tissue.

The ingenuity pathway analysis found that the only genes with a direct relationship to *HTRA1* were Tgf-βI (transforming growth factor- β) and Bmp4 (bone morphogenetic protein 4), a member of the TGF-β family (Gilicze et al. 2007). TGF-β is a known regulator of extracellular matrix deposition and angiogenesis; cellular activities that are disrupted by AMD. Oka et al. (2004) previously reported that HTRA1 was able to inhibit TGF-β signalling, acting to regulate the availability of insulin-like growth factors (IGFs) by cleaving IGF-binding proteins. HTRA1 can also directly cleave pro-TGF-β, limiting the amount of mature TGF-β available under normal conditions (Shiga et al. 2011).

Negative regulation of BMP signalling has also been attributed to HTRA1 (Oka et al. 2004). Further evidence as to the inhibition of signalling pathways by HTRA1 was provided by Canfield et al. (2007), who found BMP-2 induced matrix mineralisation was inhibited by overexpression of HTRA1.

Although some interacting partners of HTRA1 have been reported, the HTRA1 interactome, and range of substrates for this serine protease, are not well characterised. In terms of ECM components, collagens have been identified as binding partners of HTRA1 using a combination of approaches. A yeast two-hybrid screen performed using the PDZ domain of mouse HTRA1 (96% identical to human HTRA1) identified interactions with C-propeptides of fibrillar collagens (Murwantoko et al. 2004). HTRA1 was also shown to interact with collagen fibres in the extracellular matrix in a study of HTRA1 expression in the placenta (De Luca et al. 2004). On the basis of HTRA1 distribution in both the extracellular space and the cytosol, De Luca et al. (2004) speculated that HTRA1 may act on intracellular growth factors or extracellular matrix proteins, depending on the precise sub-cellular location of HTRA1. *In vitro*, HTRA1 can also degrade matrix proteins, including matrix Gla protein and decorin, and inhibits signalling to regulate physiological and pathological matrix mineralisation (Canfield et al. 2007).

Using quantitative proteomics, An et al. (2010) recently identified additional substrates for HTRA1 in the RPE secretome. These substrates - clusterin, vitronectin, and fibromodulin; proteins involved in complement regulation - may be of particular relevance to AMD pathogenesis if HTRA1 does play a role in development of this disease.

1.4.2.3 HTRA1 in diseases other than AMD

HTRA1 is down-regulated in ovarian cancer and melanoma (Baldi et al. 2002; Chien et al. 2004), and may act as a tumour suppressor by promoting serine-protease-mediated cell death. This is supported by the observation that over-expression of HTRA1 inhibits cell growth and proliferation *in vitro* (Baldi et al. 2002). Recently, over-expression of HTRA1 has been suggested to play a role in survival in mesothelioma patients (Baldi et al. 2008).

Expression of HTRA1 is also up-regulated in osteoarthritis and in skeletal muscle in Duchenne muscular dystrophy, conditions in which degradation of the ECM may be important (Bakay et al. 2002; Grau et al. 2006). Proteomic investigation of cartilage tissue extracts identified aggregan as a substrate for HTRA1 (Chamberland et al. 2009). Aggrecan is the major structural proteoglycan of cartilage. Aggregan fragments produced by HTRA1 activity were significantly more abundant in cartilage from osteoarthritic joints than in healthy joints, implicating HTRA1 in cartilage degeneration in this disease.

Down-regulation of *HTRA1* has been reported in the hippocampal region of brains affected by Alzheimer's disease, relative to disease-free controls (Li et al. 2003). Association studies have not shown a significant contribution of variants in *HTRA1* to risk of Alzheimer's disease (Li et al. 2003; Ozturk et al. 2005). However, the protease can degrade amyloid-β *in vitro* (Grau et al. 2005). This is a major constituent of amyloid plaques, the pathological hallmark of Alzheimer's disease. HTRA1 also co-localises with amyloid plaques in the brain (Grau et al. 2005).

CARASIL (cerebral autosomal recessive arteriopathy with subcortical infarcts and leukoencephalopathy) is an autosomal recessive disorder caused by mutations in *HTRA1* (Hara et al. 2009). CARASIL is characterised by ischemic, non-hypertensive, cerebral small-vessel disease with associated alopecia and spinal osteoarthritis (Fukutake and Hirayama 1995). Arteriosclerosis appears to result from intimal thickening in the cerebral small vessels by deposition of dense collagen fibres (Hara et al. 2009). Non-sense and mis-sense mutations in *HTRA1* identified in CARASIL patients reduce activity of the protease, leading to uncontrolled TGF-β

signalling (Hara et al. 2009; Shiga et al. 2011). TGF-β signalling plays a variety of roles in angiogenesis and vascular remodelling (reviewed by (ten Dijke and Arthur 2007)).

1.4.2.4 HTRA1 in AMD

HTRA1 is expressed in human RPE, and the HTRA1 protein has been detected in drusen in the eyes of AMD-affected individuals (Figure 1.12; Dewan et al. 2006; Yang et al. 2006). Although the role of HTRA1 in AMD pathogenesis is not yet known, a combination of effects may contribute to disease. HTRA1 binds and degrades components of the ECM (Murwantoko et al. 2004; Grau et al. 2006; Canfield et al. 2007), as well as complement regulators (An et al. 2010). HTRA1 negatively regulates TGF-β signalling (Shiga et al. 2011); this may have implications in extracellular matrix deposition, neuronal survival (Launay et al. 2008) and angiogenesis. Yang et al. (2006) suggest that HTRA1 overexpression could promote the growth of choroidal capillaries across the extracellular matrix of Bruch's membrane leading to CNV, although this does not seem to occur spontaneously in mice over-expressing HTRA1 in the RPE (Vierkotten et al. 2011).

HTRA1 may be involved in neovascularisation, in wound healing following chronic inflammation and in remodelling the Bruch's membrane. However, much work remains to be done before the biological significance of HTRA1 activity in normal and disease states can be fully understood.

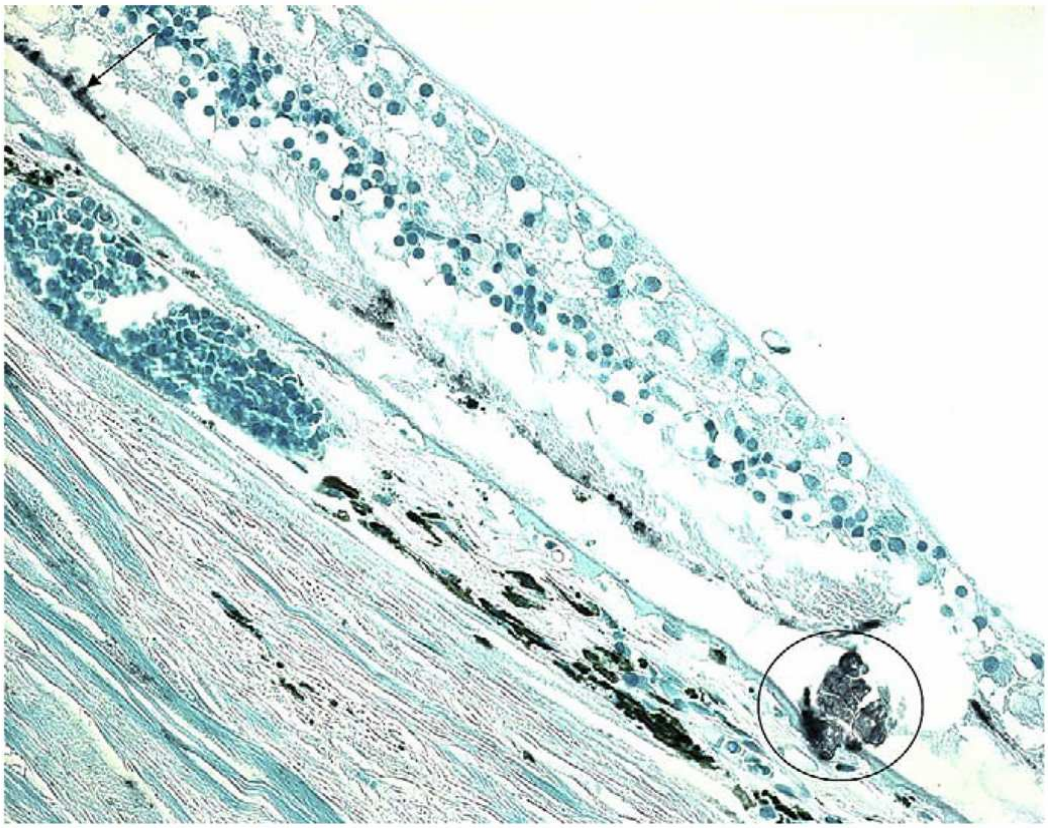

Figure 1.12 HTRA1 expression in the AMD eye.
HTRA1 is expressed by RPE cells and has been detected in drusen. This is shown by HTRA1 immunoreactivity in the AMD lesion (circle) and in residual RPE cells (arrow; top left corner) from a human eye (Ding et al. 2009).

1.5.4 Animal models of *HTRA1* and *ARMS2*

There is considerable debate about whether *ARMS2* or *HTRA1* is the AMD-susceptibility gene located on chromosome 10q26. To date, there have been no published reports of mouse models of *HTRA1* over-expression to recreate the proposed functional consequence of the risk haplotype on human chromosome 10. *ARMS2* is conserved only in higher primates, which may correlate with development of the macula (Kanda et al. 2007). Thus, rhesus macaques have been used to study the contribution of *HTRA1* and *ARMS2* to macular degeneration. A rhesus homologue of the chromosome 10q26 AMD-susceptibility locus contains *ARMS2* and *HTRA1* (Francis et al. 2008). As in humans, both proteins are expressed in the retina and RPE of macaques. A promoter polymorphism in *HTRA1* which was associated with macular degeneration in these animals resulted in over-expression of *HTRA1* in *in vitro* studies (Francis et al. 2008). A second study on independent research colonies of macaques found similar association between the *HTRA1* promoter polymorphism and macular degeneration, and no association with *ARMS2* (Singh et al. 2009).

1.6 Aims of the study

The aims of this study were to determine whether HTRA1 is likely to play a role in AMD pathogenesis, by:

- Identifying interacting partners of HTRA1, using yeast two-hybrid screening and tandem affinity purification.

- Studying candidate interactors of HTRA1 which may be relevant to AMD, using genetic and molecular approaches.

- Validating and characterising the roles of interactions involving HTRA1 in AMD development and progression using biochemical approaches.

2: Chapter 2

Materials and Methods

2.1 Introduction

This chapter describes the experimental methods and statistical approaches used to generate the data that are subsequently presented. Unless otherwise noted, consumables were obtained from HGU Technical Services.

2.2 Cell culture procedures

Human cell culture lines HEK293T, hTERT-RPE1 and THP-1, bacterial cells and yeast cells were used. Procedures for culturing and manipulating cells are described.

2.2.1 Mammalian cells

2.2.1.1 Standard culture conditions for mammalian cells

Mammalian cell cultures were maintained at 37°C in 5% CO_2. HEK293T cells were grown in Dulbecco's modified Eagle's medium (DMEM; Gibco) supplemented with 10% fetal calf serum (FCS) and penicillin/ streptomycin. hTERT-RPE1 (RPE1) cells were grown in Dulbecco's Modified Eagle Medium: Nutrient Mixture F-12 (DMEM/F-12; Gibco) containing 15 mM HEPES, 2 mM L-Glutamine and 0.348% sodium bicarbonate (Gibco), 10% FCS and 100 μg/ml streptomycin, 100 U/ml penicillin. THP-1 cells were grown as a suspension culture in RPMI 1640 (Gibco) supplemented with 2 mM GlutaMAX, 10 mM HEPES (Gibco), 1 mM sodium pyruvate (Gibco), 4.5 g/l glucose, 100 μg/ml streptomycin, 100 U/ml penicillin, 0.05 mM 2-mercaptoethanol (Sigma) and 10% FCS.

THP-1 cells were passaged when cell density reached between 6-8x10^5 cells/ml, by diluting 1 in 10 in fresh media. RPE1 and HEK293T cells were passaged at 70-90% confluence. A 25 cm^2 tissue culture flask of cells was washed twice with phosphate buffered saline (PBS; 3.2 mM Na_2HPO_4, 0.5 mM KH_2PO_4, 1.3 mM KCl, 135 mM NaCl, pH 7.4), and then 2.5 ml of a 1:1 mix of trypsin (2 g/l trypsin in PBS, 0.2% Phenol Red) and versene (0.4 g/l EDTA in PBS, 0.2% Phenol Red) was added. The flask was incubated at 37°C for 2-3 minutes or until the cells detached. 7.5 ml of culture media was added to neutralise the trypsin. When appropriate, cells were counted using a haemocytometer. Cells were seeded as a 1 in 10 dilution in a new

tissue culture flask with the appropriate volume of media. Volumes were adjusted for flask/plate size.

All cell cultures were negative for mycoplasma infection (tested by HGU Technical Services).

2.2.1.2 Transfection of mammalian cells

HEK293T and RPE1 cells were transfected using microporation performed using an MP-100 machine (Digital Bio). At 70-90% confluency, HEK293T cells were transfected with pDEST *HTRA1*-CTAP or pDEST EV-CTAP. 5.6 x 10^6 cells were mixed with 5 µg of the appropriate construct. Microporation was performed using the MP-100 (Digital Bio) with 100 µl tips and Buffer E2 electrode buffer. Microporation parameters were 1300 V/ 10 ms/ 3 pulses. For each construct, ten 14 cm plates were seeded with 2 microporation reactions (~10x 10^6 cells, 10 µg DNA) in 10 ml of DMEM supplemented with 10% FCS, without antibiotics, and grown at 37°C for 48 hours. Transformation efficiency and cell viability were initially confirmed by fluorescence microscopy 12 hours following transfection of HEK293T cells with pEGFP DNA.

Optimal electric field, pulse width and pulse number for effective transfection of RPE1 cells were determined using a procedure supplied by the manufacturer (Digital Bio). RPE1 cells were grown to 70-90% confluency and harvested by trypsinisation. 2.4 x 10^5 cells were centrifuged at 1200 rpm for 3 minutes, washed in PBS and then resuspended in 288 µl Buffer R (Digital Bio). For each microporation reaction, 0.5 µg of pmaxGFP DNA (Amaxa) was added. Microporation was performed using the MP-100 with 10 µl tips and Buffer E electrode buffer. Microporation parameters are shown in Table 2.1.

Following microporation, each reaction was seeded in a well of a 24-well plate. Each well contained 500 µl of antibiotic-free media. The plate was incubated at 37°C for 24 hours. Fluorescence and light microscopy was used to determine the optimal parameters for microporation by assessment of cell viability in relation to untransfected RPE1 cells, and by assessment of transfection efficiency by observation of GFP-positive cells. Subsequently, the three optimal protocols were

scaled up for use with 14 cm plates. 5.6 x 10^6 cells were mixed with 5 µg of the pmaxGFP construct and microporation performed using the MP-100 with 100 µl tips and Buffer E2 electrode buffer. Microporation parameters tested were: 1400 Volts/ 20 ms/ 1 pulse, 1500 Volts/ 20 ms/ 1 pulse and 1600 Volts/ 20 ms/ 1 pulse. For each condition tested, a 14 cm plate was seeded with 2 microporation reactions (~10x 10^6 cells, 10 µg DNA) in 10 ml of antibiotic-free media. Transfection efficiency and cell viability were assessed as described previously. Optimised parameters (1500 Volts/ 20 ms/ 1 pulse) were used for transfection of RPE1 cells with pDEST *HTRA1*-CTAP or pDEST EV-CTAP.

	Microporation parameters		
Well	**Pulse voltage**	**Pulse width**	**Pulse number**
1	Control without microporation		
2	1400	20	1
3	1500	20	1
4	1600	20	1
5	1700	20	1
6	1100	30	1
7	1200	30	1
8	1300	30	1
9	1400	30	1
10	1000	40	1
11	1100	40	1
12	1200	40	1
13	1100	20	2
14	1200	20	2
15	1300	20	2
16	1400	20	2
17	900	30	2
18	1000	30	2
19	1100	30	2
20	1200	30	2
21	1300	10	3
22	1400	10	3
23	1500	10	3
24	1600	10	3

Table 2.1 Microporation parameters tested during optimisation of transfection of RPE1 cells.

2.2.1.3 Treating RPE1 cells to induce stress

2.2.1.3.1 Cell viability assay

The cytotoxic effects of a range of concentrations of H_2O_2 (250-2,000 µM; Sigma) or LPS (1.25-80 µg/ml; Sigma) upon RPE1 cells in culture was assessed. 8,000 RPE1 cells/well were seeded in a 96-well plate in standard culture media. After 24 hours, media was removed and the cells washed in PBS. Serum-free media containing H_2O_2 (250-2,000 µM) or LPS (1.25-80 µg/ml) was added, the cells were grown for a further 24 hours and the media removed. Cell viability was quantified using an MTT assay. 100 µl of 5 mg/ml MTT (3-(4,5-Dimethylthiazol-2-yl)-2,5-diphenyltetrazolium bromide; Sigma) in PBS was added to each well, and incubated at 37°C for 4 hours. The MTT solution was removed and replaced with an equal volume of MTT Solvent (4 mM HCl (Fisher), 0.1% Nondet P-40 (NP40; ICN Biomedicals) in isopropanol (Fisher)). The plate was wrapped in foil, and incubated at room temperature on an orbital shaker for 15 minutes. Absorbance was measured at 590 nm with a reference filter of 620 nm (Multiskan Spectrum, Thermo Electron). All assay points were determined in triplicate and all experiments were repeated three times. Cell viability was calculated relative to untreated cells, and corrected for background in the absence of cells in the well.

2.2.1.3.2 Optimised assay for non-cytotoxic stress in RPE1

RPE1 cells were cultured in 6-well plates ($0.5x10^6$ cells/well) for 24 hours until confluent. Media was removed and replaced with 250 µM H_2O_2 or 10 µg/ml LPS in serum-free media for 24 hours. Conditioned media was collected and used to measure CFD by ELISA. Cells were lysed and RNA extracted.

2.2.1.4 Differentiation of THP-1 cells

Monocyte THP-1 cells were induced to differentiate into macrophage-like adherent cells by addition of 200 nM PMA (phorbol myristate acetate; Sigma) in DMSO (Sigma) for 72 hours. Morphological changes were apparent under light microscopy (Leica DM1L). After 4 days in culture in serum-free media, conditioned media was

collected and protein measured by Bradford assay for analysis by Western blotting. Cells were lysed and RNA extracted using the RNeasy Kit (Qiagen).

2.2.2 Bacterial cells

2.2.2.1 Standard culture conditions for bacterial cells

Escherichia coli cultures were used to produce recombinant human proteins and for propagation of plasmids. *E. coli* cultures were incubated at 37°C, either on Luria-Bertani (LB) agar plates supplemented with the appropriate antibiotic, or in liquid culture in LB rotated at 225 rpm. LB was supplied by HGU Technical Services. Bacterial clones were obtained from Invitrogen (CFD Ultimate ORF) or made by transfection of *E. coli* with DNA constructs made in the lab or provided as gifts. Glycerol stocks of all bacterial cultures were stored at -80°C. Expression constructs and their antibiotic resistance are shown in Table 2.2.

2.2.2.2 Plasmid amplification in *E. coli*

50 µl of freshly thawed *E. coli* TOP10 cells (Invitrogen) were mixed with 1µl of plasmid and incubated on ice for 30 minutes. Cells were heat-shocked at 42ºC for 30 seconds, then placed on ice for 2 minutes. 250µl Super Optimal broth with Catabolite repression (SOC) medium (Invitrogen) was added before incubation at 37ºC with shaking for 1 hour. 50-200 µl of the cell suspension were spread on LB-agar plates containing 100 µg/ml ampicillin (provided by HGU technical services) or 50 µg/ml kanamycin, as appropriate (Table 2.2). Plates were incubated overnight at 37ºC. Individual colonies were amplified overnight at 37ºC in 5 ml LB under antibiotic selection. Cell pellets were collected by centrifugation at 2500 rpm for 10 minutes.

Plasmid DNA was purified from the cell pellets using the QIAprep Spin Miniprep Kit (Qiagen), following the manufacturer's instructions and supplied buffers. Centrifugation steps were performed using a bench-top microcentrifuge (Thermo Scientific). The cell pellet was resuspended in 250 µl Buffer P1 plus RNase A and mixed with 250 µl Buffer P2 by inversion. 350 µl Buffer N3 was added. After mixing by repeated inversion, the mixture was centrifuged at 13,000 rpm for 10

minutes. The supernatant was spun through a QIAprep spin column. The column was washed with 0.5 ml Buffer PB and then with 0.75 ml Buffer PE. After the second wash, an additional centrifugation step removed any residual wash buffer. Centrifugation was performed at 13,000 rpm for 60 seconds. The flow-through was discarded after each spin. Plasmid DNA was eluted from the column in 30 µl dH_2O or in TE Buffer (10 mM Tris-Cl, 1 mM EDTA, pH 7.5).

2.2.2.3 Protein expression in *E. coli*

100 µl of *E.coli* BL21 (DE3) pLysS cells (Stratagene) were transformed with 0.5 µl of one of the expression vectors shown in Table 2.2. Cells were transformation by incubating the bacteria and DNA on ice for 30 minutes, followed by 45 seconds at 42°C and 2 minutes on ice. Transformed bacteria were grown in SOC media and plated on LB agar as described in Section 2.1.2.2. Individual colonies were used to make glycerol stocks, and to inoculate 10 ml overnight starter cultures. The following day, 400ml of LB medium containing 100 µg/µl ampicillin and 34 µg/µl chloramphenicol was inoculated with the starter culture and grown at 37^{o}C until the OD_{600} reached 0.6–0.8 (UV1101 Biotech Photometer, WPA). 1 mM isopropyl β-D thiogalactoside (IPTG) was added to induce protein production. After incubation at 25°C for 4 hours, the cells were harvested by centrifugation at 4,000 x *g* for 20 minutes and frozen at -20°C prior to protein purification.

2.2.3 Yeast cells

2.2.3.1 Yeast two-hybrid screening for HTRA1-binding proteins

A GAL4-based yeast two-hybrid system (Matchmaker, Clontech) was used to screen a human oligo-dT primed placental cDNA library (in pAD_GAL4_2.1/DEST vector) for proteins interacting with HTRA1 in PJ69-4α yeast cells. Full-length *HTRA1* was fused to the DNA binding domain in the pYes-Dest52 vector to create a bait plasmid, which was transformed into PJ69-4A yeast cells using the lithium acetate procedure (Becker and Lundblad, 1994). Cell-to-cell mating of PJ69-4α cells, containing the bait plasmid, with the mating library, containing human oligo-dT primed placental

cDNA fused to an activation domain, was >5% efficient. Transformation and cell-to-cell mating was performed by Dr. Elod Kortvely. Resultant diploid cells were cultured on selection plates lacking tryptophan, leucine, histidine and adenine (-WLHA) at 30°C. Yeast capable of growing on selective medium were positive clones.

Plasmid DNA was extracted from positive clones following culture for 2 days at 30°C in 2ml of SD-tryptophan-leucine (SD-WL) media supplemented with 1% glucose, to select for the pAD_GAL4_2.1/DEST prey plasmid. Yeast cells were pelleted by centrifugation at 3,000 x *g* for 5 minutes, and resuspended in 250 µl of Buffer A1 (Macherey-Nagel) supplemented with 570 µg/ml Lyticase (Sigma) and 400 µg/ml RNAse I (Macherey-Nagel). Cell lysis was achieved by incubation at 37°C for 2 hours with vigorous shaking. Plasmid DNA was purified using the NucleoSpin Multi-96 Plus Plasmid kit (Macherey-Nagel) and used to transform *E. coli* DH5α cells. Bacterial cells were plated on L-AMP plates using glass beads, and grown at 37°C overnight. Plasmid DNA was purified as described previously using the NucleoSpin Multi-96 Plus Plasmid kit (Macherey-Nagel) and processed for DNA sequencing using the primer pACT2_7848F, which anneals to the GAL4 activation domain sequence within the pACT2-AD vector backbone.

Table 2.2 Details of DNA constructs used.

DNA Construct Name	Vector Backbone	Insert	Tag	Expression	Bacterial resistance
pDEST HTRA1 CTAP	pDEST CTAP	full-length HTRA1 (amino acids 1-480)	C-terminal Strep-Strep-FLAG	Mammalian	Ampicillin
pDEST EV	pDEST CTAP	No insert	C-terminal Strep-Strep-FLAG	Mammalian	Ampicillin
pmaxGFP	pmax	No insert	GFP	Mammalian	Kanamycin
CFD Ultimate ORF	pDONR221	full-length preproCFD (amino acids 1-253)	-	-	Kanamycin
pENTR proCFD	pDONR221	proCFD (amino acids 21-253)	-	-	Kanamycin
pENTR ΔN HTRA1	pDONR221	ΔN HTRA1 (amino acids 157-480)	-	-	Kanamycin
pENTR HTRA1 ΔC	pDONR221	ΔC HTRA1 (amino acids 21-160)	-	-	Kanamycin
pENTR CTGF	pDONR221	full-length CTGF	-	-	Kanamycin
GST ΔN HTRA1	pDEST15	ΔN HTRA1 (amino acids 157-480)	N-terminal GST	Bacterial	Ampicillin
GST ΔN HTRA1 S328A	pDEST15	ΔN HTRA1 (amino acids 157-480)	N-terminal GST	Bacterial	Ampicillin
His_6 ΔN HTRA1	pDEST17	ΔN HTRA1 (amino acids 157-480)	N-terminal His_6	Bacterial	Ampicillin
GST HTRA1 ΔC	pDEST15	ΔC HTRA1 (amino acids 21-160)	N-terminal GST	Bacterial	Ampicillin
GST CTGF	pDEST15	full-length CTGF	N-terminal GST	Bacterial	Ampicillin
GST	pGEX 6-P-1	No insert	N-terminal GST	Bacterial	Ampicillin
GST-cleavable-proCFD	pGEX6P1-DEST (Gateway-modified)	proCFD (amino acids 21-253)	N-terminal cleavable GST	Bacterial	Ampicillin
pACT2 AD_GAL4_2.1/DEST	pACT2 (Gateway-modified)	placental cDNA library	GAL4-activation domain fusion	S. cerevisiae	Ampicillin
pDBD DEST HTRA1	pYes-Dest52	full-length HTRA1 (amino acids 1-480)	GAL4-DNA binding domain fusion	S. cerevisiae	Ampicillin

2.3 DNA and RNA procedures

2.3.1 Agarose gel electrophoresis

Agarose gel electrophoresis was used to separate and purify DNA. Agarose gels were made with 1% or 2% agarose, depending on the size of DNA being resolved. To make a 1% agarose gel, 1 g agarose (biogene) was added to 100 ml 0.5x TBE buffer (1 litre of 20x stock: 216 g Tris base, 110 g boric acid, 18.6 g EDTA, dH_2O) and heated until boiling to dissolve the agarose. 0.2 mg/ml ethidium bromide (VWR International) was added when the liquid had cooled to approximately 60°C. The agarose solution was allowed to set in a gel tray for at least 1 hour, prior to immersion in 0.5x TBE buffer and loading of the DNA samples. DNA samples were mixed with 6x loading buffer (Promega) before loading. Gels were run at 150 Volts. DNA size markers were used in combination: 100 bp ladder (Promega), 1 kb ladder (Promega), DNA marker III (Roche).

2.3.2 Gel purification

The QIAquick PCR Purification Kit (Qiagen) was used to purify DNA from agarose gel slices, following the manufacturer's instructions and supplied buffers. 3 volumes of buffer PB was added to 1 volume of gel slice containing DNA in an eppendorf tube. The gel was dissolved by incubating at 50°C for 10 minutes, and then added to the QIAquick column. After centrifugation for 1 minute, the column was washed with 0.5 ml Buffer QG and then with 0.75 ml Buffer PE. After each wash, the column was centrifuged at 13,000 rpm for 60 seconds. After the second wash, an additional 60 second spin removed any residual wash buffer. The flow through was discarded after each spin. Plasmid DNA was eluted from the column in 30 µl dH_2O.

2.3.3 DNA constructs

Gateway cloning technology (Invitrogen) was used to generate vectors for the expression of HTRA1 and interacting proteins in *E.coli*. Sequences encoding HTRA1 and CTGF were amplified by PCR from human retinal Marathon-Ready cDNA (BD Biosciences) using gene-specific *att*B PCR primers (Table 2.3). The

proCFD sequence was amplified using the CFD Ultimate ORF (Invitrogen) as the template for amplification. Constructs for the expression of CTAP-HTRA1 and the empty vector in mammalian cells were generated previously, using vectors provided by Dr. Johannes Gloeckner.

2.3.3.1 PCR amplification of attB-flanked gene-specific sequences

A 50 µl PCR mixture contained 1 µl cDNA, 1x Phusion HF buffer (1.5 mM $MgCl_2$), 0.2 mM dNTPs, 0.5 µM each of forward and reverse primers, 0-10% DMSO and 1 U of Phusion High Fidelity DNA polymerase (Finnzymes). Samples were denatured at 98°C for 30 seconds, and then subjected to 35 cycles of 98°C for 10 seconds, annealing at 54°C for 30 seconds, extension at 72°C for 45 seconds, followed by a final extension cycle of 72°C for 10 minutes. Annealing temperature, extension time and % DMSO for specific primer pairs is shown in Table 2.3. Following successful amplification, the PCR product was purified from a 1% TBE Agarose gel using the QIAquick gel extraction kit (Qiagen) to remove *att*B primers and primer-dimers.

2.3.3.2 Gateway BP recombination

The gene-specific *att*B-flanked PCR products were used in Gateway BP recombination reactions. 150 ng of *att*P containing donor vector (pDONR221) was incubated at 25°C for 4 hours with the PCR product and 2 µl of BP Clonase (Invitrogen) in TE Buffer, pH 8. 1 µl of Proteinase K (Invitrogen) was added and the reaction incubated at 37°C for 10 minutes to terminate the reaction. The BP recombination reaction mix was used to transform chemically competent TOP10 *E. coli* (Invitrogen) The transformed cells were grown overnight at 37°C on L-KAN (50 µg/ml) agar plates to select for entry clones containing the kanamycin resistance gene encoded by pDONR221 vector. The presence of the insert in the entry vector was verified by PCR, using primers and thermocycling conditions shown in Table 2.3. Clones containing the appropriate insert were used to propagate the plasmid, which was then quantified using the ND-1000 Spectrophotometer (NanoDrop). The inserts were sequenced using M13 primers and gene-specific primers (Table 2.3).

2.3.3.3 Gateway LR recombination

*Att*L-containing entry clones were used in Gateway LR recombination reactions. The destination vectors used are shown in Table 2.2. 150 ng of destination vector was added to 150 ng of entry clone and incubated with LR Clonase II (Invitrogen) at 25°C for 1 hour. The reaction was stopped by adding Proteinase K, and used to transform TOP10 *E. coli*. Clones were selected on L-AMP plates (100 µg/ml ampicillin), and the insert verified by PCR. Restriction digests were used to confirm the insert into the vector. Appropriate restriction enzymes were identified using NEBCutter2 (tools.neb.com/NEBcutter2/). Digests were performed at overnight at 37°C using 1 U of ApaI or MluI, in specific buffers supplied with the enzymes (NEB).

2.3.3.4 Site-directed mutagenesis of DNA constructs

The active site serine residue of HTRA1 was mutated to an alanine residue (S328A), using the QuikChange Site-Directed Mutagenesis kit (Stratagene) and HPLC-purified primers containing the mutated residue:

HTRA1_S328A	5'-ccatcatcaactatggaaacgcgggaggcccgttag-3'
HTRA1_S328A_antisense	5'-ctaacgggcctcccgcgtttccatagttgatgatgg-3'

The site-directed mutagenesis of the GST ΔN HTRA1 expression construct was performed by Dr. Elod Kortvely, following the manufacturer's instructions. Samples were denatured at 95°C for 30 seconds, and then subjected to 12 cycles of 95°C for 30 seconds, annealing at 55°C for 1 minute and extension at 68°C for 14 minutes. The plasmid template was digested by 10 U DpnI at 37°C for 1 hour. 50 µl of XL1-Blue supercompetent *E.coli* cells were transformed with 1 µl of DNA, and subsequently grown on L-AMP plates overnight at 37°C. 5 ml overnight culture was established from 5 separate colonies and used for to amplify the plasmid, which were subsequently purified using the QIAprep Spin Miniprep Kit (Qiagen). The mutation was verified by sequencing using HTRA1-specific primers (Table 2.3).

		PCR conditions				
Primer Name	**5' - 3' sequence**	**Amplicon size (bp)**	**% DMSO**	**Annealing temperature ^{o}C**	**Extension time**	**Polymerase**
	attB-flanked cloning primers					
ΔSS_CFD_Gateway_F	GGGGACAAGTTTGTACAAAAAAGCAGGCT TCACCATGCCGCCCCGTGGTCGGATCC	800	10	54	45 seconds	Phusion
CFD_Gateway_R	GGGGACCACTTTGTACAAGAAAGCTGGGT CCTAGGCCAGGACGCTGCTGAT					
CTGF_Gateway_F	GGGGACAAGTTTGTACAAAAAAGCAGGCT TCACCATGACCGCCGCCAGTATG	1100	10	54	45 seconds	Phusion
CTGF_Gateway_R	GGGGACCACTTTGTACAAGAAAGCTGGGT CTCATGCCATGTCTCCGTACAT					
SP-HtrA1_F	GGGGACAAGTTTGTACAAAAAAGCAGGCT CCGAGAGGCTGCACCGGCCG	500	10	54	45 seconds	Phusion
IGFBP_HTRA1_R	GGGGACCACTTTGTACAAGAAAGCTGGGT CCTAGCACACACAGAGGCCGGC					
	ARMS2 3' UTR indel genotyping primers					
ARMS2 indel F ARMS2 indel R	TGTCACTGCATTCCCTCCTGTCAT AAGCTTCTTACCCTGACTTCCAGC	200/600	10	58	60 seconds	Platinum Taq
	CFD resequencing primers					
CFD-ex1-F CFD-ex1-R	CGACTCTGGTGTGAGTCTGG TTTCAGCGTTCAGAGCCTTC	383	5	59	60 seconds	Platinum Taq
CFD-ex2-F CFD-ex2-R	AGAGCTGGGATCCCGTCAG GCCCAGGAGAACCTGCAC	353	10	67	60 seconds	Platinum Taq
CFD-ex3-F CFD-ex3-R	CTGGAGGACGCGTGAGTG GTGAGGGTGTGGGGGTTG	387	10	65	60 seconds	Platinum Taq
CFD-ex4-F CFD-ex4-R	AGCCTAGCGGCATTCTCC CTGGGCCCTGTTCCTACTTG	425	10	57	60 seconds	ReddyMix
CFD-ex5-F CFD-ex5-R	ATTAACACGGGAGGGATGAG CCATGCTGATCTCGAACTCC	431	10	62	60 seconds	ReddyMix

RT-PCR primers						
C3_RT-PCR_For	aagtcccggacaccgagt	67	0	55	20 seconds	Platinum Taq
C3_RT-PCR_Rev	Tctgtcatctgggccactg					
CFD_RT-PCR_For	tccaagcgcctgtacgac	106	0	55	20 seconds	Platinum Taq
CFD_RT-PCR_Rev	Gtgtggccttctccgaca					
GAPDH_RT-PCR_F2	agccacatcgctcagacac	66	0	59	20 seconds	Platinum Taq
GAPDH_RT-PCR_R2	gcccaatacgaccaaatcc					
HTRA1_RT-PCR_F2	agtcccatgaccgacagg	74	0	59	20 seconds	Platinum Taq
HTRA1_RT-PCR_R2	gagtgacatcattcggatacca					
MASP1_RT-PCR_For	Ttgctcagcccttctgactt	74	0	55	20 seconds	Platinum Taq
MASP1_RT-PCR_Rev	tgctgttcattttcatctgacc					
Sequencing primers						
CFD_Seq_F	gctacagctgtcggagaagg					
CFD_Seq_R	cagcactggcaagagcac					
CTGF_Seq_F1	Gtgagcctcgtgctggac					
CTGF_Seq_R1	acgtgcactggtacttgcag					
CTGF_Seq_F2	gttccaagacctgtgggatg					
CTGF_Seq_R2	tggagattttgggagtacgg					
HTRA1 IntF	CAAGGGCAGGAAGATCCCAA					
HTRA1 IntR	AGTTGCGGAGCCCCAGCTCT					
Htra1 IntF2	Gctcttctcccgctgctg					
Htra1 IntR2	ggaagcttgcgaaacaattc					
Htra1 IntF3	ccgttttcccttcaaaacac					
Htra1 IntR3	acgtcgttttccttgagacc					
Htra1 IntF4	caaagccaaagagctgaagg					
M13 F	CACGACGTTGTAAAACGAC					
M13 R	GGATAACAATTTCACACAGG					
pACT2_7848F	CTATCTATTCGATGATGAAG					

Table 2.3 Primers and PCR conditions.

2.3.4 DNA Sequencing

Plasmid DNA and PCR products were sequenced in both directions using primers shown in Table 2.3. DNA sequencing was performed by HGU Technical Services using BigDye Terminator Cycle Sequencing on an ABI PRISM 3100 (Applied Biosystems). Sequence fidelity was confirmed using Sequencher (Gene Code) for analysis. Variants in *CFD* were identified using Mutation Surveyor (Soft Genetics).

2.3.5 Cases and controls for genetic association analysis

DNA samples were obtained from six cohorts and were genotyped to test for an association between AMD-susceptibility and variants in *CFD*. The characteristics and demographic information for the AMD case-control series used in this study are shown in the results in Chapter 4, Table 4.2. AMD cases were graded using the Clinical Age-Related Maculopathy Grading System (Bird et al. 1995). Controls were examined and free from AMD. All individuals were reported as Caucasian. Blood samples were collected at ophthalmic clinics, and genomic DNA isolated from peripheral blood leukocytes. Written consent from the individuals and appropriate ethical approval were obtained prior to the study.

2.3.6 SNP Genotyping

2.3.6.1 TaqMan 5' nuclease assay

SNPs in *CFD* were genotyped in the UK1, UK2 and Nijmegen cohorts using TaqMan genotyping technologies (Applied Biosystems). Genotyping assays for rs3826945, rs1683563 and rs1683564 were pre-validated by the supplier. 5µl reactions were set up in 384-well plates, using TaqMan Universal PCR Master Mix, No AmpErase UNG (Applied Biosystems) with 7.5 ng DNA, 1 µM of each primer, and 0.2 µM of probe. The thermal cycling reactions (95°C for 10 minutes, followed by 40 cycles at 92°C for 15 seconds and 60°C for 1 minute) were run and analyzed on a 7900HT Sequence Detection System (Applied Biosystems) with Applied Biosystems Genotyper software (SDS system, version 2.2). As controls, each plate contained multiple blank wells without DNA. The USA2 series were genotyped

using the same TaqMan assays in the laboratory of Dr. Dwight Stambolian at the University of Pennsylvania.

2.3.6.2 Alternative methods of SNP genotyping

Genotyping for the USA1 and USA3 series was performed using alternative methods. The USA3 series was genotyped for rs3826945 using the Sequenom iPLEX assay (Yu et al. 2011) in the laboratory of Dr. Johanna Seddon at Tufts University School of Medicine, USA. The USA1 case-control series was genotyped for rs1683563 and rs3826945 using direct sequencing. This was performed in the laboratory of Dr. Anand Swaroop at the University of Michigan, USA. The following primers were used for PCR:

rs1683563 : Forward primer 5'AGTGTGGCCTTCTCCGACAG
Reverse primer 5'AAATCTCTCCTGCTGCACTGA.

rs3826945: Forward primer 5'CACGTGTTAGACCCCCTCAC
Reverse primer 5'TGGAAGAGCAGGAATGAGGT.

Standard PCR conditions using TaKaRa Ex Taq polymerase (TAKARA BIO INC., Japan) were used to amplify ~100 ng DNA. Samples were denatured at 94°C for 2 minutes, and then subjected to 35 cycles of 94°C for 30 seconds, annealing at 60°C for 30 seconds, extension at 72°C for 30 seconds; followed by extension at 72°C for 7 minutes. PCR products were sequenced at the University of Michigan core facility.

2.3.7 Measuring copy number variation

Copy number variation at the CFD locus was assessed using a TaqMan copy number assay (Hs01536182_cn; Applied Biosystems) run simultaneously with a TaqMan Copy Number Reference Assay for RNAseP in a duplex real-time polymerase chain reaction. The CFD probe was FAM-labelled and the endogenous control was VIC-labelled. 10 µl reactions were set up in 384-well plates, using TaqMan Universal PCR Master Mix, No AmpErase UNG (Applied Biosystems) with 10 ng genomic DNA, 1 µM of each primer, and 0.2 µM of probe. The thermal cycling reactions (95°C for 10 minutes, followed by 40 cycles at 92°C for 15 seconds and 60°C for 1

minute) were run on a 7900HT Sequence Detection System (Applied Biosystems). Samples were analysed in triplicate, and each plate contained multiple blank wells without DNA as no template controls. The relative copy number of *CFD*, normalised to the copy number of the RNAseP reference sequence, was calculated using Applied Biosystems Copycaller software.

2.3.8 PCR amplification of *CFD* for sequencing

Primers spanning the 5 exons, intron-exon boundaries and 200 bases of the promoter of *CFD* (ENSG00000197766, Ensembl) were designed using Primer3 (frodo.wi.mit.edu/primer3/). Primer sequences are shown in Table 2.3. Primers were used to amplify specific sequences from genomic DNA of 95 AMD cases and 95 controls. Exons 1-3 were amplified using Platinum Taq. A 20 µl PCR mixture contained 1 µl 10 ng/ml DNA, 1 x PCR Buffer (Minus Mg), 1.5 mM $MgCl_2$, 0.2 mM dNTPs, 0.2 µM each of forward and reverse primers, 5-10% DMSO and 1 U of Platinum Taq polymerase (Invitrogen). Samples were denatured at 94°C for 30 seconds, and then subjected to 35 cycles of 94°C for 30 seconds, annealing at 59-67°C for 30 seconds and extension at 72°C for 60 seconds. Annealing temperature and % DMSO for specific primer pairs is shown in Table 2.3. Exons 4 and 5 were amplified using ReddyMix PCR Mix (Thermo Scientific). A 20 µl PCR mixture contained 1 µl 10 ng/ml DNA, 75 mM Tris-HCl, 20 mM $(NH_4)_2SO_4$, 1.5 mM $MgCl_2$, 0.2 mM dNTPs, 1.25 U of Thermoprime Plus DNA Polymerase and 0.2 µM each of forward and reverse primers. PCR was carried out in 0.2 ml semi-skirted 96-well plates (ABgene). PCR products were sequenced by HGU Technical Services. Sequence analysis was performed using Mutation Surveyor to identify variants compared to the reference sequence ENSG00000197766 (converted to .gbk).

2.3.9 Genotyping of indel in *ARMS2* 3'UTR

The indel in the 3' UTR of *ARMS2* was genotyped by PCR using primers designed to span the indel (Wang et al. 2010b). Primers (Table 2.3) were used to PCR amplify specific sequences from genomic DNA from 15 AMD cases using Platinum Taq, as described in Section 2.3.8. Annealing temperature and % DMSO are shown in Table

2.3. Following amplification, the PCR products were analysed on a 2% agarose gel, alongside a 100 bp DNA ladder (Promega). The wild-type sequence generates a band of 600 bp; the indel generates a band of 200 bp.

2.3.10 RNA isolation, cDNA synthesis and RT-PCR

RNA was extracted from RPE1 and THP-1 cells using the RNeasy Mini kit (Qiagen), following the manufacturer's instructions and supplied buffers. $<1 \times 10^7$ RPE1 cells or THP-1 cells differentiated by treatment with PMA were lysed directly in the culture plate, by adding 350 µl of Buffer RLT. THP-1 cells grown in suspension were centrifuged at 1200 rpm for 3 minutes to form a cell pellet, which was then lysed by addition of Buffer RLT. The cell lysate was homogenised by passing through a QIAshredder column (Qiagen). 350 µl of 70% ethanol (Fisher) was added to the homogenized lysate and mixed. The mixture was transferred to an RNeasy spin column, centrifuged for 15 seconds at 8,000 x *g*, then washed with 350 µl Buffer RW1. After centrifugation and removal of flow-through, on-column DNase digestion was performed using 10 µl RNase-Free DNase I (Qiagen) mixed with 70 µl Buffer RDD and incubating for 15 minutes at room temperature. 350 µl Buffer RW1 was added and the column centrifuged for 15 seconds at 8,000 x *g*. The column was washed twice with 500 µl Buffer RPE, and then centrifuged for 2 minutes at 8,000 x *g*. RNA was eluted in 30 µl RNase-free water by centrifugation at 8,000 x *g* for 1 minute. RNA was quantified by quantitated using the NanoDrop ND-1000 Spectrophotometer.

The Transcriptor High Fidelity cDNA Synthesis Kit (Roche) was used for synthesising cDNA from 1 µg RNA, following the manufacturer's protocol and supplied buffers and enzymes. 1200 pmol of random hexamer primer was denatured at 65^{o}C for 10 minutes with 1 µg RNA (or without RNA, as a control) in a final volume of 11.4 µl, before chilling on ice. The reaction volume was increased to 20 µl by addition of Transcriptor High Fidelity Reverse Transcriptase Reaction Buffer (1x, 8 mM $MgCl_2$), Protector RNase Inhibitor (20 U), 1 mM dNTPs, 5 mM DTT and 10 U Reverse Transcriptase (RT). A control lacking Reverse Transcriptase (-RT) was

performed. After incubation at 45^{o}C for 30 minutes to allow cDNA synthesis, Reverse Transcriptase was inactivated by heating to 85^{o}C for 5 minutes.

50-250 ng of cDNA was amplified by PCR using Platinum Taq and gene-specific intron-spanning primers to test for expression of transcripts for *HTRA1*, *CFD*, *C3*, *MASP1* and *GAPDH*. Primers, annealing temperatures and extension times are shown in Table 2.3. Following amplification, the PCR products were analysed on a 2% agarose gel, alongside a 100 bp DNA ladder.

2.4 Protein procedures

2.4.1 Bradford Assay

The concentration of protein in solution was determined using the Bradford Assay. Protein standards were prepared in the same buffer as the samples to be assayed. A 10 mg/ml BSA (96%, Sigma) solution was subjected to doubling dilutions into an appropriate diluent (such as PBS or distilled water) to obtain seven standard solutions with the following range of concentrations of BSA: 0, 0.078, 0.156, 0.313, 0.625, 1.25 and 2.5 mg/ml. 0.98 ml of 1x Bradford reagent (5x; BioRad) diluted in distilled water was mixed with 20 µl of either standard sample or protein solution in disposable 1 ml cuvettes. Colour was allowed to develop for 10 minutes at room temperature. The OD_{595} of each sample and standard was measured using the UV1101 Biotech Photometer. A standard curve was created from the OD_{595} of the standard solutions, allowing the concentrations of protein solutions to be determined.

2.4.2 Protein separation by polyacrylamide gel electrophoresis

For reducing gels, samples were mixed with 1 x Reducing Agent (Invitrogen) and 4 x NuPAGE LDS (lithium dodecyl sulfate) Sample Buffer (Invitrogen) and denatured by heating to 70^{o}C for 10 minutes. Samples run under non-reducing conditions were mixed with 4 x NuPAGE LDS Sample Buffer and loaded directly on the gel, without heating. Gel electrophoresis was performed using pre-cast 10%, 12% or 4-12% Bis-Tris NuPAGE gels (Invitrogen), depending on the required resolution of proteins. Gels were run using the XCell SureLock Mini-Cell system (Invitrogen). Running

buffer was either 1 x MOPS (3-(N-morpholino)propanesulfonic acid; Invitrogen) or 1 x MES (2-(N-morpholino)ethanesulfonic acid; Invitrogen). Gels were run at 200V for 55 minutes. SeeBlue Plus 2 pre-stained molecular weight marker (Invitrogen) was the protein standard used on all gels.

Gels were silver-stained, Coomassie-stained or transferred to Hybond-P PVDF membrane (GE Healthcare) for Western blotting.

2.4.3 Coomassie staining

Following electrophoresis, gels were either stained with Gelcode Blue stain reagent (Pierce) or with InstantBlue stain (Expedeon). For Gelcode Blue-staining, the gel was rinsed 3 times in 100 ml of ultrapure water for 5 minutes. 20 ml of Gelcode Blue stain reagent was then added to the gel, and incubated for 1 hour at room temperature with gentle shaking a rotary shaker. After 1 hour, the staining solution was removed and destaining of the gel background was achieved by washing in ultrapure water for an hour or more. For gel staining using InstantBlue, there was no wash step in ultrapure water prior to immersion of the gel in 20 ml of stain reagent for 1 hour at room temperature with gentle shaking on a rotary shaker. After 1 hour, the staining solution was removed and destaining of the gel background was achieved by washing in ultrapure water for an hour or more.

2.4.4 Silver staining

Silver staining was performed using the SilverQuest Silver staining kit (Invitrogen). The gel was fixed in Fixing Solution (40% ethanol (Fisher), 10% acetic acid (Sigma)) for 20 minutes, and then washed for 10 minutes in 30% ethanol. In order to increase the sensitivity and contrast of the stain, the gel was incubated in Sensitizing solution (30% ethanol, 10% Sensitizer (Invitrogen)) for 10 minutes. The gel was washed twice, firstly with 30% ethanol and then with ultrapure water for 10 minutes each. The gel was stained in Staining solution for 15 minutes, washed for 1 minute in ultrapure water, and then developed in Developer solution (Invitrogen) until the required band intensity was obtained.

2.4.5 Western Blotting

Samples were subjected to gel electrophoresis and then transferred to Hybond-P PVDF membrane (GE Healthcare) in 1 x NuPAGE Transfer Buffer (Invitrogen) containing 10% methanol (Fisher) using the XCell SureLock Mini-Cell Blot Module system (Invitrogen). The PVDF membrane was cut to the appropriate size, wetted in methanol and then placed directly on the gel. The gel and membrane was sandwiched between two pieces of Whatman filter paper, and then the transfer apparatus assembled. Transfer was performed for 1 hour at 30V. Following transfer of proteins from the gel to the membrane, membranes were blocked in 5% non-fat milk in PBST (Phosphate-buffered Saline-Tween 20; 3.2 mM Na_2HPO_4, 0.5 mM KH_2PO_4, 1.3 mM KCl, 135 mM NaCl, 0.05% Tween 20, pH 7.4) for 1 hour at room temperature, or overnight at 4°C. Antibodies used in the following steps are shown in Table 2.4.

Membranes were incubated with primary antibody diluted in PBST for 1 hour at room temperature, followed by three 5-minute washes in PBST. Membranes were incubated in horseradish peroxidase (HRP)-conjugated secondary antibody, diluted 1:5,000 in PBST, for 1 hour followed by three more washes in PBST. The secondary antibodies were detected by addition of Enhanced Chemiluminescence (ECL) Western blotting detection reagents (GE Healthcare) for 1 minute. The membrane was exposed to Kodak BioMax XAR film (Sigma) in an X-ray film exposure cassette for sufficient time to detect an ECL signal. The film was developed using a phosphorimager X-ray machine (Konica Minolta). Densitometry analysis of scanned films was performed using ImageQuantTL software (GE Healthcare).

Antibody	Raised in	Clonality	Supplier	Stock concentration	Application	Dilution
anti-Bb	Mouse	Monoclonal	Quidel	1 mg/ml	Western Blot primary	1 in 1000
anti-C3 (B-9)	Mouse	Monoclonal	Santa Cruz Biochemicals	0.2 mg/ml	Western Blot primary	1 in 2000
anti-CFD (C-16)	Goat	Polyclonal	Santa Cruz Biochemicals	0.2 mg/ml	Western Blot primary	1 in 2000
anti-CFD	Mouse	Monoclonal	R&D Systems	0.72 mg/ml	ELISA Capture	1 in 180
biotinylated anti-CFD	Goat	Polyclonal	R&D Systems	0.036 mg/ml	ELISA Detection	1 in 180
anti-CFD MAB#255719	Mouse	Monoclonal	R&D Systems	0.5 mg/ml	Serum depletion	-
anti-CFD GAU 008-01	Mouse	Monoclonal	Antibody Shop	1 mg/ml	Serum depletion	-
anti-CTGF (L-20)	Goat	Polyclonal	Santa Cruz Biochemicals	0.2 mg/ml	Western Blot primary	1 in 2000
anti-FLAG M2	Mouse	Monoclonal	Sigma-Aldrich	2 mg/ml	Western Blot primary	1 in 4000
anti-GST-HRP conjugate	Rabbit	Polyclonal	Sigma-Aldrich	9 mg/ml	Western Blot	1 in 1000
anti-His_6	Mouse	Monoclonal	Veronica van Heynigen	ND	Western Blot	1 in 100
anti-HTRA1 PDZ	Rabbit	Polyclonal	Michael Erhmann	ND	Western Blot primary	1 in 1000
anti-HTRA1**	Rabbit	Polyclonal	Jeremy Chien	ND	ELISA Capture	1 in 100
anti-HTRA1 MAb 10	Mouse hybridoma	Monoclonal	Jeremy Chien	ND	ELISA Detection	1 in 10
anti-HTRA1 MAb 4.1	Mouse hybridoma	Monoclonal	Jeremy Chien	ND	ELISA Detection	N/A
anti-THBS1	Rabbit	Polyclonal	Abcam	1 mg/ml	Western Blot primary	1 in 400
anti-mouse IgG HRP	Rabbit	Polyclonal	Sigma-Aldrich	-	Western Blot secondary	1 in 5000
				-	ELISA secondary Detection	1 in 12500
anti-rabbit IgG HRP	Donkey	Polyclonal	Amersham Pharmacia	-	Western Blot secondary	1 in 5000
anti-goat IgG HRP	Donkey	Polyclonal	Santa Cruz Biochemicals	0.4 mg/ml	Western Blot secondary	1 in 5000

Table 2.4 Antibodies used for Western blotting, serum depletion and ELISA.

2.4.6 Purification of bacterially expressed recombinant proteins

Bacterial cells were induced to express recombinant proteins as described in Section 2.2.2.3. Proteins were affinity purified using the N-terminal tags.

2.4.6.1 Purification of GST-tagged recombinant proteins

The bacterial cell pellet was resuspended in STE Buffer (50 mM Tris-HCl pH 7.5, 150 mM NaCl, 1 mM EDTA, 10 mM DTT (Sigma)) with 1 mg/ml of lysozyme (Novagen) and rotated on an end-on-end shaker at 4°C for 1 hour to achieve lysis. Subsequently, Sarcosyl (Sigma) was added to a final concentration of 1% and the cells disrupted by sonication for 6 x 10 seconds at 24 µ. Triton X-100 (Sigma) was added to a final concentration of 1% prior to clearing of the lysate by centrifugation at 10,000 x *g* for 20 minutes at 4°C. Soluble material was incubated for 2 hours at 4°C with glutathioine-agarose (GE Healthcare), previously equilibrated with STE Buffer. The agarose was washed with 60 bed volumes of STE Buffer + 0.5% Triton X-100, prior to elution of bound GST-tagged proteins in 200 µl fractions using GST-Elution Buffer (200 mM Tris-HCl pH 7.5, 150 mM NaCl, 5 mM EDTA, 0.1% Triton X-100 and 100 mM reduced glutathione (Sigma)). For on-column cleavage of the GST tag from proCFD, after washing the resin to remove contaminating proteins, Prescission protease was added to the resin in Cleavage Buffer (20 mM Tris pH 7.0, 150 mM NaCl, 1 mM DTT) and incubated for 2 hours at 4°C. Free proCFD was collected in the flow-through and dialysed into TBS.

2.4.6.2 Purification of His_6-tagged recombinant HTRA1

Bacterial cells were resuspended in His_6-Lysis Buffer (50 mM NaH_2PO_4, 300 mM NaCl, 5 mM imidazole (Acros), pH 8.0) and lysozyme was added to 1 mg/ml. The suspension was rotated end-on-end at 4^{o}C for 1 hour to achieve lysis. Cells were then further disrupted by sonication for 6 x 10 seconds at 100% power. Insoluble material was removed by centrifugation at 10,000 x *g* for 20 minutes at 4^{o}C. The cleared lysate (soluble fraction) was applied to a Ni-NTA (Ni^{2+}-nitrilotriacetate)-agarose (Qiagen) column, pre-equilibrated by washing with 10 bed volumes of His_6-Lysis

Buffer. The lysate was incubated on the column for 2 hours at 4°C. The column was washed twice with His_6-Lysis Buffer, before elution of bound His_6 ΔN HTRA1 from the column in 0.5 ml fractions with His_6-Elution Buffer (50 mM NaH_2PO_4, 300 mM NaCl, 250 mM imidazole pH 8.0).

2.4.6.3 Assessment of protein purity

Protein fractions were quantified by Bradford assay, and 2-5 µg of protein was analysed by reducing and denaturing gel electrophoresis, followed by Coomassie staining. Fractions containing pure protein were identified and pooled for dialysis into Storage Buffer (50 mM Tris pH 8, 150 mM NaCl, 10% glycerol (Fisher), and in some cases, 0.1% Triton X-100). Proteins were also assessed by Western blotting using antibodies specific to the protein and the tag (Table 2.4).

2.4.7 Zymography of recombinant forms of the HTRA1 protease

Proteolytic activity of recombinant HTRA1 was assessed using zymography, using premade buffers and following a protocol provided by BioRad. Briefly, 5 µg of each GST ΔN HTRA1, GST ΔN HTRA1 S328A and His_6 ΔN HTRA1 was mixed with an equal volume of Zymogram sample buffer (62.5 mM Tris-HCl, pH 6.8, 4% SDS, 25% glycerol, 0.01% Bromophenol Blue). Samples were loaded on a 12% Zymogram gel with casein as a substrate (BioRad) and run for 90 minutes at 100 V in Zymogram Running Buffer (25 mM Tris, 192 mM glycine, 0.1% SDS).

Proteins were renatured within the gel by incubating in Renaturation Solution (2.5% Triton X-100) for 30 minutes at room temperature. Subsequent incubation in Development Solution (50 mM Tris, 200 mM NaCl, 5 mM $CaCl_2$, 0.02% Brij-35 (Pierce), pH 7.5) overnight at 37ºC allowed proteolysis of the casein contained in the gel. The gel was stained with Coomassie Brilliant Blue R-250 staining solution (40% methanol. 10% acetic acid. 0.5% Coomassie Blue R-250 (BDH)) for 1 hour at room temperature. Destaining was performed in a solution of 40% methanol and 10% acetic acid, for 1 hour until clear bands were apparent.

2.4.8 Protein interaction assays

2.4.8.1 Tandem Affinity Purification (TAP)

48 hours post-transfection, media was removed from transfected RPE1 or HEK293T cells (Section 2.2.1.2), and centrifuged at 1200 rpm for 10 minutes to remove cell debris. Each 14 cm plate of cells was scraped in 1 ml of Lysis Buffer (50 mM Tris-HCl pH 7.5, 150 mM NaCl, 1 % NP40, 1 mM EDTA, 1 PhosStop phosphatase inhibitor tablet (Roche)/10 ml). Cell lysis was achieved by snap-freezing in liquid nitrogen. Media was snap-frozen in liquid nitrogen for storage at -80°C. Upon thawing, media was concentrated approximately 10-fold to a final volume of 5 ml, by centrifugation in a Sorvall Legend RT centrifuge using a Centriprep centrifugal filter device (Amicon; 3 kDa MW cut-off) at 3,000 x *g* at 4^{o}C. Cell lysates were centrifuged at 1,0000 rpm for 10 minutes to remove cell debris.

Streptactin Superflow beads (IBA Technologies) were pre-equilibrated by washing with 1 ml of Lysis Buffer (details as above), and 2 x 1 ml of Wash Buffer (50 mM Tris-HCl pH 7.5, 150 mM NaCl, 0.1 % NP40, 1 mM EDTA). Cell lysate or concentrated media was added to 20 µl settled volume of Streptactin Superflow beads per 14 cm plate and incubated, on an end-on-end shaker, for 2 hours at 4^{o}C. Subsequently, beads were washed 3 times in 0.5 ml of Wash Buffer. Bound proteins were eluted by resuspension of Streptactin Superflow beads in 0.5 ml of Elution Buffer (2 mM D-Desthiobiotin; IBA Technologies) for 10 minutes at 4 ^{o}C. The elution mixture was transferred to Illustra Microspin columns (GE Healthcare). Eluates were recovered by centrifugation at 2,000 rpm for 5 seconds and incubated for 2 hours at 4°C with 30 µl settled volume of pre-equilibrated anti-FLAG M2 Agarose beads (Sigma) per construct in Microspin columns.

Anti-FLAG M2 Agarose beads were washed 3 times with 0.5 ml of Wash Buffer before elution with 200 µl of 200 µg/ml FLAG peptide (Sigma) by gentle mixing for 10 minutes. Eluates were concentrated by centrifugation using Microcon centrifugal filter devices (3kDa MW cut-off; Millipore) at 10,000 rpm for ~100 minutes at 4 ^{o}C.

Eluates were precipitated and analysed by mass spectrometry, performed by Dr. Karsten Boldt at the Helmholtz Zentrum, Munich.

2.4.8.2 Protease Activity Assay

The protease activity of GST ΔN HTRA1 was assayed by incubation of recombinant HTRA1 (0.1-5 µg) with other recombinant proteins (proCFD, GST-CTGF), synthetic peptides (CFD_Y2H, GeneCust; 20 µg) or proteins purified from human plasma (THBS1 (Affinity Bioreagents), C3 (Sigma), CFB (Calbiochem); CFD (Sigma); 0.5-5 µg). Assays were performed in a 20 µl mixture containing 50 mM Tris-HCl, pH 8, 150 mM NaCl for 3-18 hours at 37°C. GST only and GST ΔN HTRA1 S328A were incubated with potential substrates under the same conditions and served as controls. The reaction was terminated by the addition of 10 µl of LDS loading buffer (Invitrogen), and where appropriate, reducing agent. For denaturing gels, the mixture was boiled for 5 minutes. Proteins were separated by gel electrophoresis and stained with Coomassie Blue, silver stained or analysed by Western blot.

2.4.8.3 GST Pull-downs

For pull-down assays using GST-tagged proteins, equimolar amounts of a GST-tagged protein (GST ΔN HTRA1, GST HTRA1 ΔC, GST CTGF or GST alone) were incubated together with a potential binding partner (His_6 ΔN HTRA1, CFD, C3, THBS1).GST-tagged proteins and interactors were bound to 25 µl of glutathione-Sepharose beads (GE Healthcare) in 500 µl TEN150 buffer (50 mM Tris-HCl, pH 7.5, 150 mM NaCl) for 2 hours at 4°C. Beads were washed with 4 x 1ml of TEN150 buffer containing 0.1-0.5% NP40 and resuspended in 4 x LDS loading buffer and 10 x Reducing Agent. Samples were heated at 70°C for 10 minutes. Eluted proteins were then analysed by LDS-PAGE and Western blotting using antibodies specific to the protein and/or the tag (Table 2.4).

2.4.9 Mass spectrometry

2.4.9.1 Identification of interactors from TAP experiments

Eluates from tandem affinity purification were analysed by liquid chromatography coupled with tandem mass spectrometry (LC-MS/MS) to identify components of the purified complexes following tryptic digestion. Mass spectrometry was performed by

Dr. Karsten Boldt at the Helmholtz Zentrum, Munich, according to the published protocol (den Hollander et al. 2007). Peptides were identified using the MASCOT search engine (Matrix Science in the GPS Explorer software (Applied Biosystems) to search the Swiss Prot database. Positive identification of proteins required representation by one or more unique peptides with a MASCOT confidence interval >90%.

2.4.9.2 Peptide Mass Fingerprinting of proCFD

Following overnight incubation of HTRA1 with proCFD at 37°C, the digested and untreated proCFD were subjected to reducing gel electrophoresis, and the gel was Coomassie stained. Bands corresponding to CFD and proCFD were excised from the gel using sterile razor blades. The gel slices were frozen and sent to Dundee Cell Products for peptide mass fingerprinting. Gel slices were destained and in-gel digests using the V8 Protease (NEB) in buffer containing 50 mM Tris-HCl, 0.5 mM Glu-Glu, pH 8.0 was performed overnight at 37°C. Peptide fragments were separated by HPLC using the Dionex Ultimate 3000 nanoflow LC-System with a reverse-phase ReproSil-Pur C18-AQ 3 μm column, using a gradient of 10-60% solvent B over 100 minutes with a constant flow of 200 nL/minute. The HPLC system was coupled to an LTQ-Orbitrap mass spectrometer (ThermoFisher Scientific) to detect peptides. Data were acquired using the Xcalibur software, and peptides quantitated using MS-Quant (http://msquant.sourceforge.net) and identified using Protein Center (Proxeon Bioinformatics) proteomics data mining and management software.

2.4.10 Plasma and serum

2.4.10.1 Plasma

Plasma samples used in the CFD and HTRA1 ELISAs were collected from 751 cases and 474 controls from the UK1 and UK2 AMD case-control cohorts. 208 plasma samples were obtained from the SOCCS disease-free control series (Prof. Malcolm Dunlop). Blood samples were collected in dipotassium EDTA-coated tubes. Plasma was separated from blood cells by centrifugation within 3 hours of collection and

was frozen in aliquots at -80°C until use. Human blood and blood products were handled following protocols for Containment Level 2.

2.4.10.2 Serum

2.4.10.2.1 Normal Sera

Blood samples from 5 healthy Caucasian volunteers were processed to produce normal sera. After clotting for 1 hour at room temperature, sera were separated by centrifugation for 25 minutes at 3,000 rpm. Separated serum was collected, pooled for all samples and frozen immediately then stored at −80 °C. This represents normal serum in the subsequent assays. Normal serum was heat-inactivated at 65°C for 25 minutes to remove alternative complement pathway activity.

2.4.10.2.2 CFD-depleted serum

Normal human serum was thawed and used to test protocols for depleting sera of CFD on affinity columns. CFD-depleted human serum was also obtained from Quidel.

2.4.10.2.2.1 CFD-depletion using antibodies

0.2 µg of the monoclonal CFD-specific antibodies GAU-008-01 (Antibody Shop) or MAB#255719 (R&D Systems) were coupled to 0.2 ml of CNBr-activated Sepharose 4B (GE Healthcare). Prior to coupling, the Sepharose was swelled in 1 mM HCl for 20 minutes at room temperature, collected by centrifugation at 500 x *g* for 10 minutes at 4°C and then washed 3 times with 10 ml of 1 mM HCl. The beads were washed twice more with Borate Buffered Saline (BBS; 200 mM H_3BO_3, 150 mM NaCl, pH 8) containing 0.02% sodium azide (Sigma). Beads were resuspended in antibody solution containing 0.2 mg/ml antibody in BBS and incubated end-on-end overnight at 4°C. The beads were washed three times with BBS, and excess reactive sites blocked by incubation in 1M ethanolamine (Sigma) for 2 hours at room temperature. Beads were washed three times with BBS and equilibrated by extensive washing in veronal buffered saline (VBS; 2.8 mM barbituric acid, 145.5 mM NaCl,

0.8 mM $MgCl_2$, 0.3 mM $CaCl_2$, 0.9 mM sodium barbital, pH 7.2 (Lonza)). Beads were transferred to Microspin columns and incubated for 1 hour with freshly thawed serum at 4°C. Serum was passed over the column and collected. The column was washed with VBS, and then with 50 mM glycine-HCl (Fisher) to remove bound proteins, before re-equilibrating in VBS. The serum was passed over the column a second time, and the least dilute fractions of depleted sera, assessed visually by colour, were collected and pooled for each antibody.

2.4.10.2.2.2 BioRex70 chromatography

0.2 g of BioRex70 cation-exchange resin (BioRad) was equilibrated by repeated washing in VBS until pH 7.2 was maintained. 1 ml of normal serum was incubated for 1 hour at 4°C with the resin. CFD-depleted-serum was recovered from the resin by centrifugation at 10,000 x *g* for 10 minutes.

2.4.10.2.2.3 Testing depletion of CFD in sera

CFD-depleted sera were tested using CFD-specific ELISA, Western blotting of 1 µl of sera with anti-CFD, and by assessing haemolytic activity using a red cell lysis assay in the presence and absence of 0.1 µg of exogenous human CFD.

2.4.10.2.3 CARASIL Sera

Sera obtained from three Japanese CARASIL patients, and two healthy Japanese controls, were provided by Professor Osamu Onodera (Niigata University, Japan) These samples were collected and processed as described previously. Samples were shipped on dry ice, and immediately stored at -80 °C upon arrival.

2.4.10.3 An ELISA for CFD

2.4.10.3.1 Optimisation of the CFD Duoset for measuring CFD in plasma

The DuoSet ELISA development kit for human Complement Factor D (R&D Systems) was optimised for use in plasma. Following the manufacturer's recommended protocol, the ability of the assay to measure CFD in a plasma dilution series was assessed. Serial dilutions of three internal control plasma samples (P1, P2 and P3), ranging from 1/400 to 1/4,000, were made in 1% BSA (98%, Sigma) in PBS. A standard curve was made by serial dilutions of recombinant human CFD, ranging from 0 - 2.5 ng/ml. Plasma dilutions and standards were mixed end-on-end for 10 minutes to ensure proper mixing before additional dilution or use in the assay. All samples and standards were performed in duplicate or triplicate during the optimisation assays. At the end of the assay, absorbance was measured at 450 nm, corrected for background at 540 nm. Mean absorbance values (minus background absorbance of the zero standard) were used to create a standard curve, and subsequently calculate plasma CFD concentration in the three plasma samples for all dilutions. The most suitable plasma dilution to detect CFD in the range of 1-3 µg/ml was determined.

The internal control plasma samples P3, P6 and P9 were measured multiple times within the same assay to assess intra-assay variation, and measured multiple times in different assays to assess inter-assay variation.

2.4.10.3.2 Optimised protocol for measuring CFD in plasma

Round-bottomed ELISA plates (Greiner-Bio) were coated overnight at room temperature with 50 µl of 4.0 µg/ml mouse anti-human Complement Factor D capture antibody diluted in PBS. The wells were washed three times with 200 µl of PBST and then blocked in 1% BSA in PBS for 2 hours. The wells were washed three times with 200 µl of PBST, and then 50 µl of standards and plasma samples, diluted 1:4,000 in 1% BSA in PBS, were added for 2 hours. The wells were washed three times with 200 µl of PBST. Captured CFD was detected by incubation with 50 µl of 200 ng/ml of the biotinylated goat anti-human Complement Factor D detection

antibody in 1% BSA in PBS for 2 hours. The wells were washed three times with 200 µl of PBST, and 50 µl of a 1 in 200 dilution of Streptavidin-HRP in 1% BSA/PBS was added for 20 minutes. The wells were washed three times with 200 µl of PBST, followed by incubation with 50 µl of TMB (Tetramethylbenzidine) substrate (Sigma). Colour was allowed to develop for 20 minutes before the reaction was stopped by adding 25 µl of 1N sulphuric acid (Fisher). Incubation steps were performed at room temperature on an orbital shaker. Absorbance was measured at 450 nm, corrected for background at 540 nm. A CFD standard curve (0-2.5 ng/ml) was made by serial dilution of 110 ng/ml recombinant human Complement Factor D, which was included on each plate. The mean absorbance for each standard (minus the background absorbance from the zero standard) was used to create the standard curve in Microsoft Excel. The equation of the line of best fit was obtained by polynomial regression and used to calculate the concentration of CFD in plasma samples (accounting for the dilution factor) from the UK1 and UK2 AMD case-control series. AMD cases and control samples were included on each plate and all samples and standards were measured in duplicate. CFD was measured without prior knowledge of disease status for each sample.

2.4.10.3.3 Measuring CFD in cell culture supernatants

The CFD ELISA protocol outlined above was used to measure CFD in the cell culture supernatants collected from RPE1 cells that had been treated with LPS or hydrogen peroxide, or from untreated cells. 50 µl of conditioned media was used undiluted, alongside a standard curve of 0-2.5 ng/ml recombinant CFD.

2.4.10.4 An ELISA for HTRA1

2.4.10.4.1 Antibodies

An HTRA1-specific sandwich ELISA was developed using a mouse monoclonal capture antibody (MAb 10) and a polyclonal detection antibody (HTRA1**). Antibodies were gifts from Dr Jeremy Chien (Mayo Clinic, Rochester, USA).

2.4.10.4.2 Optimisation of the HTRA1 ELISA

2.4.10.4.2.1 Testing antibodies in an indirect ELISA

Purified recombinant protein (0.3-5 ng/ml) was diluted in Coating Buffer (50 mM carbonate buffer, pH 10.6) and incubated overnight at 4^{o}C in an ELISA plate to allow binding of antigens to the microplate. The wells were washed three times with 200 µl of Tris-buffered saline (50 mM Tris, 150 mM NaCl, 2 mM KCl, pH 7.4) containing 0.05% Tween-20 (TBST) and blocked in 5% non-fat dried milk in TBST for 2 hours. After washing three times, primary antibodies (HTRA1** diluted 1:100, mixed monoclonals 1:1, MAb 10 diluted 1:2 or MAb 4.1 diluted 1:2 in 1% BSA in TBST) were added for 2 hours to bind to the immobilised antigen. The wells were washed three times with 200 µl of TBST. Detection was performed using HRP-conjugated IgG from rabbit or mouse as appropriate for the primary antibody to process the TMB substrate. Absorbance was measured at 450 nm and corrected for background by subtraction of absorbance at 540 nm and absorbance measured at 450 nm for the zero standard (1% BSA in TBST).

2.4.10.4.2.2 Capture Antibody HTRA1** Optimisation

Dilutions of the polyclonal capture antibody HTRA1 ** (1:100, 1:250, 1:500, 1:1,000, 1:5,000, 1:10,000) were used in a sandwich ELISA to determine the optimal dilution for detection of recombinant GST ΔN HTRA1 S328A (0.78-50 ng/ml). Dilutions of the capture antibody were made in TBS, and were mixed end-on-end for 10 minutes before use. 50 µl of each antibody dilution was added to the plate in duplicate, and incubated at 4^{o}C overnight with shaking on an orbital platform. The wells were washed three times with 200 µl of TBST and then blocked in 5% NFDM in TBST for 2 hours. The wells were washed three times, and then the recombinant protein – diluted in 1% BSA in TBST, and each concentration added in duplicate for each capture antibody dilution - was added for 2 hours. After repeating the wash procedure, the monoclonal detection antibody MAb 10 was added to the plate. For optimisation of the capture antibody, the detection antibody was diluted 1:2 in 1% BSA in TBST. 50 µl of detection antibody was added to each well and incubated for 2 hours, with shaking. Washing was repeated and then 50 µl of anti-mouse IgG HRP

(Sigma) diluted 1:5,000 in 1% BSA in TBST was added to the wells for 30 minutes. The wells were washed three times, and then 50 µl of TMB substrate was added. After 30 minutes, colour development was stopped by addition of 25 µl of 1N sulphuric acid. Absorbance was measured, corrected for background, and used to determine the dilution of capture antibody which was not saturated by 50 ng/ml of HTRA1.

2.4.10.4.2.3 Detection Antibody MAb 10 Optimisation

The capture antibody was diluted 1:100 in TBS, and 50 µl was added to each well of the plate. The plate was incubated at 4^{o}C overnight. Following the protocol outlined previously, the plate was washed, blocked and then washed again. A dilution series of GST ΔN HTRA1 S328A (0.78-50ng/ml) was prepared and added to the plate before incubation for 2 hours. After repeating the wash procedure, 50 µl of the monoclonal detection antibodies MAb 10, MAb 4.1 or a mix of MAb 10 and MAb 4.1 were added to the plate for 2 hours. The hybridoma supernatants containing the monoclonal antibodies were tested undiluted, or diluted 1:2, 1:5, 1:10, 1:25 in 1% BSA in TBST, with each antibody dilution assayed in duplicate for each concentration of HTRA1 detected. After washing three times, 50 µl of anti-mouse IgG HRP diluted 1:5,000 in 1% BSA in TBST was added to the wells for 30 minutes. The wells were washed three times, and then 50 µl of TMB substrate was added. After 30 minutes, colour development was stopped by addition of 25 µl of 1N Sulphuric acid. Absorbance was measured, corrected for background, and used to determine the dilution of detection antibody which was not saturated by 50 ng/ml of HTRA1.

2.4.10.4.2.4 Anti-mouse IgG HRP Optimisation

Two internal control plasma samples, P8 and P9, were diluted 1:10 in 1% BSA in TBST and assayed for HTRA1 using the optimised antibody dilutions for capture and detection, following the procedure outlined above. Following wash steps after the incubation with the detection antibody, a dilution series of anti-mouse HRP-conjugated IgG was used to detect binding of MAb10 to HTRA1 from plasma which

had been captured by HTRA1**. The IgG-HRP was diluted as follows in 1% BSA in TBST: 1:5,000, 1:10,000, 1:25,000, 1:50,000, 1:75,000, 1:100,000. 50 µl of each dilution was assayed in duplicate for each plasma dilution. After 30 minutes, the wells were washed and TMB added. Colour development was stopped after 30 minutes and the absorbance was measured. A range of dilutions of IgG-HRP giving rise to identical plasma HTRA1 concentrations were identified, and used for the selection of the optimal IgG-HRP dilution for subsequent assays.

2.4.10.4.2.5 Plasma dilution optimisation

The ability of the optimised antibody dilutions to capture and detect HTRA1 in plasma was assessed. Three internal control plasma samples were assayed following the procedure outlined above. 50 µl of each sample was assayed in duplicate, undiluted or diluted 1:3, 1:10, 1:50 and 1:100 in 1% BSA in TBST. When absorbance was measured, it was apparent that lower absorbance readings were obtained when the plasma was less dilute. The apparent inhibition of the assay was tested by making an HTRA1 standard curve, ranging from 0.312 to 50 ng/ml of GST ΔN HTRA1 S328A in either the standard dilution buffer (1% BSA in TBST) or diluted in plasma (P7), diluted either 1:10 or 1:50 in 1% BSA in TBST. The optimised HTRA1 ELISA was performed to measure HTRA1 in these samples, and to determine the plasma dilution at which the ELISA was not inhibited.

2.4.10.4.3 Optimised protocol for measuring HTRA1 in plasma

Round-bottomed ELISA plates (Greiner-Bio) were coated with a 1:100 dilution of the polyclonal capture antibody in 50 µl TBS overnight at 4°C. The wells were washed three times with 200 µl of TBST and then blocked in 5% NFDM in TBST for 2 hours. The wells were washed three times with 200 µl of TBST, and then 50 µl of plasma samples, diluted 1:50 in 1% BSA in TBST, and standards were added for 2 hours. The wells were washed three times with 200 µl of TBST, and captured HTRA1 was detected by incubation with 50 µl of a 1:10 dilution of the mouse monoclonal detection antibody in 1% BSA in TBST for 2 hours. The wells were washed three times with 200 µl of TBST, followed by incubation with 50 µl of anti-

mouse IgG HRP, diluted 1:25,000 in 1% BSA in TBST for 30 minutes. The wells were washed three times with 200 µl of TBST. 50 µl of TMB substrate was added, and the plate incubated for 30 minutes to allow colour to develop. The reaction was stopped by adding 25 µl of 1N sulphuric acid. All assay incubations were performed at 20°C on an orbital shaker. Absorbance was measured at 450 nm, corrected for background at 540 nm. Plasma HTRA1 concentrations were calculated relative to a recombinant HTRA1 S328A standard curve (0-2.5 ng/ml), made by serial dilution and included on each plate. The inter-assay coefficient of variation, as determined by two internal standard plasma samples included on each ELISA plate, was below 10%. HTRA1 was measured without prior knowledge of disease status or genotype for each sample. All samples and standards were measured in duplicate. The mean absorbance for each standard (minus the background absorbance from the zero standard) was used to create the standard curve in Microsoft Excel. The equation of the line of best fit was obtained by linear regression and used to calculate the concentration of HTRA1 in plasma (accounting for the dilution factor).

HTRA1 was measured without prior knowledge of genotype for each sample, and without knowledge of disease status for the AMD case-control series.

2.4.10.5 Assays of complement activation

The functional consequence of HTRA1-mediated cleavage of proCFD was assessed using assays of alternative complement pathway activation *in vitro*. In the following assays, recombinant proCFD was incubated with GST ΔN HTRA1 overnight at 37°C to allow cleavage of the activation peptide to occur.

2.4.10.5.1 Reconstitution Assay

1 µg of purified Cobra Venom Factor (CVF; Quidel) was incubated overnight at 37°C with combinations of purified human factor B (1 µg; Calbiochem), CFD (0.2 µg; Sigma), recombinant proCFD (0.2 µg) and recombinant GST ΔN HTRA1 (0.1 µg). The final volume was 20 µl, in TBS containing 5 mM $MgCl_2$ and 5 mM $CaCl_2$, The reaction was stopped by adding 4 x LDS Loading Buffer. Proteins were

separated by non-reducing gel electrophoresis on 4–12% Bis-Tris gels in 1xMOPS Buffer. Gels were stained with InstantBlue (Expedeon).

2.4.10.5.2 Cleavage of factor B in human sera

1 µl of normal human serum (pooled serum, collected from healthy volunteers) or CFD-depleted serum (Quidel) were supplemented with combinations of 1µg CVF, 0.2µg CFD, 0.2 µg proCFD and 0.1 µg HTRA1. The find reaction volume was 10 µl, in TBS containing 5 mM $MgCl_2$ and 5 mM $CaCl_2$. Factor B cleavage in CARASIL sera was assessed by incubating 1-3 µl of CARASIL sera (or 1 µl of control sera) with 1 µg of CVF in the presence of increasing concentrations of $MgCl_2$ (0-5 mM). Mixtures were incubated at 37°C for 3 hours, then 4 x LDS Loading Buffer was added. Samples were separated by non-reducing gel electrophoresis and transferred to PVDF for immunoblotting with anti-Bb antibody to detect Factor B cleavage.

2.4.10.5.3 Haemolysis Assays

Erythrocytes from 2 ml of sheep's blood in Alsevers solution (TSC Biosciences) were washed in PBS containing 0.5 mM EDTA, and then twice in 10 ml of Incubation Buffer (10 mM sodium phosphate, 140 mM NaCl, pH5.5). The cells were counted and resuspended to a concentration of 1×10^9 cells/ml. Following the protocol described by Carroll et al. (2009), 2.5 units of neuraminidase from *Clostridium perfringens* (Sigma) were added for every 1×10^{10} cells and incubated with gentle shaking at 37^{o}C for 1 hour. Erythrocytes were recovered by centrifugation at 3,000 rpm for 10 minutes and washed with PBS containing 0.5 mM EDTA. Neuraminidase-treated erythrocytes and untreated erythrocytes (used in reactive lysis assays with CVF) were then washed twice in 10mM ethylene glycol-bis(2-aminoethylether)-N,N,N,N'-tetraacetic acid (EGTA), 7 mM $MgCl_2$, 2.1 mM sodium barbital, 59 mM NaCl, 2.08% (w/v) glucose, 0.08% (w/v) gelatin, pH 7.4 (DGVB-MgEGTA) and resuspended to a concentration of 10^9 cells/ml in DGVB-MgEGTA. Lysis of 10^8 neuraminidase-treated cells in DGVB-MgEGTA in 20 µl of normal, heat-inactivated or CFD-depleted human sera, with and without the addition

of 0.05 µg CFD, 0.2 µg proCFD and 0.1 µg HTRA1 wastested. The alternative complement pathway-specific reactive lysis of untreated red blood cells was also tested by mixing 10^8 erythrocytes in DGVB-MgEGTA with 20 µl of normal, heat-inactivated or CFD-depleted human sera, with and without the addition of 1 µg CVF, 0.05 µg CFD, 0.2 µg proCFD and 0.1 µg HTRA1. Reactive lysis was also assessed in 20 µl of sera from CARASIL patients and Japanese controls. Following incubation at 37°C for 1 hour, cells were pelleted by centrifugation, the supernatant transferred to a 96-well ELISA plate *(*Greiner Bio), and the absorbance at 412 nm (or 541 nm for neuraminidase-treated cells) was measured. Background haemolysis (0%) was monitored by incubating erythrocytes in DGVB-MgEGTA buffer only. 100% lysis was achieved by addition of 20 µl of H_2O to 10^8 erythrocytes in DGVB-MgEGTA. The absorbance of the serum dilution was accounted for by correcting for absorbance measured in heat-inactivated serum.

2.4.11 Synthetic peptide assays

2.4.11.1 Protease assay with CFD_Y2H fragment

The CFD_Y2H peptide (PPRGRILGGREAEAHARPYMASVQLNGAHL), obtained from GeneCust, was resuspended in H_2O to a stock concentration of 2 mg/ml. Subsequent dilutions were made in TBS. 0.1 - 1 µg recombinant HTRA1 (wild-type or S328A) was incubated with 20 µM of CFD_Y2H in a 20 µl mixture containing 50 mM Tris-HCl pH 7.5, 150 mM NaCl for 16 h at 37°C. The reaction was terminated by adding 4 x LDS loading buffer and 10 x Reducing Agent and boiling for 5 minutes. Samples were separated under reducing conditions in 12% Bis-Tris gels in 1xMES Buffer and stained with InstantBlue. The degree of cleavage of CFD Y2H peptide by HTRA1 was quantified using ImageQuantTL, expressed as a percentage reduction compared with CFD Y2H peptide incubated with inactive HTRA1±SD in two independent experiments.

2.4.11.2 AMC assay with MCA-peptides

Fluorogenic substrates were synthesised corresponding to the activation peptide (PPRGR-MCA) or the last 5 amino acids of mature CFD (DSVLA-MCA), linked to

a C-terminal MCA moiety (GeneCust). Peptides were resuspended in H_2O to a stock concentration of 2 mg/ml, and subsequently diluted in TBS. Fluorescence measured from an 7-amino-4-methyl coumarin (AMC; Calbiochem) standard curve ranging from 0.049-200 µM was prepared by serial dilution in TBS. The standard curve was used to calculate the amount of free AMC released by cleavage of the synthetic substrates.

The optimal pH for the reaction was determined by incubating the protease and synthetic substrate (20 µM) in TBS, in the pH range 6- 8.5, in a final volume of 50 µl at 37°C for 6-24 hours. Specificity of the assay was validated by comparing the relative fluorescence generated by HTRA1-mediated cleavage of PPRGR-MCA with DSVLA-MCA.

Recombinant HTRA1 (0-200 nM) was incubated in TBS pH 7.5, in a final volume of 50 µl at 37°C with the synthetic substrate (0 - 240 µM). Thrombin, purified from plasma (Sigma), was used as a positive control for the assay in the same concentration range. Fluorescence was monitored at excitation and emission wavelengths of 355 nm and 460 nm using a VICTOR plate reader (PerkinElmer). Non-specific background fluorescence was measured in the absence of enzyme, which was used to calculate AMC release due to protease activity.

Enzyme kinetics were calculated using the Michaelis-Menten equation:

$$V = \frac{V_{\max}[S]}{K_m + [S]}.$$

[S] is substrate concentration, V is reaction rate, V_{max} is the maximum rate achieved at saturating substrate concentration, and K_m (the Michaelis constant) is the [S] at which the reaction rate is half of V_{max}. Kinetic data ($1/V$ and 1/[S]) were used to draw a Lineweaver-Burk plot in Microsoft Excel.

2.5 Statistical analysis

For all analyses, a p-value ≤ 0.05 was considered statistically significant. Unless otherwise noted, statistics were performed using Microsoft Excel software.

2.5.1 Statistical Analysis of *CFD* SNP association and copy number variation

Genotyping, copy number variation and plasma CFD measurements were maintained using SPSS Version 17, a statistical analysis and data management software (SPSS Inc.) used for subsequent analyses.

SNP genotyping was assessed for deviation from Hardy-Weinberg equilibrium in AMD cases and controls using a Chi^2 test. The association of SNPs in CFD with AMD was tested using logistic regression analysis to model the probability of disease occurrence, including known risk factors - age, sex and smoking history - as variables along with SNP genotype in the analyses. Using a dominant genotypic model for regression, SNP genotype was categorised as 0 = major allele homozygote, or 1 = minor allele homozygote or heterozygote. Age was included as a continuous variable. Sex and smoking history (ever/never) were considered as categorical values. Correction for multiple testing was not necessary. Each cohort was analysed individually, and in a combined meta-analysis. Cohorts were also stratified by gender. In these analyses, SNP genotype, age and smoking status were included as variables. Stepwise logistic regression was also performed to investigate interactions between rs3826945 and smoking (ever/never), rs3826945 and age, rs3826945 and sex and rs3826945 and BMI (categorised as <25, 25-29.99, or >30). Odds ratios (OR) and 95% confidence intervals (C.I.) for association were calculated by the software. A Forest plot for OR and 95% confidence intervals for each cohort was constructed using GraphPad Prism 5.

Association of AMD with copy number variation (defined as either deletion or duplication) at the *CFD* locus was evaluated using Fisher's exact test.

2.5.2 Statistical Analysis of plasma CFD

The coefficient of variation (CV; the ratio of the standard deviation σ observed in replicates for the same sample to the mean μ) was used to estimate variation observed between measurements of the same sample to determine inter-assay and intra-assay variability. CV was calculated as follows:

$$CV\ (\%) = (\sigma/\mu) \times 100$$

Normalising for experimental variables which affected assay performance was performed using the following calculation:

Normalised measurement = (*A/B*) actual measurement

A is the mean of the means of the three internal control plasmas measured across all plates (>30). *B* is the mean of the means of the three internal controls obtained from one assay.

The Mann-Whitney *U* Test performed in SPSS was used to assess differences between median values of CFD measured in plasma for AMD cases (GA, CNV and total AMD) and controls. Logistic regression, controlling for age (<65 years of age/ 65-80 years of age, and aged >80 years), gender and smoking (ever/never), was performed to compare the first and fourth quartiles of plasma CFD values in AMD cases and controls, and to calculate ORs and 95% confidence intervals. BMI (<25, 25-29.9, >30) was included as a covariate in analysis of the UK2 cohort.

2.5.3 Statistical Analysis of plasma HTRA1

Assessment of inter- and intra- assay variability, and normalisation of plasma HTRA1 measurements was performed as described for the CFD ELISA. Demographic, genotyping and HTRA1 ELISA data were maintained and analysed using SPSS Version 19. SNP genotyping was assessed for deviation from Hardy-Weinberg equilibrium in AMD cases, in AMD-free individuals and in the combined series using a Chi^2 test. Differences in mean age and BMI between genotype groups were assessed by t-tests. Fisher's exact test was used to assess difference in gender, smoking history and % AMD between genotype groups. Non-parametric tests including the Mann-Whitney U test, Kruskal-Wallis test, median test and test of extreme outliers were used to determine whether altered distribution of raw plasma HTRA1 was associated with genotype (GG or GT/TT), and demographic characteristics including BMI (<25, 25-29.99, >30) and age (<65 years, 65-80 years, >80 years).

The association between each plasma HTRA1 quartile and the risk allele of rs10490924 (GT/TT) was tested using logistic regression, including age and BMI as continuous variables in the analyses. Odds ratios and 95% confidence intervals for

association were also calculated in AMD cases, in AMD-free individuals and in the combined series.

2.5.4 Power calculations

The Genetic Power calculator (http://pngu.mgh.harvard.edu/~purcell/gpc/cc2.html; Purcell et al., 2003) was used to estimate the required number of cases and controls for the well-powered replication of the *CFD* SNP association study, using the effect size observed in the discovery cohort. The probability of detecting an effect of a given size (power) is calculated as 1- β, where β is the probability of a false-negative or type II error. The required level of statistical significance (α, the false-positive or type I error) influences the calculated sample size. Power was calculated for dominant and additive models of AMD-susceptibility related to SNP genotype, accounting for linkage disequilibrium between rs3826945 and rs1683563.

The power to detect a significant difference in plasma CFD between AMD cases and controls, and in plasma HTRA1 between genotype groups was retrospectively assessed using an Altman Nomogram (Figure 2.1) and the standardised difference. Use of the Altman Nomogram requires normally distributed data. The plasma CFD measurements were normalised by log-transformation. The plasma HTRA1 measurements were normalised by cube-root transformation of detectable HTRA1. Transformation was performed in SPSS. Standardised differences were calculated as follows:

Standardised difference = difference in means between groups/standard deviation

The standardised difference was found on the left-hand axis of the Altman Nomogram, and used to determine the required sample size to detect a statistically significance (p=0.05) difference of that magnitude with 80% power (right-hand axis).

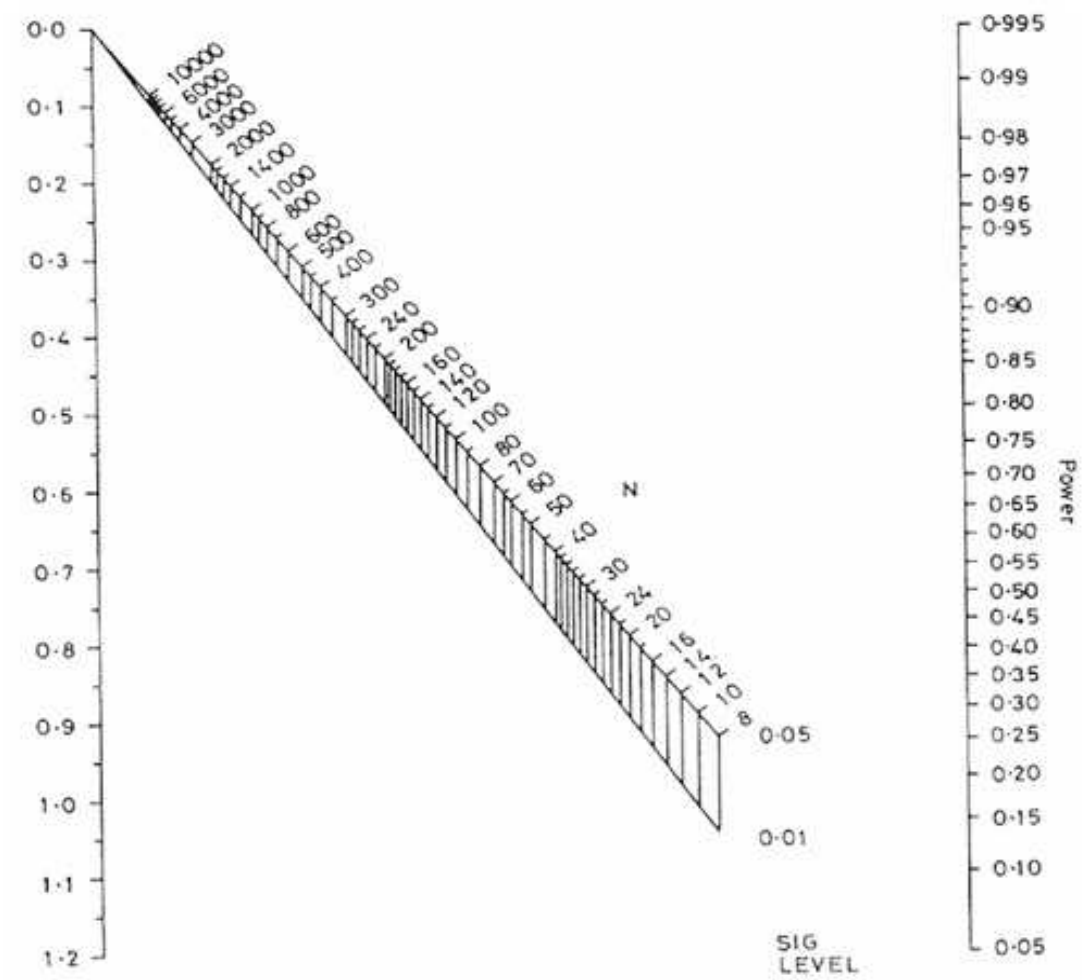

Figure 2.1 Altman Nomogram.

The Altman Nomogram was used to calculate the statistical power of a two-sample study to detect a significant difference in a continuous variable, relating sample size to the standardised difference. Standardised difference is shown on the y-axis at the left-hand side, N= sample size (Altman 1980).

2.6 Bioinformatic analyses

2.6.1 Analysis of Prey Sequences

Analysis of the prey sequences was performed using NCBI BLAST (Basic Local Alignment Search Tool; //blast.ncbi.nlm.nih.gov/Blast.cgi). Nucleotide sequences of the isolated prey DNA were used to search a nucleotide database for sequences of highly significant similarity (BLASTN). Nucleotide sequences were also translated and used to search a protein database (BLASTX) for regions of similarity. Multiple sequences showing significant similarity to the same gene/protein were aligned using ClustalW *(*www.ebi.ac.uk/clustalw/) to identify the minimal sequence required for a positive interaction between bait and prey.

2.6.2 Data-mining for components of the HTRA1 interactome

The Human Protein Reference Database (www.hprd.org) was used to identify previously reported interactions for the proteins identified as putative interactors of HTRA1. A proposed extracellular interactome for HTRA1 was constructed based on these data, and including novel interactors identified in yeast two-hybrid screening or by tandem affinity purification.

3: Chapter 3

Characterising the HTRA1 interactome

3.1 Introduction

An AMD risk locus on chromosomal region 10q26 (chr10q26) spans two genes - *ARMS2* and *HTRA1* - and controversy exists as to whether one or both genes contribute to AMD. The purpose of this study is to investigate the protein interaction network of the serine protease HTRA1 (high temperature requirement A 1), to elucidate its role in AMD pathogenesis.

HTRA1 is a secreted protein expressed in a variety of tissues, but expression appears to be strongest in placenta (Zumbrunn and Trueb 1996; De Luca et al. 2003). In this tissue, HTRA1 is proposed to have a role in extracellular matrix remodelling and trophoblast migration and invasion (Ajayi et al. 2008; Lorenzi et al. 2009).Elsewhere, *HTRA1* expression increases with age (Ly et al. 2000), and degradation of the ECM by HTRA1 has been implicated in arthritis (Grau et al. 2006). In AMD, HTRA1 expressed by the RPE (Yang et al. 2006; Chan et al. 2007), may remodel extracellular matrix proteoglycans in the Bruch's membrane, along with collagenases and matrix metalloproteinases. ECM components, including collagens, interact with HTRA1 *in vitro* and *in vivo* (De Luca et al. 2004; Murwantoko et al. 2004). Other ECM components, including matrix Gla protein and decorin, are degraded by HTRA1 *in vitro* (Canfield et al. 2007). This is further supported by recent work that shows HTRA1 over-expression in mouse RPE results in fragmentation of the Bruch's membrane (Vierkotten et al. 2011). However, it remains unclear how HTRA1 activity contributes to AMD-susceptibility, as these mice do not appear to develop AMD-like features.

This chapter describes work undertaken to identify interacting partners of HTRA1 that may contribute to the development of AMD pathology. A modified method of tandem affinity purification was performed (Puig et al. 2001; Kumar et al. 2004; Gloeckner et al. 2007). Additionally, a yeast two-hybrid screen using full-length human HTRA1 as bait in a placental cDNA library was undertaken in collaboration with Dr. Elod Kortvely in the laboratory of Professor Marius Ueffing at the Helmholtz Zentrum, Munich. These approaches are complimentary to one another, and greatly expand upon the previously reported interactome of HTRA1.

3.2 Identification of proteins interacting with HTRA1 by yeast two-hybrid screening

To elucidate the role of this secreted serine protease, a yeast two-hybrid screen was performed using full-length human HTRA1 as the bait protein to identify novel interacting proteins. As HTRA1 is expressed highly in the placenta (De Luca et al. 2004), a cDNA library derived from this tissue was utilised in the screen. The principles of the yeast two-hybrid system are shown schematically in Figure 3.1.

The bait construct consisted of the sequence for full-length HTRA1 (active protease) fused to the GAL4 transcription factor DNA-binding domain. Prior to screening for interacting proteins, auto-activation of the bait plasmid was assessed by co-transformation with HTRA1 and the empty prey plasmid (pACT2 AD_GAL4_2.1/DEST). The pACT2 AD_GAL4_2.1/DEST is a Gateway-cassette modified version of the pACT2 vector (Clontech), created by Dr. Elod Kortvely, and subsequently referred to as pACT2. After 2 weeks, no yeast cells grew on triple dropout medium (-tryptophan, leucine, histidine; -WLH), indicating auto-activation did not occur.

Cell-to-cell mating of yeast containing the bait plasmid to the placental cDNA library was performed. Diploid cells in which there was a positive interaction between bait and prey grew on selective media lacking tryptophan, leucine, histidine and adenine (-WLHA). Of the 480 colonies which grew on selective medium (-WHLA), 389 clones were successfully isolated from yeast. The sequences recovered identified 64 proteins as potential interactors of HTRA1, of which the majority were extracellular (Figure 3.2). Table 3.1 shows the interacting proteins for which multiple clones were identified, and their cellular localisation. Potential interactors for which a single positive clone was isolated are shown in Table 3.2.

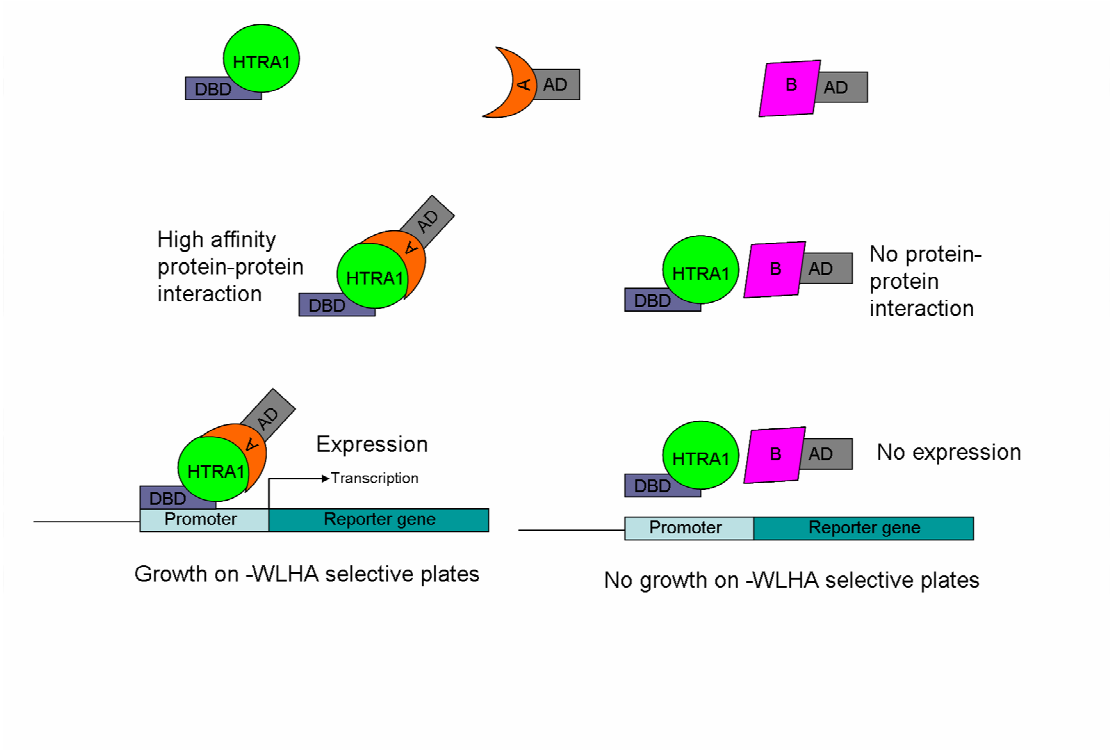

Figure 3.1 GAL4-based yeast two-hybrid screening.
Yeast two-hybrid screening was utilised to identify interactions between HTRA1 and proteins expressed in the human placenta. HTRA1 was fused to the GAL4 transcription factor DNA-binding domain (DBD) to create a bait plasmid. Placental cDNAs were expressed as a fusion protein with the GAL4 activation domain (AD). When the HTRA1 bait and placental cDNA library fusion proteins interact (HTRA1 and A), the proximity of DBD and AD activates transcription of the reporter genes; *HIS3*, *ADE2*, *lacZ* and *MEL1* are used for selection of positive clones. If two proteins do not interact (HTRA1 and B), there is no expression of the reporter gene. In this assay, *ADE2* and *HIS3* reporters were used for stringent selection of positive clones by nutritional selection on -WHLA media.

Potential interactor	Gene name	Number of clones	Cellular localisation	Molecular Function	Biological process
Chorionic somatomammotropin hormone 1	CSH1	127	Extracellular	Peptide hormone	Cell communication; signal transduction
Collagen, type III, alpha 1	COL3A1	100	Extracellular	Extracellular matrix structural constituent	Cell growth and/or maintenance
Collagen, type I, alpha 1	COL1A1	12	Extracellular	Extracellular matrix structural constituent	Cell growth and/or maintenance
Telomeric repeat binding factor (NIMA-interacting) 1	TERF1	9	Nucleus	Inhibitor of telomerase	Regulation of nucleic acid metabolism
ADAM metallopeptidase domain 12 (meltrin alpha)	ADAM12	9	Plasma membrane	Metallopeptidase activity	Protein metabolism
Eukaryotic translation initiation factor 3, subunit F	EIF3F	8	Cytosol (Ribosome)	Translation initiation factor activity	Protein metabolism
HLA-B associated transcript 3	BAT3	8	Nucleus	Molecular function unknown (apoptosis)	Apoptosis
CutC copper transporter homolog (E. coli)	CUTC	6	Nucleolus	Copper homeostasis	Unknown
Tuberous sclerosis 2	TSC2	6	Cytoplasm/Membrane	GTPase activator activity	Cell communication; signal transduction
Fibulin 1	FBLN1	5	Extracellular	Extracellular matrix structural constituent	Cell growth and/or maintenance
Solute carrier family 2 (facilitated glucose transporter) 1	SLC2A1	5	Plasma membrane	Auxiliary transport protein activity	Transport
Connective tissue growth factor	CTGF	4	Extracellular	Extracellular matrix structural constituent	Cell growth and/or maintenance
Follistatin-like 3	FSTL3	4	Extracellular	Extracellular matrix structural constituent	Unknown
Growth differentiation factor 15	GDF15	4	Extracellular	Growth factor activity	Cell communication; signal transduction
Wilms tumor 1 interacting protein	WTIP	4	Nucleus	Transcription regulator	Regulation of gene expression, epigenetic
Pleckstrin homology-like domain, family B, member 3	PHLDB3	4	Unknown	Unknown	Unknown
Collagen, type V, alpha 2	COL5A2	3	Extracellular	Extracellular matrix structural constituent	Cell growth and/or maintenance
Secreted protein, acidic, cysteine-rich (osteonectin)	SPARC	3	Extracellular	Extracellular matrix structural constituent	Cell growth and/or maintenance

Complement factor D	CFD	3	Extracellular	Serine-type peptidase activity	Immune response
Golgi autoantigen, golgin subfamily a, 2	GOLGA2	3	Golgi apparatus	Vesicular transport	Cell growth and/or maintenance
Mitochondrion, complete genome		3	Mitochondria		
Zinc finger and AT hook domain containing	ZFAT	3	Nucleus/Cytoplasm	Transcriptional regulation	Unknown
Protein phosphatase 4, regulatory subunit 1,	PPP4R1	2	Centrosome	Signal transduction	Cell communication; signal transduction
Calcium regulated heat stable protein 1	CARHSP1	2	Cytoplasm	Calcium ion binding	Cell communication; signal transduction
ATG4 autophagy related 4 homolog B (S. cerevisiae)	ATG4B	2	Cytoplasm	Cysteine protease (Autophagy)	Proteolysis
FERM domain containing 4B	FRMD4B	2	Cytoplasm	Insulin receptor signaling	Unknown
Histamine N-methyltransferase	HNMT	2	Cytoplasm	Inactivates histamine by N-methylation	Amino acid metabolism
Eukaryotic translation initiation factor 4A	EIF4A1	2	Cytosol (Ribosome)	Translation initiation	Protein metabolism
Selenoprotein P, plasma, 1,	SEPP1	2	Extracellular	Peroxidase activity	Metabolism; Energy pathways
Flotillin 1	FLOT1	2	Integral to membrane	Unknown	Unknown
Transmembrane protein 87A	TMEM87A	2	Integral to membrane	Unknown	Unknown
Dedicator of cytokinesis 9	DOCK9	2	Intracytoplasmic membrane	Guanine nucleotide-exchange factor	Cell communication; signal transduction
Forkhead box J3	FOXJ3	2	Nucleus	Unknown	Regulation of nucleic acid metabolism
Zinc finger protein 302	ZNF302	2	Nucleus	Transcriptional regulation	Regulation of nucleic acid metabolism
Chromosome 9 open reading frame 97	C9orf97	2	Unknown	Unknown	Unknown

Table 3.1 Potential multi-hit interactors of HTRA1 identified by yeast two-hybrid screening in a placental cDNA library.

Proteins are arranged by the frequency with which they were identified by sequencing of the isolated prey plasmids in a yeast two-hybrid screen. The Human Protein Reference database (www.hprd.org) was used to assign cellular localisation and molecular function to each protein. Extracellular proteins are shaded in orange.

Potential interactor	Gene name	Number of clones	Cellular localisation	Molecular Function	Biological process
A kinase (PRKA) anchor protein 10	AKAP10	1	Mitochondria	Cytoskeletal anchoring activity	Cell communication ; Signal transduction
Absent in melanoma 1-like	AIM1L	1	Unknown	Unknown	Unknown
Ankyrin repeat domain 33	ANKRD33	1	Unknown	Unknown	Unknown
BCL2-like 12 (proline rich)	BCL2L12	1	Cytoplasm	Unknown	Apoptosis
CAP, adenylate cyclase-associated protein, 2	CAP2	1	Plasma membrane	Unknown	Cell communication ; Signal transduction
Centaurin, delta 2	CENTD2	1	Cytoplasm/ Golgi	GTPase activator activity	Cell communication ; Signal transduction
Chromosome 1 open reading frame 172	C1orf172	1	Unknown	Unknown	Unknown
Chromosome 10 open reading frame 10	C10orf10	1	Mitochondria	Unknown	Unknown
C-type lectin domain family 3, member B	CLEC3B	1	Extracellular	Unknown	Unknown
Inhibitor of DNA binding 1, dominant negative helix-loop-helix protein	ID1	1	Nucleus	Inhibitor of DNA binding	Nucleic acid metabolism
Inosine triphosphatase (nucleoside triphosphate pyrophosphatase)	ITPA	1	Cytoplasm	Hydrolase activity	Metabolism ; Energy pathways
Junction plakoglobin	JUP	1	Cytoplasm	Cell adhesion molecule activity	Cell communication ; Signal transduction
Macrophage erythroblast attacher	MAEA	1	Integral to membrane	Cell adhesion molecule activity	Cell adhesion
Mediator complex subunit 12	MED12	1	Nucleus	Transcriptional regulation	Cell communication ; Signal transduction
NADH dehydrogenase (ubiquinone) Fe-S protein 1	NDUFS1	1	Mitochondria	Electron transport	Metabolism ; Energy pathways
Nuclear receptor subfamily 2, group F, member 6	NR2F6	1	Nucleus	Transcription factor	Nucleic acid metabolism
Polymerase (RNA) III (DNA directed) polypeptide F	POLR3F	1	Nucleus	DNA-directed RNA polymerase activity	Nucleic acid metabolism
PRP8 pre-mRNA processing factor 8 homolog (S. cerevisiae)	PRPF8	1	Nucleus	RNA binding	Nucleic acid metabolism
Son of sevenless homolog 2 (Drosophila)	SOS2	1	Cytoplasm	guanine nucleotide exchange factor	Cell communication ; Signal transduction
Spectrin repeat containing, nuclear envelope 2	SYNE2	1	Nucleus/Cytoplasm	Structural constituent of cytoskeleton	Cell growth and/or maintenance
TBC1 domain family, member 12	TBC1D12	1	Intracellular	GTPase activator activity	Cell communication ; Signal transduction

Topoisomerase (DNA) III beta	TOP3B	1	Nucleus	DNA topoisomerase	Nucleic acid metabolism
Transmembrane 7 superfamily member 2	TM7SF2	1	Integral to membrane	Cholesterol biosynthesis	Metabolism ; Energy pathways
Ubiquinol-cytochrome c reductase, Rieske iron-sulfur polypeptide 1	UQCRFS1	1	Mitochondria	Electron transport	Metabolism ; Energy pathways
USP6 N-terminal like	USP6NL	1	Cytoplasm	GTPase activator activity	Cell communication ; Signal transduction
Zinc finger, X-linked, duplicated A	ZXDA	1	Nucleus	Transcription factor	Nucleic acid metabolism

Table 3.2 Potential single-hit interactors of HTRA1 identified by yeast two-hybrid screening in a placental cDNA library.

Proteins identified only once by sequencing of the isolated prey plasmids in a yeast two-hybrid screen. The Human Protein Reference database (www.hprd.org) was used to assign cellular localisation and molecular function to each protein. Extracellular proteins are shaded in orang

3.2.1 HTRA1 interacts with CSH1, a placental lactogen

The most common interaction to be identified was between HTRA1 and the placental lactogen, chorionic somatomammotropin hormone 1 (CSH1; 127 clones). CSH1 is a secreted peptide hormone, which, like HTRA1, is highly expressed in the placenta during the third trimester (Sciarra et al. 1963; De Luca et al. 2004). CSH1 has been postulated to play a role in insulin growth factor (IGF) signalling during pregnancy, influencing fetal growth and metabolism (Handwerger 1991). This is interesting in terms of a role for HTRA1 during development, but the interaction between CSH1 and HTRA1 is unlikely to influence AMD and was not investigated further.

3.2.2 HTRA1 interacts with extracellular matrix components

The majority of interacting proteins identified by yeast two-hybrid are extracellular, including a number of extracellular matrix (ECM) components (Figure 3.2). One of the most common interactions detected is a previously reported interaction with collagen type 3A1 (Table 3.1; (Murwantoko et al. 2004). A representative back-transformation to verify the interaction between COL3A1 and HTRA1 is shown in Figure 3.3. Collagen type 1A1 (COL1A1) and collagen type 5A2 (COL5A2) were also identified as interacting with HTRA1 (Table 3.1), in agreement with a proposed role for HTRA1 in the degradation of collagen-rich extracellular membranes (Murwantoko et al. 2004).

Other proteins found to interact with HTRA1 are also localised to the ECM. Of these, connective tissue growth factor (CTGF), fibulin-1 (FBLN1) follistatin-like 3 and osteonectin, together with the collagens COL1A1, COL3A1 and COL5A2, are all extracellular matrix structural constituents, as defined by the AmiGo Gene Ontology database (amigo.geneontology.org/). C-type lectin domain family 3, member B (also known as tetranectin) is also a secreted protein, found as a component of plasma and the extracellular matrix (Table 3.2). The function of CLEC3B is unknown.

ECM components bind one another, and secreted proteins. An HTRA1 interactome in the extracellular matrix was proposed (Figure 3.8) based on these data

and previously published information (available from the Human Protein Reference Database (Mathivanan et al. 2008); www.hprd.org, accessed January 2009).

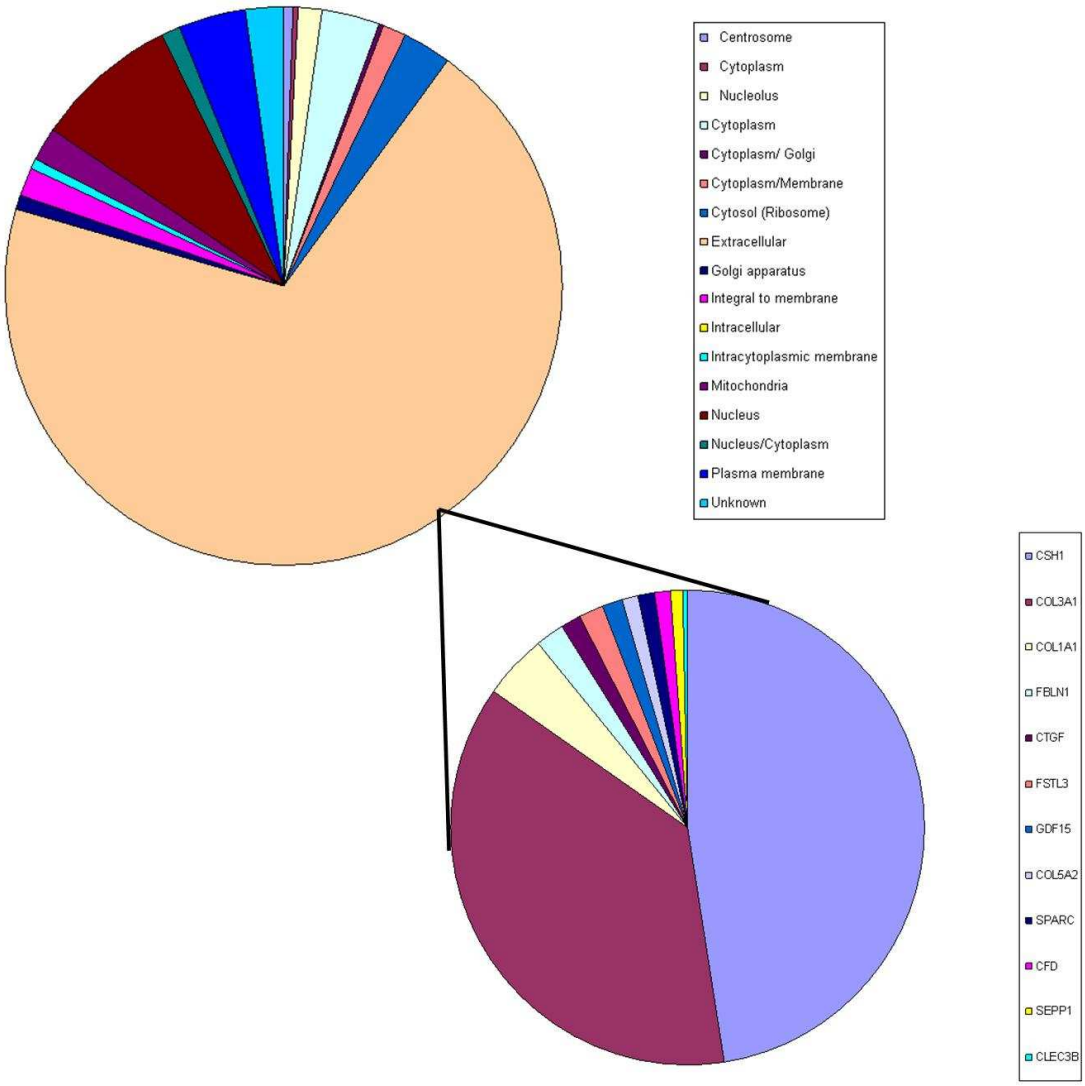

Figure 3.2 Interactors of HTRA1 identified by yeast two-hybrid screening are enriched for extracellular proteins.

The interactors of HTRA1 that were identified by yeast two-hybrid screening in a placental cDNA library were classified according to cellular localisation using the Human Protein Reference Database (www.hprd.org). Extracellular proteins made up the greatest proportion of interactors, accounting for 70% of the 389 positive clones that were screened (upper chart). The most frequently identified extracellular interactors of HTRA1 were a placental lactogen, CSH1, and the extracellular matrix constituent COL3A1 (lower chart).

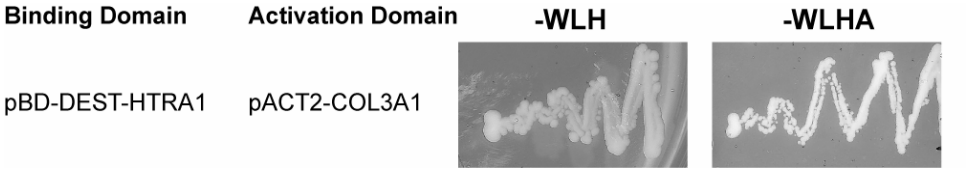

Figure 3.3 COL3A1 interacts with HTRA1 in a yeast two-hybrid screen.

Of the numerous interactors of HTRA1 identified by sequencing of the prey plasmid in an initial yeast two-hybrid screen, several candidates were selected for back-transformation to confirm the interaction. Prey vectors for COL3A1 (pACT2-COL3A1) were co-transformed with the pBD-DEST-HTRA1 bait plasmid into yeast cells. Double transformants were grown on SD-WL plates (under no selection for an interaction). Individual colonies for COL3A1 were subsequently streaked onto selective media of increasing stringency (-WLH and -WLHA) to confirm the interaction. Supplements missing from the SD media are tryptophan (W), leucine (L), histidine (H) and adenine (A). Images and back-transformations were produced by Elod Kortvely.

3.2.3 HTRA1 interacts with proteins involved in angiogenesis, inflammation and scarring

Interactions between HTRA1 and components of the extracellular matrix have previously been reported (De Luca et al. 2004; Murwantoko et al. 2004; Canfield et al. 2007; An et al. 2010). In addition to these, several novel interactors with potential relevance to the development and progression of AMD were identified by yeast two-hybrid screening.

3.2.3.1 An interaction between HTRA1 and Complement Factor D (CFD)

CFD was identified as a potential interactor of HTRA1 in the yeast two-hybrid screen (Table 3.1, Figure 3.8). This links the alternative complement pathway - known to be dysregulated in AMD - and HTRA1, and was considered an attractive candidate for further study. Additional work to characterise the functional relevance of an interaction between HTRA1 and CFD is described in Chapter 5.

3.2.3.2 An interaction between HTRA1 and Connective Tissue Growth Factor (CTGF)

CTGF was identified as a potential interactor of HTRA1 in the yeast two-hybrid screen (Table 3.1, Figure 3.8. Four *CTGF* clone sequences were aligned to the human full-length *CTGF* cDNA reference sequence (NM_001901.2), using ClustalW *(*www.ebi.ac.uk/clustalw/). Although three clones contained the complete *CTGF* cDNA sequence, one clone contained only 477 nucleotides of the cDNA sequence (data not shown). This defined the minimal sequence required for a positive interaction between the active HTRA1 bait and CTGF prey sequences as spanning the first 159 amino acids of CTGF, including the Insulin growth factor-binding protein (IGFBP) and von Willebrand factor (vWF) type C domains, shown schematically in Figure 3.15A.

3.3 Tandem Affinity Purification of HTRA1 and interacting proteins

To identify proteins which interact with HTRA1 in a native, functional state, a fusion protein of HTRA1, tagged at the C-terminal end with the tandem affinity purification tag (CTAP), was expressed in HEK293T cells and in hTERT-RPE1 cells. The TAP procedure is shown schematically in Figure 3.4.

3.3.1 Tandem Affinity purification of HTRA1 in HEK293T cells

HEK293T cells are a transformed human embryonic kidney cell-line, which can be readily transfected. Endogenous HTRA1 is present in HEK293T cells, as demonstrated by the detection of an immunoreactive band of ~51 kDa when untransfected HEK293T cell lysate is subjected to Western blotting with an anti-HTRA1 antibody (Figure 3.5, lane 1). HEK293T cells were transfected with a construct encoding HTRA1 with a C-terminal TAP tag or with a corresponding empty vector (EV). 48-72 hours post transfection, cell lysates and concentrated conditioned media were subjected to tandem affinity purification (TAP). The TAP procedure is shown schematically in Figure 3.4.

Western blotting analysis, using antibodies against the FLAG tag, show that both HTRA1-CTAP (~57 kDa) secreted into the media from the transfected HEK293T cells and intracellular HTRA1-CTAP was successfully purified using TAP (Figure 3.5). Whole eluates were analysed by liquid chromatography coupled with tandem mass spectrometry (LC-MS/MS). This was performed by Karsten Boldt at the Helmholtz Zentrum in Munich.

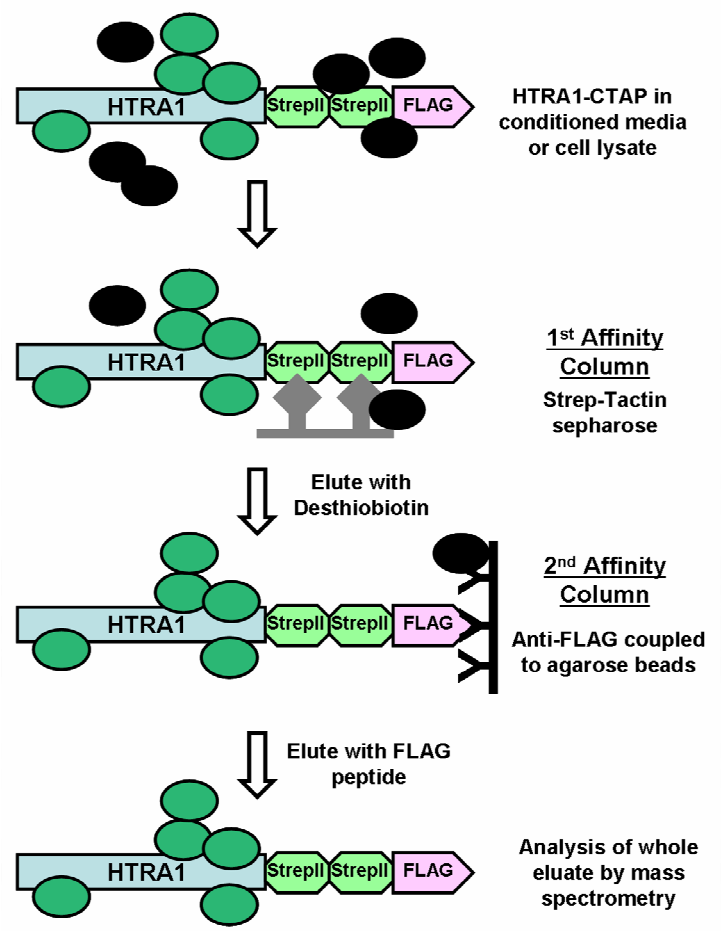

Figure 3.4 Tandem Affinity Purification of HTRA1.
An overview of the TAP procedure, using a C-terminally tagged form of full-length HTRA1 (HTRA1-CTAP). Mass spectrometry was used to identify interactors of HTRA1 in the whole eluate following purification of the tagged protein from the conditioned media and cell lysates of HEK293T and RPE1 cells. HTRA1-interacting proteins are indicated in green; proteins that bind non-specifically to the tags and resin are shown in black.

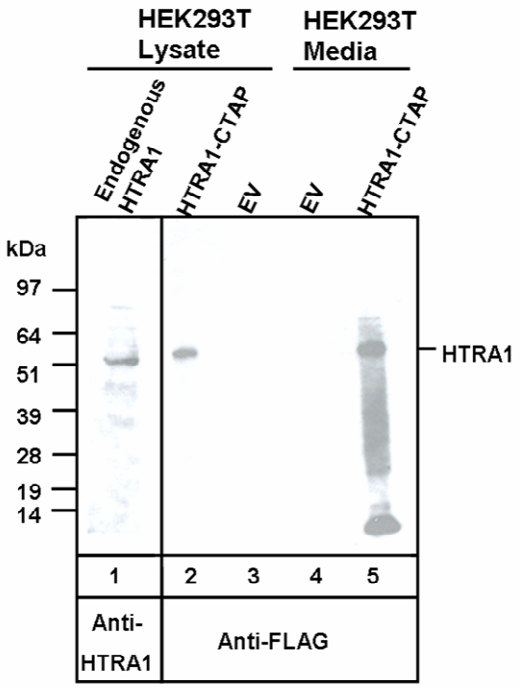

Figure 3.5 HEK293T cells transfected with HTRA1-CTAP express tagged-HTRA1.

HEK293T cells endogenously express HTRA1 (lane 1). HEK293T cells were transfected with the HTRA1-CTAP construct for use in tandem affinity purification. Expression of the tagged HTRA1 construct was verified by Western blotting of cell lysate and conditioned media from transfected cells, probed with anti-FLAG antibody to detect FLAG-tagged HTRA1. HTRA1-CTAP was detected in both cell lysate (lane 2), and more abundantly, in conditioned media of transfected cells (lane 5). The CTAP FLAG and Strep2 tag adds approximately 6 kDa to the molecular weight of HTRA1. The FLAG peptide (1 kDa) produced by HEK293T cells which were transfected with the empty vector EV was not detected by Western blotting.

3.3.2 Tandem Affinity purification of HTRA1 in hTERT RPE1 cells

Dysfunction and cell death of retinal pigment epithelial (RPE) cells is considered to have an important role in the pathogenesis of AMD. For this reason, proteins interacting with HTRA1 in the physiologically relevant cell line hTERT-RPE1 were also investigated.

3.3.2.1 Optimisation of microporation conditions for transfection of hTERT-RPE1

Parameters for the transfection of the hTERT-RPE1 cell line using microporation had not previously been described. Therefore, the optimal conditions for high transfection efficiency and cell viability were determined in a series of experiments.

3.3.2.1.1 Assessment of transfection efficiency and cell viability in 24-well plates

$1x10^5$ cells/well of a 24-well plate were subjected to microporation using the MP-100 (Digital Bio), with 0.5 µg pmaxGFP plasmid DNA in a 10 µl gold tip. A range of pulse voltages, pulse widths and pulse number were tested to determine microporation parameters with optimal transfection efficiency and cell viability (Table 3.3).

After 24 hours of growth at 37^{o}C, transfection efficiency was determined by assessing the proportion of GFP-positive cells. Viability was assessed by comparison to cells which were not microporated. The optimal parameters for microporation, producing cell viability comparable to untransfected cells and transfection efficiency >75% of viable cells, were 1500 Volts/ 20 ms pulse/ 1 pulse and 1600 Volts/ 20 ms pulse/ 1 pulse.

Table 3.3 Optimisation of microporation parameters for the transfection of RPE1 cells.

$1x10^5$ cells/well of a 24-well plate were subjected to microporation with 0.5 µg pmaxGFP in a 10 µl gold tip using a range of pulse voltages, pulse widths and pulse number. Transfection efficiency was determined 24 hours post-microporation by assessing the proportion of GFP-positive cells. For cell viability, +++ is cell viability comparable to untransfected cells; ++ is cell viability less than 80% of untransfected cells and + is cell viability less than 50% of untransfected cells. For transfection efficiency, +++ indicates that more than 75% of viable cells are transfected, ++ indicates between 50-75% of viable cells are transfected, and + indicates that less than 50% of viable cells are transfected.

	Microporation parameters			Results	
Well	Pulse voltage	Pulse width (ms)	Pulse number	Cell viability	Transfection efficiency
1	Control without microporation			+++	-
2	1400	20	1	++	+++
3	1500	20	1	+++	+++
4	1600	20	1	+++	+++
5	1700	20	1	+++	++
6	1100	30	1	+++	+
7	1200	30	1	+++	+
8	1300	30	1	+++	++
9	1400	30	1	++	++
10	1000	40	1	+++	+
11	1100	40	1	+++	+
12	1200	40	1	+++	+
13	1100	20	2	+++	+
14	1200	20	2	+++	++
15	1300	20	2	+++	++
16	1400	20	2	++	++
17	900	30	2	+++	+
18	1000	30	2	++	+
19	1100	30	2	++	++
20	1200	30	2	+++	++
21	1300	10	3	+++	++
22	1400	10	3	+++	++
23	1500	10	3	++	++
24	1600	10	3	+	++

3.3.2.1.2 Assessment of transfection efficiency and cell viability in 14 cm plates

The microporation parameters which gave high transfection efficiency and high levels of cell viability in a small-scale microporation reaction (Table 3.3) were tested in large-scale reactions for use in 14 cm plates.

5 x 10^6 RPE1 cells were mixed with 5 µg of the pmaxGFP construct. Microporation was performed using the MP-100 (Digital Bio) with 100 µl tips and Buffer E2 electrode buffer. Transfection efficiency and cell viability were confirmed by fluorescence microscopy 24 hours post transfection. As shown in Figure 3.6, the conditions which gave optimal transfection efficiency were 1500 Volts for one pulse of 20 ms duration.

Subsequent transfection of RPE1 cells was performed using these parameters. Each 14 cm plate was seeded with 10x 10^6 cells microporated with 10 µg DNA. Transfected cells were grown at 37°C for 48-72 hours before collection of conditioned media and cell lysates.

3.3.2.2 Identification of interacting proteins of HTRA1 by TAP in hTERT-RPE1

Endogenous HTRA1 was detected in the conditioned media of untransfected RPE1 cells (Figure 3.7). This is consistent with reports of HTRA1 expression in primary human RPE cells (Yang et al. 2006; An et al. 2010). RPE1 cells were transfected with a construct encoding HTRA1-CTAP or with a corresponding empty vector (EV). Cell lysates and concentrated conditioned media were collected 48-72 hours after transfection, and subjected to TAP. Immunoblotting, using antibodies against the FLAG tag, show that HTRA1-CTAP (~57 kDa) is secreted into the media from the transfected RPE1 cells. Secreted HTRA1-CTAP and intracellular HTRA1-CTAP were successfully purified by TAP and were identified, along with putative interactors, in the whole eluates analysed by LC-MS/MS.

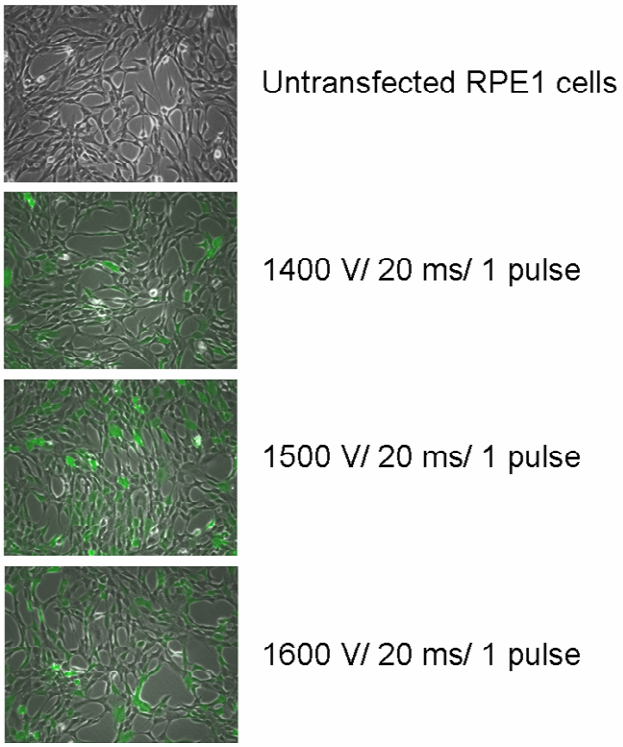

Figure 3.6 Optimised microporation parameters for transfection of RPE1 cells.

Transfection reactions were scaled-up for $5x10^6$ RPE1 cells in a 14cm cell culture dish, using 5 µg pmaxGFP in a 100 µl gold tip. Three microporation parameters, found to give high cell viability and transfection efficiencies in small-scale 24-well plate transfection were tested to determine microporation parameters with optimal transfection efficiency and cell viability for larger scale reactions. After 24 hours of growth at 37°C, transfection efficiency was determined by assessing the proportion of GFP-positive cells. Viability was assessed by comparison to cells which were not subjected to microporation. The greatest cell survival and highest transfection efficiency was obtained by microporating the cells at 1500 Volts for one pulse of 20 ms duration.

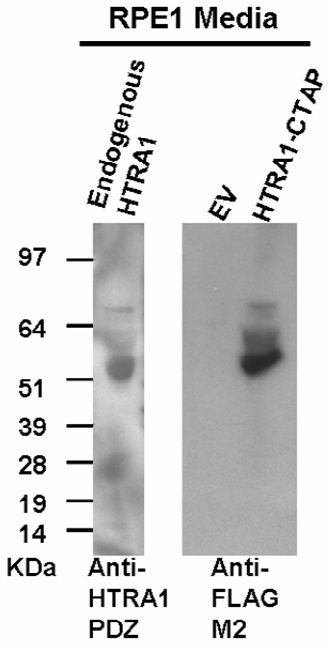

Figure 3.7 RPE1 cells transfected with HTRA1-CTAP express tagged-HTRA1.

RPE1 cells endogenously express HTRA1. RPE1 cells were transfected with the HTRA1-CTAP construct for use in tandem affinity purification. Expression of the tagged HTRA1 construct was verified by Western blotting of conditioned media from transfected cells, probed with anti-FLAG antibody to detect FLAG-tagged HTRA1. The CTAP FLAG and Strep2 tag adds approximately 6 kDa to the molecular weight of HTRA1. The identities of the higher molecular weight bands are unknown. The FLAG peptide (1 kDa) produced by HEK293T cells which were transfected with the empty vector (EV) was not detected by Western blotting.

3.3.3 Interactors of HTRA1 identified by TAP

Proteins which bind non-specifically to the affinity resins or to the TAP tag in conditioned media and cell lysate were identified by mass spectrometry analysis of the empty vector control (data not shown). Proteins that interact specifically with HTRA1 (or the binding partners of HTRA1, in the case of indirect interactions) in the extracellular environment in three separate TAP experiments are shown in Table 3.4. Table 3.5 contains the HTRA1 binding partners with a primarily intracellular localisation, also in three experiments. Cellular localisation, molecular function and biological process for each protein were obtained by data-mining in the Human Protein Reference Database (www.hprd.org, accessed January and February 2009).

3.3.3.1 ECM structural constituents interact with HTRA1

Extracellular proteins were enriched in the interactome identified by TAP in conditioned media. Of these proteins, collagen 12A1, laminin alpha 4, tenascin, agrin, fibronectin-1, thrombospondin-1 and connective tissue growth factor have a structural role in the ECM (Table 3.4). Only fibronectin was identified as a potential interactor of HTRA1 in multiple TAP experiments (performed in media from HEK293T cells). Connective tissue growth factor was identified as a binding partner of HTRA1 in only one of the TAP experiments (performed in HEK293T cells), but was also identified by yeast two-hybrid screening.

3.3.3.2 Protease inhibitors interact with HTRA1

Four protease inhibitors were found to interact with the serine protease HTRA1 extracellularly. Serpin B3 and Serpin B12 were detected only in TAP performed in HEK293T cells. Serpin C1 was detected as an interactor only in RPE1 cells. Alpha-2-macroglobulin was detected in TAP experiments performed in both HEK293T cells and in RPE1 cells (Table 3.4), reflecting a previously reported interaction (An et al. 2010). Whether these various protease inhibitors represent a tissue-specific method of regulating HTRA1, or simply reflect over-expression of an active protease is unknown.

Protein Name	Gene Name	Cellular localisation	Molecular Function	Biological Process	TAP 1 (HEK293T)	TAP 2 (HEK293T)	TAP3 (RPE1)
Alpha-2-macroglobulin	A2M	Extracellular	Protease inhibitor activity	Protein metabolism	Y		Y
Cochlin precursor	COCH	Extracellular	Unknown	Unknown	Y		
Collagen alpha-1(XII) chain	COL12A1	Extracellular	Extracellular matrix structural constituent	Cell growth and/or maintenance			Y
Thrombospondin-1	THBS1	Extracellular	Extracellular matrix structural constituent	Cell growth and/or maintenance	Y		Y
Uncharacterized protein ENSP00000332963	FOLR4	Extracellular	Unknown	Unknown		Y	
Agrin	AGRN	Extracellular	Extracellular matrix structural constituent	Cell growth and/or maintenance			Y
Antithrombin-III	SERPINC1	Extracellular	Protease inhibitor activity	Protein metabolism			Y
Complement C3	C3	Extracellular	Complement activity	Immune response		Y	Y
Connective tissue growth factor	CTGF	Extracellular	Extracellular matrix structural constituent	Cell growth and/or maintenance		Y	
Fibronectin precursor	FN1	Extracellular	Extracellular matrix structural constituent	Cell growth and/or maintenance	Y	Y	
Hemoglobin alpha 1-2 hybrid	HBA1	Extracellular	Transporter activity	Transport			Y
Hemoglobin subunit beta	HBB	Extracellular	Transporter activity	Transport		Y	
Hemoglobin subunit delta	HBD	Extracellular	Transporter activity	Transport			Y
Isoform 2 of Serum albumin	ALB	Extracellular	Transporter activity	Transport			Y
Lactoferroxin C	LTF	Extracellular	Transporter activity	Transport			Y
Laminin subunit alpha-4	LAMA4	Extracellular	Cell adhesion molecule activity	Cell growth and/or maintenance			Y

Lysozyme g-like protein 1	LYG1	Extracellular	Unknown	Unknown		Y
Tenascin	TNC	Extracellular	Extracellular matrix structural constituent	Cell communication; Signal transduction		Y
Serpin B12	SERPINB12	Extracellular/ Cytoplasm	Protease inhibitor activity	Protein metabolism	Y	
Serpin B3	SERPINB3	Extracellular/ Cytoplasm	Protease inhibitor activity	Protein metabolism	Y	
Stem cell growth factor	CLEC11A	Extracellular/ Cytoplasm	Stimulates proliferation and differentiation	Cell communication; Signal transduction	Y	

Table 3.4 Extracellular interactors of HTRA1 identified by tandem affinity purification.
Proteins identified by LC-MS/MS analysis in the eluates of tandem affinity purification of HTRA1-CTAP from the cell lysates and conditioned media of either HEK293T or RPE1 cells. The Human Protein Reference Database was used to assign cellular localisation and molecular function to each protein.

Protein Name	Gene Name	Cellular localisation	Molecular Function	Biological Process	TAP 1 (HEK293T)	TAP 2 (HEK293T)	TAP3 (RPE1)
Acetyl-CoA carboxylase 1	ACACA	Cytoplasm	Ligase activity	Metabolism; Energy pathways		Y	Y
S100-A8	S100A8	Cytoplasm	Calcium ion binding	Cell communication; Signal transduction	Y		
Cytoplasmic dynein 1 heavy chain 1	DYNC1H1	Cytoplasm	ATPase activity	Metabolism; Energy pathways			Y
Heat shock 70 kDa protein 1	HSPA1A	Cytoplasm	Chaperone activity	Protein metabolism		Y	
Neutrophil defensin 1	DEFA1	Cytoplasm	Defense/immunity protein activity	Immune response		Y	
Protein S100-A7	S100A7	Cytoplasm	Calcium ion binding	Cell communication; Signal transduction		Y	
Titin	TTN	Cytoplasm	Structural molecule activity	Muscle contraction		Y	Y
Beta-actin-like protein 2	ACTBL2	Cytoplasm/Cytoskeleton	Unknown	Unknown			Y
Keratinocyte proline-rich protein	KPRP	Cytoplasm/Cytoskeleton	Unknown	Cell differentiation			Y
Tubulin alpha-1A chain	TUBA1A	Cytoplasm/Cytoskeleton	Structural constituent of cytoskeleton	Cell growth and/or maintenance		Y	
Dimethylaniline monooxygenase [N-oxide-forming] 3	FMO3	Endoplasmic reticulum	Catalytic activity	Drug metabolism			Y
78 kDa glucose-regulated protein precursor	GRP 78	Endoplasmic reticulum	Chaperone activity	Protein metabolism	Y	Y	
Tumor rejection antigen 1	HSP90B1	Endoplasmic reticulum	Heat shock protein activity	Protein metabolism		Y	

Transmembrane emp24 domain-containing protein 9	TMED9	Endoplasmic reticulum	Unknown	Unknown		Y	
Transmembrane emp24 domain-containing protein 10	TMED10	Golgi apparatus membrane	Transporter activity	Transport	Y		
Transmembrane emp24 domain-containing protein 2	TMED2	Golgi apparatus membrane	Transporter activity	Transport	Y		
C-type lectin domain family 7 member A	CLEC7A	Integral to membrane	Unknown	Unknown		Y	
Desmoglein-1	DSG1	Integral to membrane	Cell adhesion molecule activity	Cell growth and/or maintenance			Y
Olfactory receptor 52E6	OR52E6	Integral to membrane	G-protein coupled receptor activity	Cell communication; Signal transduction		Y	
Roundabout homolog 2 precursor	ROBO2	Integral to membrane	Receptor activity	Signal transduction		Y	
Astrotactin 2	ASTN2	Integral to membrane	Unknown	Unknown		Y	
Transmembrane protein 26	TMEM26	Integral to membrane	Unknown	Unknown		Y	
Protein dispatched homolog 2	DISP2	Membrane	Unknown	Cell communication; Signal transduction			Y
Cytochrome b	CYTB	Mitochondrion	Oxidoreductase activity	Metabolism; Energy pathways		Y	
Trifunctional enzyme subunit beta, mitochondrial	HADHB	Mitochondrion	Catalytic activity	Metabolism; Energy pathways		Y	
ATP synthase subunit beta, mitochondrial	ATP5B	Mitochondrion	Transporter activity	Metabolism; Energy pathways		Y	
Trifunctional enzyme subunit alpha, mitochondrial	HADHA	Mitochondrion	Catalytic activity	Metabolism; Energy pathways	Y	Y	

Nucleoporin	TMEM48	Nuclear membrane	Structural constituent of nuclear pore	Protein transport			Y	
Heat shock cognate 71 kDa protein	HSPA8	Nucleolus	Heat shock protein activity	Protein metabolism			Y	
Coiled-coil domain-containing protein 48	CCDC48	Nucleus	Unknown	Unknown			Y	
General transcription factor II-I	GTF2I	Nucleus	Transcription factor activity	Regulation of nucleic acid metabolism	Y			
Methylcytosine dioxygenase TET1	TET1	Nucleus	DNA binding	Regulation of nucleic acid metabolism				Y
Probable histone-lysine N-methyltransferase ASH1L	ASH1L	Nucleus	Transcription factor activity	Regulation of nucleic acid metabolism			Y	
Ribonucleases P/MRP protein subunit POP1	POP1	Nucleus	RNA processing	Regulation of nucleic acid metabolism				
RNA-binding protein Raly	RALY	Nucleus	RNA binding	Regulation of nucleic acid metabolism			Y	
Cell cycle checkpoint protein RAD17	RAD17	Nucleus	Unknown	Regulation of cell cycle			Y	
Chromodomain-helicase-DNA-binding protein 3	CHD3	Nucleus	DNA binding	Regulation of nucleic acid metabolism				Y
Component of gems 4	GEMIN4	Nucleus	Unknown	Reproductive behavior			Y	
Disrupted in schizophrenia 1 protein	DISC1	Nucleus	Unknown	Unknown			Y	
Exportin-2	CSE1L	Nucleus	Transporter activity	Transport			Y	
Lamin-A/C	LMNA	Nucleus	Signal transducer activity	Cell growth and/or maintenance				Y

Activin receptor type-2A precursor	ACVR2A	Plasma membrane	Receptor signaling protein serine/threonine kinase activity	Cell communication; Signal transduction		Y	
B(0,+)-type amino acid transporter 1	SLC7A9	Plasma membrane	Auxiliary transport protein activity	Transport		Y	
Ephexin-1	NGEF	Plasma membrane	Guanyl-nucleotide exchange factor activity	Cell communication; Signal transduction		Y	
Ephrin-A5	EFNA5	Plasma membrane	Receptor binding	Cell communication; Signal transduction			Y
Free fatty acid receptor 2	FFAR2	Plasma membrane	G-protein coupled receptor activity	Cell communication; Signal transduction		Y	
Leukotriene C4 synthase	LTC4S	Plasma membrane	Glutathione transferase activity	Metabolism; Energy pathways		Y	
Plasma membrane calcium-transporting ATPase 3	ATP2B3	Plasma membrane	Transporter activity	Transport		Y	
Protocadherin alpha 10 precursor	PCDHA10	Plasma membrane	Cell adhesion molecule activity	Cell growth and/or maintenance		Y	
Vascular endothelial growth factor receptor 2	VEGFR-2	Plasma membrane	Tyrosine kinase activity	Cell communication; Signal transduction		Y	
Double-strand-break repair protein rad21-like protein 1	RAD21L1	Unknown	Unknown	Unknown		Y	
NGFRAP1 like 1	BEX5	Unknown	Unknown	Unknown	Y		
Tetratricopeptide repeat protein 21B	TTC21B	Unknown	Unknown	Unknown		Y	

Table 3.5 Potential intracellular interactors of HTRA1 identified by tandem affinity purification.
Proteins identified by LC-MS/MS analysis in the eluates of tandem affinity purification of HTRA1-CTAP from the cell lysates and conditioned media of either HEK293T or RPE1 cells. The Human Protein Reference Database was used to assign cellular localisation and molecular function to each protein.

3.3.3.3 Complement component C3 is a potential interactor of HTRA1

In addition to the extracellular matrix proteins identified by TAP, complement C3 was detected as an interacting partner in TAP experiments performed in both HEK293T and RPE1 cells (Table 3.4). C3 is an extracellular protein with an important role in complement activity, and genetic variants of the *C3* gene have been shown to confer increased susceptibility to AMD (Yates et al. 2007).

3.3.3.4 Intracellular interactors of HTRA1

Although HTRA1 is a secreted protein, the protease has been proposed to play a role in intracellular signalling pathways. Potential intracellular binding partners of HTRA1 that were identified using TAP are shown in Table 3.5.

3.3.3.4.1 Membrane proteins

Proteins that are localised to the plasma membrane, or are integral components of the plasma membrane, were detected by mass spectrometry of the TAP eluates (Table 3.5). Of these, the vascular endothelial growth factor receptor 2 (VEGFR2) may be of interest due to the previous association of VEGF with AMD.

A largely uncharacterised family of integral membrane proteins is represented multiple times as interacting with HTRA1 in TAP eluates - the emp24 domain containing proteins 2, 9 and 10 (Table 3.5). Despite only being detected in HEK293T cells, the detection of more than one member of this family of proteins may indicate a significant biological role for HTRA1 in relation to emp24 domain-containing proteins. These proteins are relatively uncharacterised, but may have a transporter function.

3.3.3.4.2 Chaperone proteins

Chaperone proteins (as determined by GO ontology terms) feature strongly in the list of potential intracellular interactors of HTRA1 identified by TAP (Table 3.5). These

include the 78 kDa glucose regulated protein (GRP78), heat shock cognate 71 kDa protein (HSPA8), and heat shock 70 kDa protein 1 (HSPA1A). This may be a consequence of over-expression of HTRA1 in cell culture, or may reflect the role of HTRA1 as a stress-responsive protein which may function as a chaperone (Runyon et al. 2007).

3.3.3.4.3 Cytoskeleton proteins

Intracellular proteins which are localised to the cytoskeleton were identified as interactors of HTRA1 in the TAP experiments (Table 3.5). Of these, Beta-actin-like protein 2 (ACTBL2) and Keratinocyte proline-rich protein (KPRP) have an unknown function within the cell. Tubulin alpha-1A is a structural constituent of the cytoskeleton, and has been previously reported as an interactor and substrate for HTRA1 (Chien et al. 2009a; Chien et al. 2009b; Campioni et al. 2011). Tubulins are also components of drusen and amyloid plaques, characteristic of AMD and Alzheimer's disease respectively (Booij et al. 2010).

3.3.3.4.4 Mitochondrial proteins

AMD has been proposed as a disease of mitochondrial dysfunction; HTRA1 is shown to interact with several proteins that are localised to the mitochondria (Table 3.5). The alpha and beta subunits of the trifunctional enzyme acetyl-CoA acyltransferase were detected. Although the alpha subunit was detected in both of the TAP experiments performed in HEK293T cells, the trifunctional enzyme has no obvious connection to the AMD phenotype, playing a catalytic role in the β-oxidation of long chain fatty acids in the mitochondria. Cytochrome b is a component of the respiratory chain complex III, and as has a role in electron transfer and ATP generation. The electron transfer chain is a key source of free-radical superoxide ions and cause of oxidative stress, which is thought to contribute to AMD (Hollyfield et al. 2008). The beta subunit of ATP synthase, the final component of the mitochondrial electron transport chain, was also detected in the analysis of the TAP eluate. The physiological relevance of these interactions is unclear as HTRA1 is not reported to be localised to the mitochondria.

3.3.3.4.5 Proteins with a role in innate immunity

Proteins with a role in pro-inflammatory processes and the innate immune response were identified as interactors of HTRA1 in TAP experiments. Neutrophil defensin-1, DEFA1, is an alpha-defensin with anti-microbial properties and was identified as an interactor of HTRA1 in an experiment performed in HEK293T cells. S100A7 and S100A8 were also identified as interactors of HTRA1 in HEK293T cells. These are calcium-binding proteins, with a suggested role in pro-inflammatory processes. S100A8 is elevated in the macular region of AMD eyes (Yuan et al. 2010).

3.4 A proposed extracellular interactome for HTRA1

A large number of potential interactors of HTRA1 were identified by the yeast two-hybrid screening and TAP. The focus of this study was on extracellular interactors of HTRA1 with a possible role in AMD. The cellular localisation of the putative interactors was used to filter proteins with a primarily extracellular localisation. A proposed extracellular HTRA1 interactome was constructed, incorporating these data and previously reported interactions from HPRD, STRING and NCBI PubMed databases. The interaction network for HTRA1 is shown in Figure 3.8. This reinforces the overlap between these data and previously reported HTRA1-interactors (for example, with COL1A1, COL3A1, fibronectin, and indirectly with TGF-β). Novel interactions were also identified (Figure 3.8). These suggest roles for HTRA1 in angiogenesis, fibrovascular scarring, inflammation and the alternative complement pathway (C3 and CFD), in addition to extracellular matrix remodelling.

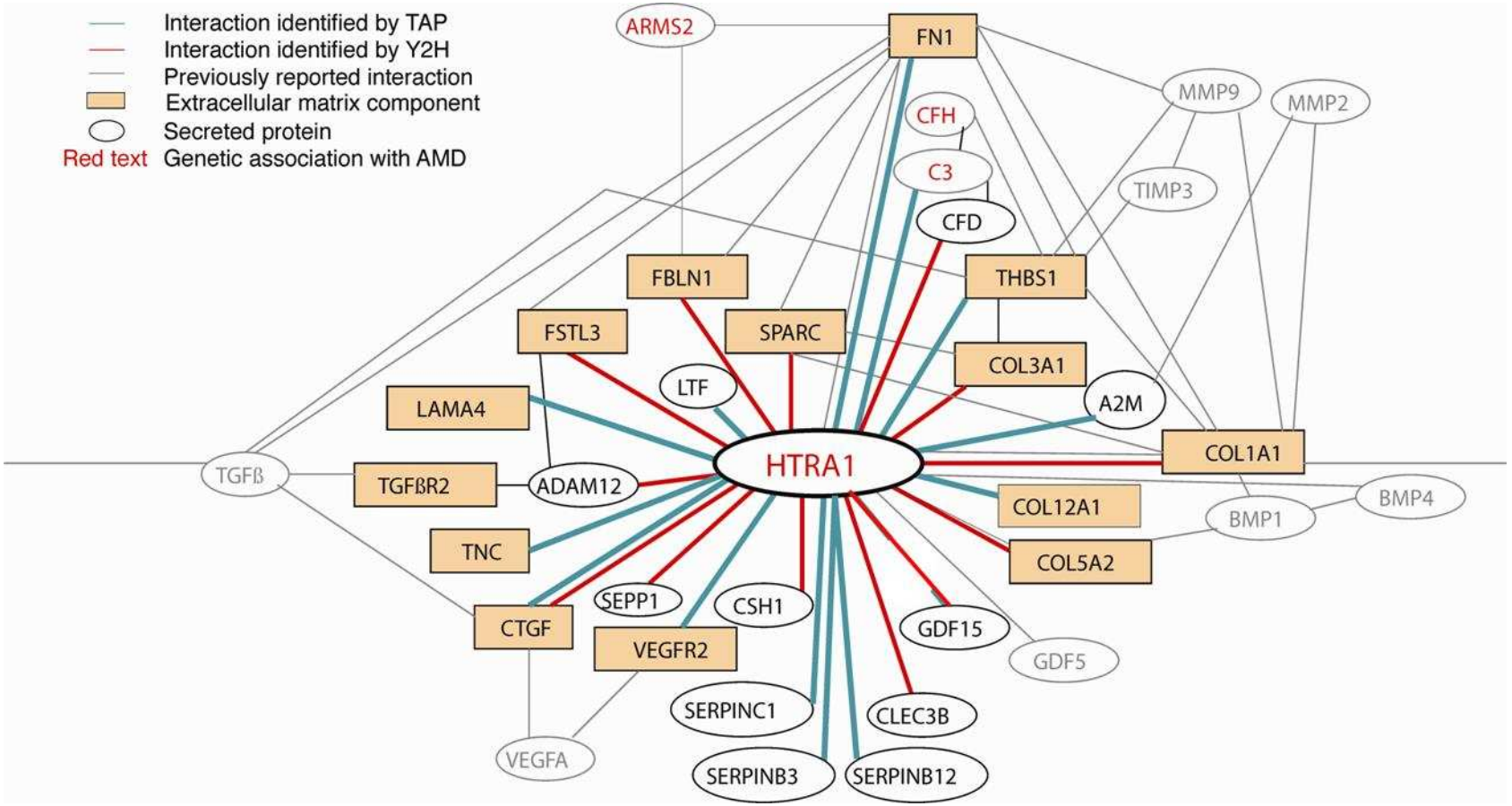

Figure 3.8 A proposed extracellular interaction network for HTRA1.
An extracellular interactome for HTRA1 was constructed using data from yeast two-hybrid and tandem affinity purification, together with data-mining for previously reported interactions in the Human Protein Reference Database (www.hprd.org), STRING string-db.org) and NCBI PubMed (www.ncbi.nlm.nih.gov/pubmed).

3.5 Verification of interactions identified by yeast two-hybrid screening or TAP

A number of putative extracellular interactors were selected for verification of an interaction with HTRA1 using additional *in vitro* approaches. Recombinant HTRA1 was expressed and purified from bacteria, and used to confirm interactions in GST-pulldown assays, and to identify substrates in protease assays.

3.5.1 Recombinant forms of HTRA1

Recombinant GST-tagged HTRA1 encoding amino acids 157-480 of the full-length protein was produced in *E. coli*. The pDEST17 construct is an *E. coli* expression vector, encoding a GST-tag at the N-terminus of the recombinant protein, with an IPTG-inducible $lacI^q$ promoter controlling expression. The expression vector for GST ΔN HTRA1 was a kind gift of Dr. Elod Kortvely.

GST ΔN HTRA1 lacks the N-terminal insulin-like growth factor-binding protein and serine protease inhibitor domain (shown schematically in Figure 3.9). This form of HTRA1 is thought to be physiologically relevant as HTRA1 undergoes auto-proteolysis to generate N-terminal truncations. A catalytically inactive mutant of HTRA1 was generated by site-directed mutagenesis (performed by Elod Kortvely) of the active site serine residue 328 to alanine (S328A). Confirmation of the necessary coding change by the alteration of the codon for serine (TCG) to alanine (GCG) is shown in Figure 3.10.

A His_6-tagged form of HTRA1, encoding amino acids 157-480 of the full-length protein was also produced in *E. coli*. The pDEST15 construct is an *E. coli* expression vector, encoding a His_6-tag at the N-terminus of the recombinant protein, with an IPTG-inducible $lacI^q$ promoter controlling expression. Gateway cloning technology was used to insert the sequence of ΔN HTRA1 into the expression vector.

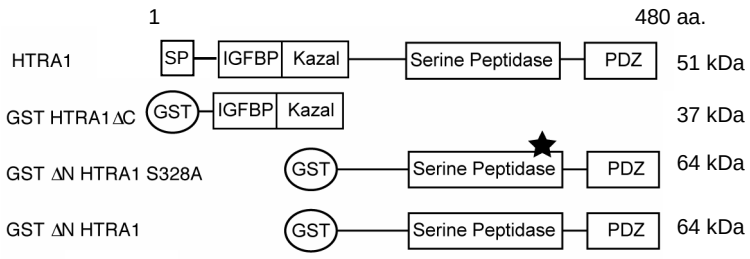

Figure 3.9 Domain structure and recombinant forms of HTRA1.
HTRA1 is a secreted serine protease, with an N-terminal secretory signal sequence, an insulin-like growth factor domain, and a Kazal-type serine protease inhibitor domain, a trypsin-like serine peptidase domain and a C-terminal PDZ domain. Full-length HTRA1 contains 480 amino acids and is 51 kDa. GST HTRA1ΔC is a recombinant form of the protein containing the two N-terminal domains. GST ΔN HTRA1 is a recombinant form of the protease, lacking the two N-terminal domains and with an N-terminal GST tag. An inactive mutant of HTRA1 replaces the active site serine residue in the peptidase domain with alanine (S328A).

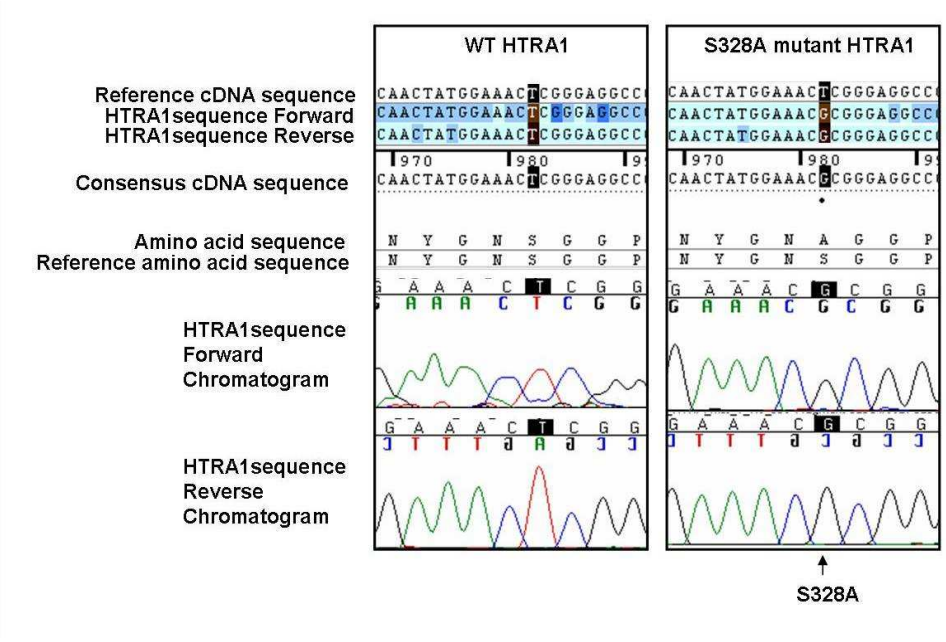

Figure 3.10 Verification of the T to G coding change in HTRA1 sequence to generate the S328A inactive HTRA1 mutant.
Site-directed mutagenesis was used to alter an amino acid codon in HTRA1 from **T**CG (Serine) to **G**CG (Alanine) and generate an inactive mutant of the enzyme. The base change was confirmed by sequencing both strands of the vector (highlighted in black).

3.5.1.1 Expression of recombinant GST ΔN HTRA1 and His_6 ΔN HTRA1

The *E.coli* strain BL21 (DE3) pLysS was used for the expression of His_6 ΔN HTRA1, GST ΔN HTRA1 or GST ΔN HTRA1 S328A.

3.5.1.2 Purification of recombinant GST ΔN HTRA1

Recombinant GST ΔN HTRA1 or GST ΔN HTRA1 S328A was purified from the soluble fraction of the bacterial cell lysate using the affinity of the GST-tag for Glutathione Sepharose resin. Following extensive washing of the immobilised protein, the GST ΔN HTRA1 was eluted. Steps in the purification procedure of GST ΔN HTRA1 and GST ΔN HTRA1 S328A are shown in Figure 3.11A and Figure 3.12 respectively.

The purity of GST ΔN HTRA1 (~64 kDa) was assessed by SDS-PAGE (Figure 3.11B). All bands observed in the Coomassie stained gel (lane 1) were recognised by the polyclonal anti-HTRA1 PDZ antibody (lane 2) or the anti-GST-HRP antibody (lane 3). Lower molecular weight bands are due to proteolytic activity of the recombinant protease, as these bands are not observed in purified GST ΔN HTRA1 S328A (Figure 3.12).

3.5.1.3 Purification of recombinant His_6 ΔN HTRA1

Recombinant His_6 ΔN HTRA1 was purified using the affinity of the His_6-tag for Ni-NTA agarose. Purity of the eluted His_6 ΔN HTRA1 (~51 kDa) was assessed by SDS-PAGE and Coomassie-staining (data not shown), prior to dialysis into TBS to remove Imidazole.

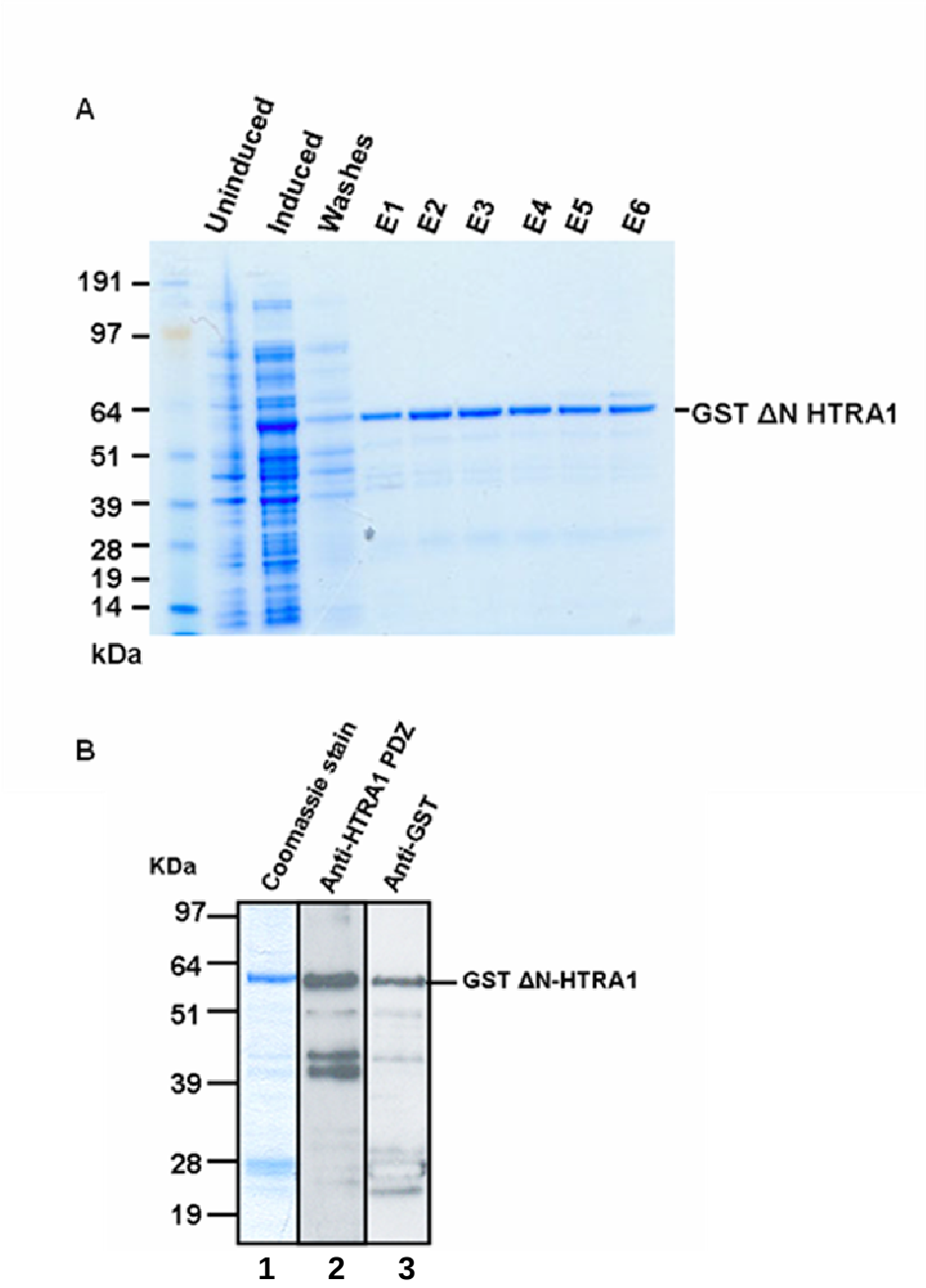

Figure 3.11 A representative purification procedure for GST ΔN HTRA1.

A. A representative Coomassie-stained gel showing stages in the purification of GST ΔN HTRA1. The band at ~64 kDa corresponding to HTRA1 is induced by IPTG, and purified from the soluble fraction of the bacterial cell lysate. Following extensive washing, GST ΔN HTRA1 is eluted from Glutathione Sepharose in successive elution steps E1-E6.

B. Lower molecular weight bands apparent in the Coomassie-stained gel are fragments of HTRA1, as shown by immunoreactivity with either anti-HTRA1 PDZ or anti-GST antibodies.

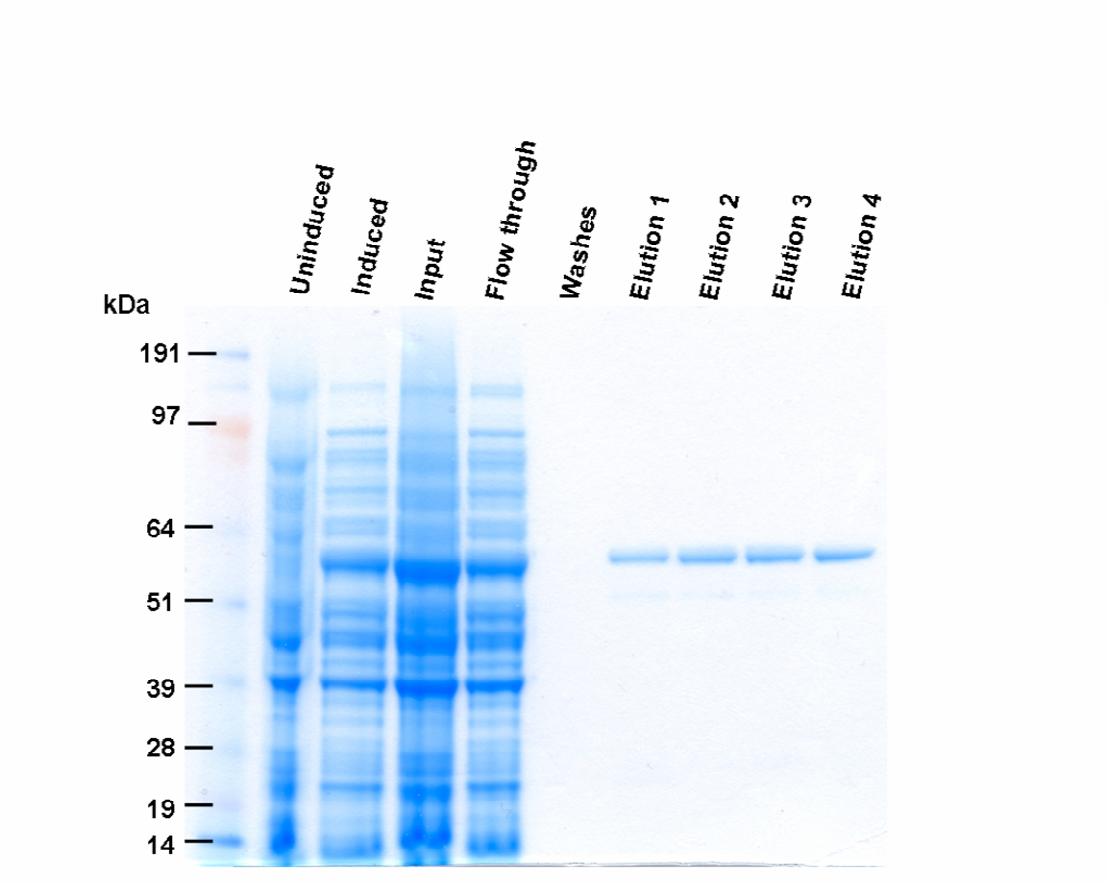

Figure 3.12 A representative purification procedure for GST ΔN HTRA1 S328A.

A Coomassie-stained gel showing steps in the purification procedure for GST ΔN HTRA1 S328A. Expression of HTRA1 is induced by IPTG, and purified from the soluble fraction of the bacterial cell lysate (Input) using the affinity of the GST tag for Glutathione Sepharose. After extensive washing, pure GST ΔN HTRA1 S328A (~64 kDa) was eluted from the resin.

3.5.2 HTRA1 interacts with Thrombospondin-1 (THBS1)

As shown in Figure 3.13A, thrombospondin-1 is a multi-domain protein of 129 kDa. Thrombospondin-1 is secreted by a variety of cell types and is a component of the extracellular matrix with diverse physiological roles. An interaction between HTRA1 and thrombospondin-1 was detected by TAP performed in HEK293T cell media (Table 3.4).

3.5.2.1 Thrombospondin-1 is a substrate for HTRA1 *in vitro*

Purified thrombospondin-1 is cleaved by recombinant GST ΔN HTRA1 in an *in vitro* protease activity assay (Figure 3.13B). Following incubation of 1 µg of GST ΔN HTRA1 with 2.25 µg of thrombospondin-1 at 37ºC for 18 hours, fragments ranging from approximately 80 kDa to 129 kDa were observed in a silver stained gel (Figure 3.13B). A higher molecular weight band of approximately 180 kDa which is not recognised by anti-THBS1, but is likely to represent an acetylated and glycosylated modified form of thrombospondin-1 (post-translational modifications are indicated in Figure 3.13A), appears to be particularly susceptible to proteolysis by GST ΔN HTRA1 (*). There was no degradation of thrombospondin-1 following incubation at 37ºC for 18 hours in the absence of the protease (lane 3, Figure 3.13B).

3.5.2.2 Thrombospondin-1 interacts directly with HTRA1 *in vitro*

The HTRA1/thrombospondin-1 interaction detected by TAP was validated using *in vitro* pull-down techniques. Full-length thrombospondin-1, purified from human platelets, was tested for the ability to associate with GST ΔN HTRA1 (Figure 3.9). Thrombospondin-1 generated an immunoreactive band with a molecular weight of ~129 kDa when subjected to Western blotting with an anti-THBS1 antibody (lane 3, Figure 3.13C). This band represents 10% input to the GST-pulldown assay. A thrombospondin-1-specific band was detected following pull-down with the GST ΔN HTRA1 fusion protein (lane 6). No binding to Glutathione Sepharose resin or to GST alone was observed (lane 4 and lane 5, Figure 3.13C).

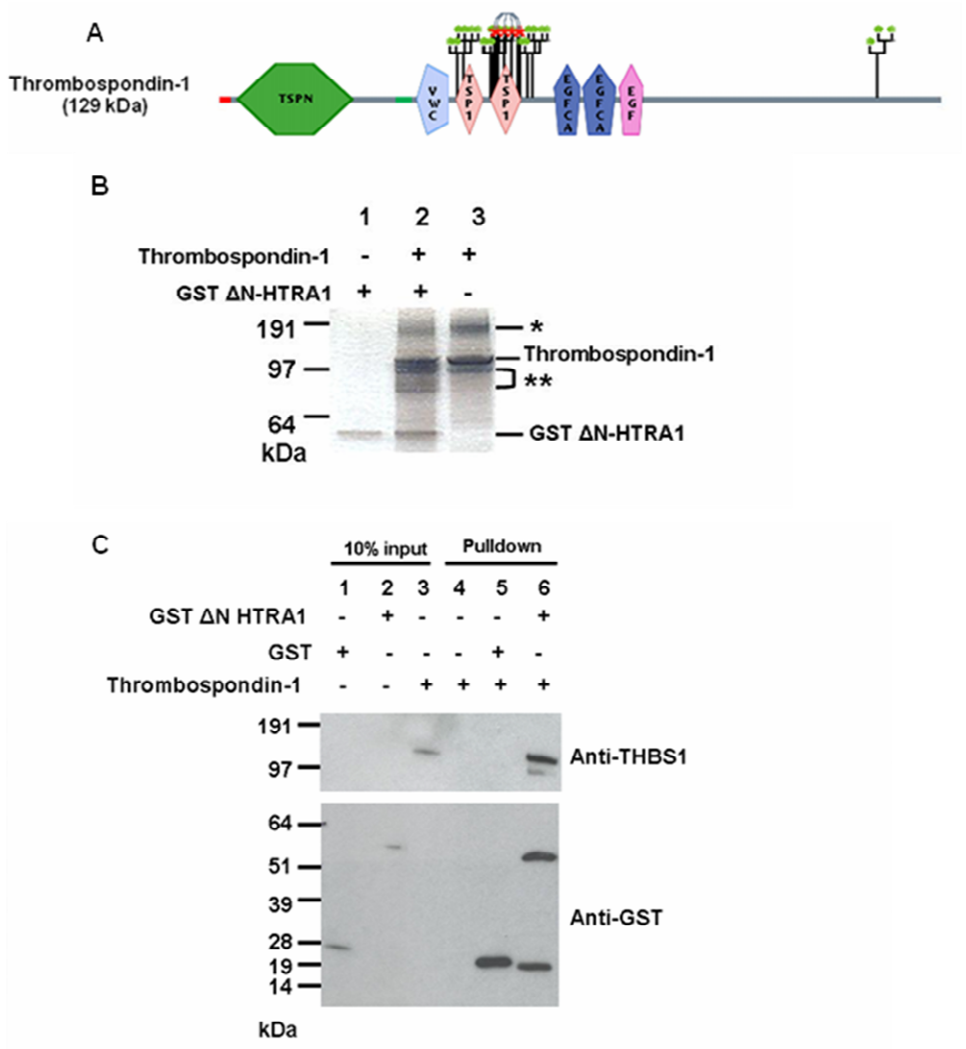

Figure 3.13 Thrombospondin interacts with, and is a substrate for, HTRA1 *in vitro*.

A. Thrombospondin-1 is a multi-domain matrix glycoprotein (N- and O-glycosylation sites indicated by green dots), which forms as a disulphide-linked (indicated by red dots) homotrimer. Domains are: Thrombospondin N-terminal -like domain (TSPN), von Willebrand factor (vWF) type C domain (VWC), Thrombospondin type 1 repeats (TSP1), Calcium-binding EGF-like domain (EGFCA) and Epidermal growth factor-like domain (EGF).
Source: www.hprd.org.
B. Thrombospondin-1 is cleaved by HTRA1 in an *in vitro* protease assay, generating fragments ranging from 80-129 kDa (lane 2, **). Unmodified thrombospondin-1 is 129 kDa; glycosylated thrombospondin-1 has a higher molecular weight (*).
C. Thrombospondin-1 interacts with GST ΔN HTRA1 in a GST-pulldown assay. 10% input to the assay is shown in lanes 1-3 of the Western blots. Upper panel is probed with anti-thrombospondin-1; lower panel is probed with anti-GST HRP. There was no interaction between Glutathione Sepharose and thrombospondin-1 (lane 4), or GST and thrombospondin-1 (lane 5). A strong interaction between GST ΔN HTRA1 and thrombospondin-1 was detected (lane 6).

3.5.3 An interaction between HTRA1 and C3 could not be verified *in vitro*

Complement component C3 has a key role in the alternative complement pathway. The putative interaction between C3 and HTRA1 identified by TAP was selected for validation. A commercially available C3, purified from human plasma, was used in *in vitro* assays with recombinant GST ΔN HTRA1.

3.5.3.1 C3 is not a substrate for HTRA1 *in vitro*

Purified C3 was tested as a substrate for HTRA1 in an *in vitro* protease assay. As shown in Figure 3.14, there was no cleavage or degradation of 2 µg of C3 following incubation with 0.2 µg of GST ΔN HTRA1 at 37ºC for 18 hours, analysed by SDS-PAGE.

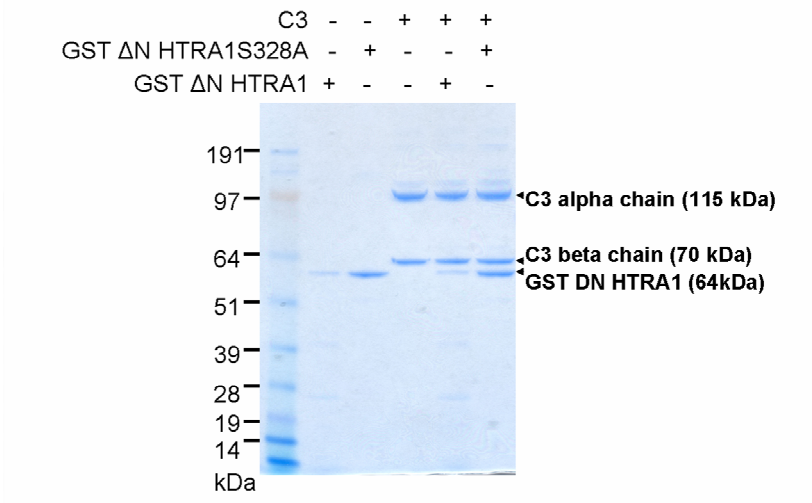

Figure 3.14 C3 is not a substrate for HTRA1 in an in vitro protease assay.

C3 purified from human plasma (comprising C3 alpha and C3 beta subunits) is not subject to proteolysis by GST ΔN HTRA1, as shown in lane 4 of the Coomassie-stained gel of the protease assay.

3.5.3.2 Non-specific binding of C3 prevented verification of an interaction in GST-pulldown assay

Recombinant GST ΔN HTRA1 was used in a series of GST pulldown assays to verify an interaction between HTRA1 and C3 *in vitro*. High background binding of C3 to Glutathione Sepharose resin was observed across a range of increasingly stringent wash conditions (0-2M NaCl; 0-2% NP40; data not shown). This prevented the verification of a direct interaction between C3 and HTRA1.

3.5.4 HTRA1 interacts with CTGF *in vitro*

An interaction between CTGF and HTRA1 was identified in the yeast two-hybrid screen and in a TAP experiment (Table 3.1, Table 3.4, Figure 3.8). The domain structure of CTGF is shown in Figure 3.15A. A direct interaction between these two proteins was verified using recombinant purified proteins in *in vitro* assays.

3.5.4.1 Generation of recombinant GST-tagged CTGF

The sequence encoding full-length CTGF (Figure 3.15A) was cloned from human retinal cDNA. Using Gateway technology, CTGF was sub-cloned into the bacterial expression vector pDEST17, to produce CTGF with a GST-tag at the N-terminus of the recombinant protein. The *E.coli* strain BL21 (DE3) pLysS was used for protein expression. Recombinant GST CTGF (63 kDa) was purified from the soluble fraction of the bacterial cell lysate. The purity of the eluted protein was assessed by SDS-PAGE followed by Coomassie staining prior to dialysis into TBS. GST CTGF alone is shown in Figure 3.15B (lane 3).

3.5.4.2 CTGF is a substrate for HTRA1 *in vitro*

Recombinant GST-tagged CTGF and ΔN HTRA1 were incubated together for 16 hours at 37°C. CTGF was cleaved by HTRA1 to generate additional lower molecular weight bands (Figure 3.15B). These additional bands were observed when the recombinant proteins were incubated together (lane 2), but not seen in each protein alone (lane 1, lane 3).

3.5.4.3 CTGF interacts directly with HTRA1 *in vitro*

GST CTGF was used in a GST-pulldown with His_6 ΔN HTRA1 (Figure 3.15C). An interaction was observed between GST CTGF and His_6 ΔN HTRA1 (lane 6). This confirms an interaction between CTGF and HTRA1 initially identified in tandem affinity purification experiments and by yeast two-hybrid screening. Non-specific interactions between His_6 ΔN HTRA1 and Glutathione Sepharose resin alone, or between His_6 ΔN HTRA1 and GST alone, were not seen.

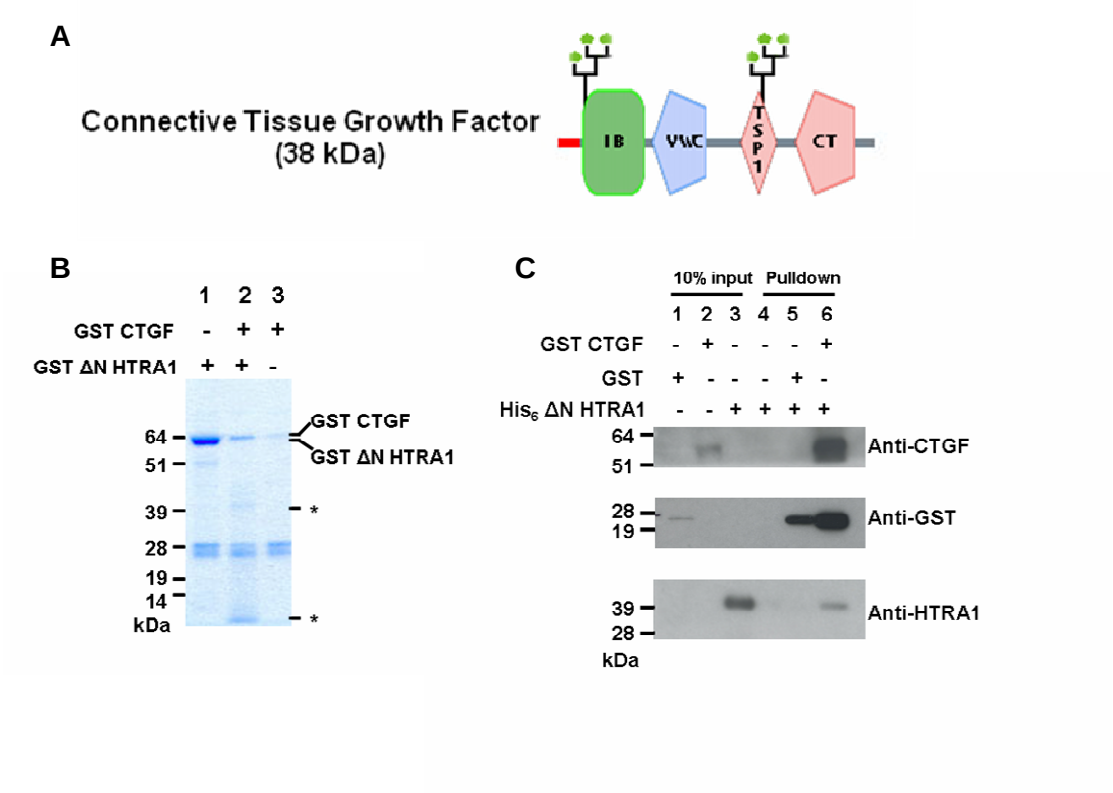

Figure 3.15 Connective tissue growth factor (CTGF) interacts with, and is a substrate for, HTRA1 *in vitro*.

A.The CTGF protein (38 kDa) contains four distinct domains; an N-terminal insulin-like growth factor binding protein domain (IB; a domain also found in HTRA1), the Von-Willebrand factor (VWC) motif (implicated as a binding site for TGF-β), a thrombospondin type 1 (TSP-1) motif, and a cysteine knot (CT). Image from www.hprd.org.

B. A GST-tagged form of CTGF (64 kDa) is susceptible to proteolysis by GST ΔN HTRA1 *in vitro*. Following incubation with the protease (lane 2), fragments of GST CTGF are observed in the Coomassie-stained gel (*). The band at 38 kDa is likely to represent CTGF cleaved from the GST-tag (25 kDa).

C. GST CTGF interacts with His_6 ΔN HTRA1 (39 kDa) in a GST-pulldown assay (lane 6). There is no interaction between Glutathione Sepharose, or GST alone, and His_6 ΔN HTRA1 (lanes 4 and 5 respectively). The Western blot of the pulldown assay was probed with anti-CTGF, anti-GST HRP and with anti-HTRA1.

3.6 Discussion

The serine protease HTRA1 has been implicated in the pathobiology of a variety of diseases, including AMD, Alzheimer's disease and osteoarthritis (Hu et al. 1998; Grau et al. 2005; Grau et al. 2006; Yang et al. 2006). HTRA1 is a stress-induced serine protease with a poorly characterised interactome and substrate specificity in healthy or diseased tissues. As such, the role of the protease and its substrates in the development of disease pathogenesis is not well understood. In this chapter, putative interactors of HTRA1 were identified by yeast two-hybrid screening and by tandem affinity purification. Candidates with a proposed role in the pathogenesis of AMD were identified, and suggest that HTRA1 may be involved in a number of pathways which are implicated in AMD.

A number of intracellular proteins of interest in AMD were identified as potential interactors of HTRA1 (Table 3.1, Table 3.2, Table 3.5). These included previously reported interactions, for example, with Tubulin alpha1 (Chien et al. 2009a; Chien et al. 2009b), and novel putative interactions with proteins involved in innate immunity and inflammatory response (DEFA1, S100 A8). However, HTRA1 is a secreted serine protease, and so the attention of this study was focussed on the extracellular interactors (Figure 3.8). Several of these will be discussed further, including those for which an interaction was successfully validated in this chapter.

Using a combination of a yeast two-hybrid screen and tandem affinity purification of a tagged-HTRA1 protein from HEK293T or RPE1 cells and conditioned media, components of the ECM have been identified as novel binding partners of HTRA1. As seen in Figure 3.8, an interactome for HTRA1 in the extracellular environment has been proposed based on these findings (although replication and verification of all interactors is still required). The combined results of the HTRA1 interactome screen showed that this protease interacts with a broad range of predominantly extracellular matrix proteins. These include proteins with a structural role in the ECM, such as type 1, 3 and 5 collagen chains (COL1A1, COL3A1, COL5A2, COL12A1). COL1A1 and COL3A1 have previously been reported as interactors of HTRA1 (De Luca et al. 2004; Murwantoko et al. 2004) and are constituents of Bruch's membrane or choroid (Booij et al. 2010). The Bruch's

membrane, separating the RPE cells from the blood supply in the choroid, is collagen-rich, and is likely to be a target for HTRA1-mediated remodelling. Murwantoko and co-workers (2004) have shown that COL3A1 is degraded by recombinant HTRA1 *in vitro*, suggesting that HTRA1 does have a role in remodelling the ECM.

Changes to the ECM may play a role in drusen development and disease progression. Histopathological analysis indicates that alterations in the collagen and elastin layers of Bruch's membrane occur in AMD (Spraul et al. 1999; Chong et al. 2005). As HTRA1 is expressed by RPE cells and appears to possess extracellular matrix remodelling activity in normal tissue, tumour progression and invasion, and in arthritis (Hu et al. 1998; Baldi et al. 2002), *HTRA1* remains an attractive candidate gene for AMD.

Fibronectin (FN) was detected by mass spectrometry of HTRA1 interactors from TAP eluates in two experiments (Table 3.4). The interaction between these proteins has been previously reported, and may play a role in cartilage degradation, arthritis pathology and in matrix mineralization (Grau et al. 2006; Hadfield et al. 2008). Fibronectin can be degraded by full-length mouse HtrA1 *in vitro* (Hadfield et al. 2008). Fibronectin fragments, generated by the action of various proteases including MMPs, increase the expression of fibronectin, promote cellular transformation and are pro-inflammatory (Labat-Robert 2002). Fibronectin levels increase with age (Labat-Robert et al. 1981). Soluble fibronectin upregulates VEGF in RPE cells and can promote angiogenesis (Mousa et al. 1999). The physiological relevance of an interaction between fibronectin and HTRA1, and a relationship to AMD pathology, is unknown.

Thrombospondin-1 (THBS1) was identified by mass spectrometry in the first analysis of TAP eluates as a potential binding partner of HTRA1 in conditioned media. As such, the interaction between HTRA1 and thrombospondin-1 was the first to be investigated further. Thrombospondin-1 is a homotrimeric glycoprotein with disulfide-linked subunits, arising from a precursor protein of 129 kDa. Thrombospondin-1 is secreted by a variety of cells during development, tissue remodelling and wound healing. In the eye, thrombospondin-1 is secreted by the RPE and is predominantly localised to the basement membrane (Carron et al. 2000;

Miyajima-Uchida et al. 2000; Hiscott et al. 2006). Following secretion, THBS1 is incorporated in the ECM as a matricellular protein, binding to matrix components including heparin, fibronectin, fibrinogen, plasminogen and collagen. It binds to a variety of extracellular proteins (including proteases, growth factors) and to cell-surface receptors, allowing the formation of multi-protein signalling complexes (Bornstein 2001).

A variety of biological roles have been attributed to thrombospondin-1, including regulation of cell-matrix interactions and cellular behaviour, both anti-angiogenic and pro-angiogenic properties, activation of TGF-β, inhibition of VEGF signalling, inhibition of MMP2 and MMP9, modulating RPE cell migration and maintenance of immune privilege in the eye (Good et al. 1990; Murphy-Ullrich et al. 1992; Nicosia and Tuszynski 1994; Gupta et al. 1999; Bein and Simons 2000; Rodriguez-Manzaneque et al. 2001; Sheridan et al. 2002; Zamiri et al. 2005). Any alteration in levels of THBS1 will affect these processes. For example, a reduction in thrombospondin-1 could lead to an increase in protease activity of MMP2 and MMP9 in the ECM. Matrix metalloproteinases degrade components of the ECM and basement membrane during tissue remodelling and in pathological processes, including the development of coronary disease and in AMD (Guo et al. 1999; Kamei and Hollyfield 1999; Blankenberg et al. 2003; Auge et al. 2004). In experimental models of choroidal neovascularisation (CNV), MMP2 and MMP9 play a role in the development of new vasculature (Lambert et al. 2002; Lambert et al. 2003). Mutations in the gene encoding tissue inhibitor of metalloproteinases-3 (TIMP3) cause Sorsby's fundus dystrophy, a rare inherited form of macular degeneration associated with deposits in the Bruch's membrane and sub-retinal neovascularisation (Weber et al. 1994). More recently, *TIMP3* has also been associated with AMD in a large genome-wide association scan (Chen et al. 2010). An association between variants in *MMP9* and AMD (Fiotti et al. 2005) has not been replicated in large genome-wide association studies (Chen et al. 2010; Yu et al. 2011).

Interestingly, although expression of *THBS1* in the retina increases with age (Chowers et al. 2003), reduced levels of thrombospondin-1 have been detected in AMD eyes (Uno et al. 2006; Bhutto et al. 2008). Thrombospondin-1 is anti-angiogenic in most tissues. However, pro-angiogenic activity of thrombospondin-1 in

the subretinal space has been suggested in an *in vitro* study using RPE cells (Mousa et al. 1999). Clearly, thrombospondin-1 is involved in the modulation of inflammatory responses, largely via the activation of TGF-β, and regulation of intraocular vasculature. Indeed, these seem to be vital roles of thrombospondin-1 in maintaining a healthy eye, as reviewed by Hiscott et al. (2006). Thus, the potential interaction between thrombospondin-1 and HTRA1 is of great interest.

An *in vitro* pull-down assay, using a recombinant form of HTRA1 and thrombospondin-1 purified from human platelets, was used to verify the interaction (Figure 3.13C). Moreover, a protease activity assay using the same recombinant HTRA1 protein shows that thrombospondin-1 is subjected to proteolytic degradation by the serine protease *in vitro*. Further experiments are required to determine the significance of this. The interactions, and resultant activities, of thrombospondin-1 may be disrupted by aberrant proteolytic degradation by HTRA1. For example, HTRA1 is known to inhibit TGF-β signalling, with some *in vitro* experiments indicating that TGF-β itself is not degraded by the protease (Oka et al. 2004). Degradation of thrombospondin-1 may affect the activation of TGF-β, preventing downstream signalling, leading to dysregulation of a number of processes which are involved in AMD pathogenesis, including ECM deposition and inflammation. Alternatively, pro-angiogenic fragments of thrombospondin-1 may be generated. Furthermore, thrombospondin-1 is known to interact with CFH, potentially providing a link between two AMD susceptibility genes (Vaziri-Sani et al. 2005).

Two clones encoding fibulin-1 (FBLN1) have been isolated as interactors of HTRA1 in a yeast two-hybrid screen performed in a placental cDNA library. Fibulin-1 is a calcium-binding secreted glycoprotein, widely expressed in basement membranes of epithelial cells and in blood vessels. The protein is incorporated into the extracellular matrix via binding to fibronectin, nidogen, aggrecan, and versican (Argraves et al. 1989; Aspberg et al. 1999).

A mutation in the fibulin-3 gene (also known as *EFEMP1*) causes autosomal dominant drusen or Doyne's honeycomb retinal dystrophy, an early onset Mendelian disease with similar pathological features to AMD (Stone et al. 1999). Variants in fibulin-6 (*HEMICENTIN-1*) and in fibulin-5 have been associated with AMD (Schultz et al. 2003; Stone et al. 2004). Subsequently, doubts have been cast upon the

contribution of variants in fibulin-6 towards AMD risk at the chromosome 1q31 locus, due to the close proximity to *CFH* (Fisher et al. 2007). Although fibulin-1 is expressed in RPE cells, no variants were identified in the FBLN1 gene on chromosome 22q13 that were significantly associated with AMD in a case-control study (Stone et al. 2004). However, the fibulins remain an interesting family of proteins to investigate with respect to AMD, and a potential interaction with HTRA1 may contribute towards AMD pathology. Additionally, fibulin-1 interacts with CFH and with ARMS2 in yeast two-hybrid screens which may indicate a role in AMD development (Kortvely et al. 2010).

Three clones encoding osteonectin (SPARC; secreted protein, acidic and rich in cysteine) were found to interact with HTRA1 in the yeast two-hybrid screen. Sequence alignment with osteonectin suggests that the minimal binding region required for an interaction between the two proteins involves the Kazal-type inhibitory domain present at the N-terminus of osteonectin (data not shown). This has interesting implications for the regulation of HTRA1, which also contains a Kazal-type inhibitory domain which appears to be involved in self-regulation and is often cleaved *in vivo* (Chien et al. 2006). Like thrombospondin-1 and CTGF, osteonectin is a matricellular protein which mediates cell interactions and signalling (Bornstein and Sage 2002), and may have a role in the migration of RPE cells (Sheridan et al. 2002). Osteonectin is a 32 kDa phosphoprotein, largely found in bone but expressed by endothelial cells in response to injury (Termine et al. 1981; Goldblum et al. 1994). Osteonectin binds to type 1 collagen fibrils, and modulates the activity of MMPs, PDGF, VEGF and FGF-2 (reviewed by (Brekken and Sage 2001). Although the full-length protein is considered anti-angiogenic, fragments of osteonectin can stimulate angiogenesis and promote wound healing (Bornstein and Sage 2002). Indeed, a role for osteonectin in regulation of VEGF signalling in choroidal neovascularisation has previously been suggested (Nozaki et al. 2006b). Further work remains to determine whether osteonectin, and a potential interaction with HTRA1, have physiological significance under normal conditions or in AMD.

Connective tissue growth factor (CTGF) is a cysteine-rich protein of 38 kDa, produced by a variety of cell types and secreted into the extracellular environment. This protein was identified as a potential interactor of HTRA1 in TAP experiments

and in a yeast two-hybrid screen (Table 3.1, Table 3.4, Figure 3.8). The domains of CTGF, shown schematically in Figure 3.15A, are separated by hinge regions which are susceptible to cleavage by proteases (Brigstock et al. 1997).

CTGF is expressed during development and is induced during wound healing, embryo implantation and is overexpressed in fibrosis (Igarashi et al. 1993; Surveyor et al. 1998). CTGF associates with components of the ECM and with cell surface receptors. TGF-β induces expression of CTGF, leading to the hypothesis that CTGF is a downstream mediator of TGF-β signalling (Grotendorst 1997). However, expression of CTGF can occur independently of TGF-β. CTGF may be induced by thrombin and angiotensin II, suppressed by TNF-α and cAMP, and under the control of glucose (Murphy et al. 1999; Abraham et al. 2000; Chambers et al. 2000; Finckenberg et al. 2003). The precise action of CTGF is unknown, but overexpression of CTGF leads to fibrosis by promoting the expression of ECM proteins including fibronectin and type IV collagen (Ruiz-Ortega et al. 2006). Fibrosis is considered to be important in many diseases, with a role for CTGF being proposed in disorders including cancer, atherosclerosis, Crohn's disease, vitroeretinal disorders and in AMD (Oemar and Luscher 1997; Koliopanos et al. 2002; He et al. 2003; Beddy et al. 2006; Kuiper et al. 2006). *In vitro* CTGF, together with additional growth factors and cytokines, also promotes a range of activities, including matrix production, photoreceptor cell survival and angiogenesis (Frazier et al. 1996 ; Shimo et al. 1999; Hauck et al. 2008).

He et al. (2003) used a variety of methods to show that *CTGF* was expressed by RPE cells of patients with wet AMD but not by the RPE in healthy eyes. CTGF was localised to the choroidal neovascular membrane in the AMD eye. Furthermore, CTGF stimulates tube formation by choroidal endothelial cells *in vitro,* potentially promoting angiogenesis *in vivo* (He et al. 2003). A similar study by Watanabe and co-workers co-localised TGF-β and VEGF with CTGF to CNV membrane (Watanabe et al. 2005). Recent work has shown that CTGF is present in the Bruch's membrane, in basal deposits and in drusen in human macula, and increases expression of matrix proteins in ARPE-19 cells (Nagai et al. 2009). Interestingly, CTGF is upregulated by oxidative stress, a process that has been implicated in AMD pathogenesis (Matsuda et al. 2005). Additionally, CTGF activates MMP2, which has

been shown to degrade ECM components and promote neovascularisation (Yang et al. 2007). CTGF may also play a role in inflammatory response, inducing a range of genes including chemokine [C-X-C motif] ligand 1 (CXCL1), chemokine [C-X-C motif] ligand 6 (CXCL6), interleukin 6 (IL6), and interleukin 8 (IL8) in primary human tenon fibroblasts (Seher et al. 2011).

An interaction between HTRA1 and CTGF was verified in a GST-pulldown assay (Figure 3.15C), complementing the results of the yeast two-hybrid screen and TAP experiments. CTGF is also known as IGFBP8 (insulin-like growth factor-binding protein 8), and contains a conserved N-terminal IGFBP motif also seen in HTRA1. However, this domain is removed in the N-terminally truncated form of HTRA1 used in the assay, suggesting that the interaction between these proteins is not dependent on the IGFBP domain. In an *in vitro* protease assay, CTGF appears to be subjected to partial cleavage by HTRA1 (Figure 3.15B). In addition to a potential role in angiogenesis, fragments of CTGF seem to increase ECM deposition and fibrovascular scarring - pathological characteristics of AMD. This is an attractive candidate for further study in relation to AMD.

The involvement of inflammatory processes in AMD has been indicated by the identification of variants in several components (*CFH, C2, C3, CFB, CFHR1* and *CFHR3* genes) of the complement pathway that influence the risk of AMD development (Conley et al. 2005; Edwards et al. 2005; Hageman et al. 2005; Haines et al. 2005; Klein et al. 2005; Magnusson et al. 2005; Gold et al. 2006; Hughes et al. 2006; Yates et al. 2007). Numerous plasma and cell-surface proteins are involved in the complement system, activating and regulating the innate immune response and facilitating adaptive immunity (reviewed by Walport, 2001). C3 is the most abundant of these proteins. Cleavage of C3 plays a central role in complement activation in the classical pathway, the lectin pathway and the alternative complement pathway (Walport, 2001). Although C3 is produced mainly by the liver, *C3* mRNA is detected in numerous other cells and tissues, including the retina, choroid and RPE cells (Mullins et al. 2000).

A potential interaction between C3 and HTRA1 was detected by mass spectrometry of TAP eluates (but has yet to be verified independently, Figure 3.14). However, due to the central role of this protein in the complement cascade, a

previous association with AMD and evidence that C3 is found in drusen (along with HTRA1), an interaction between these two proteins is potentially very interesting (Mullins et al. 2000; Yang et al. 2006; Yates et al. 2007).

Aside from connective tissue growth factor and an enrichment for ECM components, there is little overlap between the potential binding partners of HTRA1 that have been identified by TAP and those identified by the yeast two-hybrid screen. Both systems use fusion proteins, coupling HTRA1 to a Strep-FLAG tag in the case of TAP, or to a promoter-specific DNA-binding domain in the yeast two-hybrid screen. The conformation of a fusion protein may differ from that of the native protein, resulting in altered activity, inaccessibility of binding sites and modified functionality. The small size (6 kDa) of the TAP tag is believed to lead to a minimal impact on correct folding of the fusion protein (Gloeckner et al. 2007). An additional benefit of tandem affinity purification from a human cell line is that HTRA1 and interacting proteins are likely to undergo correct post-translational modifications, which may not occur in a heterologous system such as the yeast two-hybrid system. Modifications such as the formation of disulphide bridges, glycosylation and phosphorylation may not occur in yeast in the same manner as in mammalian cells. If protein-protein interactions were dependent on such modifications, a yeast two-hybrid approach would be unlikely to detect them. Thrombospondin-1, for example, undergoes acetylation, glycosylation and disulphide cross-linking. This may explain why a potential interaction with HTRA1 was detected by TAP, but not in an extensive yeast two-hybrid screen. Additionally, the protease activity assay using recombinant GST ΔN HTRA1 suggests that the modified form of thrombospondin-1 is particularly susceptible to degradation by the protease, relative to the unmodified form of the protein (Figure 3.13B).

The yeast two-hybrid screen using HTRA1 as a bait protein identified numerous components of the ECM as potential interacting partners, including collagens, fibulin-1 and osteonectin (Figure 3.8, and Table 3.1 and Table 3.2). However, as the two-hybrid system detects interactions that occur in the yeast nucleus, it is possible that interactions with some extracellular proteins or proteins that contain strong targeting signals are not detected. Furthermore, indirect interactions occurring in multi-protein complexes cannot be detected using a yeast

two-hybrid approach. Mass spectrometry analysis of TAP eluates does not discriminate between direct interactions between two proteins and a multi-protein complex which arises as a result of numerous interactions between multiple proteins.

A large number of potential interacting partners for HTRA1 were identified using a combination of TAP and yeast two-hybrid approaches. Many of these potential interactors remain to be verified, by back-transformation in the yeast two-hybrid screen, and by additional methods including pull-downs and immunoprecipitation experiments. The biological relevance of all interactions remains to be shown. Some interactions may be an artefact of the experimental procedures - that is, although two proteins are able to interact, they would never be found in close proximity to each other within the cell. HTRA1 is a secreted protein, and yet numerous proteins that are localised to distinct subcellular compartments are identified as potential binding partners of the protease in both the yeast two-hybrid screen and in TAP experiments (particularly TAP performed in cell lysate, in which the subcellular compartments are disrupted).

Neither yeast two-hybrid (a heterologous system) nor HEK293T cells are physiologically relevant to AMD. TAP was performed in RPE1 cells to partially address this issue. It is encouraging to note that many of the extracellular proteins identified as potential interactors with HTRA1 are secreted by cultured primary RPE cells (An et al. 2006). Furthermore, differential expression of several interacting proteins - including COL1A1, COL3A1, fibronectin-1 and osteonectin - between RPE derived from AMD cases and normal controls was observed (An et al. 2006).

Any of these putative interactors of HTRA1 could play a role in AMD susceptibility, given the range of roles in inflammation, angiogenesis and matrix remodelling. Aside from C3, none of the genes encoding these proteins have shown genetic associations with AMD in recent large genome-wide association studies (Chen et al. 2010; Yu et al. 2011). This suggests that common variants in these genes are not important influences in disease susceptibility – extensive further work is required to characterise the role of these proteins in AMD. One putative interactor was selected for such study in this thesis. The interaction between CFD and HTRA1 (Table 3.1, Figure 3.8) is characterised in Chapter 5, and a role for CFD in influencing the genetic susceptibility to AMD is investigated in Chapter 4.

4: Chapter 4

A role for *CFD* in AMD pathogenesis

4.1 Introduction

The alternative complement pathway is thought to contribute to the chronic inflammatory state observed in the AMD eye. Previous studies have identified strong association between AMD-susceptibility and genes encoding components of the alternative complement pathway. The *CFH* gene on chromosome 1 has been identified as a major AMD-susceptibility locus (Edwards et al. 2005; Hageman et al. 2005; Haines et al. 2005; Klein et al. 2005). This gene encodes Complement Factor H, which regulates activation of the pathway and dampens down an inflammatory response. Variants in additional components of the alternative complement pathway are also associated with altered disease-risk, including *CFB/C2, C3, CFI, CFHR1* and *CFHR3* (Gold et al. 2006; Hughes et al. 2006; Yates et al. 2007; Fagerness et al. 2009). Additionally, inflammatory peptides have been identified in drusen (Hageman et al. 2001; Crabb et al. 2002; Johnson et al. 2002), and are expressed at altered levels in AMD cases compared to disease-free controls (Hakobyan et al. 2008; Scholl et al. 2008; Reynolds et al. 2009; Hecker et al. 2010). Thus, it is clear that dysregulation of the alternative complement pathway as a result of environmental or genetic factors has a key role in development and progression of AMD.

Complement factor D (CFD; also known as adipsin) is a member of the chymotrypsin family of serine proteases and regulates a key step in the activation of the alternative complement pathway (Volanakis and Narayana 1996; Xu et al. 2001). *CFD* is expressed in several tissues and cell types, but the major source of plasma CFD in humans is adipose tissue, in which it is secreted by both mature adipocytes and macrophages (Whaley 1980; Barnum and Volanakis 1985; White et al. 1992). CFD becomes transiently active following removal of an activation peptide, and upon conformational change when bound to Factor B. This allows CFD to cleave factor B into Ba and Bb fragments. This is a rate limiting step in formation of the C3bBb complex or C3 convertase, which is crucial to activation and amplification of the alternative complement pathway (Volanakis and Narayana 1996).

Plasma CFD concentrations have been reported to be very low (1-2 µg/ml) (Barnum et al. 1984). This is much lower than other complement proteins, including plasma C3 (1-2 mg/ml) or factor B (200µg/ml) (Schreiber and Müller-Eberhard 1978). This means that CFD only ceases to be limiting at 9-10 times the

concentration generally found in plasma. Given the importance of proper regulation of the alternative complement pathway in AMD pathogenesis, it is in some ways surprising that *CFD* has not previously been implicated in the disease. This chapter investigates whether CFD may contribute to the genetic and molecular basis of AMD, by analysis of genetic association, copy number variation and plasma CFD concentrations.

4.2 Testing SNPs in *CFD* for an association with AMD

In order to test the contribution of variants in *CFD* towards genetic susceptibility to AMD, a SNP association study was performed. Several SNPs were genotyped and tested for an association with disease in a Scottish AMD case-control cohort (the discovery cohort, UK1). Subsequently, one or two SNPs were investigated in five additional "replication" cohorts from the UK, USA and one combined European cohort from Holland and Germany.

4.2.1 SNP selection

CFD maps to chromosome 19p13.3, spans 3.9 kb and contains 5 exons (Figure 4.1). Three SNPs in *CFD*- rs3826945, rs1683564 and rs1683563 - with a minor allele frequency >10% in the CEPH Caucasian reference population were identified. TaqMan 5' nuclease SNP genotyping assays were ordered for these SNPs from Applied Biosystems. The position of the SNPs on chromosome 19, and in relation to *CFD*, is shown in Figure 4.2. Due to their intronic locations, these SNPs are unlikely to play a functional role in CFD activity (unless they act to alter expression levels), but may be in linkage disequilibrium (LD) with novel or rare functional variants. The Tagger-pairwiseTagging algorithm (http://hapmap.ncbi.nlm.nih.gov/) identified rs3826945 and rs1683564 as tagging SNPs.

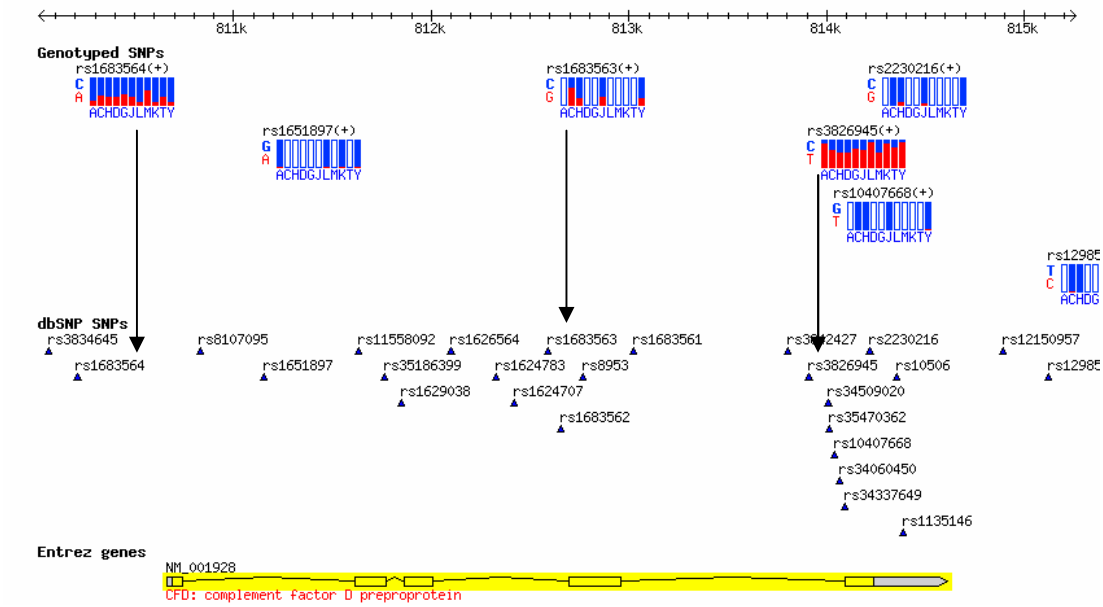

Figure 4.1 Selection of SNPs in *CFD* on chromosome 19.
The International HapMap Project (http://hapmap.ncbi.nlm.nih.gov/) was used to identify variants in CFD for investigating an association between CFD and AMD (HapMap Data Release 27, Phase 2 and 3 data, Feb09, NCBI Build 36 assembly, dbSNP126). There are 25 known SNPs in the region chr19: 810,014 to 815,259 (dbSNPs). The majority of these are rare variants or have not been genotyped in reference populations used by the HapMap project (Genotyped SNPs). Populations in which the SNPs were genotyped are: A: African ancestry in Southwest USA, C: Utah residents with Northern and Western European ancestry from the CEPH collection, H: Han Chinese in Beijing, China, D: Chinese in Metropolitan Denver, Colorado, G: Gujarati Indians in Houston, Texas, J: Japanese in Tokyo, Japan, L: Luhya in Webuye, Kenya, M: Mexican ancestry in Los Angeles, California, K: Maasai in Kinyawa, Kenya, T: Tuscan in Italy, Y: Yoruban in Ibadan, Nigeria. Three SNPs with a minor allele frequency (red portion of chart in Genotyped SNPs panel) greater than 10% in the CEPH population were identified and selected for use in this study. These SNPs are rs1683564, rs1683563 and rs3826945.

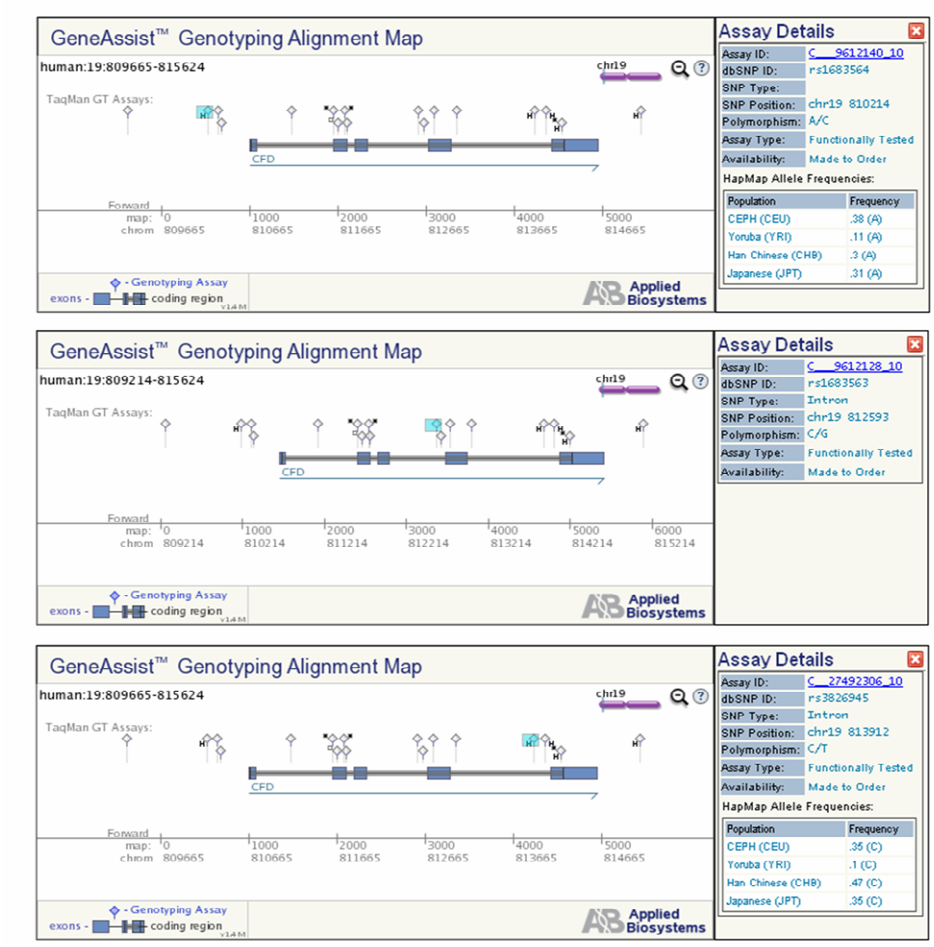

Figure 4.2 Location of SNPs selected for genotyping within the *CFD* gene.

TaqMan SNP genotyping assays were obtained for the intronic variants rs1683564, rs1683563 and rs3826945. These alignment maps, obtained from Applied Biosystems, show the location of each SNP, the polymorphism detected by the assay and the minor allele frequency in HapMap reference populations (where available).

The degree of linkage disequilibrium between the three SNPs was investigated using data from the HapMap3 Genome Browser release #2 (Phase 3 - genotypes, frequencies & LD), accessed through the International HapMap Project (http://hapmap.ncbi.nlm.nih.gov/). Pair-wise LD between the SNPs is reported in Table 4.1. As shown by LOD (Log of Odds) scores of >2 between pair-wise combination of the SNPs, there is some LD between SNPs. There is strong LD between rs3826945 and rs1683563 (D'=1). However, the SNPs are not in perfect LD (r^2=0.314), indicating that the alleles for the two SNPs are not correlated on the three possible haplotypes (ab, AB, aB, where A is the minor allele of rs3826945, and b is the major allele of rs1683563), so both SNPs remain informative.

Chr19 position 1	Chr19 position 2	Population	Marker1	Marker2	D'	r^2	LOD
810214	812593	CEU	rs1683564	rs1683563	0.764	0.184	4.12
810214	813912	CEU	rs1683564	rs3826945	0.745	0.476	11.3
812593	813912	CEU	rs1683563	rs3826945	1	0.314	7.48

Table 4.1 Linkage disequilibrium between SNPs in *CFD*.
Pair-wise linkage disequilibrium between the rs1683564, rs1683563 and rs3826945 SNPs in *CFD* has been tested in the CEPH population, and is available through the HapMap project. Measures of LD are D' (Complete LD =1), r^2 (perfect LD=1) and Log of Odds (LOD).

4.2.2 Discovery and replication AMD case-control cohorts

The characteristics and demographic information for the AMD case-control series used in this study are shown in Table 4.2. The Scottish AMD cohort was the first to be genotyped, and represents the discovery cohort (UK1).

Replication cohorts from Cambridge, England (UK2), Michigan, USA (USA1), NIH, USA (USA2), Tufts University (USA3) and Nijmegen, Holland (Nijmegen) were used. Replication cohorts had a greater proportion of late AMD cases (>85%) than the discovery cohort. Ages of cases and controls were not significantly different between cohorts (data not shown; Table 4.2).

Table 4.2 Cohort characteristics.

Late AMD includes cases of geographic atrophy (GA) and neovascular AMD (CNV). Grading was based on the Clinical Age-Related Maculopathy Grading System (*CARMS*) (Bird et al. 1995). Grading was performed by an ophthalmologist and refers to the worst eye. Controls were also examined. All cohorts were made up of Caucasian individuals. The numbers shown in the main text refer to the number of individuals that were successfully genotyped for *CFD* SNPs.

						Mean age		Sex			
Cohort	**Status**	**N**	**%**	Grading	**%**	**(years)**	**SD**	Male	%	Female	%
	Control	351	41			78	8.5	152	43.8	199	57.3
	Case	505	59	Late AMD	48.3	77.9	9.2	190	38.1	315	63.1
UK1	Total	846									
	Control	421	32.1			75.6	7.7	171	40.6	232	55.1
	Case	891	67.9	Late AMD	100	78.7	7.2	377	42.3	472	53
UK2	Total	1312									
	Control	311	33.8			76.6	5.1	143	46	168	54
	Case	608	66.2	Late AMD	85.9	79.3	7.3	222	36.5	386	63.5
USA 1	Total	919									
	Control	378	42.1			75.6	7.9	177	46.8	203	53.7
	Case	520	57.9	Late AMD	100	80	8.5	206	39.6	314	60.4
USA 2	Total	898									
	Control	887	40.1			75.4	6.1	394	44.4	501	56.5
	Case	1326	59.9	Late AMD	100	80.7	6.3	583	44	758	57.2
USA 3	Total	2213									
	Control	562	31.9			72.7	6.6	245	43.6	314	55.9
	Case	1201	68.1	Late AMD	91.3	75.9	8.2	456	38	744	61.9
Nijmegen	Total	1763									

4.2.3 *CFD* SNP Genotyping in UK1 case-control cohort

A schematic representation of TaqMan SNP genotyping is shown in Figure 4.3. Of the three single nucleotide polymorphisms selected for genotyping, only two of the genotyping assays performed satisfactorily. Representative genotype plots for each SNP, obtained from plate reads on the Applied Biosystems HT7900, are shown in Figure 4.4. One assay, for rs1683564, failed to achieve sufficient discrimination between genotype clusters to permit accurate assignment of genotype (Figure 4.4C). As a result, this SNP was not genotyped.

Allelic discrimination was achieved by the two remaining assays, with clear genotype clusters observed for the major allele homozygotes, heterozygotes and minor allele homozygotes (Figure 4.4A and B).

In addition to visual checking of genotyping cluster plots, the quality of genotyping data was assessed by call rate and deviation from Hardy-Weinberg equilibrium (HWE). Minimum call rate was found to be 93%. This is likely to represent poor DNA quality for individuals who failed to genotype, rather than a preferential assay failure for a given genotype as the same samples did not amplify for both the SNPs tested in the UK1 cohort. Hardy-Weinberg disequilibrium was not observed for either polymorphism in cases and controls ($p > 0.05$).

Genotype and allele frequencies obtained in the UK1 case-control cohort are shown in Table 4.3.

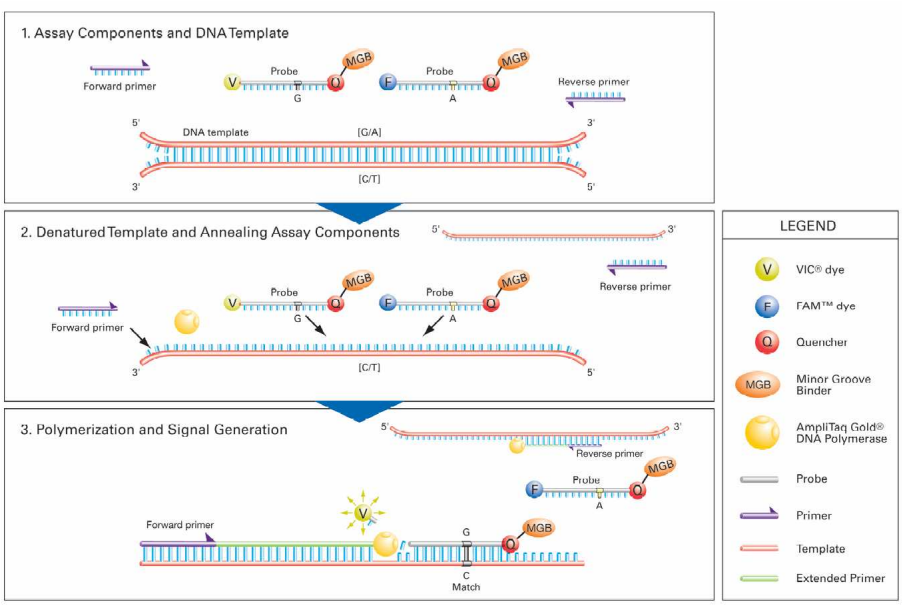

Figure 4.3 Schematic representation of TaqMan SNP genotyping technology.

TaqMan SNP Genotyping is performed by amplification of the target DNA using sequence-specific primers and two allele-specific TaqMan® MGB probes. The probes are labelled with either VIC or FAM fluorophores at the 5’ end; whilst the probe is intact, fluorescence is quenched by a 3’ quencher. During amplification, if the probe anneals to the polymorphic sequence, the 5’ nuclease activity of Taq polymerase degrades the probe, releasing the fluorophore. This causes a detectable fluorescent signal during amplification of each allele. Source: www.appliedbiosystems.com.

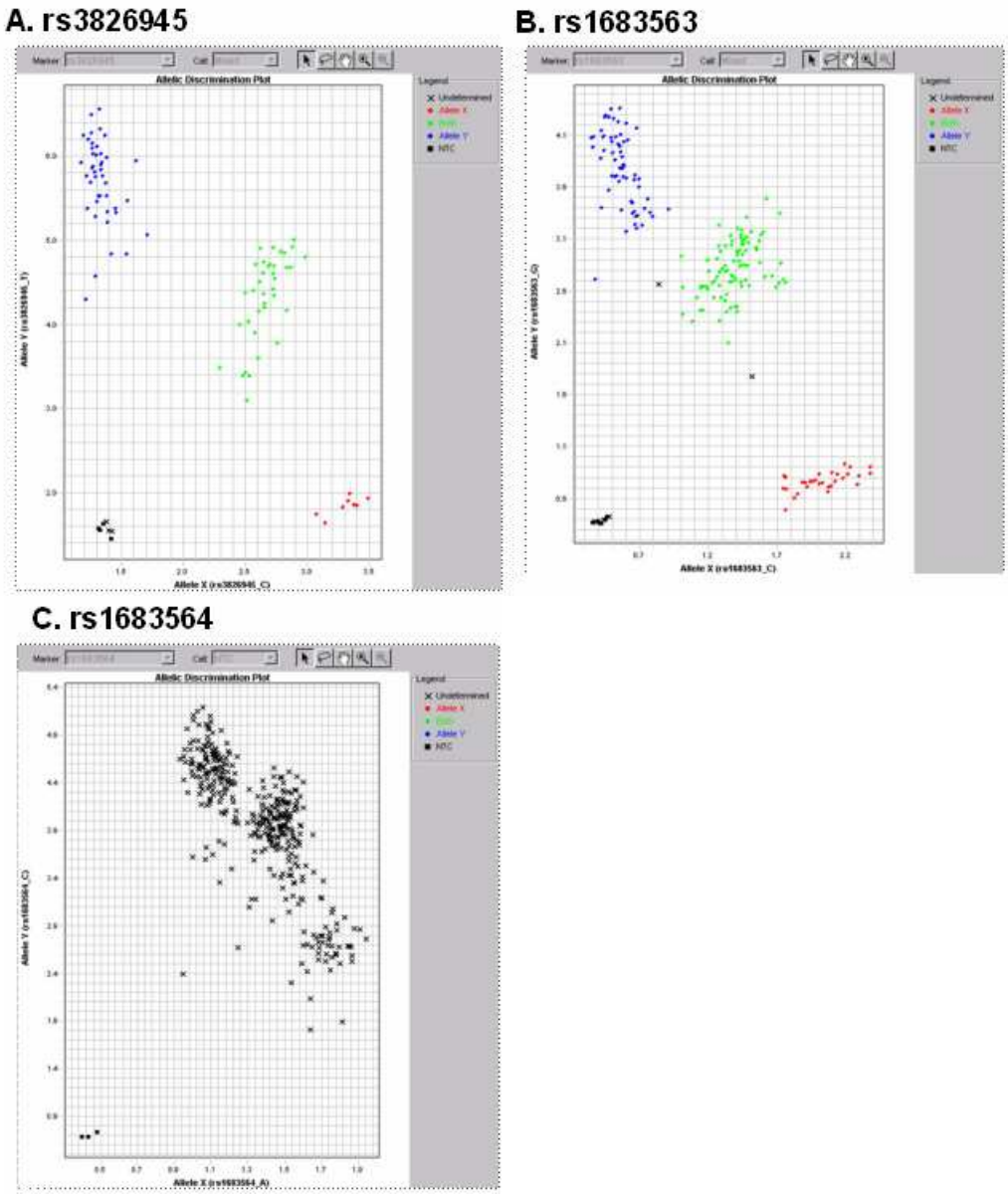

Figure 4.4 Representative genotyping plots obtained for SNPs in *CFD*.
TaqMan SNP genotyping uses fluorescent probes to detect SNP genotype. Representative genotyping plots for the three SNPs in *CFD* are shown. Assays for genotyping rs3826945 (A) and rs1683563 (B) performed well, generating distinct clusters for homozygous individuals, located at the Y (blue) or X (red) axis, whilst heterozygotes cluster in the centre (green). The assay for rs1683564 (C) did not achieve sufficient separation of genotype clusters to assign genotypes with confidence.

SNP	AMD Status	Genotype frequency	Cohort					
			UK1	UK2	USA1	USA2	USA3	Nijmegen
rs3826945	Cases	TT	0.42	0.45	0.41	0.45	0.46	0.47
		CT	0.47	0.46	0.47	0.45	0.42	0.42
		CC	0.10	0.09	0.11	0.09	0.12	0.11
		Minor allele frequency	0.34	0.32	0.35	0.32	0.33	0.32
	Controls	TT	0.47	0.50	0.48	0.46	0.45	0.51
		CT	0.41	0.41	0.43	0.41	0.44	0.39
		CC	0.11	0.09	0.10	0.12	0.11	0.10
		Minor allele frequency	0.32	0.29	0.31	0.33	0.33	0.29
		HWE p-value	***0.72***	***0.31***	***0.46***	***0.93***	***0.19***	***0.16***
rs1683563	Cases	GG	0.37	0.36	0.37	0.34	-	-
		CG	0.49	0.47	0.48	0.50	-	-
		CC	0.14	0.17	0.15	0.16	-	-
		Minor allele frequency	0.38	0.40	0.39	0.41	-	-
	Controls	GG	0.42	0.35	0.35	0.33	-	-
		CG	0.44	0.50	0.49	0.48	-	-
		CC	0.14	0.16	0.16	0.19	-	-
		Minor allele frequency	0.36	0.40	0.41	0.43	-	-
		HWE p-value	***0.91***	***0.88***	***0.60***	***0.77***	***-***	***-***

Table 4.3 Genotype and allele frequencies of rs3826945 and rs1683563 in six AMD case-control series.
Two SNPs in CFD - rs3826945 and rs1683563 - were genotyped in multiple AMD case-control series. UK1 was the discovery cohort; UK2, USA1-3 and Nijmegen were the replication cohorts. No cohort showed a significant deviation from Hardy-Weinberg Equilibrium (HWE) using Chi^2 test.

4.2.3.1 SNPs in *CFD* are associated with AMD in a British discovery cohort

Association analysis was carried out in a Scottish AMD case-control cohort (UK1) in the first instance. The UK1 series consisted of 351 controls and 505 cases (of which 48% had late AMD). The average age of cases was 77.9±9.2 years (SD) and 78.0±8.5 years (SD) for controls (Table 4.2). All individuals were unrelated and of Scottish ethnicity. Disease status and AMD grading criteria were described in Section 2.3.5.

The association between genotype at rs3826945 and rs1683563 with AMD was investigated by binomial logistic regression implemented in the statistical software package SPSS version 17. Odds ratios (OR) were calculated using the coefficient of the logistic regression (β). AMD status was included as a categorical dependant variable (AMD or disease-free control). Using a dominant genotypic model for regression, SNP genotype was categorised as 0=major allele homozygote, or 1=minor allele homozygote or heterozygote. Smoking status (ever/never), age and sex were also included in the analyses as known risk-modifiers for AMD. Smoking status and sex were categorical variables. Age was a continuous variable.

The results of the case-control association analyses of rs3826945 and rs1683563 in the UK1 cohort are summarised in Table 4.4. In this Scottish cohort, rs1683563 was suggestively associated with AMD (p=0.07). The minor allele of the rs3826945 SNP was significantly associated with AMD, increasing risk of AMD in carriers of the minor allele (OR 1.44, 95% C.I. 1.04-2.00, p=0.028).

The UK1 series was split by gender for regression analysis. As shown in Table 4.4, the association with AMD was observed only in females, who showed an OR of 1.70 (95% C.I. 1.11-2.63, p=0.016). This may represent a loss of power to detect an effect in males, due to a reduction in sample size (N male cases=175, N female cases=287).

Similar results were obtained using an additive model for logistic regression. SNP genotypes were categorised as 1 =major allele homozygote, 2 =heterozygote, 3 =minor allele homozygote. Minor allele homozygotes of rs3826945 were significantly associated with increased risk of AMD using this model (OR 1.403, 95% C.I. 1.008-1.953, p=0.045).

Analysis Group	N cases	N controls	Total	OR	95% CI	p
			Discovery cohort			
UK1 males	175	143	318	1.224	0.739-2.026	0.432
UK1 females	287	182	469	1.704	1.105-2.629	**0.016**
UK1 combined	462	325	787	1.442	1.041-1.998	**0.028**
			Replication cohorts			
UK2 males	343	154	497	1.202	0.778-1.856	0.407
UK2 females	430	208	638	1.898	1.262-2.855	**0.002**
UK2 combined	773	362	1135	1.546	1.151-2.076	**0.004**
USA 1 males	210	137	347	1.093	0.668-1.788	0.725
USA 1 females	370	159	529	1.463	0.967-2.214	**0.071**
USA 1 combined	580	296	876	1.303	0.950-1.786	0.101
USA 2 males	205	172	377	1.080	0.678-1.721	0.746
USA 2 females	307	199	506	0.882	0.580-1.342	0.522
USA 2 combined	512	371	883	0.974	0.714-1.329	0.870
USA 3 males	527	354	881	0.982	0.833-1.261	0.817
USA 3 females	684	436	1120	0.952	0.719-1.260	0.731
USA 3 combined	1211	790	2001	0.955	0.784-1.163	0.647
Nijmegen males	449	226	675	1.105	0.799-1.528	0.547
Nijmegen females	725	300	1025	1.017	0.769-1.345	0.907
Nijmegen combined	1174	526	1700	1.052	0.852-1.299	0.637
			Meta-analysis			
All males	1932	1196	3128	1.043	0.901-1.207	0.571
All females	2833	1497	4330	1.180	1.036-1.344	**0.012**
All	4765	2693	7458	1.112	1.009-1.225	**0.032**

Table 4.4 SNP association results for *CFD* SNP rs3826945.
A dominant additive model was used to assess the association of the minor allele of rs3826945 to AMD in a total of six cohorts. Analyses were controlled for age, sex and smoking. UK1, UK2, USA1 and USA2 cohorts were also genotyped for rs1683563, which was not significantly associated with AMD when included as a covariate in the analysis of these cohorts.

4.2.3.2 Power calculation

Based on the odds ratios of the association between AMD and rs3826945 in the UK1 cohort (OR 1.44, 95% C.I. 1.04-2.00), retrospective power calculations were performed to determine the appropriate sample size to detect an effect of this magnitude with a 95% confidence level. The Genetic Power Calculator programme was utilised for this analysis (Purcell et al 2003). Prevalence of AMD was reported as 1.47% in the population aged above 40 years (The Eye Diseases Prevalence Research 2004). The calculation was performed to allow for a 1% threshold for type I errors. Assuming a control:case ratio of 0.7, the number of cases required to detect an effect of this size with 95% power was calculated as 1876 cases using the dominant model, and 4332 cases using an allelic model.

4.2.4 Association analysis of *CFD* rs3826945 in 5 replication cohorts

Given that the Scottish AMD cohort had low power to reliably detect such a small effect upon AMD risk, both SNPs were genotyped in a larger set of case-controls (Table 4.2). Some individuals in these cohorts were not successfully genotyped; the number of genotyped cases and controls is indicated in the following text. Minor allele frequencies and genotype frequencies are shown in Table 4.3.

The first round of replication cohorts consisted of an additional UK series from Cambridge, England (UK2; 773 genotyped cases (all with severe AMD) and 362 examined controls) and two North American cohorts (USA1, USA2). USA1 (University of Michigan) included 580 genotyped cases (86% severe AMD) and 296 examined controls while USA2 (National Eye Institute) included 512 genotyped cases (100% severe AMD) and 371 examined controls). All cohorts comprise unrelated Caucasian individuals.

The minor allele (C) of rs3826945 was found to be associated with an increased risk of AMD in a second British AMD case-control cohort (UK2; p=0.004, OR 1.54, 95% C.I. 1.151-2.076; Table 4.4). Once again, in analysis stratified by gender, the association with AMD remained significant in females (p=0.002, OR 1.90, 95% C.I. 1.262-2.855), but not in males (p=0.40). Age and smoking history

were also significantly associated with AMD-risk in this cohort. The average age of individuals in this cohort was 78.7±7.2 years (SD) for cases and 75.6±7.7 years (SD) for controls. A small increase in risk for each year of age was observed ($p=8.9x10^{-12}$, OR 1.06, 95% C.I. 1.04-1.08). This reflects the reported increased prevalence of AMD in older individuals which is 1.47% in the population aged over 40 years, 15% in white females aged over 80 years (The Eye Diseases Prevalence Research 2004). A current or former smoker (ever smoked) in this cohort had an increased risk of AMD, relative to never having smoked (OR 1.38, 95% C.I. 1.04-1.82, p=0.025).

SNP genotyping for USA1 and USA2 was performed in America. The USA1 cohort was genotyped by dye-termination Sanger sequencing. The USA2 cohort was genotyped for rs1683563 and rs3826945 using TaqMan, as described for the UK1 and UK2 series in Section 2.3.6.1. Genotype and minor allele frequencies are shown in Table 4.3. There were no significant deviations from HWE.

Table 4.4 summarises the results of the binary logistic regression analysis performed in the USA1 and USA2 replication cohorts. Regression analysis was performed as described for the British cohorts, both combining males and females, and splitting the series by gender. The minor allele of rs3826945 showed no significant association with AMD in either of the USA 1-2 replication cohorts (p=0.10 and p=0.87 respectively). However, when stratified by gender, there was a suggestively significant association of the minor allele of rs3826945 with AMD in females from the USA1 cohort only (p=0.07, OR 1.46, 95% C.I. 0.97-2.21).

Age was significantly associated with AMD-risk in these cohorts. The average age of individuals in the USA1 cohort was 79.3±7.3 years (SD) for cases and 76.6±5.1 years (SD) for controls. In USA2, the average age of cases was 80.0±8.5 years (SD), and for controls, 75.6±7.9 years (SD). As expected, both series exhibited a small increase in risk for each year of age (USA1: $p=1.1x10^{-8}$, OR 1.07, 95% C.I. 1.04-1.09; USA2: $p=2.2x10^{-12}$, OR 1.06, 95% C.I. 1.04-1.08). Smoking history was not significantly associated with AMD in the analysis of either USA1 or USA2 series (data not shown). The USA1 series showed a significant association between gender and AMD, with males appearing to be protected from AMD ($p=3.8x10^{-4}$, OR 0.57, 95% C.I. 0.42-0.78). This is likely to reflect the composition of the cohort, with unequal distribution of males and females between cases and controls (Table 4.2).

Rs1683563 was not significantly associated with AMD in any of these three cohorts (UK2, p=0.265; USA1, p=0.911, USA2, p=0.311).

Due to the lack of conclusive replication of the association between rs3826945 and AMD that was observed in two British cohorts (UK1, UK2) in two North American cohorts (USA1, USA2), additional cohorts were investigated. The second replication group included a further large case-control series from USA (USA3, Tufts University) and another from Europe (Nijmegen, a Dutch-German series). Due to the absence of association detected between rs1683563 and AMD in the four earlier cohorts, these cohorts were genotyped for rs3826945 only. In the USA3 series, rs3826945 was genotyped using the Sequenom iPLEX assay (Yu et al 2011). The Nijmegen series was genotyped using the TaqMan 5' nuclease SNP genotyping assay for rs3826945.

The USA3 cohort consisted of 1211 genotyped cases (all with severe AMD) and 790 examined controls. The average age of individuals in USA3 was 80.7±6.3 years (SD) for cases and 75.4±6.1 years (SD) for controls (Table 4.2). In the Nijmegen series, 1174 cases (91.3% with severe AMD) and 526 examined controls were genotyped. The average age of cases was 75.9±8.2 years (SD), whilst controls were generally younger (72.7±6.6 years (SD)). Neither of these series showed evidence of association between rs3826945 and AMD (USA3, p=0.647; Nijmegen, p =0.637), as shown in Table 4.4.

Once again, advancing age was a significant AMD-risk factor; in USA3, p= $3.8x10^{-60}$, OR 1.16, 95% C.I. 1.14-1.18, and in Nijmegen, p=$1.64x10^{-13}$, OR 1.05, 95% C.I. 1.04-1.07. The USA3 series, but not the Dutch series, showed a significant association between gender and AMD, with males appearing to be protected from AMD (p=$1.4x10^{-5}$, OR 0.63, 95% C.I. 0.51-0.78). Smoking history was also a significant covariate in these analyses (in USA3, p=$7.0x10^{-9}$; in Nijmegen, p=$5.9x10^{-6}$). Individuals who had ever smoked were at increased risk of AMD.

The minor or risk allele frequency (C allele) for rs3826945 varied from 0.31 to 0.35 in AMD cases across the individual case-control series, and from 0.29-0.33 in controls (Table 4.3). These very similar minor allele frequencies observed in the UK1 (0.34) and replication series obtained from both the UK and abroad indicate

that allele frequency differences in the various populations are unlikely to account for differences between cohorts.

4.2.5 Meta-analysis of rs3826945 in six AMD case-control cohorts

The contribution of rs3826945 towards AMD risk was assessed in all of the six cohorts combined in a single meta-analysis. This was expected to increase statistical power to detect an effect of small magnitude. The combined cohorts comprised of 4765 cases and 2693 controls. The mean age of cases was 78.7±7.8 (SD) years and the mean age of the controls was 75.4±7.1 (SD) years (Table 4.2).

The combined cohort for the meta-analysis was analysed by binary logistic regression using a dominant model, as previously described for the individual cohorts. The results of the regression are shown in Table 4.4. The odds ratio (and 95% confidence interval) obtained for each of the individual cohorts, together with the combined data set, are summarised in the Forest Plot shown in Figure 4.5. Overall, there was a significant association between AMD and rs3826945 (OR=1.11, C.I. 1.01-1.23, p=0.032). As seen in the UK1-2 cohorts, and suggested in the USA1 cohort, analysis of the combined cohorts found a significant effect in females (OR=1.18, 95% C.I.1.04-1.34, p=0.012) but not in males (OR=1.04, 95% C.I. 0.90-1.21, p=0.57) for the minor allele of rs3826945. Similar results were obtained using an additive model for regression analysis, although this model has less power to detect the association (data not shown).

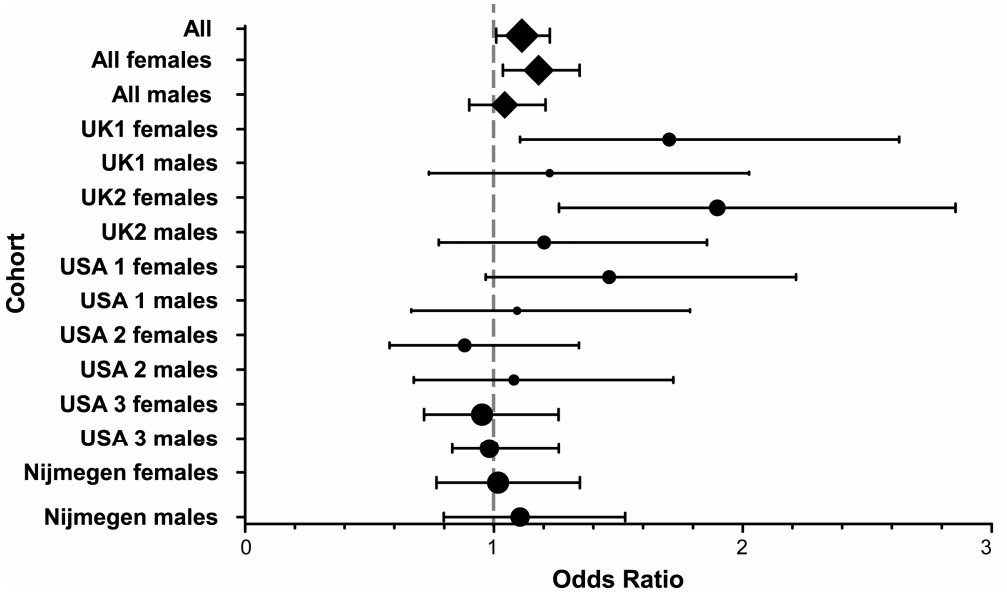

Figure 4.5 Forest plot of the results of meta-analysis for the association between *CFD* SNP rs3826945 and AMD.

Six AMD case-control cohorts were tested for an association between rs3826945 and AMD. Association varied between the three US and three European case-control series. Meta-analysis of the combined cohorts, consisting of 4765 cases and 2693 controls, showed a significant association in the combined sexes (OR=1.11, p-value=0.032) and in combined females (OR=1.18, p-value=0.012). No significant association between rs3826945 and AMD was detected in males.

4.2.6 Gene-environment interactions for *CFD* in AMD

AMD was associated with increasing age, smoking and gender (in some cohorts), as described in Section 4.2.1.6. For some of the replication cohorts (UK2, USA3, Nijmegen), body mass index (BMI) scores were available. A BMI score greater than 30 was significantly associated with AMD in these combined cohorts where data were available (p=0.037, OR 1.357, 95% C.I. 1.019-1.807).

The possibility of interactions between genotype at rs3826945 and BMI, smoking status, age or sex affecting the association with AMD was evaluated. Multinomial logistic regression was performed using a custom/stepwise approach to investigate an interaction between rs3826945*smoking (ever/never), rs3826945*age, rs3826945*sex and rs3826945*BMI (categorised as <25, 25-29.99, or >30). Models in which an interaction was included did not influence the association with AMD, compared to independent inclusion of both covariates for age and smoking (Table 4.5). In agreement with results obtained by regression analysis performed in females only, females appear to be more susceptible to AMD when they carry the risk allele of rs3826945 (OR 1.304, 95% C.I. 1.142-1.489 for the interaction; increased from OR 1.236, 95% C.I. 1.117-1.367 for females without accounting for genotype).

There was no increase in AMD susceptibility for carriers of the rs3826945 minor allele in combination with BMI. In fact, the interaction between high BMI (>30) and rs3826945 removed the significant association of BMI with AMD (p=0.037, OR 1.357, 95% C.I. 1.019-1.807 was reduced to OR 0.878, 95% C.I. 0.551-1.397, p=0.582 for the interaction).

	B	S.E.	Wald	df	p	Odds Ratio	95% C.I.for Odds Ratio	
							Lower	Upper
rs3826945	0.106	0.049	4.595	1	0.032	1.112	1.009	1.225
Exact_Age	0.056	0.003	292.949	1	$1.13x10^{-65}$	1.058	1.051	1.065
Exact_Age * rs3826945 CT/CC	0.056	0.003	264.125	1	$2.17x10^{-59}$	1.057	1.050	1.065
Sex (female)	0.212	0.051	16.984	1	$3.77x10^{-5}$	1.236	1.117	1.367
Sex (female)* rs3826945 CT/CC	0.266	0.068	15.394	1	$8.73x10^{-5}$	1.304	1.142	1.489
Smoker2 (never)	0.043	0.051	0.728	1	0.394	1.044	0.945	1.154
rs3826945* Smoker2 (never)	0.053	0.069	0.580	1	0.446	1.054	0.920	1.207
BMICAT(>30)	0.305	0.146	4.368	1	0.037	1.357	1.019	1.807
BMICAT(>30) * rs3826945 CT/CC	-0.130	0.237	0.303	1	0.582	0.878	0.551	1.397

Table 4.5 Interactions between rs3826945 and age, smoking or BMI do not increase susceptibility to AMD.
Multinomial logistic regression was performed using a custom/stepwise approach to investigate an interaction between rs3826945*smoking (ever/never), rs3826945*age, rs3826945*sex and rs3826945*BMI (categorised as <25, 25-29.99, or >30). An interaction between female gender and the risk allele resulted in an increased susceptibility to AMD. An interaction between high BMI and risk genotype resulted in a non-significant relationship of BMI and SNP genotype to AMD.

4.2.7 Searching for novel variants in *CFD*

The intronic SNPs used to search for association with AMD are unlikely to have a functional effect on the protein, unless they affect *CFD* expression. In order to investigate the possibility that novel variants in *CFD* were responsible for the association with AMD identified in theUK1 and UK2 series, a subset of cases and controls were subjected to sequencing and testing for copy number variation.

4.2.7.1 Optimisation of *CFD* sequencing primers

Primers were designed to span all 5 exons of *CFD*, together with the intron-exon boundaries. Primer sequences and optimised conditions for PCR amplification of each exon are shown in Table 2.3.

4.2.7.2 Sequencing of *CFD*

Genomic DNA from 95 AMD cases and from 95 disease-free controls was used to sequence the exonic and flanking regions of *CFD*. Sequence analysis was performed using Mutation Surveyor to identify variants in relation to the *CFD* reference sequence (ENSG00000197766), obtained from Ensembl (http://www.ensembl.org).

No novel variants in *CFD* were identified in these cases or controls. All of the variants identified by sequencing, shown in Figure 4.6, are reported in dbSNP (www.ncbi.nlm.nih.gov/projects/SNP/). Three variants are intronic. Two of the intronic variants (rs1629038 and rs1626564) are in high linkage disequilibrium with one another, commonly occurring on the same haplotype in both cases and controls. One coding change was identified, changing the glutamate (E) at position 69 in CFD to lysine (K). E69 is located close to the histidine residue (H66) of the catalytic triad of CFD. It is conceivable that altering a negatively charged amino acid (E) for a positively charged amino acid (K) may affect the active site of the enzyme. One control sample was homozygous for the E69K variant, and one AMD case was heterozygous for the same variant. Representative chromatograms for the variants are shown in Figure 4.6.

The SNPs identified by sequencing were tested for association with AMD. Two-by-two contingency tables and Fisher's exact tests determined that there is no significant difference between the frequency of these polymorphisms in *CFD* in AMD cases or controls (Figure 4.6).

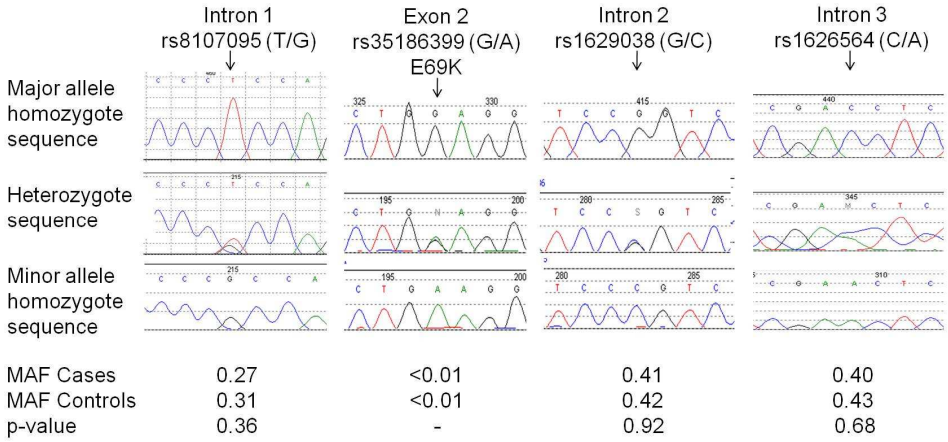

Figure 4.6 Sequencing identified known variants in *CFD*.
The exons and flanking regions of *CFD* were sequenced in 96 AMD cases and 96 controls from the UK1 cohort. No novel variants in *CFD* were identified by sequencing. The polymorphisms detected are included in the dbSNP database (www.ncbi.nlm.nih.gov/projects/SNP). Only one - rs35186399 – resulted in a coding change in CFD (E69K). Representative sequence chromatograms for the major allele homozygotes, heterozygotes and the minor allele homozygotes for each variant are shown. Minor allele frequencies (MAF) were calculated for cases and controls. There were no significant differences in MAF between cases and controls assessed with Fisher's exact test (p-value is shown).

4.3 Copy number variation at chromosome 19p13.3

The Database of Genomic Variation (http://projects.tcag.ca/variation/; (Iafrate et al. 2004)) was used to screen the human genomic assembly (Build 36, March 2006) for previously reported variations in copy number near *CFD*. A copy number variation (Variation_30054) was identified using "CFD" as the search term (Figure 4.7). Located on chromosome 19, positions 791984-850978, Variation_30054 spans almost 60 kb covering the genes *PRTN3*, *MED16*, *ELANE*, *CFD* and *C19orf22*. It was identified as a loss of copy number in one individual in 485 control samples in

the Human Genome Diversity Panel, using the Illumina HumanHap550 BeadChip (Jakobsson et al. 2008).

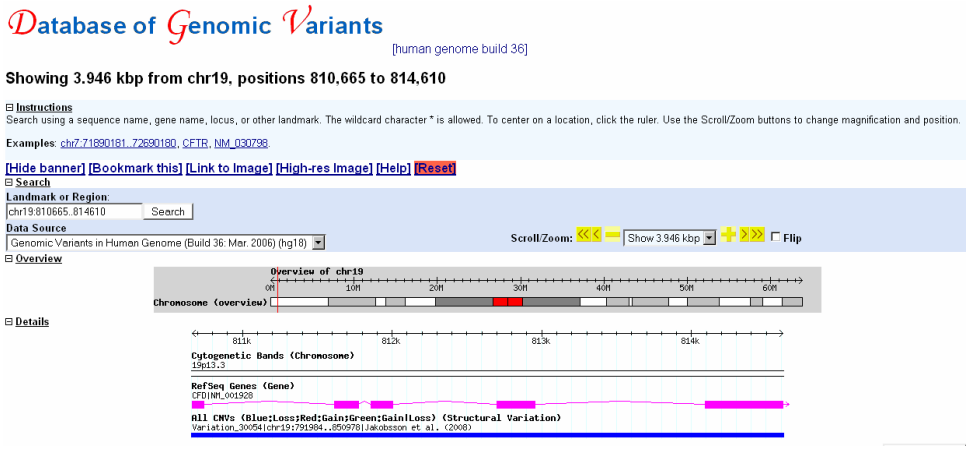

Figure 4.7 Copy number variation in the *CFD* locus.
The Database of Genomic Variation (http://projects.tcag.ca/variation) was screened for reported variations in copy number in CFD in the human genomic assembly (Build 36, March 2006). Variation_30054 is spans almost 60 kb covering the genes *PRTN3*, *MED16*, *ELANE*, *CFD* and *C19orf22*. The TaqMan Copy Number Variation assay (Hs01536182_cn) spans the exon 3-intron 4 boundary in *CFD* was selected to measure copy number variation in 311 AMD cases and 329 controls from the UK1 cohort.

4.3.1 Measuring copy number variation at CFD

Due to the copy number variation spanning *CFD*, it was proposed that copy number variation might play a role in AMD susceptibility. To assess this, TaqMan Copy Number Variation assays for Variation_30054 (Hs01536182_cn) and an *RNAseP* reference assay were used in a multiplex reaction to measure copy number. 311 AMD cases and 329 controls from the UK1 (Scottish AMD) case-control series were assayed in triplicate for each sample. Predicted copy number was calculated using Copy Caller software from Applied Biosystems. This calculates the difference in threshold cycle (C_T) values measured during amplification for *CFD* and *RNAseP*. C_T is considered proportional to the number of copies of the target gene. Alterations in *CFD* copy number are reflected by deviation of C_T ratio from 1. A C_T ratio of 0.5 indicates a reduction of one copy (compared to the normal two copies), whilst an increase in C_T ratio to 1.5 indicates an increase in CFD copy number to 3 copies. A

conservative C_T threshold value of 32 was used across all plates, with samples showing amplification later than cycle 32 excluded from the analysis.
Predicted copy number was used to calculate the proportion of AMD cases and controls with deletions or duplications spanning *CFD*. Copy number variation was identified in 4 out of 311 AMD cases (2 with a single copy and 2 with three copies) and 9 out of 329 controls (1 with zero copies, 5 with a single copy and 3 with three copies) (Figure 4.8). There was no significant difference in the frequency of duplication or deletion of *CFD* between cases and controls (1.3% of AMD cases and 2.7% of controls; p=0.51 using Fisher's exact test).

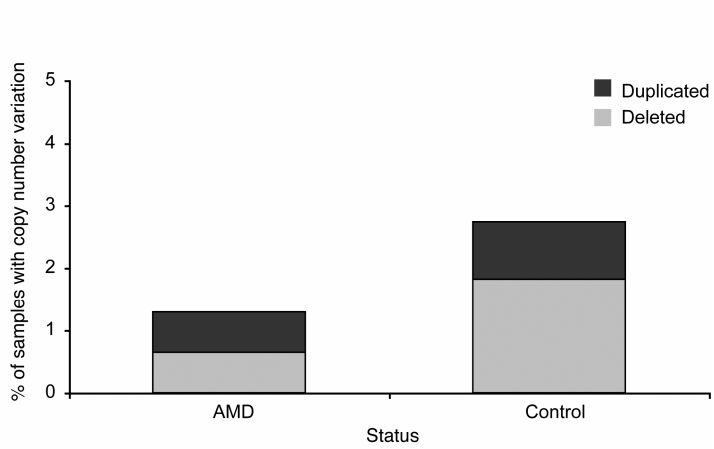

Figure 4.8 Duplication and deletion of CFD in AMD cases and controls.

Copy number variation in the CFD gene was detected in AMD cases and controls. Decreased copy number was slightly more common in controls (N=329, 1 with zero copies, 5 with a single copy) than AMD cases (N=311, 2 with a single copy). Increased copy number was identified in 2 out of 311 AMD cases 3 out of 329 controls. There was no statistically significant difference in copy number variation between AMD cases and controls.

4.4 Plasma CFD

Plasma CFD concentrations are reported to be elevated in AMD cases, relative to controls, in some but not all studies of complement proteins in plasma in small cohorts (Scholl et al. 2008; Reynolds et al. 2009; Hecker et al. 2010). Plasma CFD was measured in the UK1 and UK2 series to test for an association with AMD, and with *CFD* SNP genotype.

4.4.1 Optimisation of the CFD ELISA

The Duoset ELISA development kit for human CFD from R&D Systems is a sandwich ELISA developed for measuring CFD in cell culture supernatants. The concentration of CFD in plasma is higher than in cell culture supernatants. In order to use the mouse anti-CFD Capture antibody (4 µg/ml) and the biotinylated goat anti-CFD Detection antibody (200 ng/ml) at the recommended dilution, the optimal dilution of plasma was determined. Serial dilutions of three internal control plasma samples (P1, P2 and P3) were made, ranging from 1/400 to 1/4,000 to determine the appropriate dilution to achieve measurements in the linear range of the ELISA. The standard curve was made by serial dilutions of recombinant human CFD, ranging from 0 - 2.5 ng/ml. A representative 6-point standard curve is shown in Figure 4.9. Average absorbance at 450 nm for the three plasma samples at each dilution ± SD is shown in Figure 4.10.

Plasma CFD concentrations in the range of 1-3 µg/ml have previously been reported (Reynolds et al 2010). In this range, a plasma dilution of 1/4,000 (0.00025) was determined to be suitable for the assay.

4.4.2 Inter- and intra-assay variation for the CFD ELISA

The internal control plasma samples P3, P6 and P9 were measured multiple times within the same assay, and measurements obtained were used to assess intra-assay variability for the CFD ELISA. Figure 4.11A shows the mean measurement of plasma CFD obtained for each plasma sample (±s.e.m.) from at least 5 replicates. Coefficients of variation (CV) were around the 5% threshold or below, indicating that there was no significant difference between replicates.

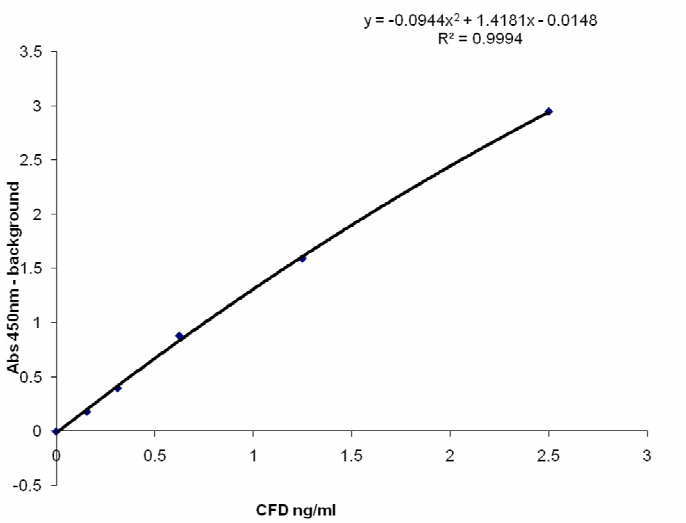

Figure 4.9 Representative standard curve for CFD ELISA.
A standard curve for CFD was obtained by serial dilution of purified recombinant human CFD of known concentration, included in the R&D DuoSet ELISA kit. The standard curve also included a blank control to obtain background absorbance at 450 nm. The equation of the line-of-best fit was obtained by polynomial regression in Microsoft Excel. Goodness of fit was assessed using the squared correlation coefficient (R^2). The standard curve was used to calculate the concentration of CFD in EDTA-plasma samples from the UK1 and UK2 AMD case-control series.

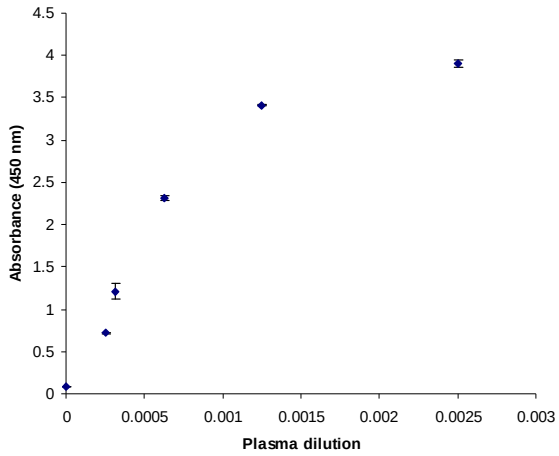

Figure 4.10 Optimisation of plasma dilutions for CFD ELISA.
The optimal dilution of human plasma samples for use with the pre-developed CFD DuoSet ELISA kit antibodies was determined. Dilutions of three human plasma samples were made, in the range of 1/400 to 1/4,000 and used in the ELISA following the recommended protocol. Plasma CFD was expected to be in the range of 1-3 µg/ml. The average absorbance at 450 nm for the three plasma samples at each dilution ± standard deviation shows that a dilution of 1/4,000 allows detection of CFD in EDTA-plasma samples within the linear range of the standard curve.

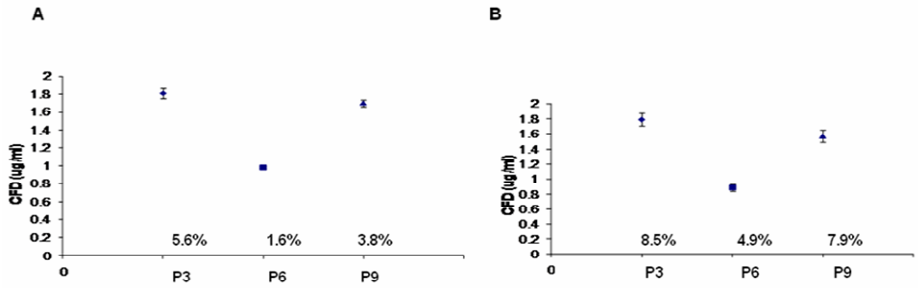

Figure 4.11 Inter- and Intra-assay variation of CFD ELISA.

A. Intra-assay variation was measured within replicates of three human plasma samples P3. P6 and P9. Each point represents at least five replicates ±s.e.m. Coefficients of variation (CV) are shown below each point.
B. Inter-assay variation was measured based on the mean of two or more replicates from at least five different assays. Each point represents the mean of replicates ±s.e.m. Coefficients of variation (CV) are shown below each point.

The internal control plasma samples P3, P6 and P9 were also used to assess inter-assay variation. The samples were measured multiple times in different assays, and measurements obtained were used to assess inter-assay variability for the CFD ELISA as described in Section 2.5.3. Figure 4.11B shows the mean measurement of plasma CFD obtained for two replicates of each plasma sample in a minimum of five assays (±s.e.m.), and indicates the coefficient of variation for each sample. There was minimal variation observed between assays (CV < 10%).

4.4.3 Plasma CFD measurements in UK1 and UK2 AMD case-control cohorts

The plasma CFD concentration was measured in 751 AMD cases and 474 controls from the UK1 and UK2 case-control series for which plasma was available. Measurements were carried out in duplicate and mean values were corrected for inter-assay variation using two internal controls (P3 and P6).

The plasma CFD measurements in the two British case-control cohorts showed a slight positive skew, leading to a small deviation from normal distribution

(Figure 4.12). To account for the deviation from normal distribution, non-parametric tests were used to investigate the relationship between plasma CFD and AMD. The effect of age, gender, smoking history and body mass index (where available, in UK2) upon plasma CFD was also investigated using non-parametric testing. The relationship of quartiles of plasma CFD with AMD status was further investigated using logistic regression, including AMD-risk factors as covariates. Plasma measurements in the UK1 and UK2 cohorts were analysed independently. Additionally, as there was no significant difference in the observations made in each cohort independently, data was subsequently combined for analysis.

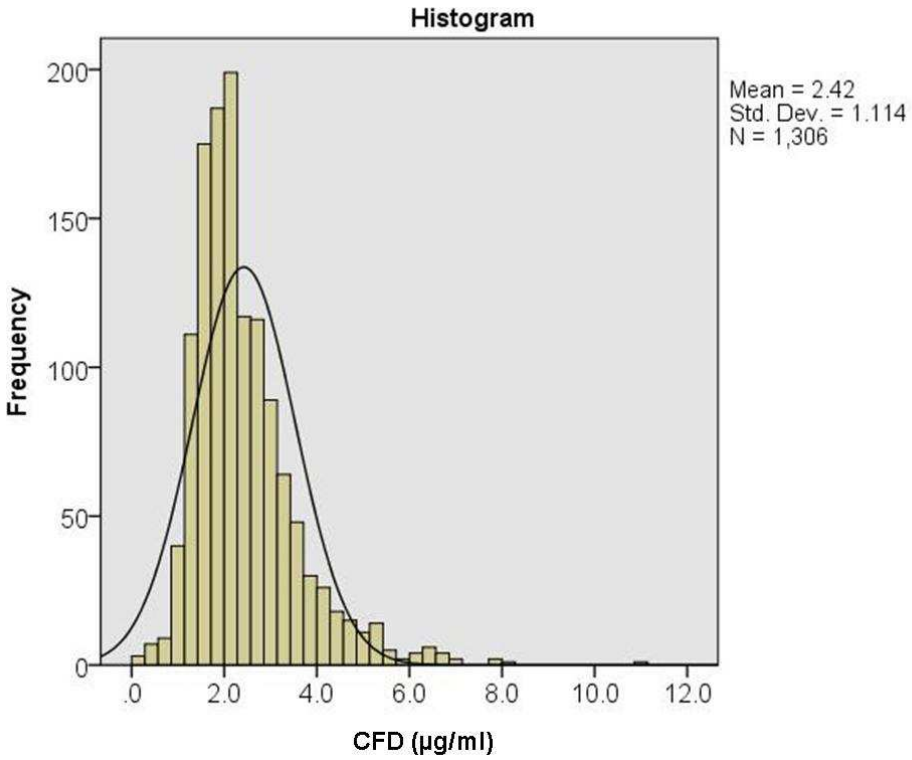

Figure 4.12 Distribution of plasma CFD measurements in combined UK1 and UK2 series.

The distribution of unadjusted plasma CFD measurements (µg/ml) in the combined UK1 and UK2 AMD case-control series. Normal distribution has a kurtosis value of less than 0.8: these data show a deviation from normal, as indicated by a kurtosis value of 5.25.

4.4.3.1 Analysis of AMD-risk factors as covariates

Expression of CFD has been reported to increase with advancing age (Reynolds et al 2010). This was confirmed in the analysis of plasma CFD measurements in the two UK cohorts combined. As shown in the box plots in Figure 4.13, there was a significant increase in plasma CFD with increasing age. The median values of plasma CFD in the group aged less than 60 years was 1.96±0.14 (s.e.m.) μg/ml. The median increased to 2.09±0.04 (s.e.m.) μg/ml in individuals aged 60-79.99 years, and again to 2.35±0.05 (s.e.m.) μg/ml in individuals aged over 80 years. This reflected a significant difference in the distribution of plasma CFD measurements in the three age groups ($p < 0.001$; Kruskal-Wallis test). A similar effect of increasing age upon plasma CFD was observed in AMD cases and controls analysed separately (data not shown).

Both UK cohorts exhibited a gender-specific difference in plasma CFD concentrations, with females having a lower median concentration (2.09±0.04 (s.e.m.) μg/ml) compared to males (2.26±0.05 (s.e.m.) μg/ml) in the combined cohorts. A Mann-Whitney U test identified a significant difference in the distribution of plasma CFD measurements between males and females ($p=0.002$, Figure 4.14). When the gender groups were split into AMD cases and controls, the significant difference in plasma
CFD was observed in controls ($p=0.001$), and not in cases ($p=0.254$).

Smoking history was categorised as never smoked, currently smokes or ex-smoker. As shown in Figure 4.15, neither of the UK cohorts showed a significant difference in plasma CFD measurements as a result of smoking history (UK1, $p=0.84$; in UK2, $p=0.224$).

Adipose tissue is a leading source of CFD (White et al. 1992). BMI scores were available for the UK2 cohort. Non-parametric testing was used to assess the association between plasma CFD and BMI category (BMI<25, 25-29.99, >30) in this series. Plasma CFD was found to be significantly elevated in individuals with BMI >30 (Figure 4.16). In this group, the median plasma concentration was 2.11±0.07 (s.e.m.) μg/ml, compared to lower median values in the groups for BMI <25 (1.77±0.06 (s.e.m.) μg/ml) and BMI 25-29.99 (1.91±0.04 (s.e.m.) μg/ml). The

difference in plasma CFD between individuals with a healthy BMI (BMI <25) and those classed as obese (BMI>30) was highly significant ($p = 3 \times 10^{-6}$).

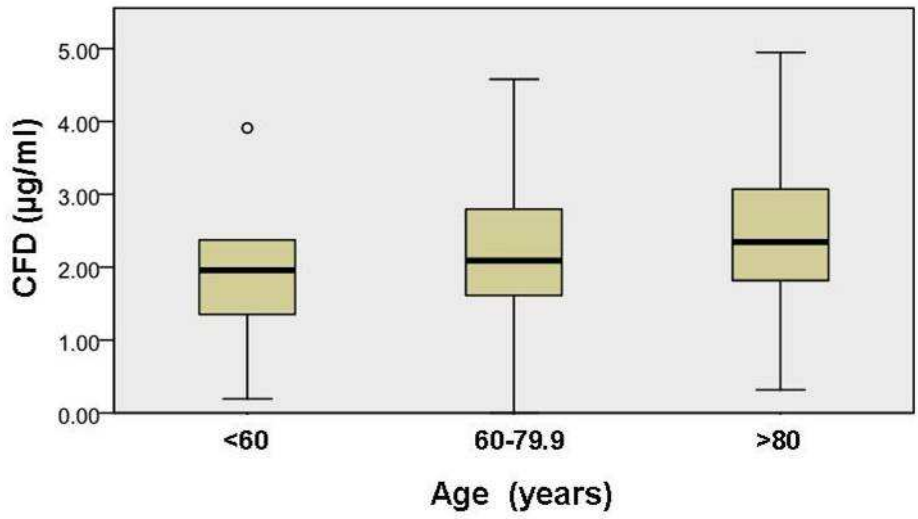

Figure 4.13 Plasma CFD increases with age.
Non-parametric testing identified a significant relationship between elevated plasma CFD concentration and increasing age (p=<0.001; Kruskal-Wallis test). Age in the combined UK1 and UK2 cohorts was categorised as <60 years (0), 60-80 years (1) and >80 years (2). A similar relationship was also observed in AMD cases and in controls analysed separately.

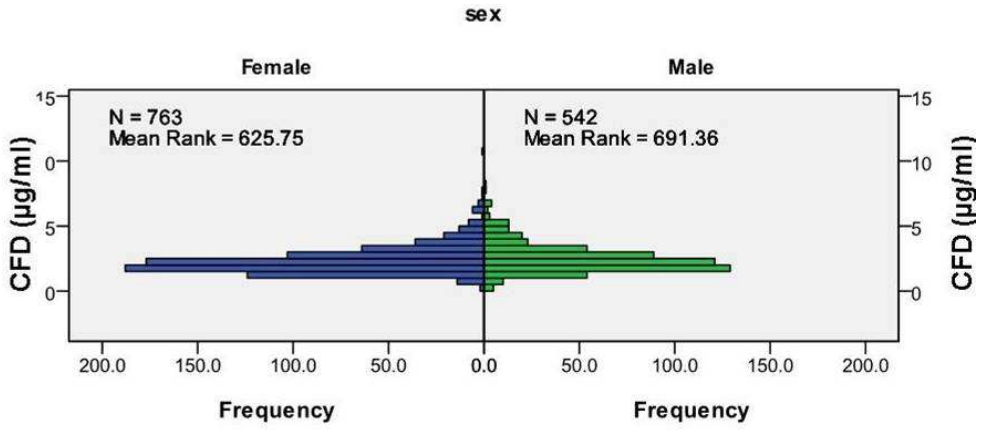

Figure 4.14 Plasma CFD has altered distribution in females.
Mann-Whitney U testing of ranked plasma CFD concentrations (µg/ml) identified a significant difference (p=0.002) in the distribution of CFD measurements in females compared to males. Females had significantly lower median plasma CFD concentrations than males (mean rank=625.75 compared to a mean rank of 691.36 in males); this effect was most pronounced in controls.

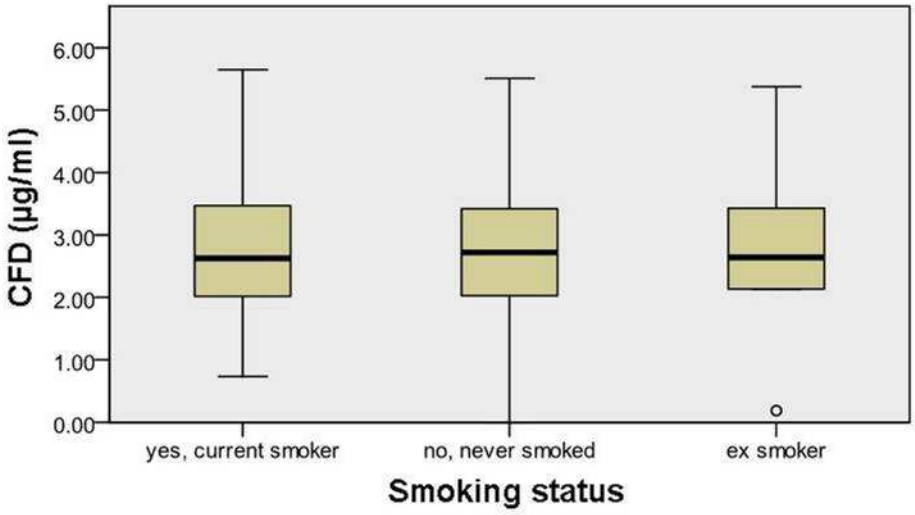

Figure 4.15 Smoking history does not affect plasma CFD.
Smoking history (categorised as current smoker, ex-smoker, or never smoked) was not found to influence plasma CFD concentrations in the combined UK1 and UK2 AMD case-control series using non-parametric testing.

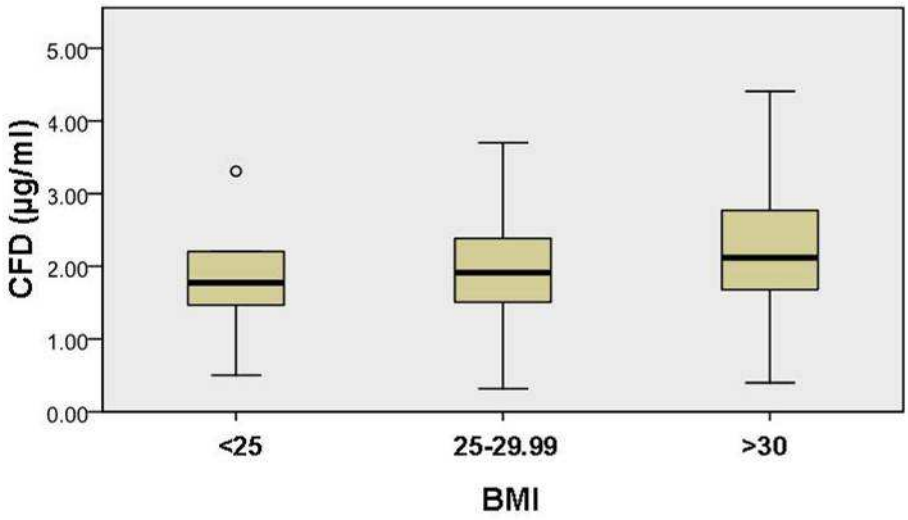

Figure 4.16 BMI affects plasma CFD.
BMI was found to have a significant relationship with elevated plasma CFD concentrations using non-parametric testing. Body mass index scores were categorised as BMI<25 (healthy), 25-29.99 (overweight) and >30 (obese). There was a highly significant difference in median plasma CFD concentrations between individuals with a BMI <25 and a BMI >30 ($p=3\times10^{-6}$).

4.4.3.2 Association of AMD status with plasma CFD

Plasma CFD was elevated in AMD cases compared with controls in the UK1-2 series assessed by non-parametric testing (Table 4.6). In the combined cohorts, the median plasma CFD concentration in cases was 2.31±0.043 (s.e.m.) μg/ml and 2.08±0.046 μg/ml in controls ($p=3.95x10^{-6}$; Figure 4.17). When samples were stratified by gender, plasma CFD was significantly greater in AMD females than control females ($p=3.76x10^{-6}$) but there was no significant difference between AMD males and control males. (p=0.112; Figure 4.17).

To correct for the confounding impact of age, sex and BMI, these were included as covariates in logistic regression analyses to assess the association of plasma CFD quartiles with AMD. In agreement with the results of non-parametric testing, elevated plasma CFD was significantly associated with AMD, and this association was found only in females. The odds ratio for those of both sexes in the highest versus lowest quartile of plasma CFD when age and smoking (ever/never) was included as a covariate was 1.81 (95% C.I. 1.27-2.57; p=0.001). In females only, the corresponding odds ratios were 2.15 (95% C.I. 1.35-3.44; p=0.001), and in males only, 1.42 (95% C.I. 0.82-2.47; p=0.215).

BMI was included as a covariate in regression analysis for 272 controls and 402 AMD cases from the UK2 series. The OR for the 4^{th} versus 1^{st} quartile of plasma CFD was 2.03 (95% C.I. 1.26-3.27; p=0.004).

4.4.3.3 Association of *CFD* genotype with plasma CFD

The minor allele of the *CFD* SNP rs3826945 was associated with increased risk of AMD. Reflecting the female-specific association between SNP genotype and AMD, there was also a female-specific association with plasma CFD and AMD. The intronic SNP rs3826945 may be in LD with an unidentified variant that affects expression of *CFD*. However, genotype at rs3826945 was not found to be associated with plasma CFD in the combined UK case-control cohorts (p=0.309).

There was no significant association between copy number variation at *CFD* and plasma CFD (p=0.857).

		Controls	Late AMD			
		Median (25th-75th Percentile)	Median (25th-75th Percentile)	*P**	OR (95% CI)	*P*
			UK1 Series			
CFD (µg/ml)	**All**	2.51 (2.02 - 3.09)	2.78 (2.12 - 3.6)	0.001	1.32 (1.07 - 1.62)	0.010
	Males	2.77 (2.22 - 3.36)	2.97 (2.28 -3.93)	0.170	1.19 (0.82 - 1.72)	0.366
	Females	2.30 (1.99 - 2.94)	2.68 (2.06 -3.42)	0.002	1.39 (1.08 - 1.80)	0.011
			UK2 Series			
CFD (µg/ml)	**All**	1.82 (1.43 - 2.25)	1.99 (1.57 - 2.60)	0.0004	1.18 (0.99 - 1.39)	0.060
	Males	1.98 (1.56 - 2.38)	2.07 (1.60 - 2.70)	0.218	1.07 (0.84 - 1.37)	0.574
	Females	1.69 (1.34 - 2.17)	1.95 (1.55 - 2.51)	0.001	1.28 (1.01 - 1.63)	0.046
			UK1 and UK2 Series			
CFD (µg/ml)	**All**	2.08 (1.59 - 2.70)	2.31 (1.76 - 3.06)	3.95×10^{-6}	1.81 (1.27 - 2.57)	0.0010
	Males	2.21 (1.74 - 2.87)	2.38 (1.78 - 3.07)	0.112	1.42 (0.82 - 2.47)	0.2150
	Females	2.01 (1.51 - 2.55)	2.25 (1.74 - 3.06)	3.76×10^{-6}	2.15 (1.35 - 3.44)	0.0004

Table 4.6 Plasma CFD is elevated in AMD cases compared to controls.

Plasma CFD was measured by ELISA in 751 AMD cases and 474 controls in two British AMD case-control series. Significant differences in the distribution of plasma CFD measured in late AMD cases (CNV and GA), determined by Mann-Whitney U testing (*), were observed in both series independently and when they were combined. When the series were split by gender, the significant difference was seen only in females. Logistic regression was used to account for the confounding effects of age and smoking history upon plasma CFD; the fourth quartile of plasma CFD measurements was significantly associated with AMD compared to the first quartile. This was also seen only in females when the cohort was split by gender. BMI was included as a covariate for the UK2 cohort in addition to age and smoking; the fourth quartile of plasma CFD remained significantly associated with AMD (data not shown).

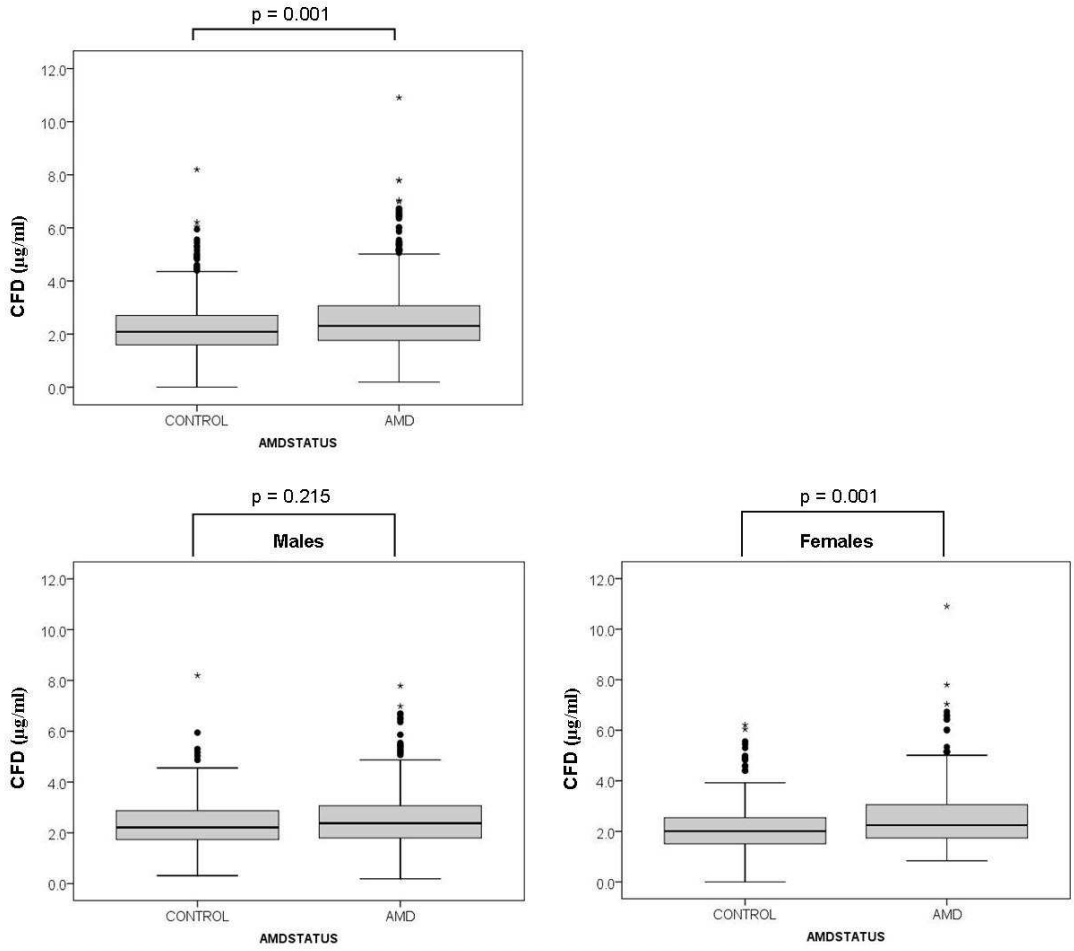

Figure 4.17 CFD is elevated in the plasma of AMD cases relative to controls.

Plasma CFD concentrations in age-related macular degeneration (AMD) and control subjects in the combined UK1 and UK2 series were measured by ELISA. The difference was statistically significant both in the combined sexes ($p=3.95x10^{-6}$) (upper Figure) and in females ($p=3.76x10^{-6}$) but not in males using Mann-Whitney U testing. P-values indicated on the figures were obtained by regression analysis, correcting for age, BMI and gender.
The 4th quartile of plasma CFD concentrations was significantly associated with AMD in the combined series, and in females.

4.4.3.4 Power Calculations for the CFD ELISA

Having observed a 10% difference in median plasma CFD between AMD cases and controls (Table 4.9), the power of the study to identify a significant difference (p=0.05) of this magnitude at 80% power was assessed. As previously described, the plasma CFD measurements showed a slight deviation from normal distribution and were assessed using non-parametric testing. Calculation of power using the Altman Nomogram assumes that data are normally distributed. This was achieved by log-transforming the plasma CFD measurements in SPSS (Figure 4.18). Log-transformed plasma CFD remained significantly elevated in AMD cases relative to controls, using non-parametric tests (p=0.001) and logistic regression (4th quartile, p=0.001, OR 1.78, 95% C.I. 1.26-2.50).

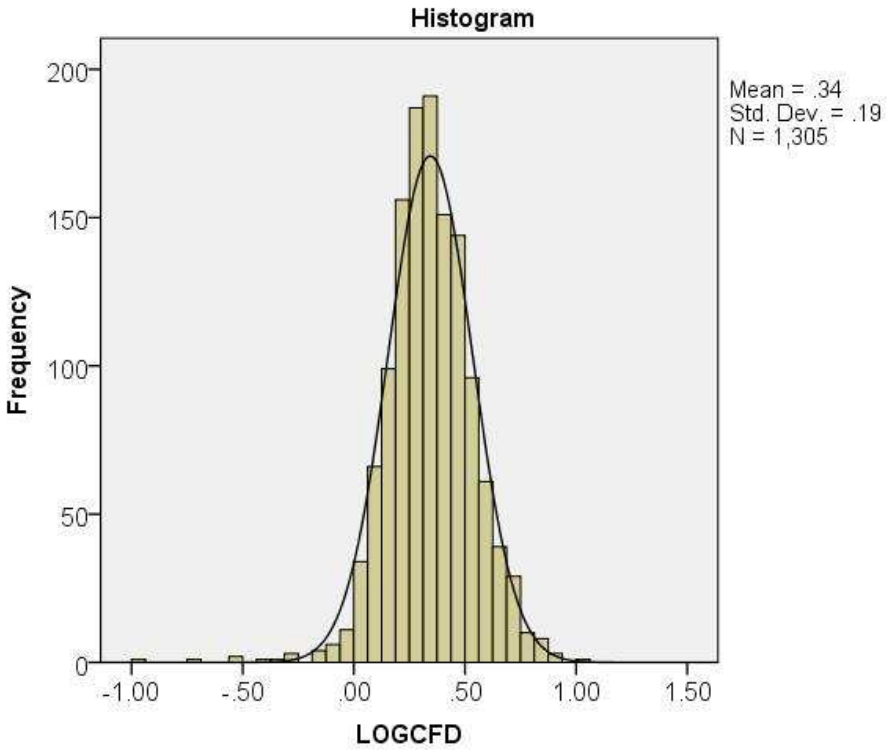

Figure 4.18 Normalisation of plasma CFD distribution by log transformation.

Plasma CFD measurements in the combined UK1 and UK2 series showed a leptokurtic distribution. Log-transformation of raw CFD concentrations reduced kurtosis, normalising distribution.

The difference in mean of log plasma CFD in AMD cases (0.368) and controls (0.318), and the observed standard deviation (0.19) were used to calculate the standardised difference. The standardised difference was applied to an Altman Nomogram. A sample size of 450, comprising an equal number of cases and controls would be sufficient to successfully identify a difference in plasma CFD of this magnitude with 80% power. Given that this study involved 751 AMD cases and 474 controls, the study is adequately powered.

4.5 Discussion

Genetic association studies and proteomic approaches implicate uncontrolled activation of the alternative complement pathway in the pathogenesis of AMD. This chapter describes investigation of Complement factor D, the central activator of the alternative pathway, as a candidate for a role in AMD.

A commercially available ELISA for measuring CFD was optimised for use in plasma samples from two British AMD case-control series. In agreement with previous reports (Scholl et al. 2008), median plasma CFD was 2.16±1.13 (SD) µg/ml across these series. The median value of plasma CFD was significantly raised (11% increase, p-value=0.001) in 751 AMD cases compared with 474 disease-free controls, correcting for age (Figure 4.17).

The levels of complement components and activation fragments in the plasma of AMD cases and controls have previously been investigated. These studies have provided clear evidence that activation products, such as Ba, Bb, C3a and C5a, are elevated in AMD cases (Reynolds et al. 2009; Hecker et al. 2010). This is consistent with the hypothesis that AMD pathogenesis involves chronic activation of the alternative complement pathway, perhaps spilling over into the systemic circulation from the eye. Although two studies reported elevated levels of CFD (Scholl et al. 2008; Hecker et al. 2010), one study did not identify any significant difference in plasma CFD between 120 AMD cases (all with severe disease) compared to 60 controls (Reynolds et al. 2009). These previous studies were performed in small series. The present study was conducted in a substantially larger number of cases and controls, and has much greater power to detect a small difference in CFD (> 80% power to detect a difference of this magnitude). Of the 751 cases, 82% of the

combined UK1 and UK2 cases had severe AMD (GA or CNV), so disease severity is unlikely to affect comparison between studies. This study confirms that CFD, the central activator of the alternative pathway, is elevated in AMD cases compared to controls. This has important implications on alternative pathway activity in AMD, further contributing to the activation observed during normal ageing and in those with high BMI.

Increasing age has a significant effect upon the concentration of CFD in plasma (Hecker et al. 2010). In agreement with this, plasma CFD concentrations were significantly higher in individuals aged 60-79.99 years, and higher again in individuals aged over 80 years, compared to those aged less than 60 years ($p < 0.001$; Figure 4.13). Plasma CFD increased with age, regardless of AMD status. Controls have lower plasma CFD than cases in each age category, reflecting both an age-related and AMD-related increase in complement activation.

In addition to an effect of advancing age, females had a significantly lower median concentration of plasma CFD (2.09±0.04 (s.e.m.) μg/ml) than males (2.26±0.05 (s.e.m.) μg/ml) in the combined cohorts ($p=0.002$, Figure 4.14). The significant difference in plasma CFD measurements between genders was only observed in controls ($p= 0.001$). This is consistent with female cases, and to a lesser extent male cases, having elevated levels of CFD regardless of gender when suffering from AMD (Figure 4.17).

The majority of complement components circulating in the plasma are synthesised by the liver, with the exceptions of CFD and C1q (Morgan and Gasque 1997). The major source of plasma CFD is adipose tissue (White et al. 1992). The most abundant cell type in adipose tissue is adipocytes. Bone-marrow derived macrophages are also present, possibly recruited by chemokines such as monocyte chemoattractant protein -1 (MCP-1) that are expressed by adipocytes. Both adipocytes and macrophages are known to synthesise CFD, although adipocytes appear to be the major source of plasma CFD in normal individuals. Consistent with this, there is a clear relationship between increased body fat (indicated by BMI score) and increasing plasma CFD measurements in the UK2 cohort (Figure 4.16). Median plasma CFD was significantly higher in obese individuals compared to those with a BMI <25 ($p=0.000003$). Fat is increasingly regarded as an endocrine organ, secreting

a variety of hormones, such as leptin, as well as immune and inflammatory mediators, including CFD and tumor necrosis factor-α (Fantuzzi 2005). Reynolds et al. (2009) report an association between high BMI and elevated C3, CFB, and CFH, in addition to elevated concentrations of complement activation fragments Bb, C3a, and iC3b.

Although BMI was significantly associated with plasma CFD in the UK2 cohort, plasma CFD level remained significantly associated with AMD when BMI was included as a covariate. Similarly, the contribution of advancing age to plasma CFD did not remove the significant association with AMD.

CFD is constitutively secreted at a high level, but is rapidly catabolised in tissues such as the kidney (White et al. 1992; Volanakis and Narayana 1996). The fractional catabolic rate of plasma CFD has been estimated to be 60% per hour (Pascual et al. 1988), contributing to its low serum concentrations. No information regarding kidney function (e.g. creatinine levels) was available for the UK cohorts. High CFD concentrations in plasma as a result of impaired renal function in some individuals cannot be excluded. Given the large number of individuals involved in this study, this is unlikely to play a significant role in elevating CFD in AMD cases compared to controls.

Plasma CFD is elevated in AMD cases compared to controls (Table 4.6). This seems likely to result in activation of the alternative complement pathway in AMD. Uncontrolled complement activity appears to have detrimental effects in AMD. However, the source of elevated CFD in AMD remains unclear. Although the majority of circulating CFD is synthesised by adipose tissue, non-adipose sources of plasma CFD include circulating monocytes/macrophages, lung, placenta, muscle, synovial tissue and brain astrocytes (White et al. 1992; Morgan and Gasque 1997). The blood-retinal barrier may restrict entry of the CFD in plasma to the neural retina, although the RPE and choroid are exposed to systemically available complement proteins. Systemic and locally expressed complement components in the eye may contribute to the chronic inflammatory process observed in AMD.

Anderson et al (2010) investigated the expression of *CFD* in the eye using quantitative real-time PCR (qPCR). In tissue isolates, choroidal cells were shown to express CFD at over tenfold higher levels than either neural retina or RPE (Anderson

et al. 2010). The complement regulators CFH, DAF and CFI and the initial components of both the alternative and classical complement pathways, including C3 and factor B, are also expressed more highly in the choroid than in RPE or neural retina. Macrophages and the choroidal capillaries adjacent to Bruch's membrane may express alternative complement pathway proteins, including CFD, in the choroid, although this remains unconfirmed.

Regardless of the cellular source, *CFD*, factor B and C3, are co-expressed in choroidal tissue. However, alternative complement pathway activation mediated by CFD requires the deposition of C3 and factor B on a surface upon which control by CFH, CFI, DAF, MCP and complement receptors can be evaded (Walport 2001). Drusen deposits, characteristic of AMD, are considered by-products of a chronic inflammatory response at the Bruch's membrane which contributes to the pathogenesis of AMD (Mullins et al. 2000; Hageman et al. 2001; Anderson et al. 2002). Druse form between the RPE and Bruch's membrane, and contain most components of both the classical and alternative complement pathways and their regulators. Whilst drusen do not contain CFD, this may be a consequence of low levels of CFD in relation to other complement proteins in circulation. Thus, a high level of complement activation occurring in the choriocapillaris-Bruch's membrane-RPE region in response to an unknown trigger may contribute to both tissue damage locally, and to the elevated plasma CFD concentration measured in AMD cases compared with controls systemically. Alternatively, AMD may be a systemic disease which manifests itself at the tissues most vulnerable to attack by complement, including the macula.

A genetic association between AMD and variation within the *CFD* gene was observed in several AMD case-control series, and in a meta-analysis, including 4765 predominantly severe AMD cases and 2693 examined controls. The association was detected with a single non-coding SNP, rs3826945, located in intron 4 of the *CFD* gene. The region in chromosomal region 19p13.3 in which *CFD* spans 3.9 kb has a high gene density, high levels of recombination and relatively low linkage disequilibrium (http://hapmap.ncbi.nlm.nih.gov). This suggests that the association may not extend far on either side of rs3826945. The effect size of the association in

the meta-analysis was small (odds ratio 1.11) and almost confined to females (Table 4.4, Figure 4.5).

Zeng et al (2010) investigated SNPs in *CFD* for an association with AMD in a smaller AMD cohort (178 cases and 161 controls). They did not identify an association between rs3826945 and AMD (although minor allele frequencies in cases and controls - 35% and 31% respectively - were comparable to those observed in the UK1 and UK2 series (Table 4.3)). The small study (Zeng et al. 2010) would lack power to detect an effect of the size observed in the meta-analysis described within this chapter (OR 1.11). Furthermore, their analysis did not account for confounding factors such as age, sex, smoking history or BMI. Although no interaction was observed between environmental factors and rs3826945 in the study described in this chapter, only partial BMI information was available. BMI is a modifiable factor, which has previously been associated with AMD-susceptibility. Furthermore, BMI affects levels of inflammatory biomarkers in addition to CFD (Seddon et al. 2006a; Reynolds et al. 2009), and may also modify genetic susceptibility. This raises the possibility that BMI may contribute to the variability in replication across case-control series used in the SNP association study, as there may be differences in BMI between populations. This cannot be excluded, as BMI data were only available in some series (UK2, USA1, Nijmegen).

Both the genetic and proteomic association between CFD and AMD appear to have a greater impact on females than males. The cohorts investigated generally had a greater proportion of females than males, so this may reflect a loss of power to detect the small differences observed in males. However, sex differences in the heritability of complex traits are common (Weiss et al. 2006). This may indicate that an unidentified variant in linkage disequilibrium with rs3826945 regulates plasma CFD levels in females. There was no significant association between rs3826945 in *CFD* and plasma CFD measurements. Almost 5,000 cases were required to show the genetic association with AMD, so this study is likely underpowered to detect such an effect. Deletions and duplications of *CFD* could affect expression, although no significant difference in frequency of these was observed between AMD cases and controls (Figure 4.8). No correlation could be made between copy number and plasma CFD. Furthermore, sequencing of the exonic and flanking regions of *CFD* in

95 cases and 95 controls did not identify any candidate regulatory variants. However, such variants may be identified in the future by re-sequencing of additional samples and would be subject to functional studies to examine the effects on *CFD* expression in adipocytes or macrophages.

The genetic association between rs3826945 in *CFD* and AMD may contribute only a small increase in risk for AMD, but further implicates the alternative pathway in AMD pathogenesis. Ablation of CFD is neuroprotective and reduces photoreceptor cell death in response to light-induced damage in a *CFD* $^{-/-}$ mouse model (Rohrer et al. 2007). The central role of CFD in the alternative complement pathway makes this an attractive candidate for therapeutic intervention, regardless of whether plasma CFD is a cause or a secondary effect of the disease. Partial (or local) inhibition of CFD in individuals at high genetic risk of AMD might reduce the risk of development and progression of disease by minimising tissue damage. Recent studies have suggested the variants in complement genes (*CFH* and *C3*) are associated with risk of developing geographic atrophy, but not with disease progression in humans (Scholl et al. 2009; Klein et al. 2010). However, animal models using laser damage to induce neovascularisation from the choroid have shown that complement components including C5a are important in development of CNV (Bora et al. 2005). It therefore remains to be seen whether the inhibition of complement would be an effective therapy for treating late forms of the disease. One such complement inhibitor, an anti-complement factor D antibody fragment (*FCFD4514S)* is currently in Phase I clinical trials using intravitreal injections (Genentech / Roche; ClinicalTrials.gov identifier: NCT00973011).

5: Chapter 5

Functional relevance of the interaction between HTRA1 and CFD

5.1 Introduction

This chapter describes the validation and characterisation of an interaction between HTRA1 and complement factor D (CFD). The interaction was identified in a yeast two-hybrid screen, and selected for further study due to the role of CFD in the alternative complement pathway. Variation in genes such as *CFH*, *CFB*, *C3* and *FI* deregulate this pathway and contribute to AMD pathogenesis (Edwards et al. 2005; Haines et al. 2005; Klein et al. 2005; Gold et al. 2006; Yates et al. 2007; Fagerness et al. 2009). CFD (also known as adipsin (White et al. 1992)) is a serine protease with a key role in this pathway, cleaving factor B when it is bound to C3b to form the C3 convertase (Götze and Müller-Eberhard 1971; Müller-Eberhard and Götze 1972 ; Vogt et al. 1974). Altered CFD activity caused by an interaction between HTRA1 and CFD may affect systemic and local inflammation, which has been implicated in AMD pathogenesis.

CFD is expressed as a prepropeptide. The N-terminal signal peptide is cleaved to form an inactive zymogen, proCFD (White et al. 1992; Kim et al. 1994; Yamauchi et al. 1994; Jing et al. 1999). Subsequently, the 5-6 amino acid N-terminal activation domain in humans is removed, either within the secretary pathway or it may be rapidly cleaved in plasma. >99% of plasma CFD is CFD rather than proCFD (Fearon et al. 1974; Lesavre and Müller-Eberhard 1978; Yamauchi et al. 1994). The mature peptide becomes active as a result of a conformational change which occurs when it binds C3bB, a complex of factor B, magnesium ions and complement component 3b (C3b) (Volanakis and Narayana 1996; Jing et al. 1999).

A number of serine proteases are able to cleave the activation peptide from proCFD (Fearon et al. 1974; Yamauchi et al. 1994). A physiological role for serine proteases in serum, such as thrombin, in the activation of mouse proCFD was excluded by Takahashi et al. (2010). This group proposed a role for mannose-binding lectin-associated serine protease-1 (Masp1), a component of the lectin pathway. *Masp1*$^{-/-}$ null mice have defective activation of the alternative pathway, with proCFD rather than mature CFD circulating in serum. This suggests that Masp1 is responsible for activation of proCFD to mature CFD in serum in mice. In humans, cleavage of proCFD is thought to occur during CFD maturation and secretion

(Yamauchi et al. 1994), rather than post-secretion as proposed for Masp1 in the mouse (Takahashi et al. 2010). Masp1 is not expressed in adipose tissue, the leading source of CFD in humans (White et al. 1992; Takahashi et al. 2010). Thus, the enzyme(s) responsible for activation in human tissues, including blood, adipose tissue and the eye remain unknown.

The mechanism(s) by which the chromosome 10q26 AMD-susceptibility locus increases risk of AMD remain elusive. In addition to verifying the interaction between HTRA1 and CFD *in vitro*, a novel ability of HTRA1 to activate CFD by specific cleavage of the activation peptide was uncovered in this study, using a variety of biochemical approaches. This provides a biologically plausible mechanism for HTRA1 involvement in AMD pathogenesis.

5.2 Validation of the interaction between CFD and HTRA1

A putative interaction was identified between CFD and HTRA1 in a yeast two-hybrid screen (described in Chapter 3). A back-transformation experiment, with bait and prey plasmids isolated from the initial positive clones, confirmed an interaction between these proteins in the yeast two-hybrid system. Purified and recombinant proteins were used to further verify the interaction and to identify CFD as a novel substrate for HTRA1 *in vitro*.

5.2.1 CFD interacts with HTRA1 in a yeast two-hybrid screen

Of the numerous potential interactors of HTRA1 that were identified by yeast two-hybrid screening in a placental cDNA library and by tandem affinity purification in RPE1 and HEK293T cells, CFD was selected for further study. The specificity of the initial interaction was tested by back-transformation of the isolated bait (pBD-DEST-HTRA1) and prey plasmid (pACT2-CFD) into PJ69–4A yeast cells. Growth of co-transformed yeast on selective media of increasing stringency (-WHL and -WHLA) indicates a positive interaction between CFD and HTRA1 (Figure 5.1). Back-transformation of the isolated plasmids was performed by Dr. Elod Kortvely (Helmholtz Zentrum, Munich, Germany).

5.2.2 The minimal binding site of the CFD:HTRA1 interaction

Sequences obtained from the three *CFD* clones identified were aligned to the human full-length *CFD* cDNA reference sequence (NM_001928.2), using ClustalW *(*www.ebi.ac.uk/clustalw/). This defined the minimal sequence required for a positive interaction between the active HTRA1 bait and CFD prey (Figure 5.2). The minimal binding region for the interaction lies at the N-terminal portion of the CFD, overlapping the activation peptide sequence of proCFD (bold text in NM_001928 reference sequence, Figure 5.2).

Figure 5.1 Back-transformation of HTRA1 and CFD plasmids into PJ69–4A cells.

Prey plasmids containing *CFD* cDNA (pACT2-CFD) and the HTRA1 bait construct were back-transformed into PJ69–4A cells, and tested for growth. Yeasts that were co-transformed with pACT2-CFD and pBD-DEST-HTRA1 were capable of growth on selective media of increasing stringency (-WHL and -WHLA), indicating a positive interaction. No growth was observed in yeast that were co-transformed with the HTRA1 bait construct and empty prey plasmid. Supplements missing from the SD media are tryptophan (W), leucine (L), histidine (H) and adenine (A). Images and back-transformations were produced by Dr. Elod Kortvely.

```
CFD_1       TCNACNGANCGGCCGCCTGCGCGGCGCCGCCCCGTGGTCGGATCCTGGGC  142
CFD_2       TCGACGGAGCGGCCGCCTGCGCGGCGCCGCCCCGTGGTCGGATCCTGGGC  142
CFD_3       NCNNCGGAGCGGCCGCCTGCGCGGCGCCGCCCCGTGGTCGGATCCTGGGC  150
NM_001928   TCCTAGGAGCGGCCGCCTGCGCGGCGCCGCCCCGTGGTCGGATCCTGGGC  109
            *    ** ****************************************

CFD_1       GGCAGAGAGGCCGAGGCGCACGCGCGGCCCTACATGGCGTCGGTGCAGCT  192
CFD_2       GGCAGAGAGGCCGAGGCGCACGCGCGGCCCTACATGGCGTCGGTGCAGCT  192
CFD_3       GGCAGAGAGGCCGAGGCGCACGCNCGGCCCTACATGGCGTCGGTGCAGCT  200
NM_001928   GGCAGAGAGGCCGAGGCGCACGCGCGGCCCTACATGGCGTCGGTGCAGCT  159
            ********************** *************************

CFD_1       GAACGGCGCGCACCTGTGCGGCGGCGTCCTG------------------  223
CFD_2       GAACGGCGCGCACCTGTGCGGCGGCGTCCTGGTGG--------------  227
CFD_3       GAACGGCGCGCACCTGTGCGGCGGCGTCCTGG-----------------  232
NM_001928   GAACGGCGCGCACCTGTGCGGCGGCGTCCTGGTGGCGGAGCAGTGGGTGC  209
            ******************************
```

Figure 5.2 Minimal binding region of CFD isolated in the yeast-two hybrid screen.

Prey plasmid sequences from the three positive yeast clones for CFD were aligned with a reference sequence for human CFD (NM_001928). Asterisks indicate complete sequence agreement. Numbering refers to length of isolated sequence for the positive clones, and to nucleotide position in the full-length cDNA sequence for CFD for the reference sequence. CFD is translated as a prepropeptide; grey text indicates a region of the signal peptide for CFD, bold text marks the propeptide sequence.

5.2.3 HTRA1-mediated cleavage of the N-terminus of CFD

A peptide spanning 30 amino acid residues at the N-terminal end of proCFD, corresponding to the minimal binding site for HTRA1 in the yeast-two hybrid screen, was synthesised. The sequence of the CFD_Y2H peptide is shown in Table 5.1. The CFD_Y2H peptide (20 µM) was tested as a substrate for recombinant HTRA1 in an *in vitro* protease activity assay with increasing amounts of recombinant HTRA1 (0.1-1 µg). Following incubation at 37°C for 16 hours, samples were subjected to reducing gel electrophoresis. A significant decrease in the amount of substrate, relative to synthetic peptide in the absence of protease, was observed in a Coomassie-stained gel (Figure 5.3A). Specificity of the proteolysis was confirmed by incubation of CFD_Y2H with the inactive mutant HTRA1 (S328A); under the same conditions, no degradation of the substrate was observed (lane 2, Figure 5.3A).

The intensity of Coomassie-stained bands was quantified by densitometry (ImageQuantTL), and plotted as band intensity relative to the untreated peptide (Figure 5.3B). Incubation with 0.1 µg, 0.5 µg or 1 µg of GST ΔN HTRA1 resulted in decreased band intensity for CFD_Y2H, corresponding to a reduction of 68±1 (SD)% with 1 µg GST ΔN HTRA1 compared to untreated (p = 0.0094; t-test, n=2). Similar results were obtained by comparison of band intensity to the inactive S328A mutant HTRA1-treated peptide (data not shown).

Name of peptide	Sequence (N – C)	Molecular Weight (Da)	Purity	Modification
CFD_Y2H	PPRGRILGGREAEAHARPYMASVQLNGAHL	3225.71	85%	
Act_pep_MCA	PPRGR	738.84	88%	C-terminal MCA
Random_MCA	DSVLA	660.72	88%	C-terminal MCA

Table 5.1 Synthetic peptides.
Synthetic peptides corresponding to regions of CFD were generated. CFD_Y2H corresponds to the N-terminal amino acid sequence identified as the minimal binding region in the yeast-two hybrid screen, including the activation peptide. Act_pep_MCA corresponds to the activation peptide of proCFD, conjugated to a C-terminal MCA group. Random_MCA corresponds to the last 5 amino acids of the C-terminal end of CFD, conjugated to a C-terminal MCA moiety.

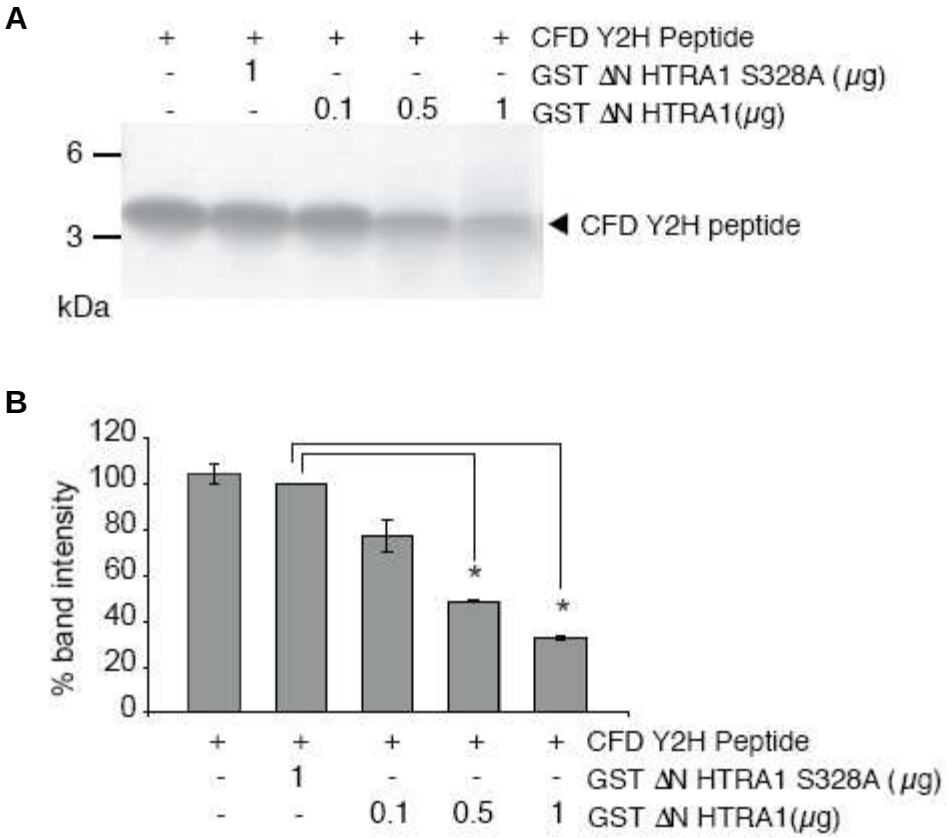

Figure 5.3 The CFD peptide sequence identified by yeast-two hybrid screening is subject to proteolysis by HTRA1 *in vitro*.

A. A synthetic peptide corresponding to the CFD activation peptide and N-terminal portion of CFD isolated in the yeast two hybrid screen (PPRGRILGGREAEAHARPYMASVQLNGAHL) was tested as a substrate for recombinant HTRA1. The 3.2 kDa peptide was incubated with increasing amounts of recombinant HTRA1 (0.1-1 µg). A Coomassie-stained gel of the reactions showed a decrease in the amount of substrate, relative to synthetic peptide in the absence of protease or when incubated with the inactive mutant GST ΔN HTRA1 S328A.

B. Analysis of band density in Coomassie-stained gels showed that increasing amounts of HTRA1 resulted in a significant ($p<0.05$) decrease of synthetic substrate, determined by a one tailed *t*-test, relative to the untreated substrate or substrate treated with an inactive mutant of HTRA1. Data is mean of two independent experiments ± SD.

5.2.4 GST ΔN HTRA1 interacts with, but does not cleave, mature CFD

A GST-pulldown assay using catalytically inactive GST-tagged ΔN HTRA1 S328A (amino acids 157-480), GST HTRA1 ΔC (amino acids 21-157) or GST alone, and mature CFD, purified from human plasma, was performed. Schematic domain structures of these proteins are shown in Figure 5.4. The S328A mutant of HTRA1 lacks protease activity, avoiding potential degradation of the CFD during the assay.

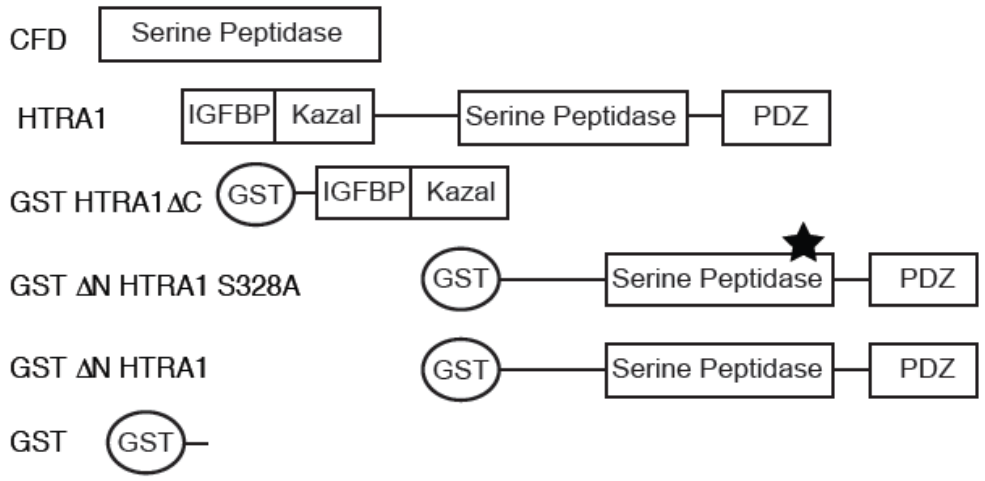

Figure 5.4 Schematic domain structure of recombinant and purified proteins used to verify the CFD-HTRA1 interaction *in vitro*.
The domain structure of proteins assayed for an interaction. CFD was purified from human plasma, and is the mature form of the protein, lacking the activation peptide. HTRA1 has an N-terminal secretory signal sequence (SP), an insulin-like growth factor binding domain (IGFBP), a Kazal-type serine protease inhibitor domain (which may be involved in self-regulation), a characteristic trypsin-like catalytic domain and a C-terminal PDZ domain. Recombinant GST-tagged forms of HTRA1, corresponding to the N-terminal domains (GST HTRA1 ΔC) and to the C-terminal domains (GST ΔN HTRA1) were expressed and purified from *E. coli*. S328A (*) is an inactive mutant of HTRA1. GST was expressed and purified from *E. coli* to test for interactions with the GST-tag.

5.2.4.1 Optimisation of wash conditions for the GST pulldown

Following a standard protocol for performing a GST pulldown, GST HTRA1 ΔC , GST ΔN HTRA1 and free GST were bound to Glutathione Sepharose beads, which were pre-equilibrated in TEN150 Buffer (50mM Tris-HCl, pH 7.5, 150mM NaCl). An equimolar amount of CFD (0.5 µg) was added to each, and to Glutathione Sepharose beads alone. Following incubation at 4^{o}C for 2 hours, the beads were washed extensively in TEN150 buffer. Bound proteins were eluted from the Glutathione Sepharose in 1 x LDS Buffer and 1 x Reducing Agent. Eluates were analysed by reducing gel electrophoresis and immunoblotting using anti-CFD (C-16) and anti-GST-HRP antibodies (data not shown).

An interaction between CFD and GST ΔN HTRA1 was observed. However, under these wash conditions, there was a non-specific interaction between CFD and GST, and between CFD and Glutathione Sepharose in the absence of any recombinant protein (data not shown).

In order to reduce the background-binding of CFD to the beads, and to GST, the stringency of the wash conditions was increased by the addition of 0.1% NP40 to TEN150 Buffer for the washes. Additionally, the number of washes was increased from three to four washes, for a total of 160 times the bead volume.

5.2.4.2 Validation of the interaction between CFD and HTRA1

The previously observed interaction between GST ΔN HTRA1 and CFD was confirmed using the more stringent wash conditions (Figure 5.5). Minimal binding was observed between the N-terminal portion of HTRA1 (GST HTRA1 ΔC) and CFD. This indicates that CFD interacts with HTRA1, and that the binding site for CFD on HTRA1 is located in the C-terminal portion of the protease, spanning the protease domain and the PDZ domain (Figure 5.4). Minimal binding of CFD to GST alone was observed using the more stringent wash conditions, thus excluding the possibility that the interaction was a result of binding to the GST tag; similarly, there was no observed binding of CFD to Glutathione Sepharose beads alone (Figure 5.5).

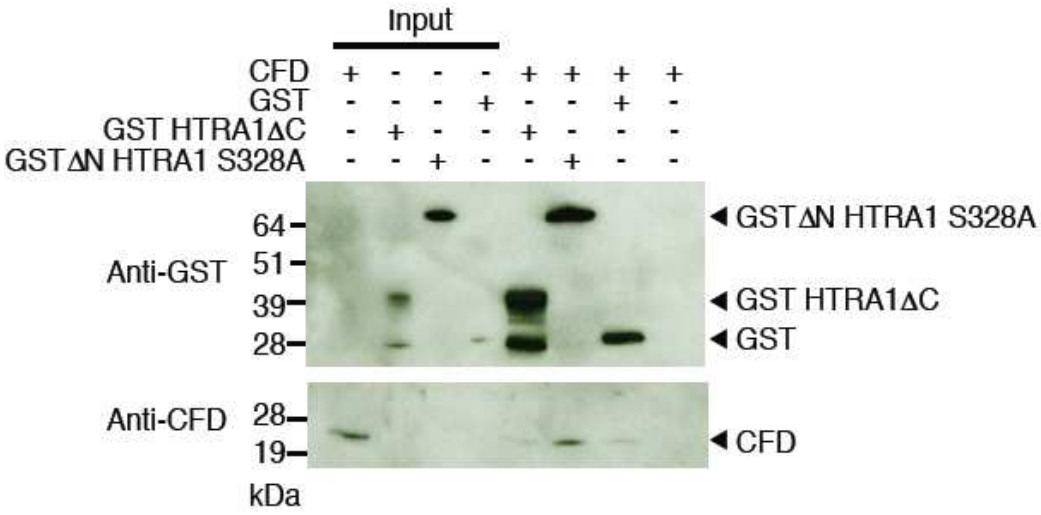

Figure 5.5 CFD interacts with GST ΔN HTRA1 in a GST pulldown assay.

An interaction between GST ΔN HTRA1 S328A and CFD was observed (lane 6) when GST or GST-tagged forms of HTRA1 were immobilised on glutathione-sepharose beads (or beads alone) and incubated with 2µg of CFD. Minimal binding was observed between the N-terminal portion of HTRA1 (GST HTRA1 ΔC) and CFD, between GST alone and CFD, and between Glutathione Sepharose beads and CFD. Samples, including 10% of input only samples (lanes 1-4) were subjected to electrophoresis and western blot following elution of bound proteins from Glutathione Sepharose beads.

5.2.5 Mature CFD is not a substrate for GST ΔN HTRA1 *in vitro*

Following confirmation of the interaction between CFD and the C-terminal domains of HTRA1 (including the protease domain; Figure 5.4), the ability of GST ΔN HTRA1 to cleave mature CFD was assessed by a protease assay. Mature CFD (1 µg) was tested as a substrate for HTRA1 by incubation with 0.5 µg proteolytically active GST ΔN HTRA1 overnight at 37^{o}C. Samples were subjected to reducing gel electrophoresis and subsequent Coomassie staining or Western blotting. There was no evidence of cleavage or degradation of mature CFD by HTRA1, as shown by a representative anti-CFD (C-16) immunoblot in Figure 5.6. This, together with the observation that the CFD_Y2H peptide is cleaved by HTRA1 (Figure 5.3), indicates that the propeptide region of CFD is subject to cleavage by HTRA1.

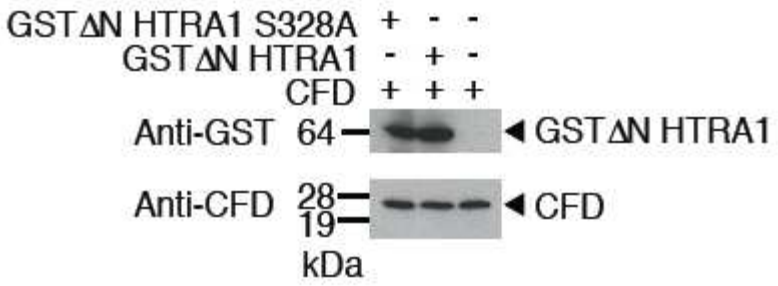

Figure 5.6 Mature CFD is not a substrate for GST ΔN HTRA1 *in vitro.* CFD purified from plasma is not a substrate for HTRA1, in an *in vitro* assay of protease activity. No cleavage of CFD was observed in the presence of active GST ΔN HTRA1.

5.3 Production of recombinant proCFD

In order to confirm the requirement for the propeptide sequence (PPRGR) for HTRA1-mediated cleavage of CFD, and to test the functional consequences of the cleavage upon CFD activity, recombinant proCFD was produced. A bacterial expression vector, encoding an N-terminal cleavable GST-tag, was used for protein expression in *E. coli*. The GST-tag was utilised for purification and then cleaved using PreScission Protease, to release proCFD with a short (27 amino acids) linker peptide remaining at the N-terminus.

5.3.1 Cloning proCFD for bacterial expression

An Ultimate ORF clone encoding the full-length prepro*CFD* cDNA sequence was obtained from Invitrogen. The sequence encoding pro*CFD* was sub-cloned from the Ultimate ORF.

5.3.1.1 PCR amplification of the proCFD insert

Pro*CFD* cDNA was cloned from the *CFD* Ultimate ORF (Invitrogen) by PCR using *att*B-containing primers to amplify the sequence encoding amino acids 21-253 of the CFD peptide (proCFD, lacking the signal peptide from amino acids 1-20 of the

preproprotein). PCR products, generated by Phusion polymerase in the presence of 10% DMSO, were separated by agarose gel electrophoresis, as shown in Figure 5.7. The band of approximately 800 bp was excised and gel purified.

5.3.1.2 Creation of the proCFD Gateway Entry Vector

Gateway cloning technology was utilised for creation of the proCFD entry vector. Gel purified *att*B-flanked pro*CFD* sequence was inserted into the *att*P-containing donor vector pDONR221 using BP Clonase II. The resulting entry vector, pENTR pro*CFD*, was selected by kanamycin resistance, and propagated in E. *coli* TOP10 cells. Sequencing with M13 and *CFD*-specific forward and reverse primers confirmed the presence, and sequence fidelity, of the pro*CFD* insert in the entry vector (data not shown).

5.3.1.3 Sub-cloning of proCFD into Gateway Destination Vector

Gateway cloning technology was utilised for creation of the proCFD bacterial expression vector. The *att*L-pro*CFD*-containing entry vector pENTR pro*CFD* was used in a Gateway LR recombination reaction to insert the pro*CFD* sequence into the destination vector pGEX6P1-DEST. This plasmid (a kind gift from Dr Martin Reijns) is a Gateway-modified form of pGEX6P1, containing the *att*R recombination cassette, to allow IPTG-inducible expression of recombinant proteins with a cleavable GST-tag at the N-terminus. Ampicillin-resistance was used to select for destination vector clones containing the pro*CFD* insert. Four clones were selected for screening for the insert into the destination vector by restriction digestion of the plasmids with ApaI or MluI. Figure 5.8 shows the separation of the digests by agarose gel electrophoresis.

ApaI cuts the pGEX6P1-DEST vector backbone twice, and the proCFD insert twice. As shown in Figure 5.8A, clones 1, 3 and 4 have the correct pattern of digestion with ApaI to confirm that proCFD has been inserted into the pGEX6P1-DEST vector. Clone 2 does not show the pattern of ApaI digestion that is characteristic for the pGEX6P1-DEST vector.

Figure 5.8B shows the pattern of restriction digest generated by MluI. This enzyme cuts the pGEX6P1-DEST vector backbone once, does not cut the proCFD insert and cuts the entry vector twice. Clones 1, 3 and 4 show the pattern of digestion with MluI expected for pGEX6P1-DEST containing the pro*CFD* insert. Clone 2 shares the restriction digest pattern of the entry vector, CFD Ultimate ORF, indicating that the LR recombination step was not successful in this instance.

pGEX6P1-DEST pro*CFD* clones 1, 3 and 4 were sequenced using gene-specific primers to confirm that the inserts matched the published proCFD sequence (NM_001928.2).

5.3.2 Expression and purification of recombinant proCFD

The pGEX6P1-DEST proCFD construct is an E. *coli* expression vector, with an IPTG-inducible $lacI^q$ promoter controlling expression of the recombinant protein. In addition to a GST-tag at the N-terminus, the vector encodes the recognition sequence for specific cleavage by PreScission Protease, between the GST domain and the site of the Gateway cloning system compatible DEST cassette. This allows sequential purification using the GST-tag on Glutathione Sepharose, followed by site-specific removal of the GST-tag by PreScission Protease.

5.3.2.1 Expression of recombinant proCFD

The *E.coli* strain BL21(DE3) pLysS was used for the expression of GST-tagged proCFD.

5.3.2.2 Purification of recombinant proCFD

Recombinant proCFD was purified from the soluble fraction of the cell lysate using the affinity of the GST-tag for Glutathione Sepharose resin. Following extensive washing of the glutathione sepharose under stringent conditions (0.5% Triton-X100 in the wash buffer) to remove contaminants from the immobilised proCFD protein, PreScission Protease was added.

PreScission Protease cleaves the GST fusion proCFD between the Gln and Gly residues of the recognition sequence Leu-Glu-Val-Leu-Phe-Gln-Gly-Pro. As seen in the flow-through (FT) in Figure 5.9A, B and C, the action of PreScission Protease releases free proCFD (27 kDa) from the GST tag (25 kDa), which together comprise the 54 kDa GST fusion proCFD observed in the input fraction of the anti-CFD and anti-GST immunoblots shown in Figure 5.9B and C respectively. The GST tag remains bound to the Glutathione Sepharose resin, and is seen following elution from the resin by reduced glutathione (Figure 5.9A, lane 2). The PreScission Protease (47 kDa) also has a GST tag, allowing it to be removed from the purified cleaved proCFD by binding to Glutathione Sepharose. Following elution with reduced glutathione, PreScission Protease was released, as shown in Figure 5.9A (lane 2) and in the anti-GST immunoblot shown in Figure 5.9C.

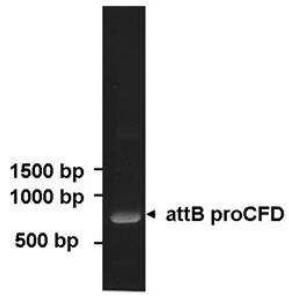

Figure 5.7 PCR amplification of the proCFD insert.
The cDNA sequence encoding amino acids 21-253 of the CFD peptide (proCFD, lacking the signal peptide from amino acids 1-20 of the preproprotein) was amplified using *att*B-containing primers. PCR products were separated by agarose gel electrophoresis and the appropriate band (800 bp) was excised and gel purified.

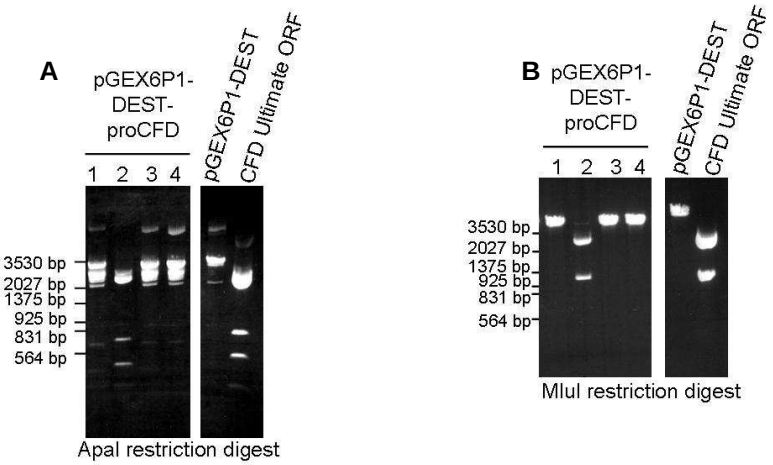

Figure 5.8 Restriction digests to verify presence of proCFD insert in the pGEX6P1-DEST vector.
Four clones containing the destination vector were screened for the insert by restriction digestion with ApaI or MluI, and separated by agarose gel electrophoresis. DNA Molecular Weight Marker III was used to calculate the size of restriction fragments.
A. Clones 1, 3 and 4 have the correct pattern of digestion with ApaI to confirm that proCFD has been inserted into the pGEX6P1-DEST vector. Clone 2 does not show the pattern of ApaI digestion that is characteristic for the pGEX6P1-DEST vector.
B. Clones 1, 3 and 4 have the correct pattern of digestion with MluI for pGEX6P1-DEST containing the pro*CFD* insert. Clone 2 has the restriction digest pattern as the entry vector, CFD Ultimate ORF, confirming that pro*CFD* was not successfully inserted into pGEX6P1-DEST in this instance.

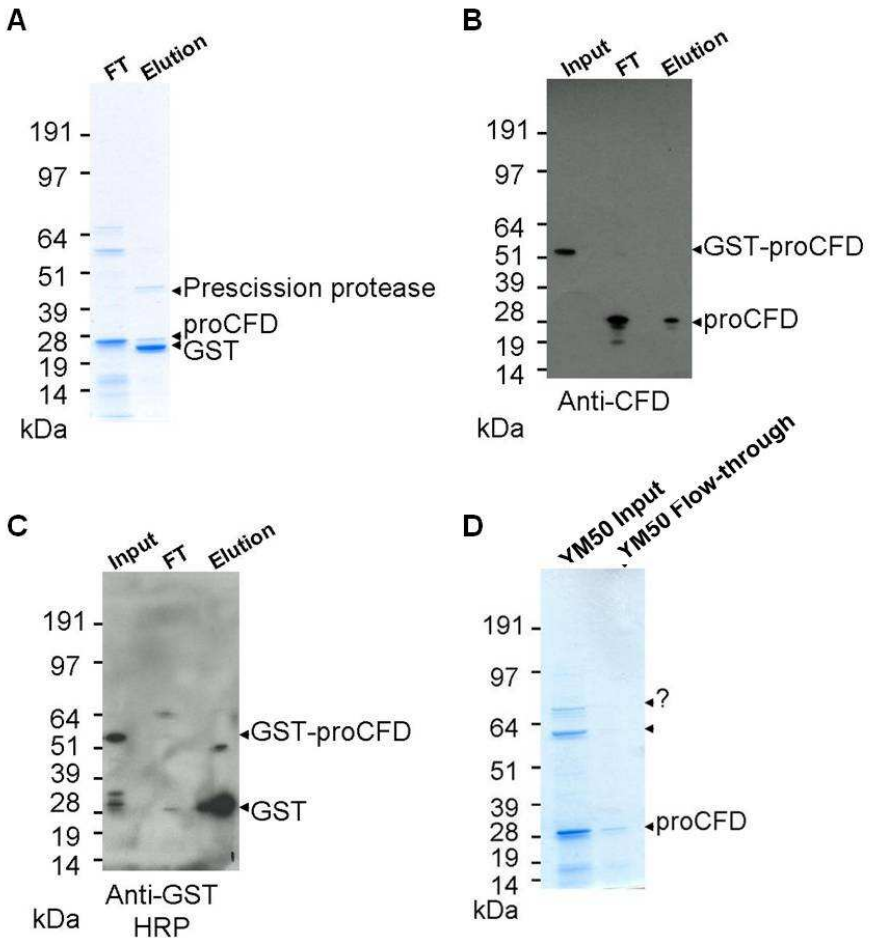

Figure 5.9 Purification of recombinant proCFD and removal of GST-tag.

- **A.** A Coomassie-stained gel showing that PreScission Protease cleaves GST-tagged proCFD, releasing free proCFD (27 kDa) from the GST tag (25 kDa) in the flow-through (FT) fraction observed on. The GST tag remains bound to the Glutathione Sepharose resin, and can be eluted using reduced glutathione (Elution).
- **B.** Anti-CFD immunoblot confirms the cleavage of GST-tagged proCFD (54 kDa) in the input fraction by PreScission Protease results in release of free proCFD (27 kDa) in the flow-through (FT) fraction, and to a lesser extent, in the Elution.
- **C.** Anti-GST immunoblot confirms the cleavage of GST-tagged proCFD (54 kDa) in the input fraction by PreScission Protease, leaving the GST tag (25 kDa) and PreScission Protease (47 kDa, with a GST-tag) bound to Glutathione Sepharose resin until eluted with reduced glutathione.
- **D.** A Coomassie-stained gel showing the removal of contaminating proteins (bands at 60 kDa and 66 kDa) from the proCFD preparation. A YM50 spin column was used to separate the proteins larger than 50 kDa from the smaller proCFD (27 kDa) in the flow-through from the PreScission Protease step (YM50 Input).

5.2.2.3 Further purification of recombinant proCFD

As seen in the flow-through (FT) fraction of the proCFD purification procedure in Figure 5.9A, there are some contaminating proteins in the purified proCFD preparation (bands at 60 kDa and 66 kDa). The presence of a weak band at 66 kDa in the FT fraction on the anti-GST western blot shown in Figure 5.9C suggests that one contaminant has some similarity to GST and thus is likely to remain bound to Glutathione Sepharose under the stringent wash conditions. Alternatively, as these contaminants are released in the mild conditions of the PreScission Protease cleavage buffer, they may be bound to proCFD.

As the contaminating proteins (60 kDa and 66 kDa) were larger than proCFD (27 kDa), an additional round of purification was performed on the FT from the PreScission Protease step. A YM50 spin column separated the proteins by size. Proteins larger than 50 kDa are less able to pass through the pores of a filter membrane and are retained above the membrane. Smaller proteins, such as proCFD, pass through the filter. Figure 5.9D shows a Coomassie-stained gel of the input to the YM50 column (i.e. the FT from the PreScission Protease cleavage step) in lane 1, and in lane 2, the YM50 FT containing proCFD. The contaminating bands at 60 kDa and 66 kDa are removed. The reduction in the amount of proCFD observed following processing in the spin column is due to incomplete passage of proCFD through the filter membrane and the unavoidable loss of sample within the column.

5.4 HTRA1 cleaves recombinant proCFD

Recombinant proCFD was tested as a substrate for HTRA1, and peptide mass fingerprinting was used in an attempt to identify the site of cleavage in the resulting fragments of proCFD.

5.4.1 HTRA1 cleaves, rather than degrades, proCFD

Increasing amounts of GST ΔN HTRA1 (0.1-1 µg) were incubated with proCFD overnight at 37 ^{o}C in order to assess whether HTRA1 is able to proteolytically process proCFD *in vitro*. Figure 5.10A shows immunoblot analysis of the digest. There is a clear shift in molecular weight of CFD in the presence of active HTRA1, which does not occur in the absence of the protease, or in the presence of the inactive mutant form of HTRA1 (Figure 5.10B). This indicates that cleavage of proCFD is specific to active HTRA1 in this assay. A linker peptide of 27 amino acids remains at the N-terminal end of the recombinant proCFD following the action of PreScission Protease (shown in Figure 5.10D). This linker peptide appears to contribute to the detectable shift in molecular weight of proCFD upon conversion to CFD following HTRA1 activity, corresponding to a loss of 3.5 kDa. This is the predicted molecular weight for the linker peptide (2.9 kDa) and the activation peptide (0.6 kDa). The distinct cleavage pattern was also detected by SDS-PAGE followed by staining with InstantBlue Coomassie stain (Figure 5.10C).

5.4.2 Peptide Mass finger printing to confirm HTRA1-mediated cleavage of proCFD

Bands corresponding to CFD and proCFD were excised from a Coomassie-stained gel (Figure 5.10C) for analysis by mass spectrometry. In-gel digests on destained gel slices were performed by Dundee Cell Products, using the V8 Protease, also known as Endoproteinase Glu-C (*EC 3.4.21.19).* This serine protease from *Staphylococcus aureus* V8 specifically cleaves the peptide and ester bonds at the carboxylic side of Glu, or both Glu and Asp, depending on the buffer used. The reaction buffer (50 mM Tris-HCl, 0.5 mM Glu-Glu, pH 8.0) utilised for the in-gel digest strongly

favours cleavage at glutamic acid residues. Figure 5.10D shows the sequence of proCFD, and indicates the expected sites of cleavage by HTRA1 and by the V8 protease. The N-terminal activated CFD fragment ILGGRE, unique to activated CFD following removal of the activation peptide PPRGR, was of particular interest.

Peptides derived from CFD following V8 protease digest are indicated in bold text in Figure 5.10D. For both bands – proCFD and putative activated CFD – the same two peptides were detected by mass spectrometry. These peptides - AHARPYMASVQLNGAHLCGGVLVAE and QWVLSAAHCLE- are located immediately adjacent to one another at the N-terminal end of activated CFD, and provide 13.8 % coverage of the complete peptide sequence of proCFD.

In agreement with the anti-CFD immunoblot shown in Figure 5.10A, detection of these CFD-specific peptides in the putative activated CFD band confirm that there is a change in molecular weight of proCFD as a result of HTRA1 activity. As the ILGGRE peptide was not detected, it was not possible to confirm activation of proCFD by HTRA1 directly using mass spectrometry. However, taken together with the cleavage of a synthetic peptide corresponding to the N-terminus of proCFD (Figure 5.3) and the absence of cleavage of mature CFD which lacks the propeptide sequence (Figure 5.6) by HTRA1 *in vitro*, it seems likely that HTRA1 cleaves the N-terminal end of proCFD at, or near to, the activation peptide.

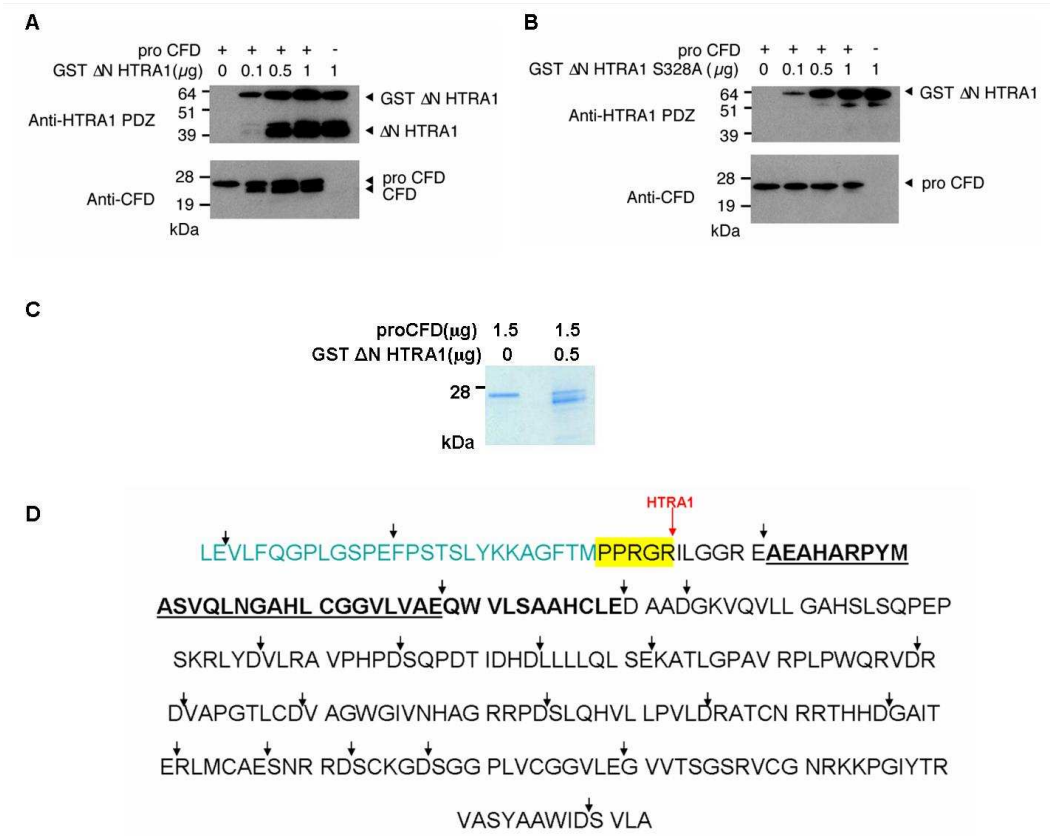

Figure 5.10 ProCFD is a substrate for HTRA1 in an *in vitro* protease assay.

A. ProCFD was incubated with increasing amounts of recombinant GST ΔN HTRA1. Immunoblotting with anti-CFD antibody (lower panel) revealed bands at 27 kDa and at 24 kDa – corresponding to the predicted mass of proCFD and activated CFD. Self-cleavage of HTRA1 generated multiple lower molecular weight bands, in addition to the band at 64 kDa in the upper panel, probed with anti-HTRA1 PDZ.

B. The absence of CFD cleavage when increasing amounts of the inactive mutant (S328A) of HTRA1 was incubated with proCFD in the lower panel (anti-CFD) indicates that active HTRA1 is responsible for the processing of proCFD seen in **A**.

C. Following the specific cleavage of proCFD by GST ΔN HTRA1, bands corresponding to proCFD and the putative activated CFD were excised from a Coomassie-stained gel for analysis by mass spectrometry.

D. The amino acid sequence of proCFD. The linker peptide is shown in blue. The activation peptide is highlighted in yellow. The expected site of cleavage by HTRA1 is indicated by a red arrow. In-gel digests were performed using V8 protease, which specifically cleaves at the carboxyl side of Glu and Asp (indicated by a black arrow). Mass spectrometry analysis of the peptide fragments identified the same two peptides for both proCFD and putative activated CFD; these are indicated in bold text, with one peptide also underlined.

5.5 HTRA1 specifically cleaves the CFD activation peptide sequence

The ability of HTRA1 to specifically cleave the activation peptide sequence of proCFD in vitro was assessed using a synthetic activation peptide (PPRGR), coupled to a C-terminal methyl coumaric acid (MCA). A measurable increase in fluorescence only occurs following cleavage of the synthetic peptide at the amino acid residue immediately adjacent to the MCA group, to release free AMC.

5.5.1 Development of the fluorescent peptide assay

A fluorescent peptide assay was developed to test whether the human CFD activation peptide was a substrate for HTRA1 *in vitro*. MCA-labelled synthetic peptides are shown in Table 5.1. Recombinant GST ΔN HTRA1 and proCFD were freshly purified to avoid loss of activity as a result of storage at -80^{o}C, and were diluted in TBS to the appropriate concentration for each assay. Thrombin, purified from human plasma, was used as a positive control for cleavage of the activation peptide. The optimal pH for HTRA1 activity was determined. All assays were incubated at 37^{o}C.

5.5.1.1 pH optimisation

The ability of recombinant GST ΔN HTRA1 to specifically cleave the five amino acid activation peptide of CFD was studied over a pH range of 6-8.5 in TBS. 50 nM of active enzyme was incubated with 20 µM fluorescent peptide for 24 hours. The final reaction volume was 50 µl. Following cleavage at the amino acid immediately adjacent to the MCA group, free AMC is released. Free AMC increases fluorescence measured at excitation wavelength of 355 nm and an emission wavelength of 460 nm. Assays were performed in duplicate, and the data shown in Figure 5.11 represents the mean ± SD of three independent experiments. Optimal cleavage activity for HTRA1, reflected by the highest measurement of relative fluorescent units (Rfu) as a result of released AMC, was obtained at pH 7.5 (Figure 5.11).

5.5.1.2 Validation of HTRA1 cleavage specificity

The specificity of the MCA-peptide assay was validated by comparing the relative fluorescent units generated by HTRA1-mediated cleavage of the CFD activation peptide-MCA peptide (PPRGR-MCA) and DSVLA-MCA, corresponding to the C-terminal five amino acid sequence of mature CFD. The relative fluorescence (corresponding to nanomoles of AMC released, Figure 5.14) increased over time for the CFD activation peptide-MCA, DSVLA-MCA did not generate detectable fluorescence over background measured when the peptide was incubated in the absence of protease (Figure 5.12). This indicates that HTRA1 could not cleave DSVLA-MCA and cleaves the activation peptide of CFD specifically.

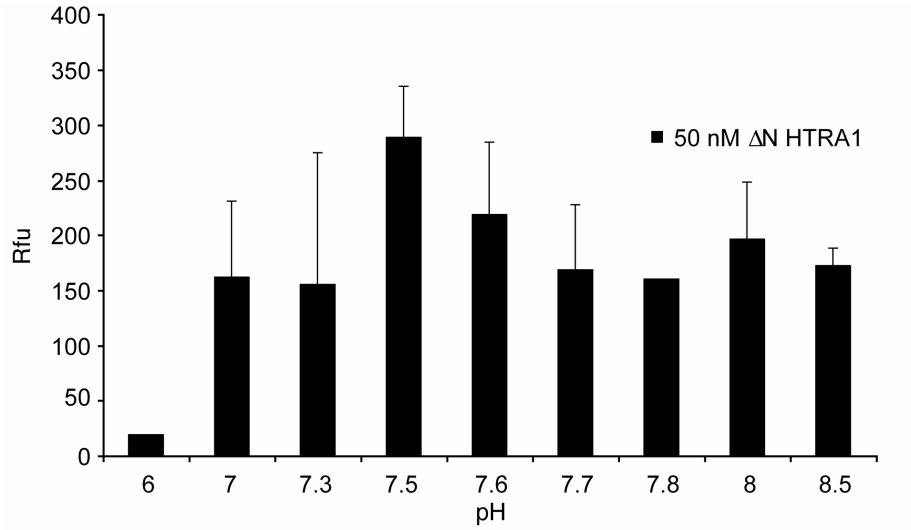

Figure 5.11 pH optimisation of the fluorescent peptide assay.
A range of pH conditions were tested in order to determine the optimal pH for ΔN HTRA1-mediated cleavage of PPRGR-MCA. AMC release, as a consequence of proteolysis of the fluorescent peptide, was measured after 6 hours. The optimal pH for HTRA1 activity was pH 7.5. Values are the mean relative fluorescent units (Rfu) obtained in three independent experiments ± SD.

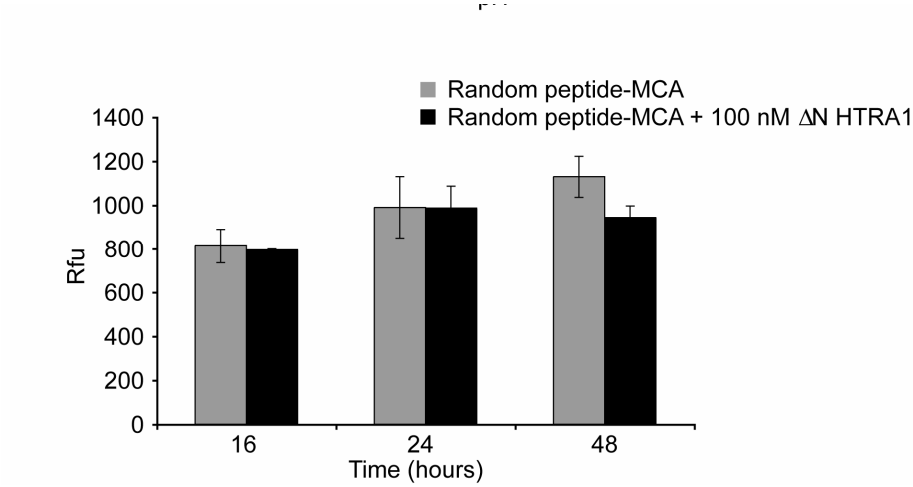

Figure 5.12 Specificity of the fluorescent peptide assay.
The specificity of the MCA-peptide assay was tested by measuring the relative fluorescent units (Rfu) generated by HTRA1-mediated cleavage of DSVLA-MCA. This is a fluorescently labelled peptide corresponding to the C-terminal sequence of mature CFD. HTRA1 could not cleave DSVLA-MCA, as there was no increase in fluorescence relative to the background Rfu measured when the peptide was incubated in the absence of protease. This indicates that HTRA1 cleaves the activation peptide of CFD specifically**.** Values are the mean Rfu obtained in two independent experiments ± SD.

5.5.1.3 The AMC standard curve

Serial dilutions of 7-amino-4-methyl coumarin (AMC) in the range of 0.05-50 µM were used to create a standard curve of AMC fluorescence (Figure 5.13). A concentration dependent, linear (R^2=0.9979) increase in AMC fluorescence was observed in the concentration range tested. The AMC standard curve was used to calculate the concentration of AMC released as a function of a measurable increase in fluorescence (Rfu) above background. Non-specific background fluorescence was measured in the absence of enzyme, and was used to calculate AMC release due to protease activity.

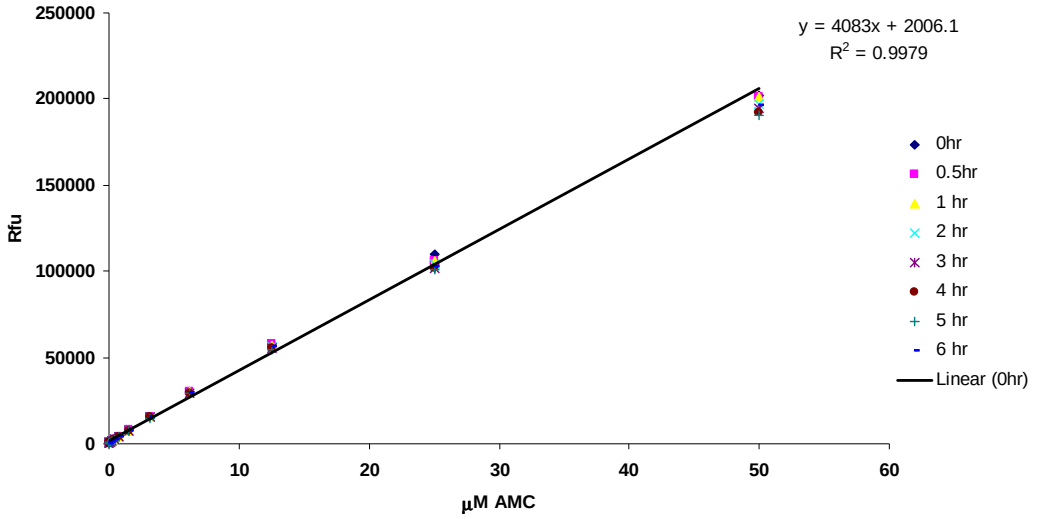

Figure 5.13 An AMC Standard Curve.
A standard curve of AMC fluorescence in the range of 0.05-50 µM was generated by serial dilutions of 7-amido-4-methyl coumarin (AMC). There was a concentration dependent, linear (R^2=0.9979) increase in AMC fluorescence observed in the concentration range tested, with little change in fluorescence over time. This standard curve was used to calculate the amount of AMC released as a function of increased in fluorescence (Rfu).

5.5.1.4 Enzyme concentration dependent increase in fluorescence

A range of enzyme concentrations were tested to determine the minimum amount of enzyme required for a detectable increase in fluorescence as a result of AMC release following peptide cleavage. Any increase in fluorescence generated by enzyme concentrations less than 10 nM was below the limits of sensitivity of the assay (data not shown). Within the range of 10-200 nM of active HTRA1 (assessed by zymography, data not shown), there was an enzyme concentration-dependent increase in free AMC over time (Figure 5.14). 50 nM of active enzyme was selected for use in subsequent assays with a range of substrate concentrations (0-240 µM, Figure 5.15).

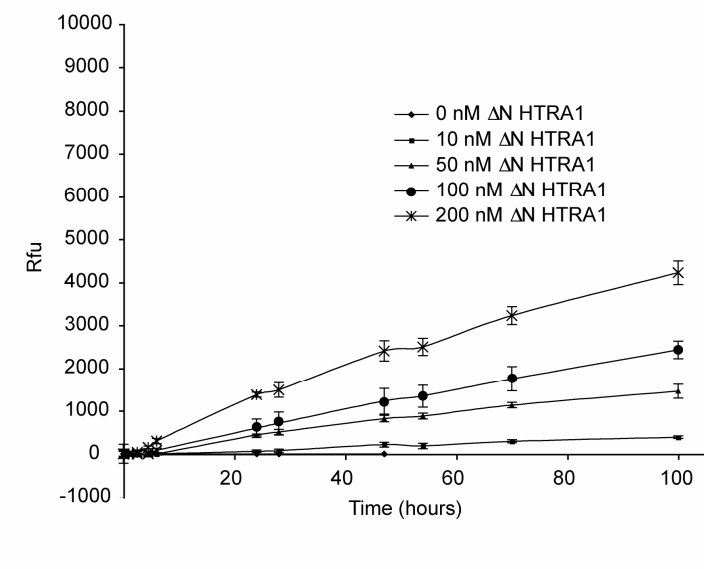

Figure 5.14 An enzyme concentration-dependent increase in fluorescence.

Increasing concentrations of active recombinant ΔN HTRA1 were used to cleave PPRGR-MCA. Fluorescence emission corresponded to the amount of cleavage product, with a clear relationship between increasing enzyme concentrations and an increase in AMC release over time. Results are shown as relative fluorescence units (Rfu), corrected for non-specific background of substrate alone. Each data point represents a minimum of three observations ±SD.

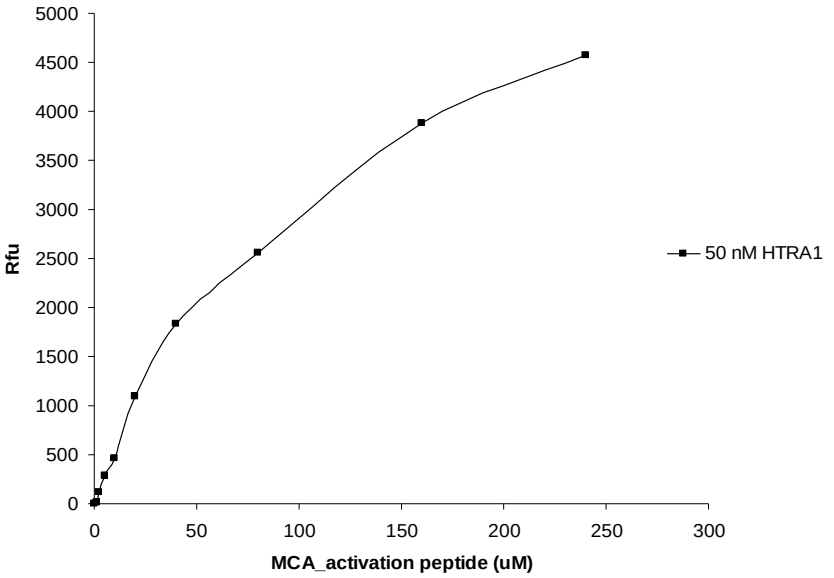

Figure 5.15 Substrate concentration-dependent increase in fluorescence.

HTRA1 is able to cleave the synthetic activation peptide across a range of substrate (0-240 µM) concentrations. A substrate concentration-dependent increase in free AMC over time was observed, with 50 nM of active ΔN HTRA1 approaching saturation at higher concentrations of substrate.

5.5.2 HTRA1 cleaves the synthetic activation peptide

50 nM of active ΔN HTRA1 (generated by self-cleavage of the GST tag) or the S328A mutant was incubated with increasing concentrations of the CFD activation peptide PPRGR-MCA (0-240 µM) for 96 hours at 37°C, following an initial incubation of 4 hours at 37°C to increase solubility of the enzyme in solution. Confirming results obtained during optimisation of the assay, HTRA1 cleaves the synthetic activation peptide (Figure 5.15). There was substrate concentration-dependent increase in free AMC over time, with the enzyme approaching saturation at higher concentrations of substrate.

Using a substrate concentration of 20 µM, and 50 nM of active ΔN HTRA1, the proteolysis of substrate by HTRA1 was observed to be of sustained duration, acting in a processive manner to release AMC in a linear fashion over the course of 96 hours of study (Figure 5.16). This is in contrast to the same experiment using 50 nM thrombin in the place of HTRA1, in which rapid generation of free AMC was observed for 1 hour, then no further increase in free AMC over the next 4 days (Figure 5.16). The inactive mutant of HTRA1, S328A, exhibited no ability to cleave the synthetic substrate, showing no increase in fluorescence above background (Figure 5.16).

Michaelis Menton kinetics were used to calculate the maximum velocity of the reaction (V_{max}) of 19.88 nanomoles AMC/hour/mg active enzyme. The K_m was calculated as 183 µM. The Lineweaver Burk plot is shown in Figure 5.17.

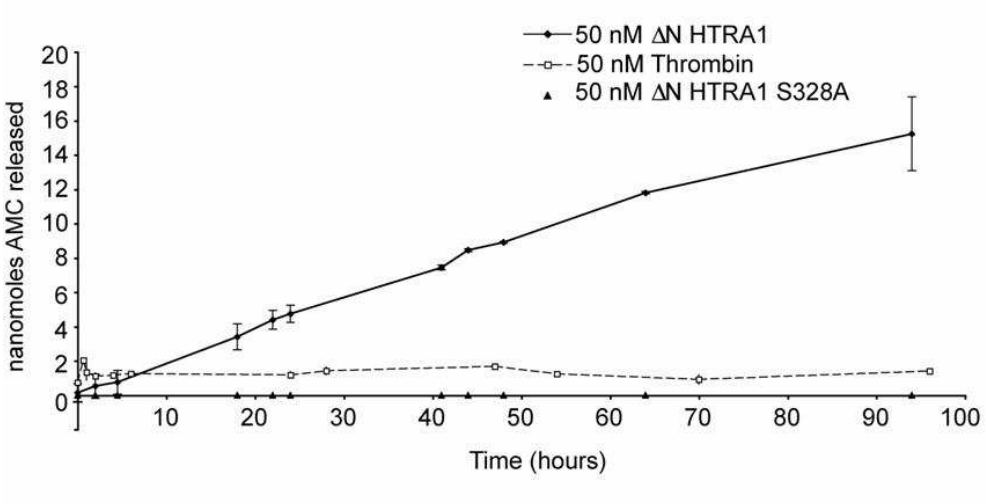

Figure 5.16 Processive cleavage of the fluorescent peptide over time by HTRA1.

50 nM active recombinant ΔN HTRA1 is able to cleave the synthetic substrate in a linear fashion for a sustained period (96 hours). This is in contrast to the activity of 50 nM thrombin, which cleaves the substrate rapidly, before reaching a plateau after one hour of reaction. There is no measurable increase in fluorescence when the fluorescent peptide is incubated with 50 nM inactive recombinant ΔN HTRA1 S328A. Each data point represents three observations, corrected for non-specific background, ±SD.

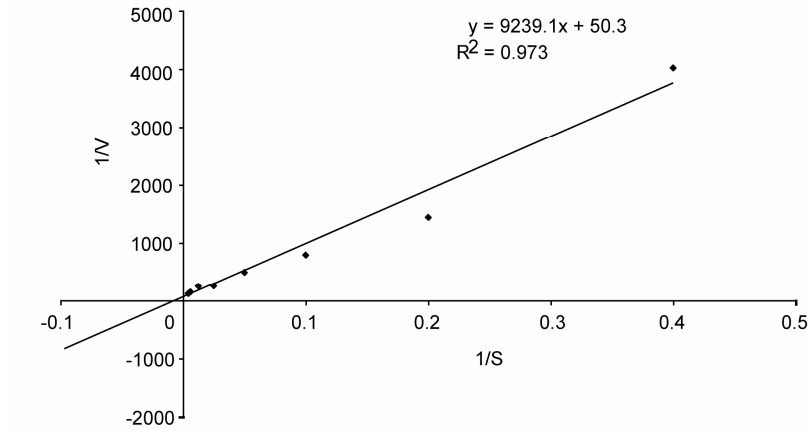

Figure 5.17 Characterisation of enzyme kinetics using a Lineweaver-Burk plot.

The cleavage reaction was performed with 50 nM active recombinant ΔN HTRA1 in the presence of increasing concentrations of PPRGR-MCA (1.25-240μM). Rate (V) was calculated as nM AMC released/hour/nM active ΔN HTRA1. V_{max} and K_M were calculated using Michaelis Menton kinetics.

5.6 Functional relevance of the interaction between HTRA1 and CFD

Recombinant HTRA1 specifically cleaves the activation peptide of proCFD. *In vitro* assays of alternative complement pathway activation were utilised to determine the functional impact on CFD activity of HTRA1-mediated cleavage. Such assays have been described previously (Biesma et al. 2001; Carroll et al. 2009; Takahashi et al. 2010), and were adapted for use with HTRA1.

The alternative complement pathway is amplified by the C3 convertase. C3b binds to Factor B, which is subsequently bound and cleaved to Ba and Bb by activated CFD to form C3bBb, the C3-convertase. Upon formation of the convertase, there is a downstream cascade of complement activation leading to the formation of the membrane attack complex and lysis of invading pathogens. The C3 convertase will only be formed when active CFD is present. The activity of the C3 convertase was assessed by visualising the cleavage of factor B to Ba and Bb, both *in vitro* and in normal and CFD-depleted human sera. Alternative complement pathway activity was measured directly by monitoring heamolysis of sheep erythrocytes in normal and CFD-depleted human sera supplemented with purified and recombinant proteins.

5.6.1 Reconstitution of the C3 convertase *in vitro*

The first assay determined whether a functional C3 convertase could be formed using purified human factor B, CVF (a structural homologue of C3b) and either CFD purified from plasma, or with recombinant proCFD which had been pre-treated with HTRA1. HTRA1 does not cleave either factor B or C3 *in vitro* (Figure 5.18). Thus, the proteolytic activity of HTRA1 is specific to proCFD under the conditions used in the subsequent assays.

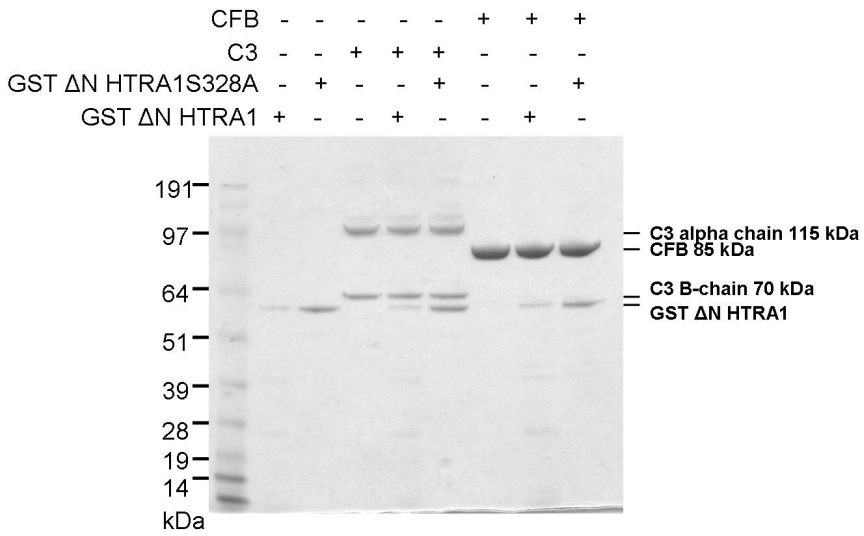

Figure 5.18 HTRA1 does not cleave factor B or C3 *in vitro.*
The C3-convertase of the alternative complement pathway is formed when C3b binds Factor B, to form C3bB. Bound Factor B is subsequently cleaved to Ba and Bb by activated CFD to form C3bBb, the C3-convertase. The ability of HTRA1 to cleave Factor B and C3 was tested in *in vitro* protease assays, with neither protein subject to proteolysis by HTRA1. This is a requirement for subsequent assays, in which the proteolytic activity of HTRA1 must be specific to proCFD.

5.6.1.1 C3 convertase is formed with proCFD activated by HTRA1 *in vitro*

0.2 µg of recombinant proCFD was incubated overnight with an equal amount of active GST ΔN HTRA1 to allow cleavage of proCFD (Figure 5.10). HTRA1-treated proCFD was added to purified plasma factor B, in the presence or absence of 1 µg of CVF at 37^{o}C overnight. Concurrently, HTRA1, proCFD or CFD purified from plasma was incubated with factor B and 1 µg of CVF. The final reaction volume was 20 µl, in TBS supplemented with 5 mM $MgCl_2$ and 5 mM $CaCl_2$. Formation of the C3 convertase was determined by cleavage of Factor B (83 kDa) to Ba (26 kDa) and Bb (57 kDa), as seen in a non-reducing Coomassie-stained gel (Figure 5.19).

HTRA1-treated proCFD or CFD purified from plasma form the C3 convertase with factor B and CVF *in vitro*, resulting in cleavage of factor B to Ba and Bb (lanes 6 and 10, Figure 5.19). Reflecting the physiological situation, all three components of the C3 convertase are required for cleavage of factor B to occur. HTRA1-treated proCFD incubated with factor B without CVF does not result in cleavage of factor B (lane 5). No cleavage of Factor B was observed when proCFD or HTRA1 alone were mixed with Factor B and CVF (lanes 7 and 8), indicating that the specific cleavage of proCFD by HTRA1 results in formation of mature CFD, necessary for formation of the C3 convertase.

5.6.1.2 Mg^{2+} ions are required for the formation of the C3 convertase

Divalent magnesium ions have a co-factor role in the formation of the C3 convertase of the alternative complement pathway, both *in vitro* and *in vivo*. Calcium ions are required in the classical complement pathway. The requirement for magnesium and/or calcium ions in the formation of the C3 convertase by HTRA1-treated proCFD, factor B and CVF was assessed. The assay was performed as above, including Mg^{2+} (2 -20 mM) or 10 mM Mg^{2+} and 10 mM Ca^{2+} in TBS. Mg^{2+} is required for the formation of the C3 convertase and cleavage of factor B to Ba and Bb. $Ca^{2+}$are not required (Figure 5.20).

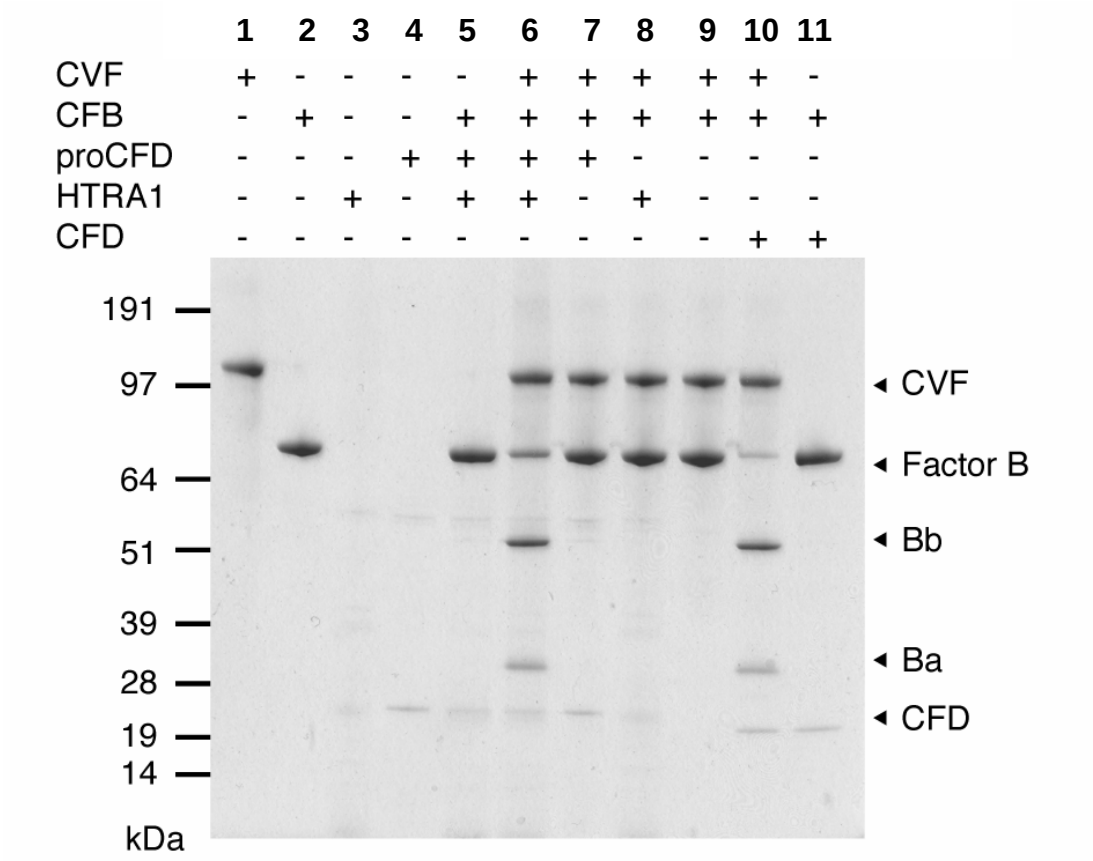

Figure 5.19 HTRA1 activates proCFD in an *in vitro* reconstitution experiment.

The C3-convertase was reconstituted *in vitro*, using purified complement components and recombinant proCFD and HTRA1. Cobra Venom Factor (CVF) is a homologue of C3b. Before the addition of CVF and Factor B, 0.2µg proCFD was preincubated with 0.2µg HTRA1 (lane 5 and 6). Samples were incubated at 37^{o}C for 16 hours and then subjected to electrophoresis under non-reducing conditions, followed by Coomassie-staining. Cleavage of Factor B to Ba and Bb - a requirement for formation of the C3-convertase - indicates that activated CFD is present. Bb and Ba were detected only when Factor B was incubated with CVF in the presence of either proCFD treated with HTRA1 (lane 6) or with CFD purified from plasma (lane 10). Results shown are representative of three independent experiments.

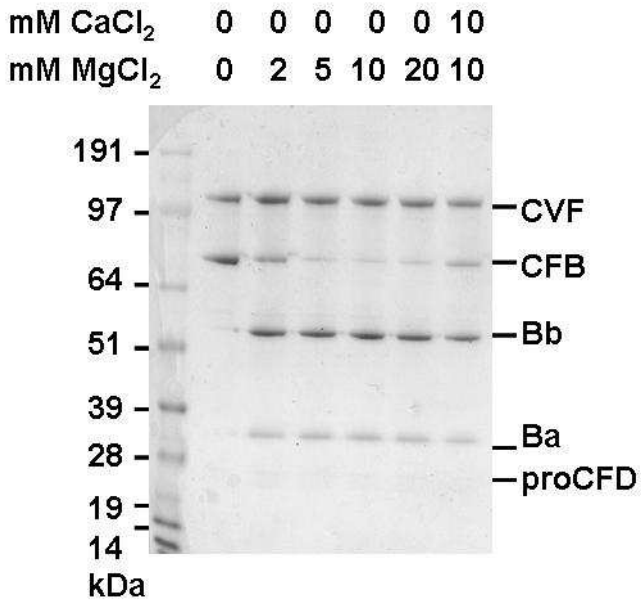

Figure 5.20 Mg^{2+} ions are required for the formation of the C3 convertase

The ability of HTRA1-activated CFD to cleave Factor B in the presence and absence of magnesium and calcium ions was assessed. All lanes in the Coomassie-stained gel contain proCFD, pre-treated with HTRA1, in addition to CVF and Factor B. There is no cleavage of Factor B in the absence of both cations. Magnesium ions are required for the cleavage of Factor B to Ba and Bb *in vivo*, and also in this *in vitro* assay. Calcium ions are not an absolute requirement for the formation of the convertase, as Factor B is cleaved when calcium ions are not included in the reaction.

5.6.2 Normal alterative complement pathway activity can be restored to CFD-depleted sera

In order to test formation of the C3 convertase from endogenous plasma components and HTRA1-treated proCFD, normal and CFD-depleted human sera were required.

5.6.2.1 CFD-depleted sera

Human serum was obtained from five healthy volunteers and pooled to provide a "normal" serum sample. CFD-depleted sera were obtained from a commercial source (Quidel) and by production of depleted serum on affinity columns. The monoclonal CFD-specific antibodies GAU-008-01 or MAB#255719 were coupled to CNBr-activated Sepharose 4B, equilibrated in veronal buffered saline (VBS). Fresh serum was passed over each column twice. The least dilute fractions of depleted sera, assessed visually by colour, were collected and pooled for each antibody.

BioRex70 chromotography was also used to deplete CFD from serum (Østerud and Eskeland 1982). The cation-exchange resin was equilibrated in VBS, and incubated for 1 hour with normal serum to adsorb CFD. Depleted-serum was obtained by centrifugation to remove the BioRex70 resin.

Depletion of CFD in serum was confirmed by CFD-specific ELISA (Table 5.2) and by Western blotting with anti-CFD (Figure 5.21A). All methods of depletion resulted in a decrease in detectable CFD in sera, by immunoblot analysis with anti-CFD and by ELISA.

5.6.2.2 Assessment of depletion in CFD-depleted sera

The completeness of CFD-depletion in sera was tested by assessment of residual haemolytic activity of sheep red blood cells (RBCs), compared to normal pooled human serum. Sera were diluted 1 in 5 with $1x10^8$ neuraminidase-treated RBCs resuspended in 10mM ethylene glycol-bis(2-aminoethylether)-N,N,N,N'-tetraacetic acid (EGTA), 7mM MgCl2, 2.1mM sodium barbital, 59mM NaCl, 2.08% (w/v) glucose, 0.08% (w/v) gelatin, pH 7.4 (DGVB-MgEGTA), and incubated for 1 hour at 37 ^oC. Haemolysis was measured in the supernatant by absorbance at 412 nm.

CFD-depleted sera showed a large reduction in haemolytic activity compared to normal serum (Figure 5.21B). Generally, there was a correlation between the proportion of retained haemolytic activity in the CFD-depleted sera and the CFD ELISA measurement and signal intensity on the anti-CFD immunoblot (Table 5.2; Figure 5.21A). The serum depleted using the monoclonal antibody GAU 008-01 showed a 56.1% reduction in CFD (0.54 µg/ml compared to 1.23 µg/ml) measured by ELISA, corresponding to a 65.6% reduction in haemolytic activity (Figure 5.21B). Likewise, the CFD-depleted sera obtained from Quidel and by depletion using the monoclonal antibody #255719 both had >85% reduction in CFD measured by ELISA, corresponding with an almost total loss of haemolytic activity compared to normal serum.

One exception was the depleted serum generated by adsorption of CFD to BioRex70; this showed a small depletion of CFD by ELISA (a reduction of 23.6%, from 1.23 µg/ml to 0.94 µg/ml) and an almost total loss of haemolytic activity.

The specificity of the serum depletion was assessed by monitoring the degree of haemolysis when purified CFD from plasma was added to the depleted sera. The three depleted sera with the least residual haemolytic activity (depletion methods, MAB#255719, BioRex70 and Quidel, Figure 5.21B) were supplemented with 0.1 µg CFD, or used alone in haemolysis assays, and compared to normal serum and to heat-inactivated serum. Figure 5.22 shows that only the CFD-depleted serum purchased from Quidel can be restored to normal levels of haemolytic activity by supplementation with CFD. Heat inactivated serum, and sera depleted by MAB#255719 and BioRex70, show no restoration of lytic activity in response to supplementation with CFD. The depletion of CFD in the CFD-depleted sera generated by MAB#255719 and BioRex70, and the observed loss of haemolytic activity in these samples, is most likely due to dilution, non-specific depletion of other complement components, or exhaustive activation of complement on the column during depletion.

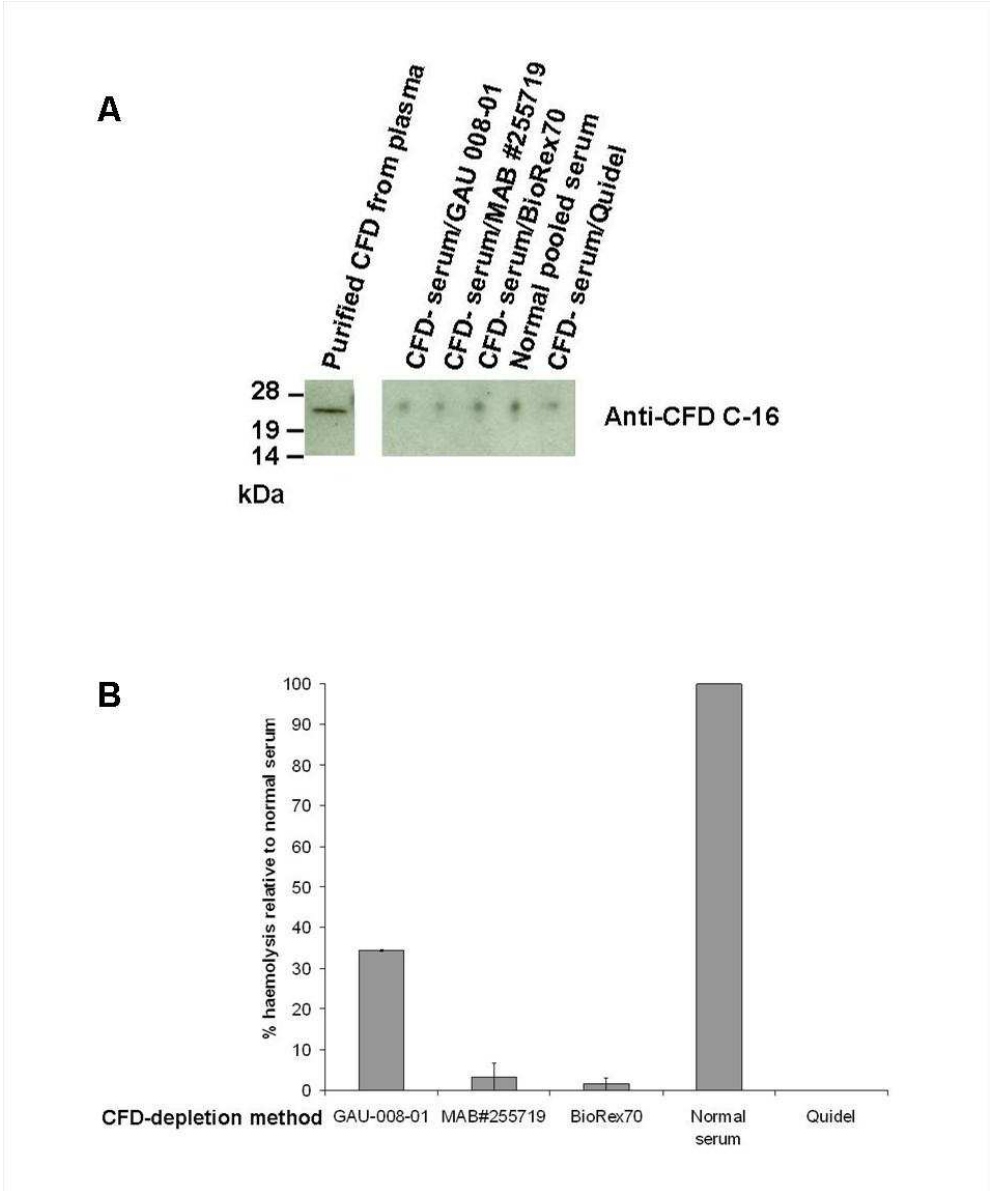

Figure 5.21 Assaying depletion in CFD-depleted sera.
Normal human serum was depleted of CFD using affinity columns, using BioRex70 chromotography or by coupling the monoclonal CFD-specific antibodies GAU-008-01 or MAB#255719 to CNBr-activated Sepharose 4B. CFD-depleted serum was also obtained from Quidel.
A. The depletion of CFD in sera was confirmed by western blotting with anti-CFD (C-16). The intensity of the CFD-specific band (24 kDa) in all depleted sera was decreased relative to the normal pooled serum sample.
B. The degree of haemolysis of sheep red blood cells was used to assess the specificity of the serum depletion. A reduction in CFD leads to a corresponding decrease in the haemolytic activity. All methods of depleting CFD reduced the residual haemolytic activity relative to normal serum.

Sera	Depletion method	CFD µg/ml
CFD-depleted serum A	GAU 008-01	0.54
CFD-depleted serum B	MAB#255719	0.14
CFD-depleted serum C	BioRex70	0.94
Normal pooled serum		1.23
CFD-depleted serum D	QUIDEL	0.13

Table 5.2 CFD measured in human serum by ELISA.
The effectiveness of CFD-depletion in human sera using a variety of methods was assessed using a CFD-specific ELISA. Depletion was determined by comparison to normal pooled serum.

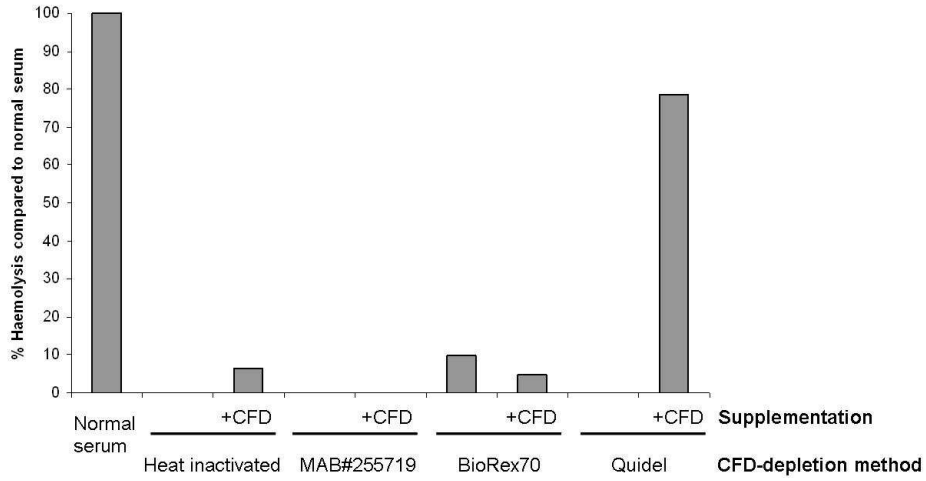

Figure 5.22 Restoration of normal alternative complement activity to CFD-depleted sera
Depleted sera with the least residual haemolytic activity (depletion methods, MAB#255719, BioRex70 and Quidel) were used alone or supplemented with 0.1 µg CFD, and compared to normal serum and to heat-inactivated serum. Heat inactivated serum, and sera depleted by MAB#255719 and BioRex70, show no restoration of haemolytic activity when supplemented with CFD. Supplementation with CFD was able to restore normal levels of haemolytic activity to the CFD-depleted serum purchased from Quidel.

5.6.2.3 Restoration of alternative complement pathway activity in CFD-depleted serum by HTRA1-treated proCFD

Having verified that the completeness and specificity of the depletion of CFD in the depletion serum purchased from Quidel, this serum was used in subsequent assays. The haemolysis of RBCs by the alternative complement pathway in normal human serum, in heat-inactivated normal serum and in CFD-depleted serum was assessed, with and without the addition of purified proteins. The assay is specific for the alternative complement pathway. EGTA in the reaction buffer chelates any calcium ions present, preventing activation of the classical pathway. 1 µg of CVF was added to all samples, including 0% and 100% lysis in water to allow reactive lysis of RBCs.

Haemolysis in normal serum after 1 hour incubation at 37 ^{o}C was considered as 100%; this activity was removed by heat-inactivation and in CFD-depleted serum (Figure 5.23). The addition of recombinant proCFD or HTRA1 alone did not restore haemolysis, although proCFD alone was able to induce slight haemolysis in the CFD-depleted serum. Addition of 0.05 µg of CFD, or of 0.2 µg proCFD pre-treated with HTRA1, restored heamolysis in CFD-depleted serum to levels observed in normal serum (data is the mean of two independent experiments ± SD). 0.2 µg of proCFD was used, compared to the 0.05 µg of CFD, to account for the incomplete cleavage of proCFD by HTRA1 to the lower molecular weight form of the recombinant protein (Figure 5.10A and C).

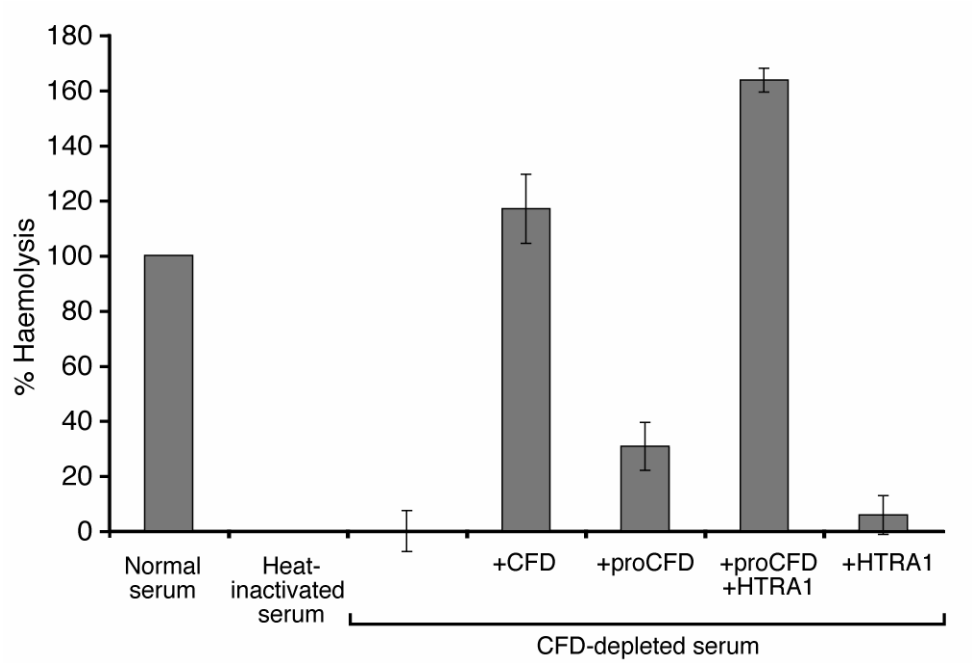

Figure 5.23 HTRA1 activates proCFD in vitro, and restores complement activity in CFD-depleted serum.

The degree of haemolysis of sheep red blood cells was assessed in normal, heat-inactivated or CFD-depleted sera with and without the addition of purified proteins. The addition of 0.05 µg of CFD, or of 0.2 µg proCFD pre-treated with HTRA1, results in the restoration of haemolytic activity in CFD-depleted serum. Neither proCFD, nor HTRA1 alone restored haemolysis to levels seen in normal serum. Results shown are the mean level of haemolysis achieved relative to normal serum in two independent experiments ± SD.

5.6.2.4 Restoration of C3 convertase activity in CFD-depleted serum *in vitro* by HTRA1-treated proCFD

Normal levels of haemolysis are restored to CFD-depleted serum upon the addition of proCFD that had been pre-treated with HTRA1. To confirm that this was a result of formation of the C3 convertase and resultant activation of the alternative complement pathway, the specific cleavage of factor B to Bb in sera was investigated by Western blotting.

The optimal conditions for Western blotting using the anti-Bb antibody were determined. 250 ng of purified factor B, from human plasma, could be detected using a 1:500 dilution of the primary antibody (data not shown). Under reducing conditions, no Bb-specific signal was obtained from serum on an immunoblot performed using a 1:500 dilution of the primary antibody (Figure 5.24A). Under non-reducing conditions, a clear signal for both factor B, and for Bb upon addition of CFD and CVF, was obtained from 1µl serum using a 1:500 dilution of the primary antibody (Figure 5.24B).

The ability of recombinant proCFD to restore C3 convertase activity to serum which was depleted of CFD was subsequently assessed. To ensure that availability of C3b was not a limiting factor in the reaction, normal and CFD-depleted sera were supplemented with 1 µg of CVF, together with either 0.2 µg of CFD purified from plasma, 0.2 µg of recombinant proCFD, 0.2 µg of HTRA1 or 0.2 µg proCFD which had been pre-treated with 0.2 µg of HTRA1. In normal serum, after incubation for 3 hours at 37^{o}C, cleavage of endogenous Factor B to Bb was detected in both the presence and absence of CVF (Figure 5.25). As seen in lane 3, Bb was dramatically increased following addition of purified CFD and CVF. In CFD-depleted serum, there was no cleavage of endogenous Factor B to Bb without supplementation with activated CFD. Both proCFD pre-treated with HTRA1 (lane 6) and CFD from plasma (lane 7) were able to restore C3 convertase activity to the CFD-depleted serum. HTRA1 (lane 8) or proCFD alone (lane 9) did not restore the alternative pathway convertase (Figure 5.25).

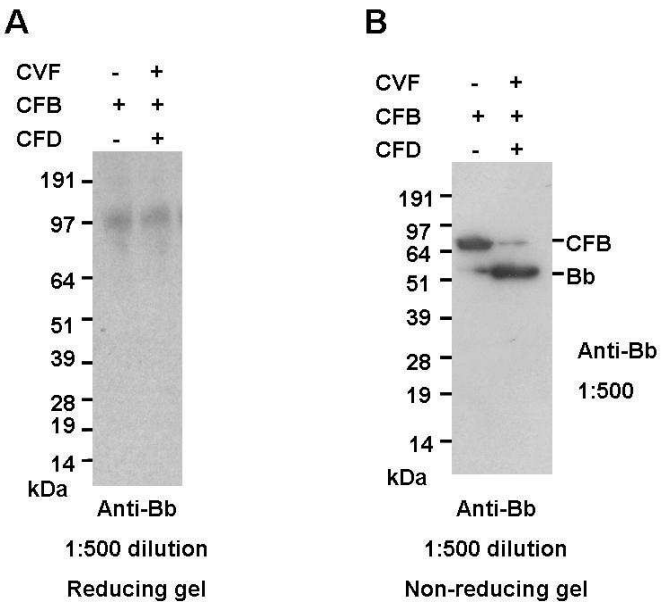

Figure 5.24 Optimisation of conditions for immunoblotting with anti-Bb

A. Reducing gel electrophoresis of normal human serum supplemented with 1 µg CVF, 1 µg Factor B and 0.1 µg of CFD, followed by immunoblotting using a 1:500 dilution of anti-Bb. No Bb-specific signal was detected under reducing conditions.

B. Non-reducing gel electrophoresis of normal human serum supplemented with 1 µg CVF, 1 µg Factor B and 0.1 µg of CFD, followedby immunoblotting using a 1:500 dilution of anti-Bb. Both Factor B and Bb were detected using a 1:500 dilution of anti-Bb.

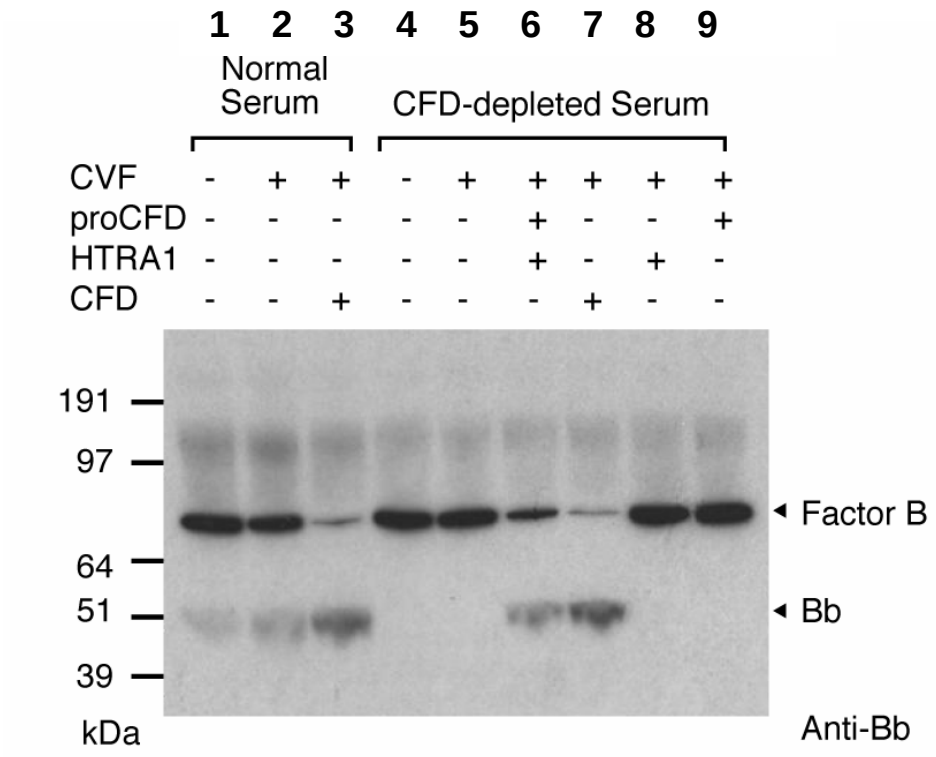

Figure 5.25 HTRA1 activates proCFD *in vitro*, and restores cleavage of Factor B to Bb in CFD-depleted serum.

Endogenous Factor B in serum is cleaved when activated CFD is present. Normal serum or CFD-depleted serum was supplemented with CVF and purified CFD, proCFD and HTRA1 as indicated. After incubation at 37^{o}C for 3 hours, samples were subjected to non-reducing gel electrophoresis and western blot. Immunoblotting with anti-Bb antibody detected both Factor B and the cleavage product Bb. Addition of CFD purified from plasma (lane 7) or proCFD pre-treated with HTRA1 (lane 6) but not with proCFD (lane 9) or HTRA1 (lane 8) alone resulted in cleavage of Factor B in CFD-depleted sera. This reflects the cleavage of Factor B observed in normal human serum (lanes 1-3) Results shown are representative of two independent experiments.

5.6.3 Reduced alternative complement pathway activity in CARASIL patients with mutations in *HTRA1* which affect protease activity

Cerebral autosomal recessive arteriopathy with subcortical infarcts and leukencephalopathy (CARASIL) is an ischemic, non-hypertensive small vessel disease associated with spondylosis and alopecia. Recently, missense and nonsense mutations in HTRA1 have been associated with CARASIL (Hara et al. 2009). Professor Osamu Onodera kindly provided serum samples from three Japanese CARASIL patients and two Japanese disease-free controls.

Sera were tested for their relative ability to lyse sheep RBCs in the presence of CVF, as an indication of alternative complement pathway activity. The CARASIL sera showed significantly reduced haemolytic activity compared to normal ethnically-matched sera (or to normal pooled sera from Caucasian individuals) in three independent experiments (Figure 5.26A). The haemolysis assays were performed without knowledge of the *HTRA1* mutation carried by the CARASIL patients. Subsequent identification of the mutations confirm that the patient whose serum showed the lowest haemolytic activity (CARASIL2, 15.7±4.1 (SD) % relative to normal sera) carries the R370X mutation in *HTRA1*. This mutation leads to nonsense-mediated decay of the HTRA1 transcript and a lack of protein in patient fibroblasts (Hara et al 2009). The two remaining CARASIL patients carry mutations which appear to reduce activity of the protease to <30% of wild-type activity *in vitro* without altering protein expression (CARASIL1; V297M, and CARASIL 3; R302X; Hara et al. 2009). CFD concentrations in the CARASIL and control sera were measured by ELISA, and determined to be within the normal range for both proteins (data not shown).

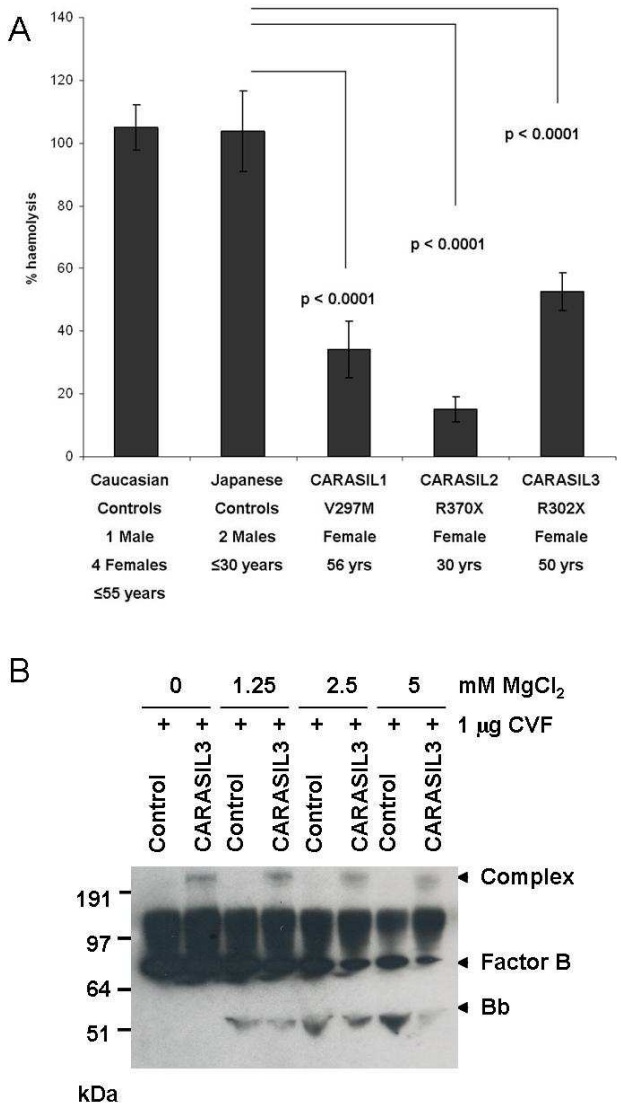

Figure 5.26 Alternative complement pathway activity in CARASIL sera.
A. Alternative complement pathway-specific reactive lysis of sheep RBCs induced by a 1 in 5 dilution of CARASIL sera were significantly reduced, compared to lysis in control sera. Data represent mean % heamolysis±SD obtained in 3 independent experiments, in which each sample was assayed 4 times. Significant differences were determined using t-tests to compare mean heamolysis.
B. Cleavage of factor B to Bb in CARASIL serum compared to normal serum was investigated in the presence of CVF and increasing Mg^{2+} concentration. The amount of factor B in the assay was equalised by using 1 µl of control serum or 3 µl of CARASIL3 serum. Bb appears less abundant in CARASIL3 serum. A high molecular weight complex, corresponding to the predicted molecular weight of the CVF-factor B complex (~240 kDa) was observed in CARASIL3 serum, but not in control serum. Data is representative of 2 independent experiments, probed with anti-Bb. 2 independent experiments using equal volumes (1 µl) of CARASIL3 and normal serum gave similar results. The complex was also observed in CARASIL1 and CARASIL2 sera (data not shown).

5.7 Co-expression of HTRA1 and CFD

HTRA1 is a stress-responsive gene, widely expressed in a range of tissues (De Luca et al. 2003). The functional data presented in Section 5.6 indicates that HTRA1 is capable of activating proCFD *in vitro*. However, a number of serine proteases, including thrombin, can activate CFD (Fearon et al. 1974; Yamauchi et al. 1994; Takahashi et al. 2010). To determine whether HTRA1 and CFD are present in the same cellular environment, thereby increasing the chances of similar activity *in vivo*, the expression of *HTRA1*, *CFD*, and of other genes implicated in local activation of the alternative complement pathway, was investigated. Expression of these genes was studied in a human tissue cDNA panel, and in the cell lines THP-1 and hTERT RPE1. THP-1 cells are a human macrophage-like cell-line, which can be differentiated from a monocyte-like cell by treatment with PMA. hTERT RPE1 is a telomerase-immortalised human retinal pigment epithelial cell line. These cell lines were investigated due to a proposed role for these cells in the development and progression of AMD pathogenesis.

5.7.1 Screening a cDNA panel by RT-PCR

Commercially available cDNA from a range of human tissues, including retina, brain, adipose, liver, kidney, skeletal muscle, thymus and peripheral blood monocytes, was screened for the expression of gene-specific transcripts. *HTRA1*-specific transcripts were detected by RT-PCR in cDNA derived from retina, brain, adipose, liver and skeletal muscle. No *HTRA1* transcripts were detected in cDNA from the kidney or peripheral blood monocytes (Figure 5.27). HTRA1 has previously been reported to be expressed in these tissues (De Luca et al 2003). *GAPDH* was used as a control, and was found to be expressed across all tissues screened. *CFD*-specific transcripts were detected in all the tissues screened (Figure 5.27). Variations in band intensity were observed, which is likely to reflect variations in the amount of *CFD*-specific transcripts within the 10 ng of cDNA used as template in the amplification reactions. Adipose cells, for example, are known to express high levels of *CFD*, correlating with high band intensity in Figure 5.27 (Cook et al. 1985; White et al. 1992).

Expression of *MASP1*, encoding an enzyme able to activate murine proCFD (Takahashi et al. 2010), was also tested. In contrast with the overlapping expression patterns of *CFD* and *HTRA1* across a range of tissues, *MASP1* transcripts were only detected in cDNA purified from the liver (Figure 5.27).

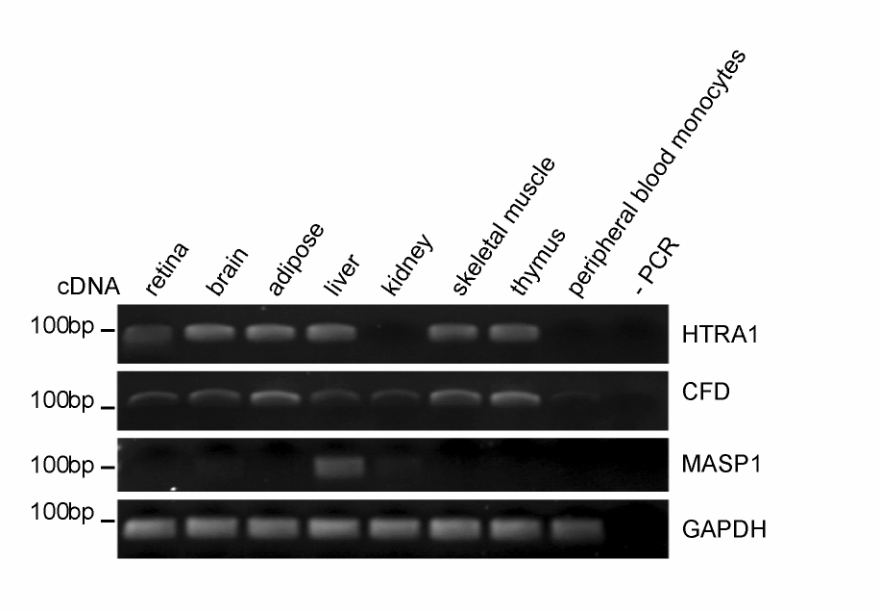

Figure 5.27 Human cDNA panel screened for HTRA1 and other genes. Co-expression of *HTRA1*, *CFD* and *MASP1* was investigated by RT-PCR in cDNA from a range of human tissues. *HTRA1*-specific transcripts were detected in cDNA derived from retina, brain, adipose, liver, thymus and skeletal muscle. *CFD*-specific transcripts were detected in all the tissues screened, with variations in expression level observed. *MASP1* transcripts, encoding an enzyme able to activate murine proCFD, were detected only in the liver. *GAPDH* was used as a control, and was found to be expressed across all tissues screened.

5.7.2 RPE1 cells

The human RPE cell line hTERT-RPE1 (RPE1) was used to investigate the expression of *HTRA1,* and other genes, in a cell line of physiological relevance to AMD. *HTRA1* transcripts were found to be constitutively expressed by RPE1 cells (Figure 5.29), in agreement with previous reports of HTRA1 expression in primary RPE cells derived from human eyes (Yang et al. 2006; An et al. 2010). Expression of *CFD* was not detected in RPE1 cells in the absence of cellular stress.

5.7.2.1 Stress conditions for RPE1 cells

In TAP experiments performed in RPE1 cells (Chapter 3, Section 3.3), CFD was not identified as an interactor of a tagged form of HTRA1. Following the observation that *HTRA1* is expressed by RPE1 cells, the concomitant expression of the interactor *CFD* was investigated. As shown in Figure 5.29, there was no *CFD*-specific transcript detected in RPE1 cDNA under normal culture conditions. Similarly, no CFD was detected by ELISA in the conditioned media from RPE1 cells (Figure 5.30).

The pathological processes underlying AMD are thought to involve dysregulation of the retinal pigment epithelium in response to a variety of triggers. In order to investigate whether stressed RPE1 exhibit an altered expression profile for *CFD*, RPE1 cells were treated with H_2O_2 to induce oxidative stress, or with lipopolysaccharide to mimic bacterial infection.

5.7.2.1.1 Hydrogen peroxide treatment

Hydrogen peroxide-treatment of cells is used to assess susceptibility to, and the response to oxidative stress (Cho et al. 2011). Oxidative stress is proposed to play a role in the degeneration of the retinal pigment epithelial cells in AMD, leading to cellular dysfunction and death, resulting in death of photoreceptor cells. The cytotoxic effects of a range of H_2O_2 concentrations (250-2,000 µM) upon RPE1 cells in culture was assessed in a 96-well plate format by monitoring the reduction of the yellow tetrazole MTT (3-(4,5-Dimethylthiazol-2-yl)-2,5-diphenyltetrazolium

bromide) to the purple formozan product. This provides an indication of cell viability as a reflection of reductase activity.

After 24 hours of treatment with 250 µM H_2O_2, cell viability was equivalent to that of untreated cells (Figure 5.28A). At higher concentrations of H_2O_2, decreased cellular metabolic activity as a consequence of increased cell death was observed. 250 µM H_2O_2 was used in subsequent experiments to investigate the non-cytotoxic effects of oxidative stress on RPE1 cells.

5.7.2.1.2 Lipopolysaccharide (LPS) treatment

LPS is a constituent of the cell wall of Gram-negative bacteria, and is an endotoxin commonly used to induce an immune response in experimental models (Cho et al. 2011). Bacterial infection may contribute to the chronic inflammatory state observed in the AMD eye (Ishida et al. 2003; Kalayoglu et al. 2003; Robman et al. 2005). A dose-response curve of LPS (1.25-80 µg/ml) was performed to determine an appropriate concentration for induction of an immune response without causing death of RPE1 cells. In the range of LPS concentrations tested, cytotoxicity was minimal (Figure 5.28B). A concentration of 10 µg/ml was selected for use in subsequent experiments to induce complement activation.

5.7.2.1.3 Constitutive expression of *HTRA1* and induction of *CFD*

RPE1 cells were cultured under standard conditions in a 6-well dish until confluency was achieved. Serum-free media was added to the cells, containing either 10 µg/ml LPS, 250 µM H_2O_2 or with no supplementation in the case of the untreated cells. Following treatment for 24 hours, the cells were harvested and RNA purified. RPE1 cDNA was synthesised by reverse transcription using random hexamer primers.

50 ng of cDNA was used as the template for amplification of transcripts specific to *HTRA1*, *GAPDH* and *C3*. 250 ng of cDNA was used for the template for amplification of the *CFD* transcript. *GAPDH* is constitutively expressed by RPE1 cells (Figure 5.29). Similarly, *HTRA1* and *C3* transcripts were detected in RPE1 cDNA regardless of treatment with LPS or H_2O_2. A transcript specific to *CFD* was detected only weakly using 50 ng of cDNA as template (data not shown). However,

when 250 ng of cDNA was used as the template for amplification, it became apparent that expression of the *CFD* transcript is not constitutive in RPE1 cells, but is induced by both oxidative stress and by treatment with LPS (Figure 5.29). Constitutive expression of *C3* - the central component of the alternative complement pathway, by RPE1 cells - suggests that expression of *CFD* may be rate-limiting in alternative complement pathway activity in this cellular environment.

Conditioned media from the untreated and treated RPE1 cells was analysed using an ELISA specific for CFD. Figure 5.30 shows that CFD is detected at low levels in the media following treatment with LPS (2.08±0.79 (SD) pg/ml) or with H_2O_2 (3.09±1.59 (SD) pg/ml, but is not detected when the cells have not been treated to induce a stress-response.

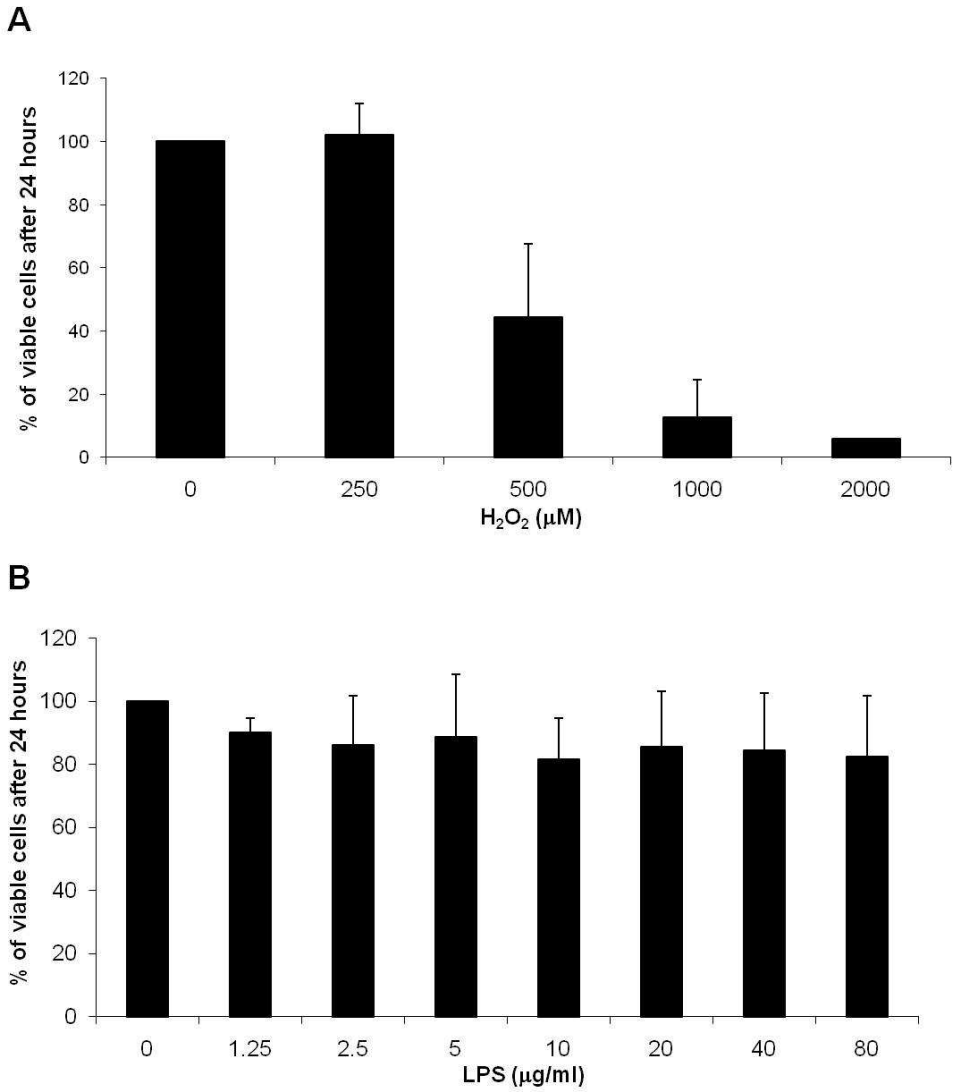

Figure 5.28 Optimisation of stress conditions for RPE1 cells.

A. Cell viability assay for RPE1 cells treated with H_2O_2 (250-2,000 µM). 250 µM H_2O_2 in the cell culture media did not cause a significant decrease of cell viability. Data are expressed as mean cell viability assessed by the MTT assay in three independent experiments (± SD), relative to the untreated control cells.

B. Cell viability assay for RPE1 cells treated with LPS (1.25-80 µg/ml). Concentrations in the media of 1.25 to 80 µg/ml of LPS did not cause a significant decrease of cell viability, assessed by the MTT assay in three independent experiments (± SD), relative to the untreated control cells.

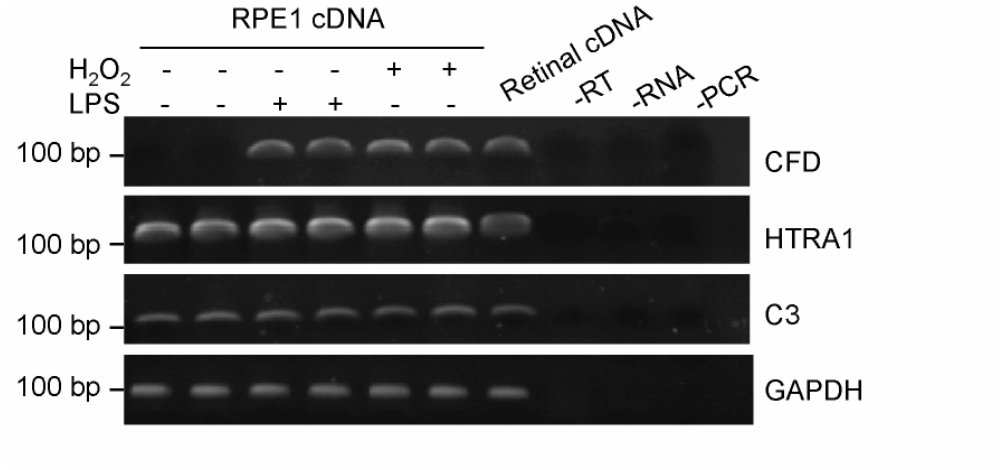

Figure 5.29 Expression of HTRA1, CFD and C3 in RPE1 cells.
HTRA1 transcripts were endogenously expressed in RPE1 cells. *CFD* was induced following treatment with LPS (to mimic bacterial infection) or H_2O_2 (to mimic oxidative stress). *C3* was detected in untreated RPE1 cells, suggesting that CFD is rate-limiting in activation of the alternative complement pathway in the local environment of the RPE. Retinal cDNA was included as a positive control. *GAPDH* was used as a control, and was found to be expressed under all conditions screened.

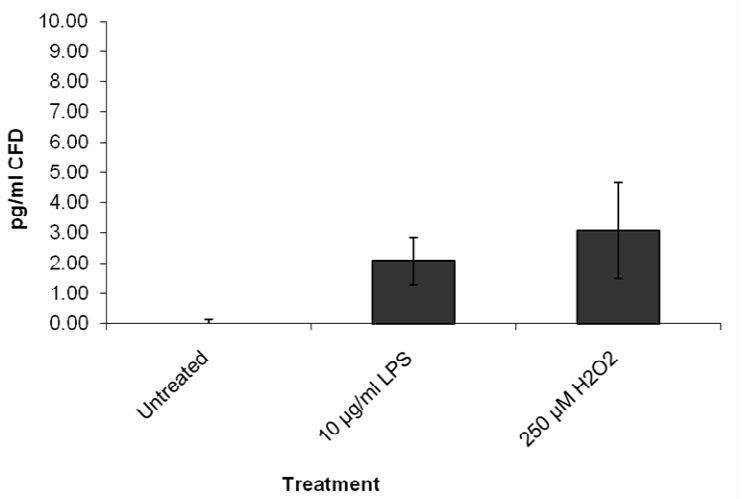

Figure 5.30 CFD is detected by ELISA in conditioned media from RPE1 cells treated with LPS or H_2O_2.
CFD is not detected in conditioned media from untreated RPE1 cells using a CFD-specific ELISA. Following treatment with LPS or with H_2O_2, CFD is detected at low levels in the conditioned media, suggesting that CFD is induced in response to stress.

5.7.3 THP-1 cells

The physiological relevance of the HTRA1-CFD interaction was also investigated by analysis of co-expression of the genes encoding HTRA1 (*HTRA1*) and CFD (*CFD*) in THP-1 cells. These are monocyte-like cells that can be induced by phorbol myristate acetate (PMA) to differentiate into macrophage-like cells. Figure 5.31 shows the morphological changes observed in THP-1 cells following treatment with PMA, when the cells differentiate and become adherent rather than growing in suspension.

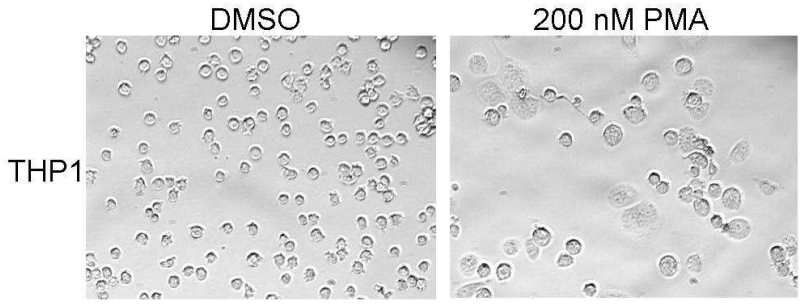

Figure 5.31 Morphological changes of THP-1 cells treated with PMA. THP-1 cells are a Human acute monocytic leukaemia cell line, which can be differentiated to a macrophage-like cell by treatment with 200 nM phorbol myristate acetate (PMA). The monocyte-like cells grow in suspension and are characterised by large, round, single cells. DMSO alone did not induce differentiation of these cells. 200 nM PMA, resuspended in DMSO, induces differentiation to a macrophage-like cell. Morphological changes can be observed, including increased adherence of cells to the cell culture plate, and an increase in cytoplasmic volume.

In THP-1 cells, *CFD* transcripts were highly expressed in both monocyte and macrophage-like cells (Figure 5.32A), whilst *HTRA1* mRNA was only detected following differentiation into macrophage-like cells (Figure 5.32A). Conditioned media from monocyte and macrophage-like cells containing 20 µg of protein was subjected to immunoblotting to detect CFD and HTRA1. CFD was highly expressed at the protein level in both undifferentiated and differentiated THP-1 cells (Figure 5.32B). HTRA1 was detected in the conditioned media from the differentiated macrophage-like THP-1 cells (Figure 5.32B). This is in agreement with the observation that HTRA1 transcripts were detected only in differentiated macrophage-like cells (Figure 5.32A).

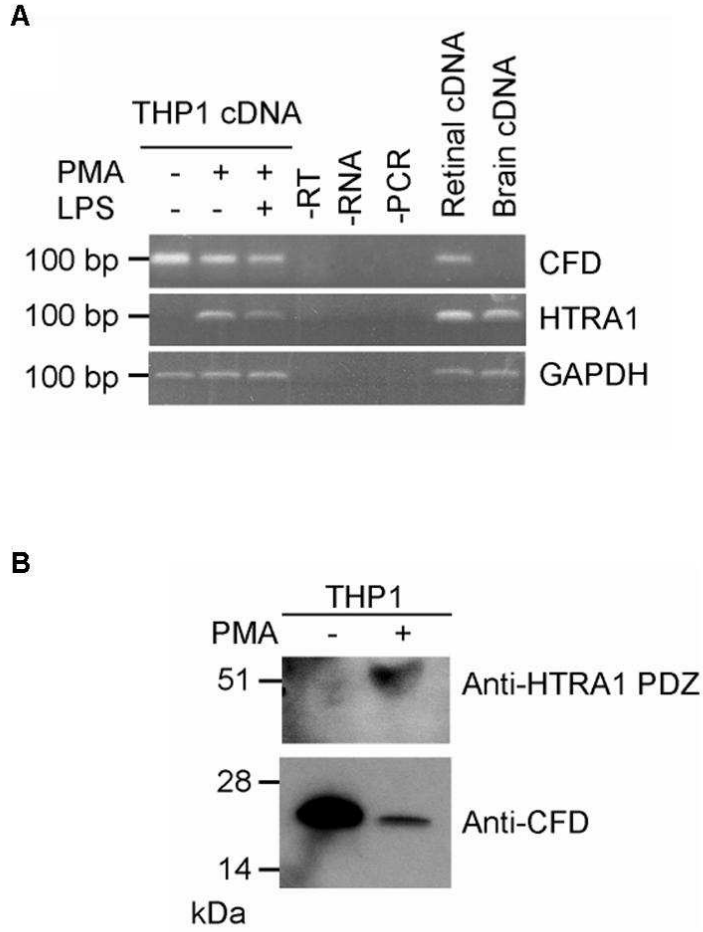

Figure 5.32 Co-expression of *HTRA1* and *CFD* in THP-1 cells.

A. *CFD* transcripts were detected by RT-PCR in cDNA from both the monocyte and macrophage-like cells which are induced to differentiate by treatment with PMA in the macrophage-like cell-line THP-1. *HTRA1* mRNA was detected only in the macrophage-like cells following treatment with PMA. Human retinal and brain cDNA were used as controls. *GAPDH* transcripts were amplified as a control.

B. The macrophage-like cell-line THP-1 was found to express high levels of CFD protein in both monocyte and macrophage-like cells. In agreement with the RT-PCR data in (A), HTRA1 protein was detected only in the macrophage-like cells following treatment with PMA.

5.8 Discussion

This chapter describes the validation and characterisation of a putative interaction between HTRA1 and CFD that was identified in a yeast two-hybrid screen. A novel function for HTRA1 was discovered – the ability to cleave the activation peptide of CFD to generate the active zymogen of the central component of the alternative complement pathway. CFD is expressed as a prepropeptide, from which a signal peptide and five amino acid activation peptide are sequentially cleaved (Volanakis and Narayana 1996). The minimal binding sequence identified by sequence alignment of the CFD prey sequences with the CFD reference sequence indicates that the interaction occurs at the N-terminus of the CFD zymogen, overlapping the activation peptide (Figure 5.2). HTRA1 is a trypsin-like serine protease, and proCFD can be activated by several such serine proteases (Fearon et al. 1974; Yamauchi et al. 1994) although the enzyme(s) responsible for physiological activation in humans remain unknown. This led to speculation that HTRA1 may be able to activate proCFD to generate mature CFD, which is known to be the rate-limiting component of the alternative complement pathway (Lesavre and Müller-Eberhard 1978; Volanakis and Narayana 1996).

Using *in vitro* assays, the interaction between HTRA1 and CFD was confirmed and localised to the C-terminal portion of HTRA1, spanning the protease domain and the PDZ domain (Figure 5.5). Although a synthetic peptide encompassing the minimal region of CFD was a substrate for HTRA1, there was no cleavage of mature CFD purified from human plasma by HTRA1 (Figure 5.6). However, recombinant proCFD (27 kDa) was susceptible to cleavage, giving rise to a cleavage product of the expected molecular weight of CFD (24kDa; Figure 5.10A and C). This suggests a requirement for the propeptide sequence of CFD for HTRA1 to cleave CFD.

This was investigated further using a synthetic fluorescently labelled activation peptide (PPRGR-MCA), which was specifically cleaved by HTRA1 to release free AMC. This site of cleavage corresponds to the position at which the activation peptide is removed from the mature CFD zymogen *in vivo*. This shows that the propeptide of CFD is both necessary and sufficient for HTRA1-mediated cleavage. PPRGR-MCA was also cleaved by thrombin, as has previously been

shown by Takahashi et al. (2010) in their analysis of CFD activation in the *Masp1*$^{-/-}$ mouse. However, there was a striking difference in the kinetics of the cleavage of PPRGR-MCA by thrombin and HTRA1 (Figure 5.16). HTRA1 had a slower rate of reaction, as indicated by the V_{max} of 19.88 nanomoles AMC/hour/mg of active protease. HTRA1 acts as a trimeric, cage-forming protease, and the minimal peptide length to effectively bridge the active site is 10 amino acid residues (Truebestein et al. 2011). This, together with the observations that some members of this family of proteases require substrate binding to the PDZ domain to induce remodelling of the active site and that the bacterial homologue DegP creates very few cleavage products of 5 residues (Murwantoko et al. 2004; Krojer et al. 2008) indicate that PPRGR-MCA is a far from optimal substrate for HTRA1. This may account for the slow rate of reaction. However, whilst thrombin activity with the synthetic peptide ceased after one hour, HTRA1 continued to cleave the synthetic substrate for 96 hours (the duration of the experiment). It is not clear why thrombin activity reaches a plateau while HTRA1 processively cleaves the substrate over 96 hours, as the substrate is not a limiting factor. Whilst the synthetic activation peptide utilised in this study is not an optimal substrate, there is clear evidence that HTRA1 is able to cleave the synthetic activation peptide of CFD specifically.

The alternative complement pathway is one of three branches of the innate immune response, and kills invading microorganisms by disrupting cell membranes. The alternative complement pathway is triggered by the spontaneous hydrolysis of C3 to C3a and C3b. When C3b binds to a “foreign” tissue surface, a conformational change allows formation of C3bB by binding Factor B. In the presence of Mg^{+2} ions, C3-bound factor B is cleaved to Ba and Bb by activated CFD to form C3bBb, the C3-convertase. Upon formation of the convertase, there is a downstream cascade of complement activation leading to the formation of the membrane attack complex and lysis of invading pathogens. CFD-catalysed cleavage of Factor B is the key activating step in this pathway, and is regarded as being rate limiting due to serum concentrations of CFD that are about nine-fold lower than C3 or factor B (Barnum et al. 1984).

Takahashi et al. (2010) report that MASP1 is responsible for the activation of proCFD in mice, but the enzyme responsible for the activation of CFD in humans has

not been described. The functional consequence of HTRA1-mediated cleavage upon proCFD was assessed in a variety of *in vitro* assays of alternative complement activity. In agreement with the proposed removal of the activation peptide, the HTRA1-treated proCFD was active in all assays of complement activity. A C3 convertase formed with Cobra Venom Factor, purified human Factor B and proCFD which had been pre-treated with HTRA1, had equivalent activity to that observed with an equal quantity of active CFD purified from plasma (Fig. 5.20). This confirms that recombinant proCFD can be activated by HTRA1 to generate a mature CFD protease. Further evidence was obtained by restoration of normal levels of alternative complement pathway activity to CFD-depleted serum, both by the specific cleavage of endogenous Factor B to Bb in human serum and in a haemolysis assay (Fig. 5.24 and 5.26).

Haemolysis assays were also used to test the alternative complement activity in sera from CARASIL patients. CARASIL is caused by homozygous mutations in *HTRA1*, which appear to either result in almost total absence of the protein due to nonsense-mediated decay, or to a severe reduction in the protease-activity of the enzyme (Hara et al. 2009). This causes uncontrolled activation of TGF-β signalling and results in cerebral small vessel disease in early adulthood. A deficiency in alternative complement pathway activity has not been described for these patients. However, sera from three CARASIL patients showed a dramatic reduction (ranging from 15-53%, Figure 5.26) in the reactive lysis of sheep RBCs, relative to ethnically-matched disease-free control sera. Due to the mutations in *HTRA1*, sera from CARASIL patients are naturally deficient (although not entirely lacking) in the active HTRA1 enzyme. The reduction in alternative complement pathway activity in these patients is strong evidence for HTRA1 having a role in the activation of this pathway.

As a result of the identification of a major susceptibility factor in *CFH*, which is known to modulate complement activation by inhibiting the formation of the C3-convertase and dampening the inflammatory response, inflammation is considered to play an important role in the degeneration of the macula and in AMD pathogenesis (Edwards et al. 2005; Haines et al. 2005; Klein et al. 2005). Several other components of the complement pathway, including C3, CFB and CFI have been

implicated in AMD, providing further evidence for the damage caused by aberrant regulation of inflammatory processes in the eye (Gold et al. 2006; Yates et al. 2007; Fagerness et al. 2009). As the rate-limiting component in the activation of the alternative complement pathway, any alterations in activation of CFD may result in an increase in alternative complement activity and consequent inflammation (depending on the amount of C3 and factor B deposited on tissue surfaces, and the complement regulators present). In agreement with the elevated plasma CFD concentrations in AMD cases compared to controls described in Chapter 4, several groups have reported elevated levels of plasma CFD and downstream activation products in AMD cases compared to controls (Scholl et al. 2008; Reynolds et al. 2009; Hecker et al. 2010). It is not clear whether this represents a systemic increase in complement activity, spill-over from the AMD eye or both.

Others have suggested a link between HTRA1 over-expression and regulation of the complement pathway based on its effects on other complement regulators (clusterin, vitronectin, fibromodulin), or upon inflammation (An et al. 2010; Yasuma et al. 2010). This is the first evidence however that HTRA1 can directly activate the central component of the alternative complement pathway by cleaving the activation peptide from proCFD.

Takahashi et al. (2010) proposed a role for mannose-binding lectin-associated serine protease-1 (*Masp1*), a component of the lectin pathway, in activation of proCFD to mature CFD in serum in mice. However, *Masp1* is not expressed in adipose tissue in mice (Takahashi et al. 2010), the major source of CFD in the circulation (White et al. 1992). Most of the CFD circulating in human plasma consists of mature CFD, although a small amount of proCFD can be detected (Fearon et al. 1974). Cleavage of proCFD in humans is therefore thought to occur during maturation and secretion of the protein (Kim et al. 1994; Yamauchi et al. 1994), rather than after secretion as proposed for Masp1 in the mouse (Takahashi et al. 2010). The co-expression of *HTRA1* with *CFD* was investigated to assess whether the enzymes were likely to be present in the same tissues. Expression data from a panel of human tissues, including blood, adipose tissue and the eye, suggest that HTRA1 is a strong candidate for the activation of proCFD, as there is substantial overlap in the expression of the two genes (Figure 5.27). Expression of *CFD* in

adipose tissue was high, which may contribute to the correlation between obesity and systemic inflammation as a result of adipose-expressed pro-inflammatory adipokines (Hotamisligil et al. 1995; Yudkin et al. 1999; Weyer et al. 2002). Obesity is also associated with an increased risk of developing AMD (Seddon et al. 2003a). HTRA1 expression was detected in adipose tissue cDNA. However, in agreement with the expression data from Takahashi et al. (2010) of *Masp1* in mouse adipose tissue, *MASP1* transcripts were not detected in adipose tissue (or indeed, any tissue except the liver which is a minor producer of CFD in humans (Morgan and Gasque, 1997, Figure 5.27). MASP1 synthesised by the liver is likely to be the major source of MASP1 measured in human serum (1-12 µg/ml), where active MASP1 is rapidly neutralised by C1 esterase inhibitor (Terai et al. 1997; Matsushita et al. 2000).

There is co-expression of *HTRA1* and *CFD* in the human cell-lines hTERT-RPE1 and THP-1 macrophages (Figure 5.29, 5.32). These are cell-lines with physiological relevance to AMD, given the role of RPE cells and macrophages in the disease. Interestingly, expression of *CFD* was only detected in RPE1 cells following the application of cellular stress, either with LPS to mimic bacterial infection, or with H_2O_2, to mimic oxidative stress (Figure 5.29, 5.30). RPE cell dysfunction is considered a key factor in the development of AMD, leading to the loss of photoreceptor function. Both oxidative stress (for example, caused by cigarette smoking (Fujihara et al. 2008)) and infection with *C. pneumoneiae* have been suggested as triggers for RPE cell degeneration (Ishida et al. 2003; Kalayoglu et al. 2003; Robman et al. 2005). Constitutive expression of *C3* in RPE1 cells suggests that, as in plasma where the concentration of CFD is nine-fold lower than of other complement components (Lesavre and Müller-Eberhard 1978), CFD may be limiting in order to prevent activation of the alternative complement pathway under normal cellular conditions. This is in agreement with low expression levels of *CFD* in RPE cells and the choroid, relative to other complement components (Anderson et al. 2010).

Tight regulation of inflammatory processes is important in delicate tissues such as the eye to avoid tissue damage. The contribution of the alternative complement pathway to tissue damage as a consequence of cellular stress was recently explored by microarray analysis of the *Cfd*$^{-/-}$ mouse retina when subjected to

light-induced damage (Rohrer et al. 2007). *Cfd*$^{-/-}$ mice are protected from degeneration of the photoreceptors compared to wild-type mice, implicating the complement pathway activity that results from activation of CFD in AMD pathogenesis. Interestingly, *Htra1* (also known as protease, serine, 11 (Igf binding)), a stress-responsive protein (Clausen et al. 2002), is significantly upregulated in the microarray analysis of the *Cfd*$^{-/-}$ mouse retina when subjected to light-induced damage (Rohrer et al. 2007). Oxidative stress, induced in cell cultures of ARPE-19 cells by H_2O_2, has also been shown to contribute to RPE cell injury mediated by the complement pathway (Thurman et al. 2009).

Inflammation as a consequence of activation of the alternative complement pathway is clearly involved in the pathobiology of AMD. However, the cellular events which lead to activation of complement are not fully understood. In addition to the contribution of RPE cells, a role for circulating monocytes and infiltrating macrophages has been proposed. This is based on the identification of macrophages associated with drusen and with CNV membranes in AMD eyes (Killingsworth et al. 1990; Lopez 1991; Penfold et al. 2001; Grossniklaus et al. 2002). Although the accumulation of macrophages in AMD lesions may be a contributory factor to the development of AMD, the dynamic nature of macrophage recruitment makes studying their contribution to pathology in humans difficult. Studies in animal models have shown that depletion of macrophages can diminish severity of CNV in laser-induced models (Espinosa-Heidmann et al. 2003; Sakurai et al. 2003). This may be due to a reduction in VEGF, which is secreted by macrophages. Conflicting data from (Apte et al. 2006) found that increased recruitment of macrophages inhibits laser induced CNV in IL-10 deficient mice. It seems likely that macrophages have multiple roles in the eye; some are anti-inflammatory and are recruited to clear drusen, whilst others are pro-inflammatory and contribute to chronic and damaging inflammation.

Macrophages are a source of CFD in humans (but not in mice; White et al. (1992)). In agreement with this, the human monocytic cell-line THP-1 expresses high levels of *CFD* at both the mRNA and protein level (Figure 5.31A and B) in both monocyte and differentiated macrophage-like cells. Interestingly, expression of *HTRA1* was not detected in the monocytes, but there was a significant up-regulation

of both *HTRA1* mRNA and protein following treatment with PMA. If HTRA1 is indeed able to activate proCFD *in vivo*, this is consistent with activated macrophages having a pro-inflammatory role, and contributing to activation of the alternative complement pathway, in AMD pathology.

HTRA1 and *CFD* are likely to be expressed in the same cells, and more specifically, in cells with a known role in AMD pathogenesis, either endogenously or in response to stress. Co-expression of *HTRA1* and *CFD* in adipose tissue, as well as in cell lines with physiological relevance to AMD, makes the *in vivo* activation of CFD by HTRA1 an exciting possibility to explore in the future. Certainly, the reduced level of alternative complement pathway activity in the sera from CARASIL patients supports a role for HTRA1 in activating proCFD *in vivo*. Activation of proCFD by HTRA1 may contribute to both systemic and local activation of the alternative complement pathway. Although work remains to determine the physiological relevance of this interaction, there is a link between activation of the alternative complement pathway and one of the major genetic-risk factors for AMD.

6: Chapter 6

Systemic and local levels of HTRA1

6.1 Introduction

An AMD-risk haplotype on chromosomal region 10q26, comprising the strongly associated indel in the 3' UTR of *ARMS2* and the minor alleles of the SNPs rs10490924 (T) in *ARMS2*, and rs11200638 (A), a putative *HTRA1* promoter polymorphism has been reported (Fritsche et al. 2008). Given the intractable nature of identifying the variants responsible for increased risk at this locus because of strong LD, recent studies have investigated the expression of *ARMS2* and *HTRA1*. The effect of the risk haplotype upon expression of the two proteins has been controversial. There is evidence that loss of ARMS2 is necessary, but not sufficient, for disease (Yang et al. 2010). *HTRA1* appears to be upregulated in carriers of the risk haplotype in some studies (Dewan et al. 2006; Yang et al. 2006; Chan et al. 2007; Yang et al. 2010) but not all (Kanda et al. 2007; Chowers et al. 2008; Kanda et al. 2010; Wang et al. 2010a; Wang et al. 2010b). These studies have been localised to specific tissues, such as the RPE (Yang et al. 2006), the retina (Kanda et al. 2007; Kanda et al. 2010; Wang et al. 2010b), placenta (Kanda et al. 2010) and blood (Yang et al. 2006; Chowers et al. 2008), and have failed to replicate consistently. Thus, it remains unclear whether the risk haplotype, or indeed a single variant on the risk haplotype, is linked to alterations in the expression of either gene.

The systemic concentration of HTRA1 in plasma has not been reported, but may reflect small changes at the local level. This chapter describes the development and optimisation of an enzyme-linked immunosorbent assay (ELISA) for measuring HTRA1 in plasma. The aim was to determine whether the risk haplotype was associated with a difference in plasma HTRA1.

The effect of covariates that are known to influence susceptibility to AMD upon plasma HTRA1 was also assessed (Klein et al. 2004). Body mass index (BMI) was identified as a significant covariate for plasma HTRA1. High BMI has been associated with increased risk of developing AMD (Seddon et al. 2003b). The contribution of BMI and genotype at the chromosome 10q26 locus to the expression of *HTRA1* was also investigated in a small number of adipose tissue biopsies.

6.2 Optimisation of an ELISA to measure the systemic levels of HTRA1 in plasma

The expression level of *HTRA1* in specific tissues or cell lines has previously been associated with risk genotype at the chromosome 10q26 locus, although this remains controversial. In order to investigate the systemic level of HTRA1 in relation to risk genotype at this locus, plasma HTRA1 was measured in the UK2 AMD case-control cohort, genotyped for the rs10490924 SNP. Antibodies specific to HTRA1 were kindly provided by Dr Jeremy Chien (Rochester, Minnesota) for use in development of a sandwich ELISA to measure HTRA1 in human plasma samples.

6.2.1 Testing HTRA1 antibodies in an indirect ELISA

The antibodies that were used in the development of the optimised HTRA1 ELISA are shown in Table 6.1. Three antibodies were provided; one purified polyclonal antibody raised in rabbit (HTRA1**) and two monoclonal antibodies (MAb 4.1 and MAb 10) which were obtained as unpurified supernatants from murine hybridoma cell cultures. All were raised against a recombinant purified protein spanning amino acids 140-480 of human HTRA1. Precise epitopes are unknown.

The ability of the HTRA1 antibodies to specifically bind and detect a recombinant purified form of HTRA1 was initially tested by indirect ELISA. Figure 6.1 shows the standard curves obtained by indirect ELISA in the range of HTRA1 concentration from 0.312-5 ng/ml. As seen in Figure 6.1A, the polyclonal antibody HTRA1** (1 in 100 dilution) generates a linear standard curve (R^2= 0.9923). The monoclonal antibodies were tested as a 1:1 mixture, and also individually. Polynomial regressions fitted to the standard curves show that MAb 10 is able to detect HTRA1 in the range of 0.312-5 ng/ml (R^2=0.987; Figure 6.1C), but MAb 4.1 did not detect HTRA1 (Figure 6.1D). The mixture of monoclonal antibodies did detect HTRA1, but provided no greater sensitivity than using MAb 10 alone (Figure 6.1B).

Antibody Name	Clonality	Raised in	Purity	Performance in indirect ELISA	Performance in Western Blot	Optimised dilution for use in sandwich ELISA
HTRA1 **	Polyclonal	Rabbit	Purified IgG	Detects HTRA1	Detects HTRA1	1:100
HTRA1 MAb 10	Monoclonal	Mouse hybridoma cells	Unpurified supernatant	Detects HTRA1	Detects HTRA1	1:10
HTRA1 MAb 4.1	Monoclonal	Mouse hybridoma cells	Unpurified supernatant	Does not detect HTRA1	Not tested	N/A

Table 6.1 Antibodies tested for use in HTRA1 ELISA.

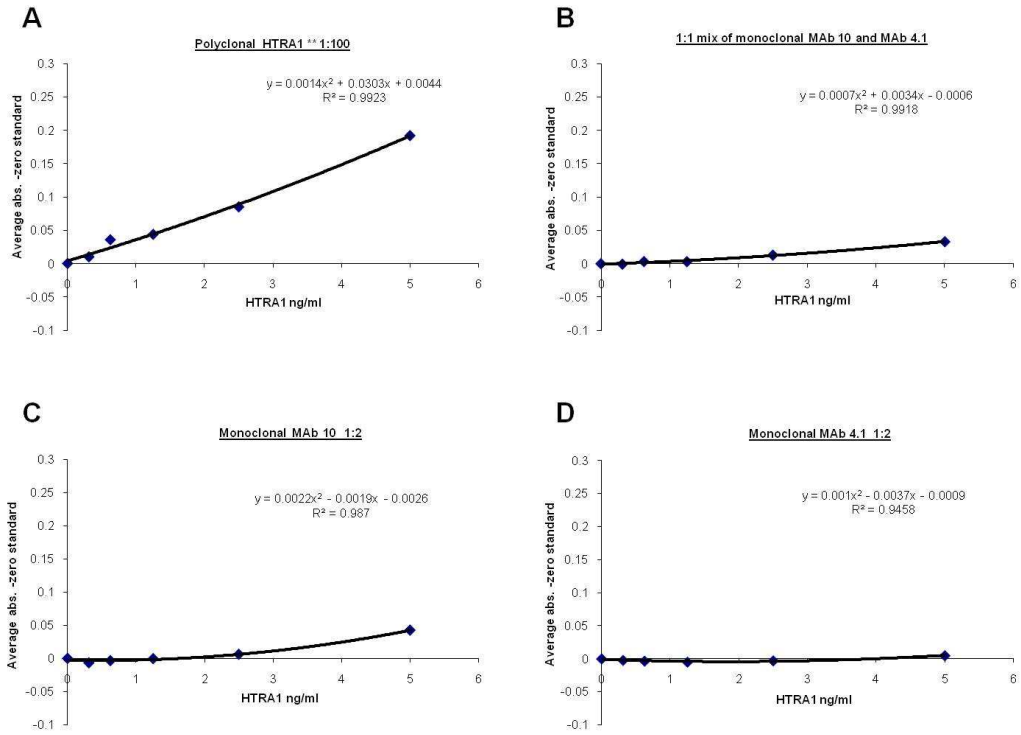

Figure 6.1 Testing the performance of anti-HTRA1 antibodies by indirect ELISA.

Three antibodies raised against unknown epitopes of recombinant human HTRA1 were tested in indirect ELISA for the ability to specifically bind and detect a recombinant purified form of HTRA1. The standard curves obtained by indirect ELISA in the range of HTRA1 concentration from 0.312-5 ng/ml are shown. The equation of the line-of-best fit was obtained by polynomial regression in Microsoft Excel. Goodness of fit was assessed using the squared correlation coefficient (R^2). **A**. The purified rabbit polyclonal antibody HTRA1** generates a linear standard curve (R^2= 0.9923). The monoclonal antibodies MAb10 and MAb 4.1 were tested as a 1:1 mixture (**B**), and also individually (**C** and **D** respectively). The mixture of monoclonal antibodies did detect HTRA1 (**B**). MAb 10 is able to detect HTRA1 in the range of 0.312 -5ng/ml (R^2=0.987; **C**), but MAb 4.1 did not detect HTRA1 (**D**).

6.2.2 Testing HTRA1 antibodies by Western blotting

The polyclonal antibody HTRA1** and the monoclonal antibody MAb 10 were able to detect purified recombinant HTRA1 in an indirect ELISA. These antibodies were used to assess the purity of the recombinant HTRA1 standard, GST ΔN HTRA1 S328A by Western blotting. The inactive mutant of HTRA1 was used for the standard to avoid degradation of the protease and antibodies by the active protease. Figure 6.2A shows a Coomassie-stained gel of 2 µg of the purified GST ΔN HTRA1 S328A. The recombinant protein has a predicted molecular weight of 64 kDa and is visualised as the major band at approximately 62 kDa in the Coomassie-stained gel. 1 µg of protein was immunoblotted with anti-HTRA1** (Figure 6.2B), anti-HTRA1 MAb10 (Figure 6.2C), or with anti-HTRA1-PDZ (Figure 6.2D). Anti-HTRA1 PDZ is the antibody used throughout this thesis to detect HTRA1 in Western blots, and is shown as a control.

Both HTRA1** (1:1,000 dilution) and MAb 10 (1:100 dilution) were able to detect the recombinant protein by Western blot. In agreement with the Coomassie-stained gel, the predominant HTRA1-immunoreactive band for each antibody is observed at approximately 64 kDa. Minor HTRA1-immunoreactive bands are observed at 51 kDa (also seen in the Coomassie-stained gel) and at approximately 130 kDa and 200 kDa. The higher molecular weight bands are thought to result from incomplete reduction of HTRA1 dimers and trimers. HTRA1 is thought to oligomerise via interactions at the C-terminus (Truebestein et al. 2011), thus only the monomer is detected by anti-HTRA1 PDZ, which recognises the PDZ domain of the protease.

Figure 6.2 also shows that no HTRA1-specific signal was observed in 5 µl of human plasma or serum by Western blotting. This may be due to the low abundance of HTRA1 in serum and plasma.

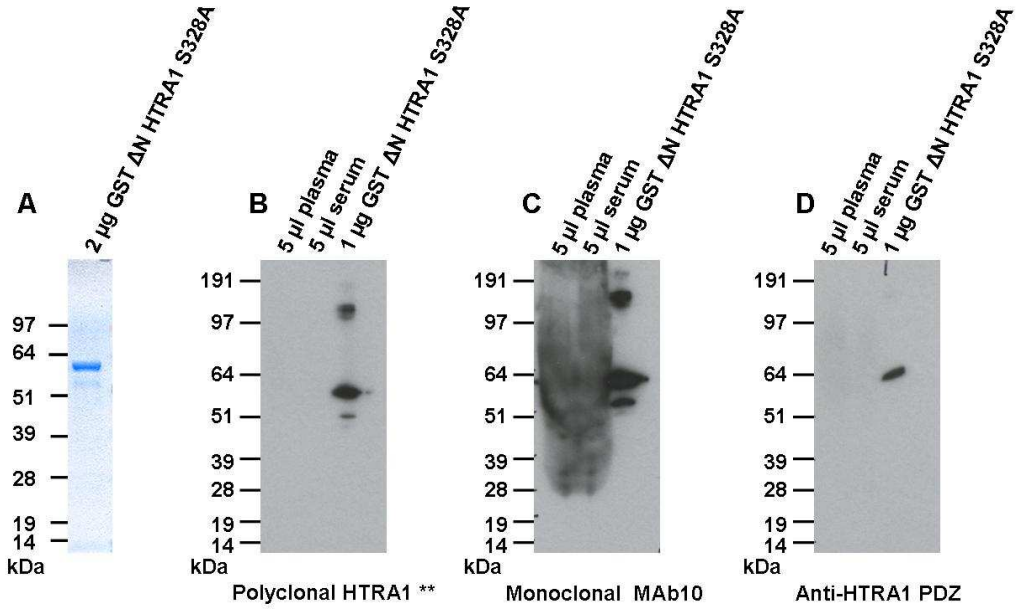

Figure 6.2 Testing anti-HTRA1 ELISA antibodies in Western blots.
A. A Coomassie-stained gel of 2 µg of the purified GST ΔN HTRA1 S328A (predicted molecular weight of 64 kDa). GST ΔN HTRA1 S328A, human plasma and human serum was separated by reducing SDS-PAGE and then immunoblotted with anti-HTRA1** (**B),** anti-HTRA1 MAb10 (**C**) or anti-HTRA1-PDZ (**D)** and appropriate secondary antibodies**.** Anti-HTRA1 PDZ is the antibody used throughout this thesis to detect HTRA1 in Western blots, and is shown as a control. The predominant HTRA1-immunoreactive band for each antibody is observed at approximately 64 kDa. Minor HTRA1-immunoreactive bands are observed at 51 kDa (also seen in the Coomassie-stained gel) and at approximately 130 kDa and 200 kDa in **B** and **C**. The higher molecular weight bands are thought to result from incomplete reduction of HTRA1 oligomers. None of the antibodies were able to detect HTRA1 in human plasma or serum.

6.2.3 Optimisation of the HTRA1 ELISA

A sandwich ELISA for HTRA1 was developed, modifying the suggested protocol provided by Dr Jeremy Chien. The polyclonal antibody HTRA1** was used as a capture antibody, and the monoclonal antibody MAb 10 was used as a detection antibody. The appropriate dilution of each antibody to detect HTRA1 in plasma was determined, along with the optimal dilution of anti-mouse IgG HRP-conjugate and a suitable plasma dilution. A schematic representation of the optimised assay is shown in Figure 6.3.

6.2.3.1 Capture Antibody HTRA1**

A dilution series of HTRA1** was used to capture a range of concentrations of GST ΔN HTRA1 S328A (0.78-50 ng/ml) by sandwich ELISA. The optimal dilution of HTRA1** is able to capture all of the HTRA1 present at the highest concentration of HTRA1. Figure 6.4 shows that a dilution of 1:100 of the antibody is sufficient to capture 50 ng/ml of the protein, without the antibody becoming saturated.

6.2.3.2 Detection Antibody MAb 10

The optimal dilution of the MAb 10 detection antibody for use in the sandwich ELISA was determined using a dilution series against a range of GST ΔN HTRA1 S328A (0.78-50ng/ml), captured with HTRA1**. Figure 6.5 shows that a 1:10 dilution of the murine hybridoma culture supernatant is sufficient to detect 50ng/ml HTRA1, without saturation of the detection antibody. In agreement with the results from the indirect ELISA to test the specificity of the antibodies, MAb 4.1 did not detect any HTRA1 captured by HTRA1** in a sandwich ELISA (Figure 6.5). A corresponding decrease in the sensitivity of detection was observed using a 1:1 mix of the monoclonal antibodies MAb10 and MAb 4.1.

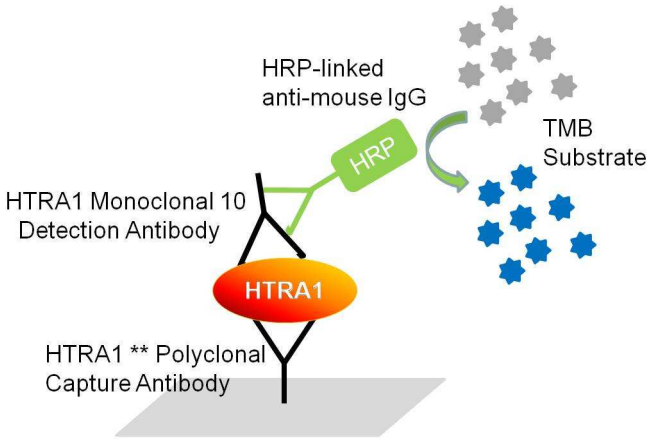

Figure 6.3 Schematic representation of the HTRA1 sandwich ELISA.
A polyclonal anti-HTRA1 antibody (HTRA1**) was used as the capture antibody, in combination with a monoclonal detection antibody (MAb10). Precise epitopes of the antibodies are unknown. The detection antibody was recognised by horse radish peroxidise (HRP)-conjugated anti mouse IgG. Absorbance at 450 nm was used to detect the HRP-mediated conversion of TMB substrate and allow quantitation of HTRA1 in EDTA-plasma.

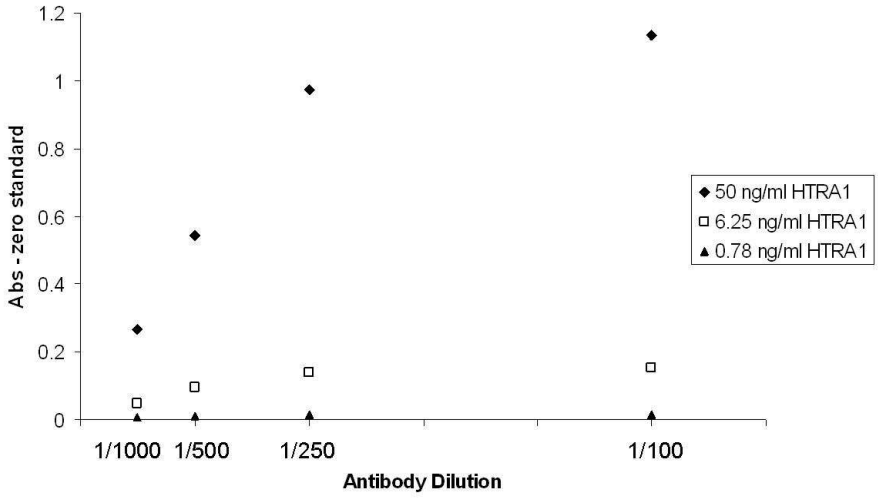

Figure 6.4 Optimisation of the polyclonal capture antibody.
The polyclonal antibody HTRA1** was tested for the ability to detect purified recombinant HTRA1 in the range expected in human plasma (<50 ng/ml). Fluorometric detection at 450 nm was used to measure HTRA1. Data points represent different concentrations of HTRA1, detected using HTRA1** diluted in the range of 1 in 100 to 1 in 1,000. The optimal dilution of HTRA1** was determined as 1 in 100, as this was not saturated at higher HTRA1 concentrations.

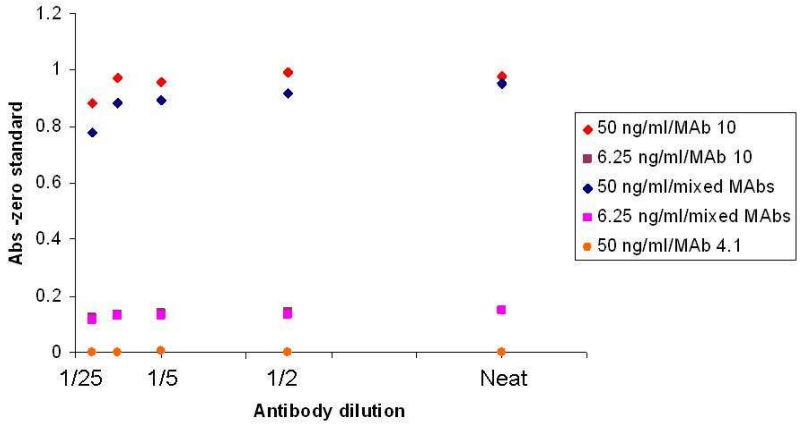

Figure 6.5 Optimisation of the monoclonal detection antibody.
Monoclonal antibodies MAb10 and MAb4.1 were obtained as hybridoma cell culture supernatants. The supernatants were tested (undiluted, or diluted in the range of 1 in 2 to 1 in 25) to detect recombinant purified HTRA1 in the range expected in human plasma (<50 ng/ml). Fluorometric detection at 450 nm was used to measure HTRA1. MAb 4.1 (orange) did not detect HTRA1. A 1:1 mixture of MAb4.1 and MAb10 (blue) was less sensitive at detecting HTRA1 than the equivalent dilution of MAb 10 only (red).

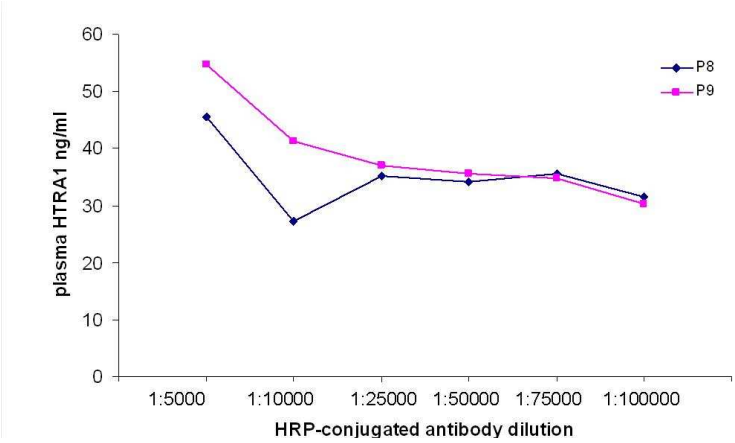

Figure 6.6 Optimisation of anti-mouse IgG HRP.
Rabbit anti-mouse IgG HRP was optimised for the purpose of detecting HTRA1 in human plasma by sandwich ELISA. A dilution series of HRP-conjugated antibody was used to detect binding of MAb10 to HTRA1 captured by HTRA1** in two internal control plasma samples, P8 and P9. Lower dilutions of IgG HRP-conjugate generated falsely high measurements of plasma HTRA1. High dilutions of IgG HRP were saturated by the secondary detection antibody. Dilutions in the range of 1:25,000 to 1:75,000 were considered optimal for the accurate detection of HTRA1 by sandwich ELISA.

6.2.3.3 Anti-mouse IgG HRP

The detection antibody in this sandwich ELISA is unlabelled, so acts as a primary detection antibody. A secondary detection antibody, specific to the primary detection antibody but not the capture antibody, is required to generate an output signal corresponding to the detection of HTRA1. In this assay, the output signal is the blue colour arising from the oxidation of tetramethylbenzidine (TMB) chromagen, catalysed by HRP in the presence of hydrogen peroxide.

Rabbit anti-mouse IgG HRP was optimised for the purpose of detecting HTRA1 in human plasma by sandwich ELISA. Two internal control plasma samples, P8 and P9, were diluted 1 in 10 and assayed for HTRA1 using the optimised antibody dilutions for capture and detection. A dilution series of HRP-conjugated antibody was used to detect binding of MAb10 to HTRA1 from plasma which had been captured by HTRA1** (Figure 6.6). Lower dilutions of IgG HRP-conjugate generated falsely high measurements of plasma HTRA1, as a result of non-specific binding of the secondary detection antibody. High dilutions of IgG HRP generated falsely low measurements of plasma HTRA1 as a result of saturation of the secondary detection antibody. Dilutions in the range of 1:25,000 to 1:75,000 were considered optimal for the accurate detection of HTRA1 by sandwich ELISA. 1:25,000 was selected for use in the assay to ensure that any high plasma HTRA1 levels encountered would not saturate the secondary detection antibody.

6.2.3.4 Inhibition of the sandwich ELISA in human plasma

The optimised antibody dilutions were used in a sandwich ELISA to detect HTRA1 in a dilution series of plasma samples, ranging from undiluted plasma to a 1 in 100 dilution. Neat plasma and low dilutions of plasma were found to inhibit the assay, decreasing the amount of HTRA1 measured in plasma (data not shown). To further investigate the plasma inhibition of the assay, an HTRA1 standard curve, ranging from 0.312 to 50 ng/ml of GST ΔN HTRA1 S328A was measured in either the standard dilution buffer (1% BSA/TBST) or diluted in plasma (P7), either 1:10 or 1:50 in 1% BSA/TBST. The standard curves for each dilution buffer are shown in Figure 6.7A, B and C. Inhibition of the assay was observed when recombinant

HTRA1 was diluted in a 1 in 10 dilution of plasma (Figure 6.7B). Direct comparison of the measured absorbance at 450 nm (minus background of the appropriate zero standard) is shown in Figure 6.7D. The ability of the assay to detect a known amount of HTRA1 in a 1 in 50 dilution of plasma was roughly equivalent to detection of the same amount of HTRA1 diluted in 1% BSA/TBST. In order to minimise the inhibition of the assay when measuring endogenous plasma HTRA1, plasma samples were subsequently diluted 1 in 50.

6.2.3.5 Analysis of intra-assay variation

The internal control plasma standards P8 and P9 were measured multiple times within the same assay, and measurements obtained were used to assess intra-assay variability for the optimised HTRA1 sandwich ELISA. Figure 6.8A shows the mean measurement of plasma HTRA1 obtained for each plasma sample (±s.e.m.) from at least 5 replicates. Coefficients of variation (CV) were around the 5% threshold, indicating that there was no significant difference between replicates.

6.2.3.6 Analysis of inter-assay variation

Internal control plasma standards P8 and P9 were used to assess inter-assay variation. The samples were measured multiple times in different assays, and measurements obtained were used to assess inter-assay variability for the HTRA1 sandwich ELISA as described in Section 2.5.3. Figure 6.8B shows the mean measurement of plasma HTRA1 obtained for two replicates of each plasma sample in a minimum of five assays (± s.e.m.), and indicates the coefficient of variation for each sample. There was minimal variation observed between assays (CV<10%). Previous work by Morad Ansari has shown that variation of this magnitude can be caused by pipetting error.

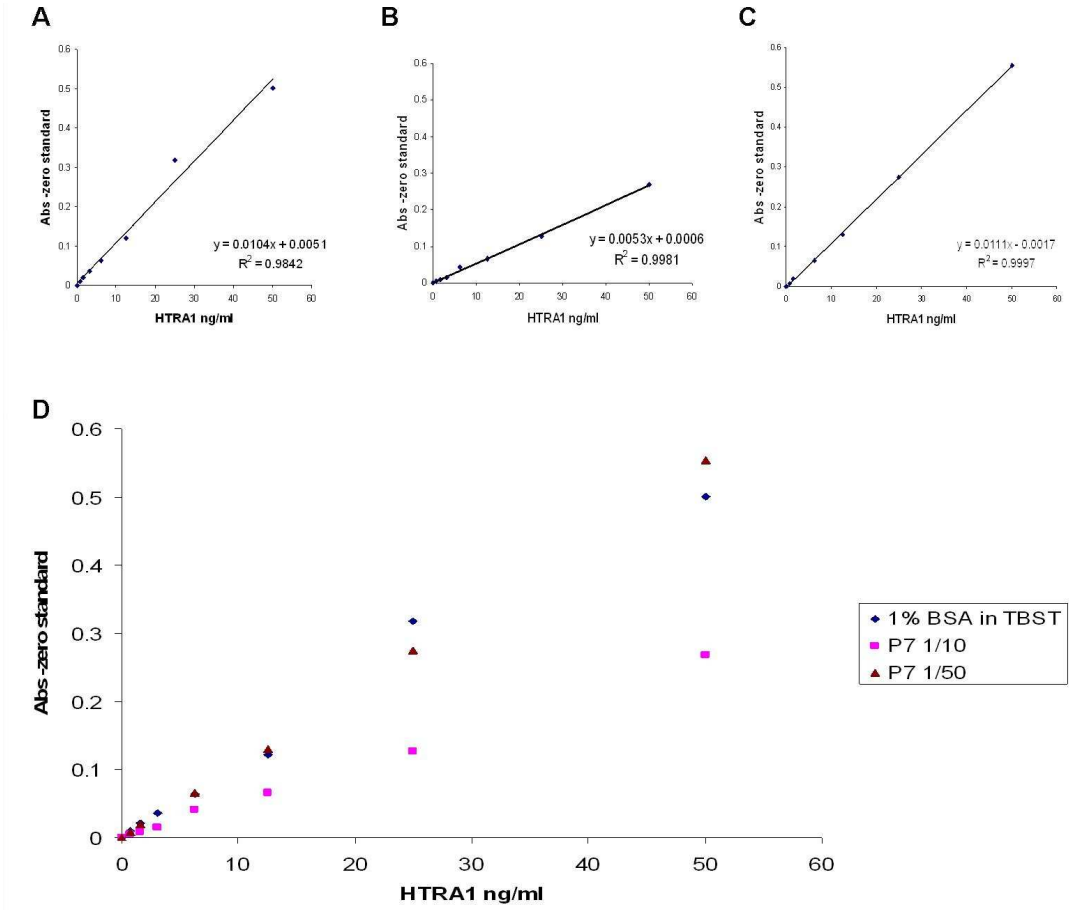

Figure 6.7 Optimisation of plasma dilution for the HTRA1 ELISA.
Inhibition of the ELISA was observed in plasma diluted 1 in 10.

A. An HTRA1 standard curve, ranging from 0.312 to 50 ng/ml of GST ΔN HTRA1 S328A was measured in the standard dilution buffer (1% BSA/TBST).
B. An HTRA1 standard curve, ranging from 0.312 to 50 ng/ml of GST ΔN HTRA1 S328A was measured in 1 in 10 in plasma (P7) in 1% BSA/TBST. Inhibition of the assay was apparent compared to (A).
C. An HTRA1 standard curve, ranging from 0.312 to 50 ng/ml of GST ΔN HTRA1 S328A was measured in 1 in 50 in plasma (P7) in 1% BSA/TBST.
D. Direct comparison of the measured absorbance at 450 nm (minus background of the appropriate zero standard) for each standard curve A-C. The performance of the assay is approximately equivalent in a 1 in 50 dilution of plasma and in 1% BSA/TBST.

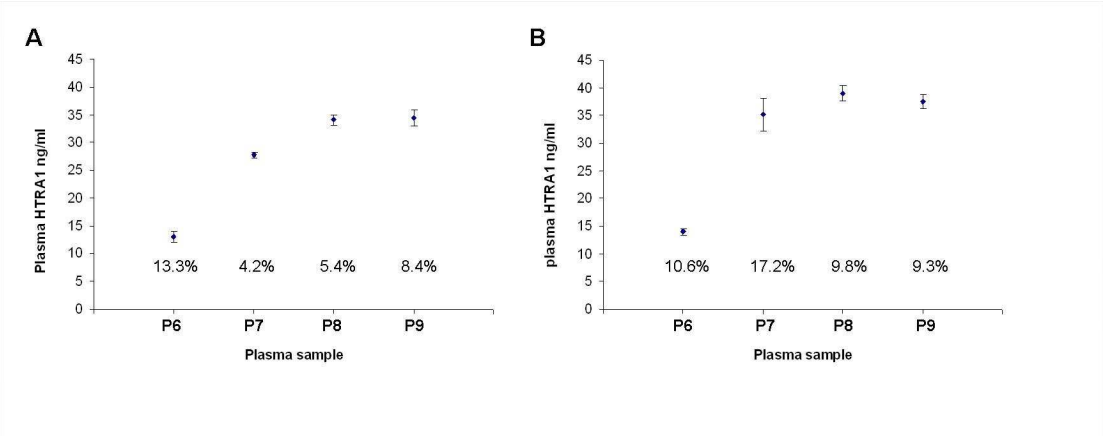

Figure 6.8 Intra- and Inter assay variability of the HTRA1 ELISA.
A. Intra-assay variation was measured within replicates of four human plasma samples P6. P7, P8 and P9. Each point represents at least five replicates ±s.e.m. Coefficients of variation (CV) are shown below each point.

B. Inter-assay variation was measured based on the mean of two or more replicates of four human plasma samples P6. P7, P8 and P9 from at least five different assays. Each point represents the mean of replicates ±s.e.m. Coefficients of variation (CV) are shown below each point.

6.3 Plasma HTRA1 measurements

In healthy human tissues, *HTRA1* is widely expressed, with strongest expression in the epidermis, liver and kidney tubules (De Luca et al. 2003). Systemic levels of HTRA1 in plasma are likely to result from spill-over from tissues. The effect of genotype at the chromosome10q26 haplotype on plasma levels of HTRA1, as a reflection of expression of *HTRA1*systemically, was investigated by measuring plasma HTRA1 in 769 individuals from a British AMD case-control cohort, UK2. 680 of these individuals were genotyped for rs10490924; missing genotypes were due to assay failure or missing DNA for these individuals. Table 6.2 shows the characteristics of the genotyped individuals. Measurements were carried out in duplicate. Mean values were corrected for inter-assay variation using two internal controls. In addition to the effect of genotype, the contribution of age, sex, smoking and body mass index (BMI) to plasma HTRA1 in this cohort was investigated.

Table 6.2 Demographic characteristics for the UK2 case-control series genotyped for rs10490924.

Demographic characteristics for the UK2 case-control series are shown according to rs10490924 genotypes. Statistically significant differences between GG and GT/TT groups were identified between mean age and % AMD. Exact test of Hardy–Weinberg equilibrium (number), *t-test* (mean age and mean BMI), exact test (gender, smoking history and % AMD) and median test (median HTRA1 (ng/ml)) were applied to calculate p-values. Abbreviations: SD, standard deviation; BMI, body mass index.

UK2 Case-Control Series				
Genotype	**Total**	**GG**	**GT/TT**	**p-value**
Number	680	284	396	<0.0001
Mean age (yrs)	78.0	77.6	79.0	
SD	7.9	7.9	7.5	0.013
Mean BMI	27.48	27.25	27.49	
SD	5.15	5.17	5.01	0.537
% Males	44.5	45.6	43.7	0.819
Smoking				
never	257	110	147	
former	374	158	216	
current	46	15	31	0.653
AMD (%)	59.5	42.0	72.1	2.92×10^{-14}
Median HTRA1 (ng/ml)	20.81	18.05	22.26	0.062

6.3.1 Analysis of plasma HTRA1 by genotype

The rs10490924 SNP encodes a serine to alanine change at position 69 of ARMS2, and is in high linkage diseqilibrium (r^2>0.88) with other variants on the risk haplotype, including an indel and a putative HTRA1 promoter polymorphism (Fritsche et al. 2008). Some, but not all, reports have suggested increased HTRA1 expression at the local level in individuals carrying risk alleles at the chromosome 10q26 locus (Yang et al 2010; Wang et al 2010, Fritsche et al 2008, Friedrich et al 2011, An et al 2010, Yang et al 2006, Chan et al 2007, Kanda et al 2007, Tuo et al 2008, Chowers et al 2008, Wang et al 2010b).

6.3.1.1 Confirmation of haplotype by PCR amplification of indel

Genotyping of these samples for rs10490924 had previously been performed by Susan Campbell using a TaqMan SNP genotype assay. PCR amplification of the indel-spanning region in the 3' UTR of *ARMS2* was used to confirm that rs10490924 genotype tagged the indel correctly in a subset of individuals (Figure 6.9). Consistent with previous reports of high LD (D' 0.99) between these variants (Wang et al. 2010b), the wild-type, non-risk, G allele of rs10490924 was always associated with a haplotype in which the indel was absent (band of 600 bp; Figure 6.9), whilst the risk allele (T) was associated with a haplotype in which the indel was present (band of 200 bp; Figure 6.9).

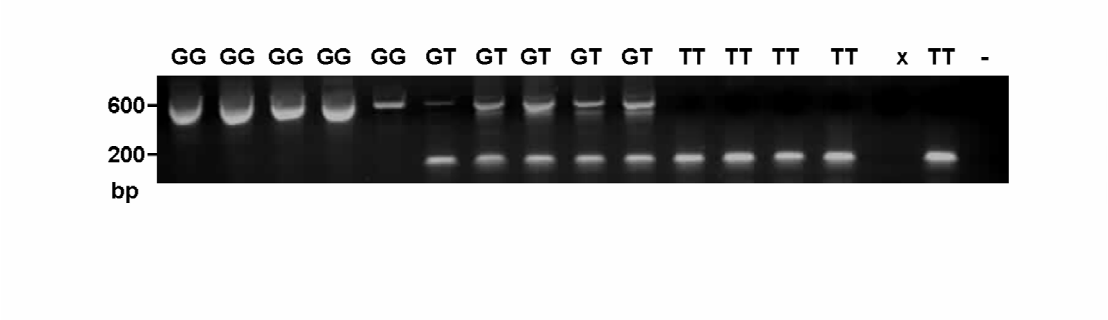

Figure 6.9 The *ARMS*2 3' UTR indel is linked to SNP genotype.
680 samples in the UK2 cohort were genotyped at SNP rs10490924. This SNP genotype was used to tag the AMD-risk haplotype covering SNP rs10490924 in *ARMS2*, 3' UTR indel in *ARMS2* and rs11200638 in *HTRA1* (Fritsche et al. 2008, Wang et al. 2010). To confirm the association of SNP genotype with the indel, the region spanning the indel was amplified by PCR. Expected PCR products are 598 bp for the wild-type allele and 209 bp for the indel allele. Five samples for each genotype of rs10490924 were amplified by PCR and subjected to gel electrophoresis. All GG samples show a single band at 600 bp, TT homozygotes show a single band at 200 bp and heterozygotes show two bands, representing the wild-type and risk allele of the indel.

6.3.1.2 Analysis of raw plasma HTRA1 by rs10490924 genotype

Plasma HTRA1 measured by ELISA was used to assess whether genotype was associated with alterations in plasma HTRA1. Due to the low frequency of minor allele homozygotes (12.4%), minor allele (T) homozygotes and heterozygotes were combined (n=396) for comparison with major allele (G) homozygotes (n=284).

The plasma HTRA1 measurements in the British case-control cohort showed a leptokurtic distribution. There was a significant deviation from normal, as indicated

by a skewedness factor of 5.93±0.088 (standard error of skewedness). Skewedness is a measure of departure from normality: normally distributed data has a value of zero. The positive or right-skewed nature of these data is mostly due to the wider range of plasma HTRA1 measured in GT/TT individuals. This is supported by the high kurtosis measure for GT/TT data (85.8±0.245 standard error of kurtosis) compared to samples with a GG genotype (4.27±0.288). Exclusion of extreme outliers (mean±3 SD; seven samples) reduced kurtosis but did not otherwise affect the subsequent analysis. Figure 6.10 shows the distribution of plasma HTRA1 measurements following exclusion of extreme outliers.

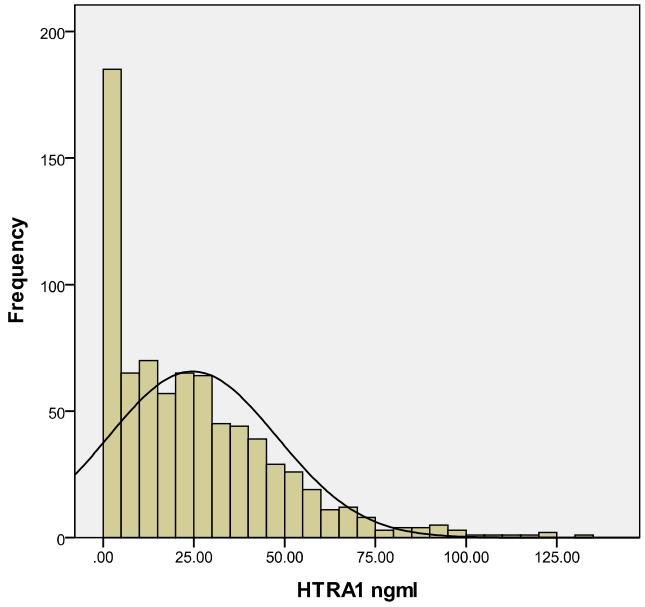

Figure 6.10 Distribution of plasma HTRA1 measurements.
The distribution of unadjusted plasma HTRA1 measurements (ng/ml) in the UK2 AMD case-control series, trimmed for extreme outliers (mean ±3 SD). These data show a deviation from normal, as indicated by a kurtosis value of 1.91 (S.E. 0.177) and skewedness value of 1.25 (S.E. 0.088).

To account for the deviation from normal distribution, non-parametric tests were used to investigate the relationship between genotype and plasma HTRA1. As shown in the box plot in Figure 6.11, there was a suggestively significant (p=0.06) increase in median level of HTRA1 measured in carriers of one or two copies of the T risk allele (22.26 ±1.76 (s.e.m.) ng/ml) compared to GG homozygotes (18.05 ±1.56 (s.e.m.) ng/ml). The range of plasma HTRA1 measured was significantly wider in GT/TT individuals, compared to GG homozygotes (Moses test of extreme reaction, in which data was trimmed for extreme outliers, p=0.045).

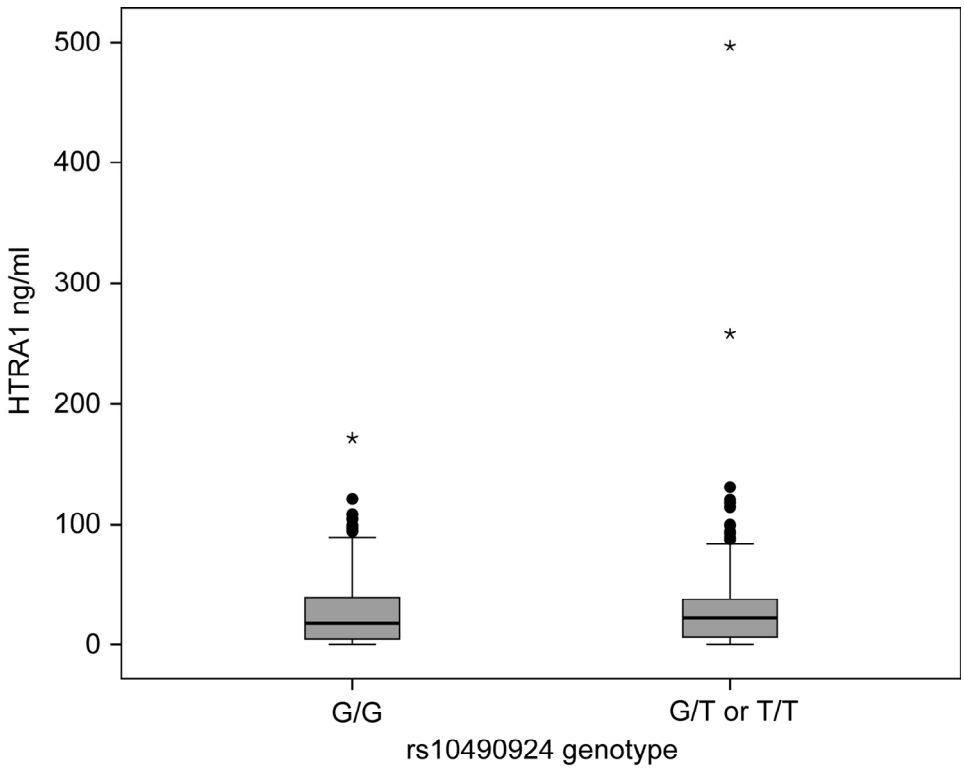

Figure 6.11 The risk allele of rs10490924 is associated with elevated plasma HTRA1 concentrations in the UK2 cohort.

Plasma HTRA1 was measured by ELISA in 680 samples from a British AMD case-control cohort which were genotyped for rs10490924. Logistic regression was used to test the association between genotype at rs10490924 (GG or GT/TT) and plasma HTRA1, accounting for the confounding effect of age and BMI. The 3rd (p=0.03) and 4th (p=0.04) quartiles of plasma HTRA1 were significantly associated with carriers of the T allele, which is associated with risk of AMD in this cohort ($p=2.73x10^{-13}$). Extreme outliers are indicated by *.

6.3.1.3 Analysis of AMD-risk factors as covariates

The known AMD risk factors of increasing age, gender and smoking history (reviewed by Klein et al 2004) showed no correlation with alterations in plasma HTRA1 using non-parametric tests of median, range and distribution for categorical variables (Table 6.3). For non-parametric testing, age was categorised as <65 years, 65-80 years, or >80 years of age. The median HTRA1 level in plasma for the individuals aged <65 years (N=46) was 17.87 ±11.9 (s.e.m.) ng/ml compared to a median of 21.27±1.19 (s.e.m.) ng/ml in the 65-80 years category (N=395), and to 20.16±1.54 (s.e.m.) ng/ml in the >80 years category (N=331). Due to the small number of individuals aged <65 years, an effect of increasing age on plasma HTRA1

cannot be completely excluded. Smoking was categorised as ever/never, and was also assessed in terms of packyears (the number of cigarettes smoked per day multiplied by the years of smoking; none, <20, >20).

Body mass index (BMI) was significantly associated with an alteration in the distribution of plasma HTRA1 measurements (Figure 6.12A). Individuals with BMI > 30 had a median HTRA1 level in plasma of 25.65 ±2.64 (s.e.m.) ng/ml compared to a median of 19.2±1.41 (s.e.m.) ng/ml for individuals with a BMI<25 (p=0.022). There was also a significant difference between the BMI groups at the extremes of distribution, as indicated by the Moses test of extreme reaction (p=<0.001).

Stratifying analysis by BMI category showed that the largest difference in median plasma HTRA1 by genotype was observed in individuals with a BMI<25 (Figure 6.12B, Table 6.3). In individuals with BMI<25, the median HTRA1 level in plasma for the GG non-risk genotype (N=99) was 17.91 ±2.17 (s.e.m.) ng/ml compared to a median of 21.53±2.15 (s.e.m.) ng/ml for individuals with GT/TT genotype (N=120; p=0.374). Stratifying the samples by BMI causes loss of power so that the differences in median are not significant. However, the range of plasma HTRA1 concentrations between genotypes was significantly different in this BMI group (p=0.038). In the BMI>30 group, the proposed effect of genotype upon plasma HTRA1 was barely observed, with only a slight (and not statistically significant) elevation in median plasma HTRA1 between genotype groups (Table 6.3).

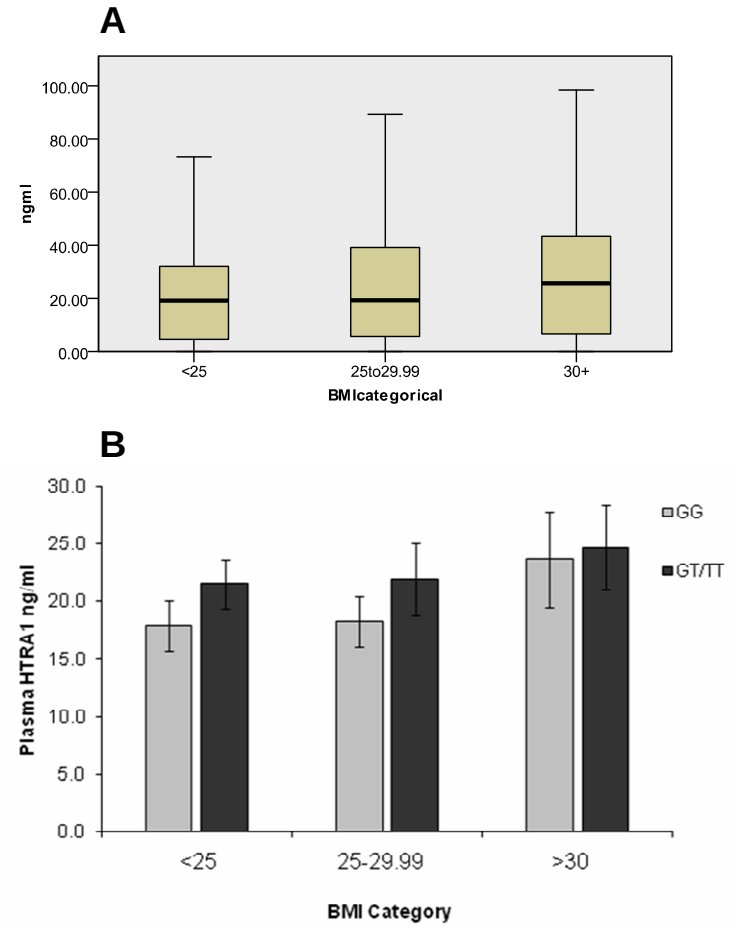

Figure 6.12 BMI is a confounding factor in the association between genotype and plasma HTRA1 in the UK2 cohort.

A. The distribution of plasma HTRA1 measurements were significantly different (p=0.022) between BMI categories (<25, 25-29.99, >30), as assessed by non-parametric tests using SPSS v17.

B. The association between rs10490924 genotype and median plasma HTRA1 concentration was affected by BMI. The difference in median plasma HTRA1 was most obvious in BMI<25 (although this was not statistically significant), and was barely apparent in the BMI>30 category. Error bars represent standard error of the mean.

plasma HTRA1 ng/ml

	Category	N plasma HTRA1 measured	N genotyped	Median	25th-75th percentile	Range	S.E.M.	Regression *p*	Mann-Whitney U *p*	Median test *p*	Moses test *p*
Combined		769	680	20.81	5.29 - 37.91	497.13	1.11				
	Male	308	303	20.79	4.63 - 38.83	497.13	2.1				
Gender	Female	380	317	20.78	5.90 - 38.06	257.87	1.33		0.821	1	**0.005**
	Ever	471	422	20.08	5.23 - 36.05	497.13	1.51				
Smoking	Never	297	258	21.95	5.92 - 39.11	257.87	1.6		0.341	0.266	**0.008**
	0	260	259	21.04	5.71 - 38.97	257.87	1.75				
	<20	221	217	22.63	5.46 - 43.32	497.13	2.66				
Pack years	>20	207	204	17.52	5.22 - 31.56	171.65	1.7		0.2	0.193	
	GG	284	284	18.05	4.95 - 39.81	171.65	1.53	3rd Quartile **0.03**			
rs10490924	GT/TT	396	396	22.26	6.49 - 37.97	497.13	1.76	4th Quartile **0.04**	0.307	**0.062**	**0.031**
	<65 years	42	31	17.87	5.83 - 38.36	497.13	11.91				
	65-80 years	395	349	21.27	6.28 - 39.95	168.62	1.19	3rd Quartile 0.94			
Age	>80 years	331	300	20.16	4.35 - 35.35	257.87	1.54	4th Quartile 1.0	0.552	0.253	**(< 0.001)**
	GG		151	19.76	5.22 - 40.81	120.8	1.91	3rd Quartile 0.11			
rs10490924 (65-80 years)	GT/TT		198	21.59	6.31 - 39.07	114.07	1.61	4th Quartile 0.457	0.893	0.478	**0.062**
	GG		116	17.02	3.04 - 35.34	171.65	2.62	3rd Quartile 0.249			
rs10490924 (>80 years)	GT/TT		184	24.1	6.89 - 38.06	257.87	2.16	4th Quartile **0.064**	0.171	**0.033**	0.127

	<25	248	219	19.2	4.56 - 32.01	120.27	1.41	3rd Quartile **0.041**			
	25-29.99	327	287	19.3	5.65 - 39.11	497.13	1.85	4th Quartile **0.062**			
BMI	>30	179	160	25.65	6.66 - 43.35	257.87	2.64		**0.072 (0.022)**	0.099 (**0.057**)	**(< 0.001)**
	GG		99	17.91	4.35 - 30.52	97.41	2.17	3rd Quartile 0.952			
rs10490924 (BMI <25)	GT/TT		120	21.53	6.03 - 33.96	120.27	2.15	4th Quartile 0.713	0.463	0.374	**0.038**
	GG		65	23.64	5.28 - 46.53	171.65	4.1	3rd Quartile 0.187			
rs10490924 (BMI >30)	GT/TT		95	24.7	7.92 - 40.64	257.87	3.69	4th Quartile 0.465	0.867	0.872	0.2
	Control	277	274	18.43	5.64 - 40.22	120.8	1.36	3rd Quartile **0.019**			
AMD Status	Case	411	406	21.68	5.30 - 36.90	497.13	1.78	4th Quartile **0.065**	0.728	0.244	**< 0.001**
	Else	341	274	19.36	6.22 - 39.43	120.8	1.21	3rd Quartile **0.032**			
	GA only	101	98	16.65	2.19 - 32.62	117.46	2.33	4th Quartile **0.085**	**0.090 (0.044)**	0.099 (0.086)	**(< 0.001)**
CNV	Any CNV	319	307	22.63	6.00 - 38.06	497.13	2.21				

Table 6.3 Plasma HTRA1 analysis in the UK2 series.

Plasma HTRA1 concentrations were tested for an association with gender, smoking history, age, BMI and AMD status, in addition to rs10490924 genotype. Raw plasma HTRA1 (ng/ml) was tested using non-parametric tests to account for skewed distribution. Quartiles of plasma HTRA1 were tested for an association with genotype, correcting for age and BMI by logistic regression. P-values shown in brackets are calculated for comparisons of the following groups: age, <65 years, >80 years; BMI, <25, >30; CNV, Else, any CNV.

Increasing age was not shown to be a confounding effect upon plasma HTRA1 concentration. However, when the cohort was split into age categories (<65 years, 65-80 years, or >80 years), the association between elevated median plasma HTRA1 and risk genotype at rs10490924 was most significant in the group aged over 80 years. Table 6.3 shows the median and quartile ranges of plasma HTRA1 measurements for each age group, split by genotype. In the group aged 65-80 years, the difference in median plasma HTRA1 is suggestively significant (p=0.06; 19.76 ±1.91 (s.e.m.) ng/ml for GG genotype compared to 21.59±1.61 (s.e.m.) ng/ml for GT/TT genotype). In individuals aged over 80 years, there is a more significant difference between median plasma HTRA1 in individuals with a GG genotype (17.02±2.62 (s.e.m.) ng/ml), compared to individuals carrying a risk allele (24.10±2.16 (s.e.m.) ng/ml), p=0.033. There was no significant difference in mean BMI between age groups, suggesting that the confounding effect of BMI is not responsible for this observation (data not shown).

6.3.1.4 Analysis of plasma HTRA1 quartiles

To account for the skewed distribution of plasma HTRA1 and the large number of low plasma HTRA1 measurements, quartiles of plasma HTRA1 were tested for an association with SNP genotype. Quartiles were calculated for the combined data set, and plasma HTRA1 measurements were classified as 1st quartile (1), 2nd quartile (2), 3rd quartile (3) or 4th quartile (4) for analysis. Quartile ranges for the combined data are shown in Table 6.3, and for the cohort split by genotype in the box plot shown in Figure 6.11. Using a dominant model of logistic regression, the 3rd and 4th quartiles of plasma HTRA1 were significantly associated with carriers of the HTRA1 rs10490924 minor allele (for each quartile, p=0.036, OR 1.608, 95% C.I, 1.032-2.504).

BMI was included as a covariate in binary logistic regression analysis to correct for the confounding effect of high BMI upon plasma HTRA1. The upper quartiles of plasma HTRA1 remained significantly associated with carriers of the HTRA1 rs10490924 minor allele (3rd quartile, p=0.03; 4th quartile, p=0.04), independent from the contribution of high BMI to plasma HTRA1. The addition of

age as a covariate had little effect upon the association of upper plasma HTRA1 quartiles with risk genotype (3rd quartile, p=0.029; 4th quartile, p=0.046).

6.3.1.5 Association of plasma HTRA1 with AMD

The genotype of rs10490924 was significantly associated with AMD in this cohort (GT/TT, $p=2.73x10^{-13}$, OR 3.618 (95% C.I. 2.56–5.11)). Median plasma HTRA1 in controls was 18.43±1.36 ng/ml, which was lower than in AMD cases (21.68±1.78 ng/ml). This was not significantly different when assessed by non-parametric tests (p=0.244, Table 6.3). However, binary logistic regression of plasma HTRA1 quartiles, including the known AMD-risk factors of age, sex, smoking history and BMI, indicate that higher plasma HTRA1 measurements are significantly or suggestively associated with AMD (3rd quartile, p=0.015, 4th quartile p=0.063). These analyses may indicate that there is a confounding factor affecting the 4th quartile of plasma HTRA1 which is not corrected for, or alternatively, insufficient power.

The chromosome 10q26 risk locus has been suggested to increase the risk of development and progression of wet AMD, possibly as a consequence of HTRA1 activity promoting choroidal neovascularisation (CNV; Dewan et al. 2006; Sobrin et al. 2011; Chen et al. 2011). The risk locus tagged by rs10490924 was significantly associated with CNV in this cohort (GT/ TT, $p=2.99 x10^{-17}$, OR 4.445 (95% C.I. 3.145 – 6.284)). The relationship between plasma HTRA1 and CNV was assessed using non-parametric tests and logistic regression.

As shown in Table 6.3, individuals with CNV had a higher median plasma HTRA1 (22.63±2.21 ng/ml) compared to individuals with only geographic atrophy (16.65±2.33 ng/ml) or to disease-free controls (19.36±1.21 ng/ml). Due to the smaller number of GA cases (N=98) potentially affecting power, CNV cases (N=307) were compared to controls (N=274). There was a significant difference in the distribution of plasma HTRA1 concentrations measured in controls compared to AMD cases with CNV (p=0.044). The range of plasma HTRA1 concentrations was also significantly different between controls and CNV cases (p<0.001). Binary logistic regression of plasma HTRA1 quartiles, including the known AMD-risk

factors of age, sex, smoking history and BMI, confirmed that higher plasma HTRA1 measurements are significantly or suggestively associated with AMD (3rd quartile, p=0.03, 4th quartile p=0.083).

6.3.2 Association of rs10490924 risk allele with elevated plasma CFD

Plasma CFD was shown to be significantly elevated in AMD cases compared to controls in Chapter 4.4.3.2. In light of the interaction between HTRA1 and CFD at the protein level, the association between plasma CFD and rs10490924 genotype was assessed. The median plasma CFD concentration in individuals with the GG genotype was 1.82±0.049 µg/ml); in GT/TT individuals, median plasma CFD was 1.95±0.053 µg/ml). The risk allele (T) was associated with higher plasma CFD measurements (p=0.005, Mann Whitney U).

AMD status is a confounding factor, given that plasma CFD was elevated in AMD cases compared to controls (p =0.00025). BMI is also a confounding factor, as shown in Chapter 4.4.3.1. Logistic regression, including age, sex, smoking, BMI and AMD status as covariates, was performed to test for an association between elevated plasma CFD and rs10490924 genotype. When comparing the 1st to 4th quartiles of plasma CFD, there was a significant association with the risk allele (GT/TT; p=0.01, OR 1.96, 95% C.I. 1.18-3.26). Furthermore, there was no association between the CFH Y402H variant (rs1061170) and plasma CFD (p=0.345). This suggests that the association of plasma CFD with AMD may reflect a contribution (by an unknown mechanism) of the chromosome 10q26 locus to systemic inflammation.

6.4 Power calculations for HTRA1 ELISA

There are no published reports of plasma HTRA1 measurements. Having observed a difference in mean and median plasma HTRA1 between genotype groups corresponding to a 8.1 % increase in the median plasma HTRA1 concentration in carriers of the risk haplotype (Table 6.3), the power of the study to identify a significant difference (p=0.05) of this magnitude at 80% power was assessed.

6.4.1 Normalisation of plasma HTRA1 measurements

Plasma HTRA1 measurements showed a considerable deviation from normal distribution, as shown in Figure 6.10. A combination of non-parametric testing and quartile normalisation was used to allow for this in the analysis of the data. However, in order to calculate power, normal distribution of data is required.

Cube root ($\sqrt[3]{}$) transformation of the detectable plasma HTRA1 measurements was performed to achieve normalisation of the plasma HTRA1 measurements for analysis of a relationship with rs10490924 genotype. As shown in Figure 6.13A, normal distribution is achieved following cube root transformation of detectable HTRA1. This is also seen in the Q-Q plot (Figure 6.13B). There was no significant difference between the proportion of plasma samples with HTRA1 below the detectable limits of the ELISA between genotype groups (p=0.345).

6.4.2 Calculation of required sample size using the Altman Nomogram

Mean values of cube root ($\sqrt[3]{}$) transformed plasma HTRA1 were used to calculate the required sample size to detect a significant difference in plasma HTRA1 between genotype groups. The mean value of $\sqrt[3]{}$transformed plasma HTRA1 in the rs10490924 GG group (N=283) was 2.33±0.081 (s.e.m.), compared to 2.43±0.066 (s.e.m.) in the GT/TT group (N=394). The difference in means and the observed standard deviation (1.33) were used to calculate the standardised difference. The standardised difference was then applied to an Altman Nomogram (Figure 2.1). This indicates that a sample size of 4,000 would be required to identify a difference in plasma HTRA1 of this magnitude with 80% power (p=0.05).

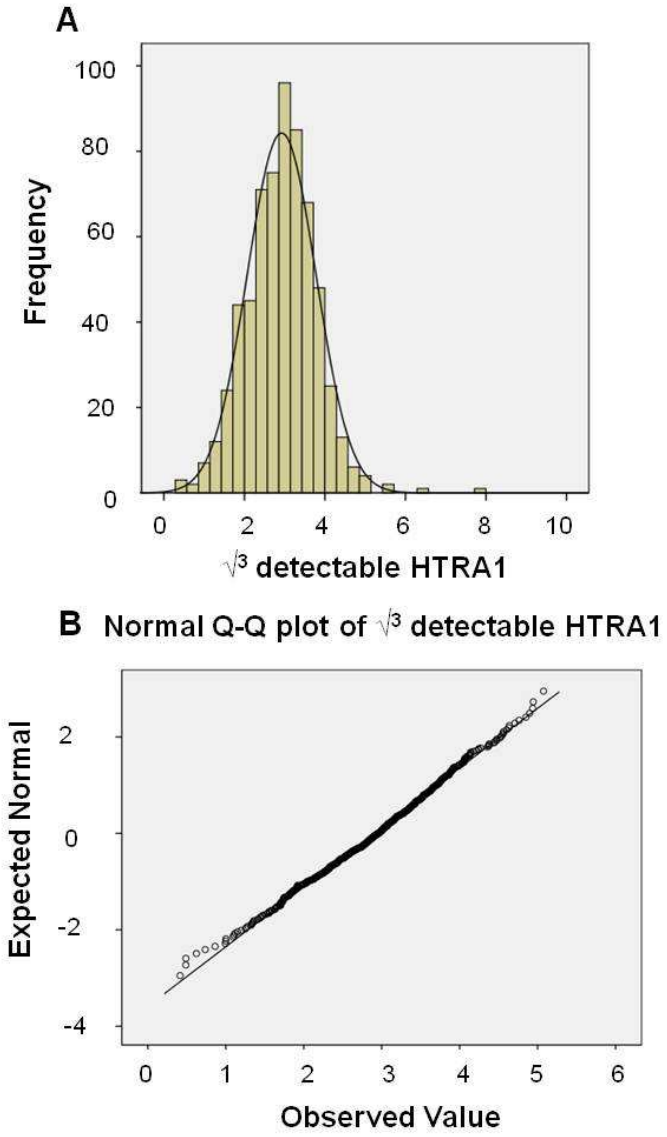

Figure 6.13 Normalisation of the distribution of plasma HTRA1 measurements in UK2.

A. Detectable HTRA1 (measurements above zero) were cube root ($\sqrt[3]{}$) transformed to attain a normal distribution. Skewedness and kurtosis were reduced.

B. A Q-Q plot showing that cube root transformation successfully normalises the distribution of plasma HTRA1 measurements, allowing calculation of power.

6.4.3 Confounding effect of BMI

High BMI is significantly associated with elevated plasma HTRA1 (p=0.022, Table 6.3, Figure 6.12A). Although the effect of BMI does not remove the significant association between higher plasma HTRA1 measurements and the risk haplotype on chromosome 10q26, it does act to reduce the significance of the association, particularly with the 4th quartile of plasma HTRA1 measurements. Thus, the inclusion of individuals with high BMI is a confounding factor in the power of the study to identify a significant association between genotype and plasma HTRA1. The measured difference in mean cube root-transformed plasma HTRA1 in GG versus GT/TT individuals stratified by BMI group (< 25, 25-29.99, >30) was used to calculate the standardised difference for each group. Application of these data to the Altman Nomogram (Figure 2.1) indicates that in individuals with BMI<25, as few as 500 samples would be sufficient to detect a significant difference (p=0.05) of the expected magnitude with 80% power. Substantially more samples are required in groups with higher BMI.

6.4.4 Plasma HTRA1 was measured in a Scottish cohort with BMI<25

In order to minimise the confounding effect of increasing body mass, and to increase the power to detect a significant difference in plasma HTRA1 between genotype groups, EDTA-plasma samples from an additional 210 individuals with BMI<25 were obtained. These samples are disease-free SOCCS controls, and were kindly provided by Prof. Malcolm Dunlop. The characteristics of this series are shown in Table 6.4. Mean age was substantially lower than in the UK2 cohort used for the initial plasma HTRA1 measurements (50.9±6.8 (SD) years, compared with 79.0±7.5 (SD) years in the UK2 series). Mean BMI was 22.6±1.6 (SD).

Genotyping the SOCCS samples for rs10490924 was performed by Susan Campbell, using a TaqMan SNP genotyping assay. Genotype frequencies are shown in Table 6.4. Eight samples were not successfully genotyped for the SNP.

Table 6.4 Demographic characteristics for the SOCCS series genotyped for rs10490924.

Demographic characteristics for the SOCCS series are shown according to rs10490924 genotypes. No statistically significant differences between GG and GT/TT groups were identified. Exact test of Hardy–Weinberg equilibrium (number), *t-test* (mean age and mean BMI), exact test (gender, smoking history) and median test (median HTRA1 (ng/ml)) were applied to calculate p-values. Abbreviations: SD, standard deviation; BMI, body mass index.

	SOCCS			
Genotype	**Total**	**GG**	**GT/TT**	***p*-value**
Number	200	119	81	0.796
Mean age (yrs)	50.9	50.9	50.9	
SD	6.8	6.7	6.8	0.96
Mean BMI	22.64	22.79	22.51	
SD	1.6	1.46	1.72	0.227
% Males	43.0	42.0	44.4	0.773
Smoking				
never	100	61	39	
former	51	30	21	
current	48	28	20	0.946
AMD (%)	Not examined			
Median HTRA1 (ng/ml)	10.85	10.36	11.79	0.223

6.4.4.1 Plasma HTRA1 measurements in SOCCS

Plasma HTRA1 was measured in the SOCCS samples as previously described for the UK2 cohort. Internal control plasma samples P8 and P9 were included on all plates to ensure the assay performed in a consistent manner across the two series. Median plasma HTRA1 concentrations in this cohort (10.85±1.22 (s.e.m.) ng/ml) were lower than in the UK2 cohort (20.81±1.11 (s.e.m.) ng/ml).

Plasma HTRA1 concentrations in the SOCCS series showed a leptokurtic distribution, with measurements ranging from 0-84.2 ng/ml (Figure 6.14). Non-parametric tests were used to investigate associations between plasma HTRA1 concentrations with rs10490924 genotype (GG versus GT/TT).

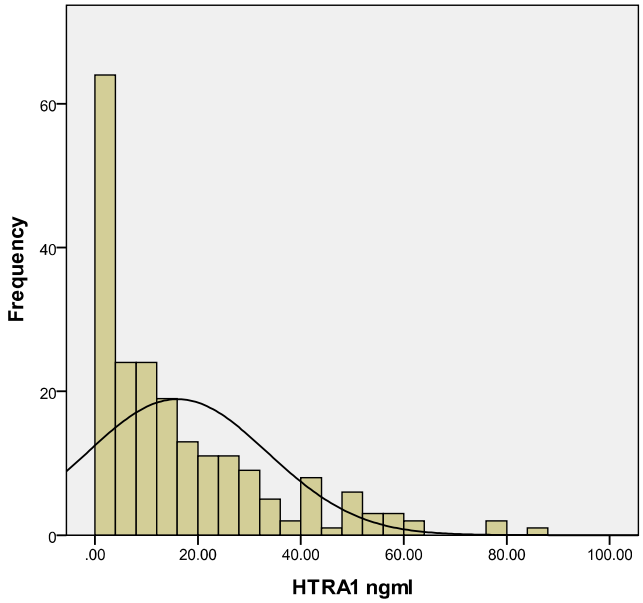

Figure 6.14 Distribution of plasma HTRA1 measurements in SOCCS cohort.

The distribution of unadjusted plasma HTRA1 measurements (ng/ml) in the SOCCS control series. These data show a deviation from normal, as indicated by a kurtosis value of 1.81 (S.E. 0.336) and skewedness value of 1.42 (S.E. 0.169).

6.4.4.2 Analysis of raw plasma HTRA1 measurements by rs10490924 genotype in SOCCs

The median level of HTRA1 measured in GG homozygotes (N=121) was 10.36±1.17 (s.e.m.) ng/ml, which was lower than in carriers of one or two copies of the T risk allele (N=81; 11.79±2.28 (s.e.m.) ng/ml). This was not statistically significant (p=0.31). However, the range of plasma HTRA1 measured was significantly wider in GT/TT individuals than in GG homozygotes (Moses test of extreme reaction, in which data was trimmed for extreme outliers, $p< 0.001$).

6.4.5 Combined analysis of UK2 and SOCCS plasma HTRA1 measurements

The plasma HTRA1 measurements made in UK2 and SOCCS cohorts were combined for analysis. This allowed further assessment of the relationship between the confounding factors of BMI, age and AMD status upon plasma HTRA1. There was also an increase in power to detect a significant difference in plasma HTRA1 concentration by genotype in the BMI<25 group (N=418).

6.4.5.1 Analysis of raw plasma HTRA1 by rs10490924 in the combined cohorts

The relationship between genotype and plasma HTRA1 in the combined UK2 and SOCCS cohorts was assessed using non-parametric testing to account for the deviation from normal distribution (skewedness 1.32±0.078 standard error of skewedness). As shown in the box plot in Figure 6.15, there was a significant (p=0.045) increase in median level of HTRA1 measured in carriers of one or two copies of the T risk allele (20.56±1.05 (s.e.m.) ng/ml) compared to GG homozygotes (14.81 ±1.10 (s.e.m.) ng/ml). This reflected a significant difference in the distribution (p=0.017) and range (p<0.001) of plasma HTRA1 measured in GT/TT individuals, compared to GG homozygotes (Table 6.5).

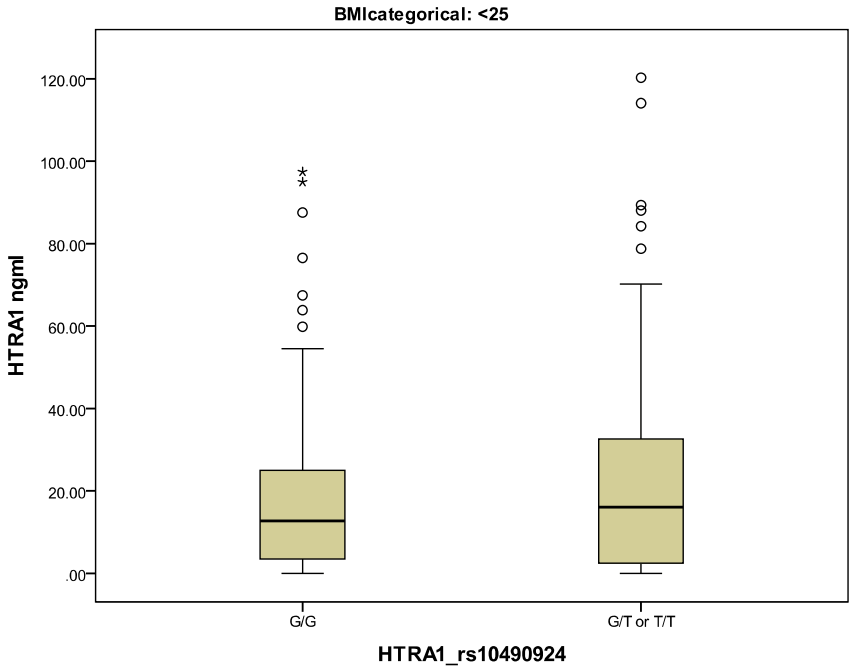

Figure 6.15 Elevated plasma HTRA1 is associated with risk genotype in BMI<25 goup for combined cohorts.

Plasma HTRA1 was measured by ELISA in 418 samples with BMI<25 which were genotyped for rs10490924. Non-parametric testing performed in SPSS v19 identified a significant (p=0.045) increase in median level of HTRA1 measured in GT/TT individuals compared to GG homozygotes. Significant differences in the distribution (p=0.017) and range (p<0.001) of plasma were also identified.

		plasma HTRA1 ng/ml									
Covariate	**Category**	**N plasma HTRA1 measured**	**N genotyped**	**Median**	**25th-75th percentile**	**Range**	**S.E.M.**	**Regression *p***	***p* Mann-Whitney U**	***p* Median test**	***p* Moses test**
					SOCCS						
SOCCS	All measured HTRA1	208	202	10.85	1.34 - 24.89	84.23	1.22				
Gender	Male	90	86	12.90	1.13 - 25.84	61.01	1.76		0.268	0.05	0.016
	Female	118	114	8.69	1.13 - 22.4	84.23	1.68				
Smoking	current	52	48	10.96	0.00 - 21.4	52.66	2.28		0.598	0.827	
	former	54	51	10.19	0.00 - 18.47	77.27	2.30				
	never	101	100	11.12	2.88 - 26.29	84.23	1.84				
rs10490924	GG		119	10.36	2.52 - 21.04	59.86	1.17		0.223	0.313	<0.001
	GT/TT		81	11.79	0.25 - 32.68	84.23	2.28				
					SOCCS and UK2 combined						
Combined	All measured HTRA1	973	916	17.37	4.57 - 34.9	130.75	0.72				
Gender	Male	396	387	17.79	3.84 - 35.16	130.75	1.15		0.556	0.482	
	Female	497	490	16.36	4.93 - 35.07	120.80	1.00				
Smoking	Current	104	357	14.82	0.42 - 24.77	63.25	1.59		0.05	0.158	
	Former	470	425	17.48	5.14 - 35.46	130.75	1.05				
	Never	397	94	18.15	4.61 - 36.95	120.80	1.16				
rs10490924	GG		402	14.81	3.78 - 31.03	120.80	1.10	4th Quartile 0.143	0.017	0.045	<0.001
	GT/TT		475	20.56	5.32 - 37.26	130.75	1.05				
Age	<65 years	247	228	10.88	2.48 - 26.22	93.94	1.27		<0.001	<0.001	
	65-80 years	395	349	21.27	6.28 - 39.95	168.62	1.19				
	>80 years	331	300	20.16	4.35 - 35.35	257.87	1.54				

BMI	<25	455	418	14.72	3.01 - 29.7	120.85	0.96		<0.001	0.002	
	25-29.99	329	287	19.10	4.47 - 39.08	99.31	1.15				
	>30	176	158	24.94	6.44 - 41.9	30.75	2.06				
rs10490924 (BMI <25)	GG		217	12.72	3.37 - 25.0	97.41	1.21	4th Quartile 0.026	0.048	0.063	<0.001
	GT/TT		201	16.08	2.30 - 32.96	120.27	1.59				
rs10490924 (disease free only)	GG		283	13.21	3.46 - 27.88	120.80	1.23	4th Quartile 0.045	0.097	0.223	<0.001
	GT/TT		191	16.09	4.37 - 39.05	89.36	1.51				

Table 6.5 Plasma HTRA1 analysis in the SOCCS series, and in the UK2 and SOCCS combined series.

Plasma HTRA1 concentrations were tested for an association with gender, smoking history, age, and BMI, in addition to rs10490924 genotype. Raw plasma HTRA1 (ng/ml) was tested using non-parametric tests to account for skewed distribution. Quartiles of plasma HTRA1 were tested for an association with genotype, correcting for age and BMI by logistic regression

6.4.5.2 Analysis of AMD-risk factors as covariates in the combined cohorts

A significant difference between plasma HTRA1 concentrations was observed between genotype groups in the combined cohorts. The potential confounding effect of age, sex, smoking history and BMI was assessed using non-parametric testing as described for the UK2 cohort. As was seen in analysis of the UK2 cohort alone (Table 6.3) using non-parametric tests, there was no significant relationship between plasma HTRA1 and sex ($p=0.525$), or between plasma HTRA1 and smoking history ($p=0.158$) in the combined UK2 and SOCCS cohorts (Table 6.5).

The SOCCS cohort has a mean age of 50.9±6.8 (SD) years, which increases the ability to identify a relationship between plasma HTRA1 and increasing age in the combined cohorts. Age was categorised as less than 65 years, 65-80 years, or aged over 80 years of age for non-parametric testing. The median HTRA1 level in plasma for the individuals aged<65 years in the combined cohort (N=249) was 10.88±1.26 (s.e.m.) ng/ml. Comparison of this to a median of 21.27±1.19 (s.e.m.) ng/ml in the 65-80 years category (N=395), and to 20.16±1.54 (s.e.m.) ng/ml in the >80 years category (N=331) identified a significant relationship between increasing age and increasing plasma HTRA1, irrespective of rs10490924 genotype ($p< 0.001$; Figure 6.16A, Table 6.5).

The relationship between increasing age and plasma HTRA1 may be confounded by the lower mean BMI in the group aged<65 years (due to the inclusion of the SOCCS cohort). In the two groups with BMI<30, the effect of age remained significant, and was most pronounced in individuals with BMI<25 ($p=0.003$, Kruskal-Wallis test; Figure 6.16B). In the combined cohorts, the median HTRA1 level for individuals with a BMI<25 was 14.7±0.96 (s.e.m.) ng/ml (Table 6.5). This group showed a significant alteration in distribution compared to the group with BMI>30 who had a median of 24.94±2.06 (s.e.m.) ng/ml ($p<0.001$).

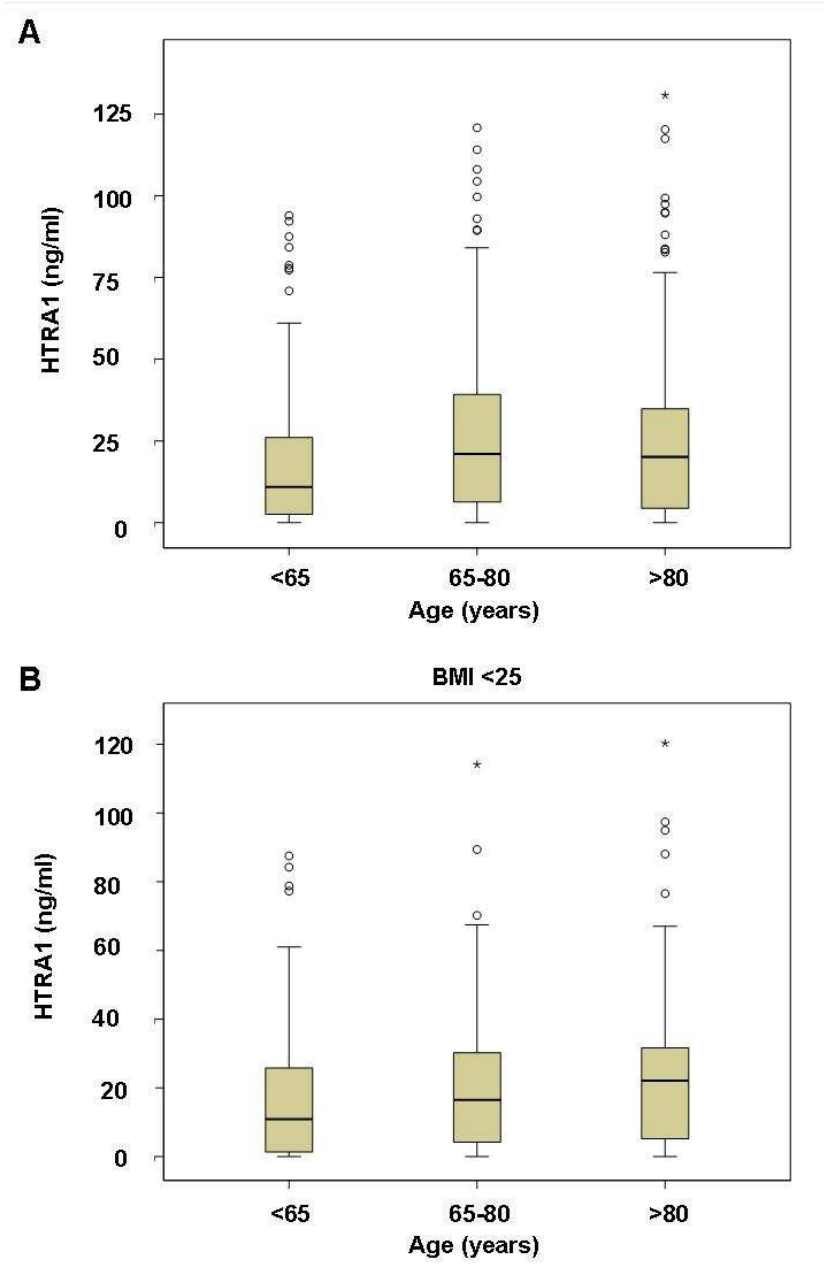

Figure 6.16 Increasing age is associated with elevated plasma HTRA1.
A.Increasing age was significantly associated with elevated plasma HTRA1, irrespective of genotype ($p<0.001$, Kruskal-Wallis test) in the combined UK2 and SOCCS cohort.
B. The association between increasing age and plasma HTRA1 in the combined cohorts remained significant in individuals with BMI<25 ($p=0.003$, Kruskal-Wallis test).

6.4.5.3 Analysis of plasma HTRA1 quartiles in the combined cohorts

To account for the skewed distribution of plasma HTRA1 and the confounding factors of age, BMI and AMD status, quartiles of plasma HTRA1 were tested for an association with SNP genotype by logistic regression. Quartiles of plasma HTRA1 measurements were calculated for the combined cohorts. Quartile ranges for the combined data are shown in Table 6.5, and for the cohort split by genotype in the box plot shown in Figure 6.15. Using a dominant model of logistic regression, including age, sex, smoking history, BMI and AMD status as covariates, the 4th quartile of plasma HTRA1 was not significantly associated with the HTRA1 rs10490924 minor allele (p=0.132).

Based on the previous observation that the effect of genotype upon plasma HTRA1 appears most obvious in the BMI<25 group, the combined cohorts were stratified by BMI category for analysis. A dominant model of logistic regression was used, including age, sex, smoking history and AMD status as covariates. As was previously predicted in the power calculations for the HTRA1 ELISA, there was a lack of power to detect a significant difference between genotypes in the groups with BMI >25. However, in the BMI<25 group, the 4th quartile of plasma HTRA1 was significantly associated with the HTRA1 rs10490924 minor allele (p=0.026, OR 2.03, 95% C.I, 1.09-3.78), corrected for confounding factors.

Similar results were obtained when only disease-free individuals (either controls from the UK2 AMD case-control cohort, or SOCCs controls) were investigated (Table 6.5). The median level of HTRA1 measured in 283 GG homozygotes was 13.21 ±1.23 (s.e.m.) ng/ml while risk (T) allele carriers (N=191) had a slightly higher median level of 16.09±1.51 (s.e.m.). In a regression analysis, including age and BMI as covariates, the upper quartile of plasma HTRA1 was significantly associated (p=0.045) with carriers of the AMD-risk (minor) allele of rs10490924.

6.4.5.4 Retrospective power calculation for plasma HTRA1 in BMI<25

The distribution of plasma HTRA1 measurements in the combined cohorts was normalised by $\sqrt[3]{}$-transformation of detectable HTRA1. The standardised difference was calculated using the difference in mean transformed HTRA1 measurements (GG=2.57±0.056 (s.e.m.), GT/TT 2.86±0.063 (s.e.m.)) and the standard deviation of the measurements. Application of the standardised difference to the Altman Nomogram (Figure 2.1) indicate that a sample size of 230 individuals would be sufficient to identify a difference in plasma HTRA1 of this magnitude with 80% power (p=0.05). In the combined UK2 and SOCCS cohorts, plasma HTRA1 measurements were made in 217 individuals with a GG genotype for rs10490924, and 201 individuals with either a GT or TT genotype. This indicates that the study is adequately powered to detect a significant difference in plasma HTRA1 by genotype, given that confounding factors of increasing age, AMD status and BMI are corrected for by regression analysis.

6.5 Local expression of *HTRA1* in adipose tissue

Due to the confounding effect of high body mass index upon plasma HTRA1 concentrations, expression of *HTRA1* in adipose tissue was investigated further to try to clarify the role of genotype upon expression of *HTRA1*. As shown in Figure 5.27, *HTRA1* transcripts were detected in cDNA derived from adipose tissue. The local expression of HTRA1 in adipose tissue in relation to BMI and rs10490924 genotype (as a tag for the risk haplotype) was assessed by analysis of microarray data from eleven adipose tissue biopsies, kindly shared by Professor Brian Walker.

6.5.1 Expression of HTRA1 in adipose tissue biopsies

Expression of *HTRA1* in adipose tissue correlates with elevated plasma HTRA1 in individuals with high BMI (Chapter 6.3.1.3, Table 6.3). As adipose tissue appears to contribute significantly to the systemic level of HTRA1, the expression of *HTRA1* was investigated in eleven adipose biopsy samples by microarray analysis of adipose

cDNA, provided by Professor Brian Walker. Figure 6.17A shows the *HTRA1* transcript intensity detected, showing a trend for elevated levels of *HTRA1* in relation to increasing BMI. The mean intensity detected for HTRA1 transcripts in individuals with a BMI<25 was 5495±542 (SD), compared to an average of 5813±305 (SD) for individuals with a BMI >30. This difference of 6% in the mean HTRA1 intensity from the microarray, although not statistically significant (p=0.27), reflects the observed effect of high BMI upon plasma HTRA1 in the ELISA measurements.

These individuals were genotyped for the *ARMS2* 3' UTR indel by PCR to investigate whether the risk haplotype was associated with higher HTRA1 expression in this tissue, as was seen systemically in plasma. Of the 11 individuals, 6 were homozygous wild-type for the indel (and presumed homozygous for the non-risk haplotype).Five individuals were heterozygous, carrying one copy of the indel variant associated with AMD-susceptibility. No homozygous carriers of the risk allele were identified. There was no significant difference in the intensity of HTRA1 between genotype groups (non-risk, 5462±372 (SD); risk, 5542±668 (SD), p=0.80).

The contribution of genotype within the BMI groups <25 and >30 upon *HTRA1* expression is summarised in Figure 6.17B. In the BMI<25 group, three individuals were homozygous wild-type and three were heterozygous. There was no significant difference between mean HTRA1 intensity by genotype in this group (non-risk, 5630±78 (SD); risk, 5359±821 (SD), p=0.60). In the BMI >30 group, one person was homozygous wild-type and two were heterozygous. There was no significant difference between mean HTRA1 intensity by genotype in this group (non-risk, 5809; risk, 5815±431 (SD).

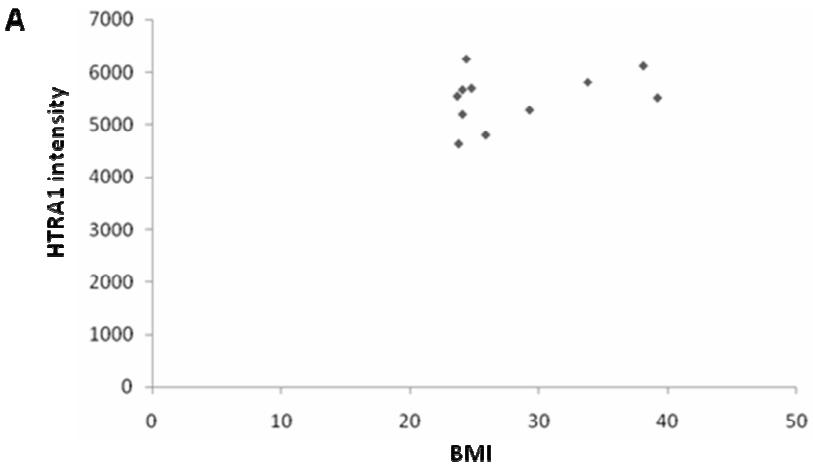

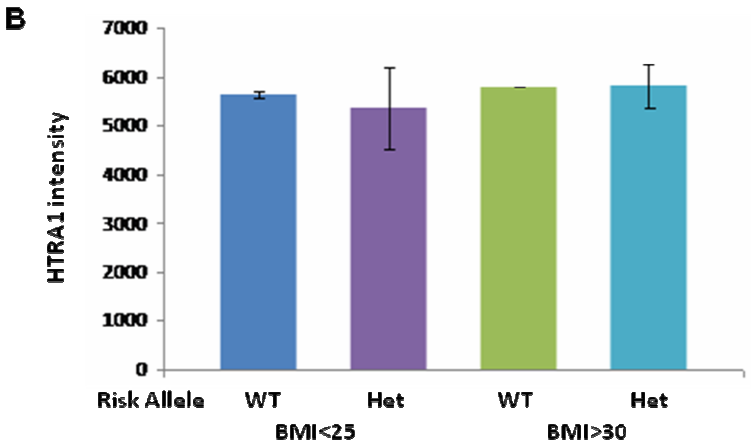

Figure 6.17 Microarray data revealed no significant relationship between BMI, genotype and HTRA1 intensity.

A. *HTRA1* expression in adipose biopsy samples obtained from 11 individuals (N=6, BMI<25; N= 2, BMI 25-29.99, N=3, BMI>30), provided by by Professor Brian Walker, was investigated using the Affymetrix probe set 201185_at. A possible trend for increased HTRA1 intensity in relation to BMI was observed.

B. *HTRA1* expression in adipose biopsy samples genotyped for the ARMS2 3' UTR indel on the chromosome 10q26 risk haplotype, divided into BMI categories. There was no clear relationship between genotype and HTRA1 intensity in this small sample size (BMI<25, WT N=3, Het N=3; BMI>30 WT N=1, Het N=2).

6.6 Discussion

The AMD-risk haplotype in chromosome 10q26 may be associated with alterations in the expression of one of, or both, *ARMS2* and *HTRA1*genes. Early studies proposed that increased HTRA1 activity, as a consequence of increased *HTRA1* expression, may increase susceptibility to AMD. The risk haplotype, tagged by rs11200638, was suggested to result in up-regulation of *HTRA1* by the AA genotype compared with the GG genotype (Dewan et al. 2006). Increased levels of *HTRA1* mRNA and protein were detected in RPE from four AMD-affected individuals carrying the AA risk allele (Yang et al. 2006). Subsequent studies have failed to replicate these findings consistently, with several studies showing no significant difference in *HTRA1* mRNA or protein in retina and placental samples of known genotype, and no increased promoter activity by luciferase assays (Kanda et al. 2007; Chowers et al. 2008; Kanda et al. 2010; Friedrich et al. 2011). However, others have shown that there is a difference in promoter activity, mRNA and protein levels for *HTRA1* in carriers of the risk haplotype using similar techniques (An et al. 2010; Yang et al. 2010).

The concentration of HTRA1 in human plasma has not previously been reported. This chapter describes the development and optimisation of a sandwich ELISA to measure HTRA1 in EDTA-plasma. The optimised assay was used to measure plasma HTRA1 in 769 individuals from a British AMD-case control cohort and subsequently, in an additional 208 Scottish disease-free controls. This allowed investigation of an association between plasma HTRA1 and the AMD-risk haplotype on chromosome 10q26. In the UK2 cohort, measurements in plasma ranged from no detectable HTRA1 to 497 ng/ml (mean 25.94, median 20.81, s.e.m. 1.11, SD 30.85). In the SOCCS cohort, the range was between 0- 84.2 ng/ml HTRA1 (mean 16.02 ng/ml, median 10.85 ng/ml, s.e.m. 1.21, SD 17.55). Measurements in each cohort, and in the cohorts combined, showed a leptokurtic distribution. Exclusion of significant outliers (mean±3 SD) reduced the range of plasma HTRA1 measurements to below 118 ng/ml, and reduced kurtosis (1.21, standard error of kurtosis 0.18).

Due to the deviation from normal distribution, the effects of categorical covariates on plasma HTRA1 were assessed using non-parametric tests. There was

no significant difference observed in plasma HTRA1 concentrations between genders in either cohort, with males having a median of 20.79±2.10 (s.e.m.) ng/ml, compared to a median value of 20.78± 1.33 (s.e.m.) ng/ml in females in UK2. Median values of plasma HTRA1 were lower in the SOCCS cohort for both sexes; there was no significant difference between measurements made in males and females (p=0.268).

Advanced age is known to increase risk of AMD development, and was associated with increased plasma HTRA1 concentrations in people aged >65 years in this cohort (p<0.001; age classified as <65 years, 65-80 years, and aged >80 years, Figure 6.16). Individuals aged <65 years had lower median plasma HTRA1 (N=249, 10.88±1.26 (s.e.m.) ng/ml) than older individuals (N=395, 21.27±1.19 (s.e.m.) ng/ml in the 65-80 years category, p=0.55).

The effect of smoking history upon plasma HTRA1 concentrations was also assessed by non-parametric testing. Schmidt et al. (2006) reported that the risk genotype of rs10490924 conferred a more substantial risk of AMD to smokers than to non-smokers, although no biological mechanism was proposed. Subsequent studies have not shown the same gene-environment interaction, so smoking is generally considered to be an independent risk factor for AMD (Hughes et al. 2007; Seddon et al. 2009; Chen et al. 2011). However, smoking increases oxidative stress, and is proposed to have damaging effects on retinal pigment epithelial cells and Bruch's membrane during the early events of AMD development (Espinosa-Heidmann et al. 2006; Fujihara et al. 2008). *HTRA1* is rapidly up-regulated following oxidative stress (Zurawa-Janicka et al. 2008) and so the effect of smoking history upon plasma HTRA1 concentration was investigated.

Smoking is a significant risk factor for AMD in this British AMD cohort (for each additional packyear, OR 1.02, 95% C.I. 1.01-1.03, p= 0.0002) and in other studies (Hughes et al. 2007; Seddon et al. 2009; Chen et al. 2011). The effect of smoking history on plasma HTRA1 concentration was tested both as ever/never smoked, and by pack years (0 pack years, less than 20 pack years, and more than 20 pack years). There was no significant difference in the median or distribution of plasma HTRA1 concentrations between these groups of smoking history, in either the UK2 cohort (Table 6.2) or the SOCCS cohort (Table 6.4). Therefore, it appears that smoking history has little effect on plasma HTRA1 levels, although it remains to

be tested whether up-regulation of *HTRA1* expression as a response to smoking occurs in specific tissues such as the RPE and choroid.

High fat diets and a high body mass index have been reported as risk factors for AMD (Cho et al. 2001; Seddon et al. 2001; Seddon et al. 2003b; Seddon et al. 2003c). BMI is not associated with increased susceptibility to AMD in this UK2 cohort (p=0.32). However, adipose tissue is a major source of a variety of pro-inflammatory adipokines, including tumour necrosis factor (TNF) and interleukin-6 (IL6). This leads to both local adipose inflammation and systemic inflammation, rendering obesity a pro-inflammatory state. In agreement with this, in Chapter 4.4.3.1, BMI was identified as a significant confounding effect upon plasma CFD concentrations. In the current chapter, obese individuals (BMI >30) had significantly higher median plasma HTRA1 concentration 24.94±2.06 (s.e.m.) ng/ml), compared to individuals with a BMI in the healthy range (BMI<25; 14.7±0.96 (s.e.m.); p<0.001) in the combined UK2 and SOCCS cohorts. In the UK2 cohort stratified by BMI, the BMI<25 group showed the largest difference in median plasma HTRA1 concentrations in relation to rs10490924 genotype (GG, 17.91±2.17 (s.e.m.) ng/ml; GT/TT, 21.53±2.15 (s.e.m.) ng/ml). Although this difference was not statistically significant, this likely reflected a lack of power due to reduced sample size.

This was confirmed by the subsequent inclusion of plasma HTRA1 measurements from 208 additional disease-free controls with BMI<25. In individuals with BMI<25 in the combined data, the median plasma HTRA1 concentration of individuals with a GG genotype was 12.72±1.21 (s.e.m.) ng/ml. This is significantly lower than median HTRA1 measured in GT/TT individuals (16.08±1.59 (s.e.m.) ng/ml) (p=0.048). Increasing age, BMI and AMD status were identified as confounding factors, all raising plasma HTRA1 concentrations. However, in logistic regression correcting for these covariates, the 4th quartile of plasma HTRA1 measurements remained significantly associated with the risk allele of rs10490924 (p=0.026, OR 2.03, 95% C.I, 1.09-3.78) in the BMI<25 group. Conversely, including only disease-free controls from either UK2 or SOCCS and correcting for BMI and age in logistic regression also found a significant association between plasma HTRA1 and risk genotype (p=0.045, N=485). Power calculations confirmed that the

study was sufficiently well powered to detect a significant difference in plasma HTRA1 measurements in this BMI category.

In the BMI >30 group, the link between genotype and plasma HTRA1 concentration was reduced (Table 6.3), suggesting that increased fat mass leads to higher systemic levels of plasma HTRA1, regardless of genotype. In order to test this hypothesis, data from a microarray experiment performed in the laboratory of Professor Brian Walker was obtained. *HTRA1* expression in adipose biopsy samples obtained from 11 individuals (N=6, BMI<25; N= 2, BMI 25-29.99, N=3, BMI>30) was investigated using the Affymetrix probe set 201185_at. As shown in Figure 6.17A, there was a suggestion of increased intensity of *HTRA1* expression detected in individuals with higher BMI (mean intensity for BMI<25, 5494.7±543.4, mean intensity for BMI>30, 5813.1±304.4). The biggest difference in plasma HTRA1 measurements by rs10490924 genotype was observed in the BMI<25 group. However, there was no obvious relationship between genotype (for the indel variant in *ARMS2*) and intensity of *HTRA1* detected in the microarray (Figure 6.17B).

The small number of samples involved affects the power of this microarray study to detect a significant difference in *HTRA1* expression level by genotype. A minimum of six biological replicates has been suggested to ensure that statistically significant conclusions can be drawn from a microarray (Lee and Saeed 2007). Using genotype and BMI as categories for analysis reduces the number of samples in this study to below this threshold. Moreover, *HTRA1* expression in healthy RPE from aged human donors exhibits intermediate levels of inter-individual variation (Booij et al. 2009). Although Booij et al. did not investigate *HTRA1* expression in relation to genotype, the work of Wang et al. (2010) and Frederich et al. (2011) confirms that *HTRA1* expression can be highly variable, irrespective of genotype. *HTRA1* is up-regulated in response to ageing, cellular stress and in diseases such as arthritis (Ly et al. 2000; Grau et al. 2006). The data shown in this chapter identify BMI as an additional confounding variable. These factors vary between individuals, and will complicate the analysis of a genotypic effect upon *HTRA1* expression. This highlights the benefit of using a large cohort of samples, which have been well characterised for confounding factors such as age, BMI and disease, to generate more robust results.

Elevated plasma HTRA1 concentration in *ARMS2/HTRA1* risk haplotype carriers compared with non-carriers supports a role for HTRA1 rather than ARMS2 in AMD susceptibility. In the UK2 cohort, there was significant or suggestively significant association between AMD and the upper quartiles of plasma HTRA1 (3^{rd} quartile, p= 0.015, 4^{th} quartile p =0.063), when correcting for AMD-risk factors of age, sex, smoking history and BMI. The association between plasma HTRA1 and AMD is not simply a reflection of the increased susceptibility of AMD for carriers of the rs10490924 risk allele in this cohort (GT/TT, $p=2.73x10^{-13}$, OR 3.618 (95% C.I. 2.56 – 5.11)), as the association differs from that seen between genotype and plasma HTRA1 in the same cohort. There was also some evidence that plasma HTRA1 concentrations are higher in AMD cases with choroidal neovascularisation (22.63±2.21 ng/ml) compared to individuals with only geographic atrophy (16.65±2.33 ng/ml). This is in keeping with the more significant association of the risk allele of rs10490924 with CNV, compared to all AMD cases in the UK2 cohort (GT/ TT, $p=2.99 x10^{-17}$, OR 4.445 (95% C. I. 3.145-6.284)). Previous studies have also suggested that the chromosome 10q26 risk-locus increases the risk of development and progression of wet AMD (Dewan et al. 2006; Chen et al. 2011; Sobrin et al. 2011). However, the relatively small number of GA cases in these studies may affect this conclusion, given that other studies find no difference between AMD sub-types and susceptibility as a consequence of chromosome 10q26 haplotype (Cameron et al. 2007).

Interrogation of a microarray data set for a selection of 11 adipose tissue biopsies for variation in *HTRA1* expression level as a function of chromosome 10q26 haplotype and BMI category proved inconclusive (Figure 6.17A and B). However, a high BMI appears to influence plasma HTRA1 concentration. Microarray data, and RT-PCR performed in Chapter 5 (Figure 5.27), detect *HTRA1* transcripts in human adipose tissue cDNA. The precise cellular source of these *HTRA1* transcripts is unclear. Adipose tissue is composed of adipocytes, fibroblasts and macrophages. De Luca et al. (2003) could not detect expression of *HTRA1* in adipocytes. However, *HTRA1* expression ratio is high in adipocytes in the GNF Expression Atlas 2 Data from U133A and GNF1H Chips (http://genome.ucsc.edu/cgi-bin). High HTRA1 levels have been detected in fibroblasts using immunohistochemistry (De Luca et al.

2003), and HTRA1 transcripts were detected in macrophage-like THP-1 cells (Chapter 5). It is therefore likely that the elevation of plasma HTRA1 observed in individuals with high BMI is a result of increased number of fat cells, macrophages and fibroblasts, all of which may express *HTRA1*. Obesity is associated with an increased risk of developing AMD (Seddon et al. 2003b). The role that increased *HTRA1* expression plays in this increased risk of AMD, as a consequence of obesity, remains to be tested. However, if HTRA1 is able to activate CFD, this would contribute to the systemic inflammatory state that is characteristic of obesity (Mathis and Shoelson 2011).

HTRA1 and CFD appear to be expressed in the same cellular contexts and the proteins interact with each other *in vitro* (Chapter 5). The relationship between rs10490924 genotype and plasma CFD in the UK2 cohort was tested using logistic regression, including age, sex, smoking, BMI and AMD status as covariates. The risk allele was significantly associated with the 4^{th} quartile of plasma CFD (GT/TT; p=0.01, OR 1.96, 95% C.I. 1.18-3.26). Although AMD status is a confounding factor, there was no association between the CFH Y402H variant (rs1061170) and plasma CFD (p=0.345). This suggests that the chromosome 10q26 locus may contribute to systemic inflammation by elevating CFD, although the mechanism is unclear. This has previously been suggested for another systemic inflammatory marker, C-reactive protein (CRP). Elevated CRP has been associated with increased risk of AMD progression (Seddon et al. 2010). A recent report suggests that the risk haplotype in chromosome 10q26 is associated with elevated CRP in the serum of 476 Japanese people without macular degeneration (Yasuma et al. 2010). This was most pronounced in individuals aged over 60 years, and is the first report of a link between the chromosome 10q26 AMD-risk locus and chronic inflammation. The association between the rs10490924 risk allele and elevated plasma CFD levels in the UK2 AMD case-control cohort provides an additional possibility to explore in considering the contribution of this locus to AMD susceptibility. Furthermore, evidence has emerged that complement activation (indicated by an elevated ratio of C3/C3d) is observed in AMD cases carrying only the rs10490924 risk allele, without additional variants in complement genes (personal communications, Dr. Anneke den Hollander).

Further investigation of the relationship between the chromosome 10q26 locus, elevated plasma HTRA1 and systemic and chronic inflammation is required. It is also necessary to determine whether elevated plasma HTRA1 concentrations reflect expression at the tissue level. This is especially important in the context of the AMD eye, and in relation to the risk haplotype in the chromosome 10q26 risk locus.

7: Chapter 7

Discussion

7.1 Introduction

Age-related macular degeneration is the leading cause of registered blindness in developed countries, affecting an estimated 50 million people worldwide (VanNewkirk et al. 2000). Despite the considerable impact upon sufferers, effective therapeutic options for this progressive loss of central vision remain elusive. A better understanding of the genetic and molecular basis of AMD is necessary. Increased knowledge of the biological and pathological processes behind the disease may identify new therapeutic targets. Furthermore, identification of genetic risk-factors may allow early identification of at-risk individuals, allowing therapeutic intervention before photoreceptor cell death occurs, thus preventing irreversible loss of vision.

In addition to environmental risk-factors, such as smoking and diet, family history of AMD is one of the most significant epidemiologically identified risk-factors (Klein et al. 2004). Since 2004, considerable progress has been made towards identifying genes in which variants can alter AMD susceptibility. Family-based linkage studies, case-control association studies and, more recently, genome-wide association scans, have led to the identification of components of the complement cascade – *CFH, C2, C3, CFB, CFI, CFHR1* and *CFHR3* genes - as containing risk-modifying variants for AMD (Conley et al. 2005; Edwards et al. 2005; Hageman et al. 2005; Haines et al. 2005; Klein et al. 2005; Magnusson et al. 2005; Zareparsi et al. 2005a; Gold et al. 2006; Hughes et al. 2006; Yates et al. 2007; Fagerness et al. 2009). This has strongly implicated the aberrant regulation of inflammation in the disease process, providing important insights into the pathogenesis of the disease.

An additional locus on chromosome 10q26 has been significantly associated with AMD risk in numerous studies (Majewski et al. 2003; Seddon et al. 2003d; Weeks et al. 2004; Fisher et al. 2005). Three genes (*PLEKHA1, LOC387715/ARMS2* and *HTRA1*) lie in a region spanning 220 kb; controversy over which of these genes contains causative variants has been on-going since the initial reports by Jakobsdottir et al. and Rivera et al. in 2005. Recently, a deletion and insertion in the 3' UTR of *ARMS2* which leads to rapid RNA decay of the *ARMS2* transcript has been identified. The indel occurs along with rs10490924 and rs11200638 in a previously

identified risk haplotype for AMD, and has led to attention being refocused on *ARMS2* as the AMD susceptibility gene (Fritsche et al. 2008). However, the indel is not always associated with loss of *ARMS2* expression (Wang et al. 2010b) and loss of *ARMS2* expression is not sufficient to explain the increased risk of AMD at this locus (Yang et al. 2010).

Meanwhile, variants in *HTRA1* cannot be excluded as susceptibility alleles for AMD. Analysis of allele frequency alone is insufficient to discriminate between potential causative variants in *ARMS2* and those in *HTRA1*, due to the strong linkage disequilibrium between the genes (D'= 0.99; Dewan et al. 2006). Correlating expression data in AMD cases and controls, and a more complete understanding of the function of each protein is vital to determining which gene contributes to AMD susceptibility. This study investigated the expression and function of HTRA1, in order to elucidate the role of the protease in health and disease.

7.2 Summary of results

In this study, interacting partners of HTRA1 were identified using a combination of yeast two-hybrid screening and tandem affinity purification (TAP). This identified a large number of potential interactions, some of which have proposed roles in AMD pathogenesis (Chapter 3). One such interactor, CFD, was selected for further study and was found to be significantly associated with AMD at the genetic and protein level (Chapter 4). The interaction between CFD and HTRA1 was investigated *in vitro* and resulted in activation of CFD and consequently, the alternative complement pathway (Chapter 5). Consistent with this, serum from patients with CARASIL – caused by reduced activity of HTRA1 – showed deficiencies in alternative complement pathway activity. Finally, plasma HTRA1 was found to be significantly elevated in carriers of the chromosome 10q26 AMD-risk haplotype, and in relation to other AMD-risk factors (Chapter 6). These data are consistent with HTRA1 contributing to AMD susceptibility.

7.2.1 Plasma HTRA1 is elevated in carriers of the chromosome 10q AMD-risk haplotype

There has been controversy about the expression level of both HTRA1 and ARMS2 in relation to the AMD-risk haplotype on chromosome 10q26. An ELISA was developed to measure HTRA1 in human plasma. The ELISA was used to measure plasma HTRA1 in 979 individuals, including AMD cases, AMD-free controls and non-examined disease-free controls. Advancing age, high BMI and AMD status were significantly associated with elevated plasma HTRA1 measurements, irrespective of genotype at the chromosome 10q26 locus. Regression analysis was used to correct for these confounding factors, and a significant association between elevated plasma HTRA1 and genotype at rs10490924 was uncovered. Further investigation of the haplotype at this locus is required. However, this is the first report of elevated plasma HTRA1 in carriers of a risk genotype on chromosome 10q26, and adds substantial weight to the argument that HTRA1 may contribute to the pathogenesis of AMD.

It is interesting to note that advancing age and high body mass have been identified as AMD-risk factors. These factors are significantly associated with elevated plasma HTRA1 measurements independently of genotype at rs10490924. Normal age-related changes are known to contribute greatly to the development of AMD, and increased expression of HTRA1 may constitute another age-related change. Likewise, high body mass and high fat diets significantly increase the susceptibility of an individual to AMD. The detection of HTRA1-specific transcripts in adipose tissue cDNA, together with expression data from microarray analysis of 11 adipose tissue biopsies, confirms that HTRA1 is expressed in adipose tissue. This is of particular relevance as CFD, an interactor of HTRA1 identified in this study, is abundantly expressed in adipose tissue. CFD contributes to the systemic inflammatory state observed in obesity. Systemic inflammation has been observed in AMD cases relative to controls (Hakobyan et al. 2008; Scholl et al. 2008; Reynolds et al. 2009; Hecker et al. 2010).

The identification of confounding factors for *HTRA1* expression levels may help to explain some of the discrepant findings previously reported for HTRA1 expression levels in relation to genotype (Dewan et al. 2006; Yang et al. 2006; Kanda et al. 2007; Chowers et al. 2008; Kanda et al. 2010). These studies used small

numbers of tissue samples, and did not account for age, BMI or other potential confounding factors in their analyses. Although measuring the systemic concentration of HTRA1 in plasma is a long way away from the site of the AMD lesion, this study has substantial power to detect differences of this magnitude, corrected for confounding factors.

7.2.2 The extracellular HTRA1 Interactome

HTRA1 is a stress-induced serine protease with a poorly characterised interactome and substrate specificity. Interacting partners of HTRA1 were identified in a yeast two-hybrid screen performed in a placental cDNA library, and by tandem affinity purification of tagged-HTRA1 and interactors from the cell lysate and conditioned media of HEK293T cells and from RPE1 cells. More than 100 potential interactors were identified using these two methods. Several of these confirmed previously identified interactions (tubulin A1, COL3A1, COL1A1), but many potential interactions had not previously been reported.

HTRA1 is a secreted serine protease, and the majority of interactors identified are localised to the ECM and extracellular environment. A proposed extracellular interactome for HTRA1 was constructed (Figure 3.8). An abundance of ECM structural constituents were identified as interacting with HTRA1 (including COL1A1, COL3A1, FBLN1, FN, SPARC, THBS1). Many of these are expressed by RPE cells and are found in the Bruch's membrane (Figure 1.4). There was substantial overlap between the HTRA1 interactome shown in Figure 3.8 and the network of proteins which are differentially expressed in AMD and disease-free primary RPE cells (An et al. 2006). Many of these proteins have known roles in angiogenesis, TGF-β signalling and regulation of matrix metalloprotease activity. Furthermore, expression of several of these interactors in the eye has been reported to increase with age, or to be altered in AMD. This suggests that ECM remodelling mediated by HTRA1 activity may influence a variety of pathways involved in AMD pathogenesis, although further work is required to confirm the mechanisms of action.

Several of the novel interactions identified in the yeast two-hybrid screening or by TAP were validated using GST-pulldown assays and protease assays using

recombinant proteins. Thrombospondin-1, identified as an interactor of HTRA1 using TAP, was shown to interact with, and to be a substrate for HTRA1 (Figure 3.13B). Thrombospondin-1 has been shown to localise to the basement membrane of RPE cells, and to play a role in activating TGF-β signalling, inhibiting the action of VEGF, MMP2 and MMP9 in the ECM. The interaction with connective tissue growth factor, which is also involved in VEGF and TGF-β signalling pathways, was similarly validated (Figure 3.15). CTGF expression is elevated in AMD eyes, and plays a role in photoreceptor survival, ECM remodelling and fibrovascular scarring. It is encouraging to note that both CTGF and THBS1 have previously been implicated in AMD (He et al. 2003; He et al. 2006; Uno et al. 2006; Bhutto et al. 2008). Further investigation of these proteins is warranted, both as substrates for HTRA1 and as independent risk-factors for disease.

Complement Factor D (CFD) was also identified as a putative interactor of HTRA1 in the yeast two-hybrid screening. This is the first report of a direct interaction between an activator of the alternative complement pathway and HTRA1. The minimal binding site for the interaction incorporated the 5 amino acid pro-peptide of CFD, which must be cleaved to activate the mature CFD protein. *In vitro* GST-pulldown assays confirmed an interaction between the mature CFD protein and HTRA1; however, the activation peptide was both necessary and sufficient for CFD to be a substrate for HTRA1.

7.2.3 The contribution of CFD to AMD-susceptibility

The alternative complement pathway is accepted to play a major role in the pathogenesis of AMD. Complement proteins have been identified in drusen (Hageman et al. 2001; Crabb et al. 2002). Variants in several alternative complement pathway genes have been associated with AMD susceptibility (Conley et al. 2005; Edwards et al. 2005; Hageman et al. 2005; Haines et al. 2005; Klein et al. 2005; Magnusson et al. 2005; Zareparsi et al. 2005a; Gold et al. 2006; Hughes et al. 2006; Yates et al. 2007; Fagerness et al. 2009). Activated components of the alternative pathway are elevated in plasma from AMD cases compared to controls (Hakobyan et al. 2008; Scholl et al. 2008; Reynolds et al. 2009; Hecker et al. 2010). However,

previous studies had not shown association between variants in CFD and AMD, although this was confounded by small numbers of cases and controls (Zeng et al. 2010). Two intronic variants in CFD were genotyped in a UK case-control cohort, and the minor allele of rs3826945 SNP was found to be significantly associated with an increased risk of AMD (OR 1.44, 95% C.I. 1.04-2.00, p=0.028). Subsequently, a further UK series, three case-control series from the USA and one comprised of Dutch and German individuals was also genotyped for this SNP. None of the four additional cohorts showed a significant association with AMD independently, but meta analysis of the combined cohorts (4765 cases and 2693 controls) identified a significant association between AMD and the minor allele of rs3826945 (OR=1.11, C.I. 1.01-1.23, p=0.032). This variant has a small effect on AMD-risk (OR =1.1) and is unlikely to explain much of the population-attributable risk of AMD. The apparent differences between the two UK series, and the series from North America and Europe is difficult to account for. Similar minor allele frequencies were observed between cases and controls in all series (and in the previously reported investigation of CFD variants in relation to AMD). This suggests that population substructure is unlikely to account for the differences observed. This is consistent with an earlier study which did not find this region on chromosome 19 to be subject to population stratification within the UK (WTCCC 2007). It seems likely that incomplete BMI (or other phenotypic characteristics) information for all cohorts may help to explain the discrepancies between series. Recent genome-wide association scans have not identified variants in CFD as AMD-susceptibility loci (Chen et al. 2010; Yu et al. 2011). A potential benefit of investigating an association between AMD with variants in a specific gene is that the stringent thresholds used in correction for multiple testing are not required. This may allow the positive identification of variants with a small effect on disease risk to be identified.

The variant in CFD that was associated with AMD is located in intron 4. This SNP is not predicted to affect exon splicing, as has been reported for other intronic variants in genes associated with AMD (Kralovicova and Vorechovsky 2009). Sequencing of the coding region of *CFD* did not identify coding changes in LD with rs3826945 that might result in altered function of CFD. A reasonable hypothesis is that this variant is in linkage disequilibrium with an unidentified variant(s) that

affects expression levels of CFD. This would be consistent with the observation of elevated plasma CFD concentrations in AMD cases relative to controls, and also to systemic inflammation having a role in AMD. The current study is underpowered to detect differences in CFD expression in relation to SNP genotype, due to the small effect size and confounding factors of age, sex and AMD.

Copy number variation is becoming increasingly well studied in relation to diseases, including systemic lupus erythematosus, autism, rheumatoid arthritis and cardiovascular disease (Fanciulli et al. 2010). Copy number variation affecting *CFD* was observed in a small number of AMD cases and controls; however, there was no significant difference in the frequency of duplications or deletions between groups. Further investigation into the role of copy number variation (as has been seen with *CFHR1* and *CFHR3*) in AMD genetics may be useful to develop a complete understanding of the genetic basis of the disease.

7.2.4 HTRA1 activates CFD in vitro: implications in AMD

CFD was identified as an interactor of HTRA1 in a yeast-two hybrid screen. The minimal binding site required for the interaction encompasses the five amino acid activation peptide of CFD. Subsequent experiments using synthetic peptides and purified CFD showed that the activation peptide is necessary and sufficient for HTRA1-mediated cleavage of CFD. The mature CFD protein, which lacks the activation peptide, is not subject to cleavage by HTRA1 *in vitro*.

The functional consequences of HTRA1 cleaving recombinant proCFD were investigated in several assays of alternative complement pathway activity. In each assay, proCFD that had been pre-treated with HTRA1 was able to activate the alternative complement pathway *in vitro*. This was determined by monitoring the cleavage of Factor B, or by the formation of the MAC and subsequent lysis of red blood cells.

The finding that HTRA1 is able to activate proCFD *in vitro* is intriguing, given that the protein responsible for the activation of proCFD in humans remains unidentified. A recent study found that Masp1 is responsible for the activation of proCFD in mice (Takahashi et al. 2010). However, in humans, CFD is thought to be

activated during secretion, and *MASP1* transcripts were not detected in adipose tissue or in other major sources of CFD production. *HTRA1* is expressed in these tissues, and in cell-lines with physiological relevance to AMD. Co-expression is required for the *in vivo* interaction of the proteins, and *CFD* and *HTRA1* appear to be co-expressed in a wide range of tissues.

7.2.5 Reduced HTRA1 activity correlates with reduced alternative complement pathway activity

Several serine proteases have been found to activate proCFD *in vitro*, although these are not considered candidates for the *in vivo* activation (Fearon et al. 1974; Yamauchi et al. 1994). The relationship between HTRA1 activity and alternative complement pathway activation (as a reflection of proCFD activation) was assessed in the sera from CARASIL patients. These individuals have mutations in HTRA1 which cause reduced function of the protease (Hara et al. 2009). Reduced HTRA1 activity causes uncontrolled TGF-β signalling, thickening of cerebral arteries and ischeamic stroke. There have been no reports of increased susceptibility to bacterial infection in CARASIL patients, such as would suggest a deficiency in the alternative complement pathway.

However, in the sera from three patients with mutations in HTRA1, reactive lysis of sheep red blood cells mediated by the alternative complement pathway was significantly reduced, relative to disease-free controls. This does not seem to reflect a systemic deficiency in alternative complement pathway components: CFD concentrations measured by ELISA were within the normal range previously reported (Hiemstra et al. 1989). Factor B concentrations, as seen in Western blots, were variable, but this is also consistent with the wide range of CFB that has been reported in healthy individuals (Reynolds et al. 2009; Scholl et al. 2008; Hecker et al. 2009). Sera were supplemented with Cobra Venom Factor (a C3b analogue), so C3 deficiency is not a factor. Additionally, the convertase formed by CVF is not subject to inhibition by CFH or CFI; high concentrations of the endogenous inhibitors of complement activation cannot explain the differences observed in CARASIL sera.

Cleavage of endogenous factor B in CARASIL sera was assessed by Western blotting of sera supplemented with CVF. Conversion of Factor B to Bb did not

appear to be grossly affected, although may be slightly reduced as a proportion of total factor B. However, a high molecular weight complex was recognised by the anti-Factor B antibody in all of the CARASIL sera, and not in control sera. The molecular weight is consistent with the CVF(C3b)-Factor B complex. This is the labile pro-C3 convertase, in which Factor B is held in an "open" conformation to allow cleavage by CFD (Forneris et al. 2010). The presence of this pro-C3 convertase in the sera of CARASIL patients is consistent with reduced CFD-mediated cleavage of Factor B to form the C3bBb convertase, implicating HTRA1 in activation of proCFD. Given that the CARASIL sera retain the ability to activate factor B and the C3 convertase, it is unsurprising that alternative complement pathway deficiency has not been described in CARASIL patients. Previous studies of CFD deficiencies caused by mutations in *CFD* have found that increased susceptibility to bacterial infection appears to affect only some individuals with a complete absence of CFD. Individuals who are heterozygous for loss of function mutations in *CFD* are not reported to have increased susceptibility to infection, and sera are normal in complement assays (Hiemstra et al. 1989; Biesma et al. 2001; Sprong et al. 2006).

7.3 Proposed roles for HTRA1 in AMD pathogenesis

Plasma HTRA1concentration was significantly elevated in disease-free carriers of the chromosome 10q26 risk haplotype. The effect of the risk haplotype on the neighbouring protein ARMS2 remains unclear, but this implicates HTRA1 in AMD susceptibility. In plasma, the concentration of HTRA1 increases with age and high BMI – factors associated with increased risk of developing AMD. Elevated plasma HTRA1 concentrations were also measured in AMD cases relative to controls.

This study has identified a number of potential substrates for the protease. These suggest a role for HTRA1 in neovascularisation, wound healing following chronic inflammation, complement regulation and thickening of Bruch's membrane with age. The proposed contribution of HTRA1 to disease is summarised in Figure 7.1.

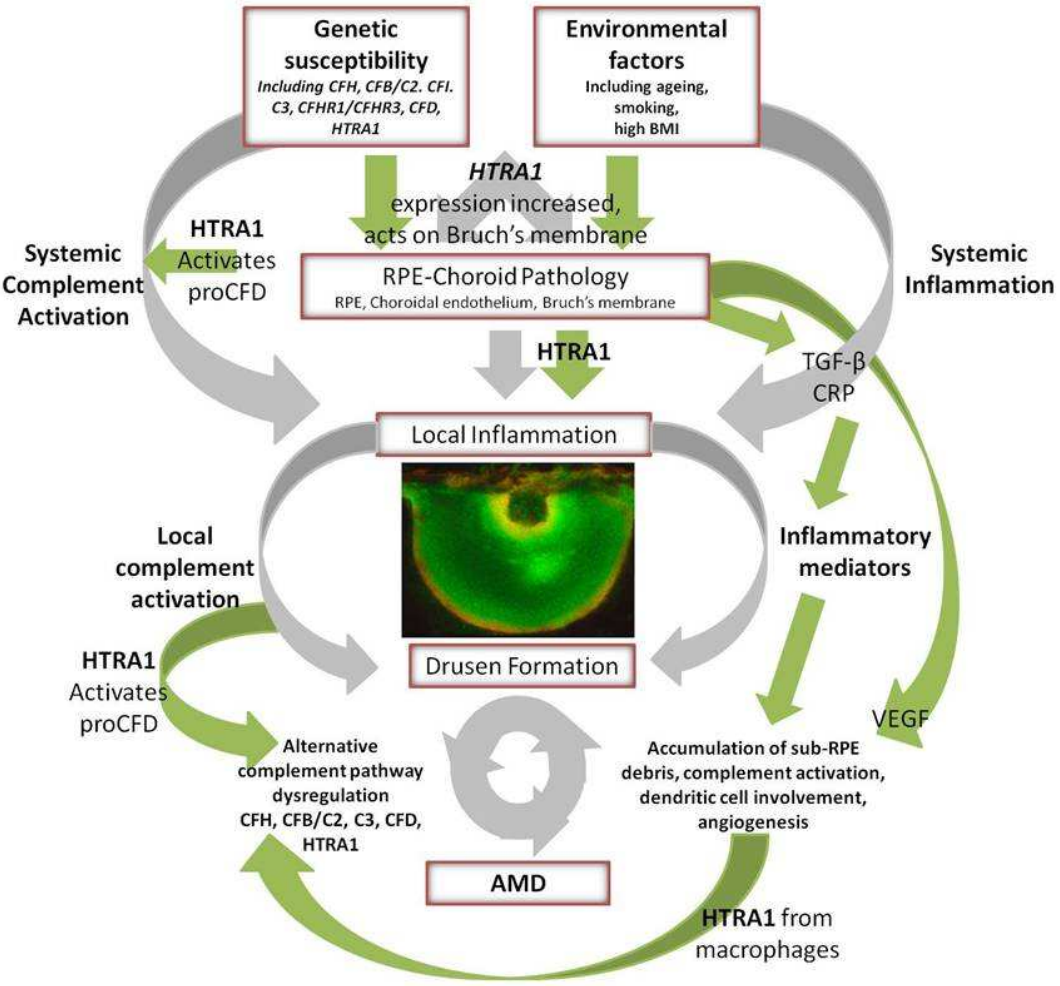

Figure 7.1 Proposed involvement of HTRA1 in AMD pathogenesis.
The formation of drusen and subsequent development of AMD pathology is increased by, and contributes to, local and systemic inflammation. Ageing, environmental factors and genetic factors alter susceptibility to disease. HTRA1 is elevated in carriers of the chromosome 10q26 AMD-risk haplotype, with increasing age, and by high BMI, and may contribute to a variety of stages in AMD pathogenesis, indicated by green arrows. Figure adapted from Anderson et al. (2010).

7.3.1 Remodelling of the Bruch's membrane by HTRA1

The interactome identified by TAP and yeast two-hybrid screening showed that HTRA1 interacts with a broad range of ECM proteins. The potential roles of several of these interactions in health and disease were discussed in Chapter 3. Many of the proteins are important components of Bruch's membrane (BM) (Booij et al. 2010), suggesting that the BM may be particularly susceptible to the activity of HTRA1. This is consistent with the expression of HTRA1 by RPE cells. Changes to the Bruch's membrane ECM may play a role in drusen formation and in initiating AMD (Spraul et al. 1999; Chong et al. 2005).

In agreement with previous reports (De Luca et al. 2004; Murwantoko et al. 2004), several types of collagen were identified as interactors of HTRA1 (COL1A1, COL3A1, COL5A2, COL12A1). These are abundant throughout Bruch's membrane, but particularly in the collagenous layers. Fibronectin was also previously reported as an interactor and substrate of HTRA1. Fibronectin is a component of the collagenous layers of the BM, and is also important in the formation of blood vessels. Novel interactions with Laminin alpha 4, and with thrombospondin-1 were identified. These proteins are found abundantly in the basement membrane of both the RPE and choroidal epithelium (Carron et al. 2000; Miyajima-Uchida et al. 2000; Booij et al. 2010).

BM is vital to maintaining healthy RPE, playing a crucial role in the exchange of biomolecules from the choroid and the photoreceptors. Damage to Bruch's membrane – for example, caused by age-related changes or oxidative damage – compromises the RPE layer, and has detrimental consequences for the overlying photoreceptors. Indeed, age-related changes in BM are a contributing factor for the development of AMD. It is possible that HTRA1-mediated degradation or cleavage of some components of the BM may further exacerbate such damage. Such a sequence of events has previously been suggested as a result of the proteolysis of vitronectin and clusterin by HTRA1 (An et al. 2010). These proteins inhibit the formation of the terminal complex of the complement pathway. Their degradation may result in increased RPE cytolysis and inflammation. For example, expression of *THBS1* increases in the retina with age (Chowers et al. 2003) but is

decreased in AMD eyes (Uno et al. 2006; Bhutto et al. 2008). If reduced *THBS1* expression is pathogenic in AMD as has been suggested, the activity of HTRA1 may contribute further to the associated processes.

Thrombospondin-1 is a multi-functional protein. It is feasible that the cleavage of thrombospondin-1 by HTRA1 may affect a diverse array of processes in the eye including ECM deposition and turnover (through inhibiting MMP2 and MMP9), RPE cell-matrix interactions and regulation of inflammation. Furthermore, this protein has both anti-angiogenic and pro-angiogenic properties, including inhibition of VEGF signalling and activation of TGF-β signalling (Good et al. 1990; Murphy-Ullrich et al. 1992; Nicosia and Tuszynski 1994; Gupta et al. 1999; Bein and Simons 2000; Rodriguez-Manzaneque et al. 2001; Sheridan et al. 2002; Zamiri et al. 2005). Dysregulation of these processes following aberrant proteolysis may have profound effects, in relation to both the dry and wet forms of AMD.

A second possibility is that HTRA1 cleaves components of the ECM, releasing peptide fragments that have different roles to the full-length protein. This has been observed with fragments of CTGF and THBS1, amongst others. If the balance of proteolysis is disturbed – by increased levels of HTRA1 as a result of genotype, age, or BMI – it may have detrimental effects. Fragments of CTGF have fibrotic activity, and lead to deposition of additional ECM components (Ruiz-Ortega et al. 2006). This has been implicated in fibrovascular scarring but may also have a role in the pathological thickening of the BM. Given that CTGF has been reported to enhance survival of photoreceptor cells *in vitro* (Hauck et al 2008), the activity of HTRA1 towards this particular substrate may also affect photoreceptor cells directly.

Thirdly, cleavage of ECM components such as collagen may have a direct effect on signalling pathways, via the release of ligands which are normally bound to matrix proteins. MMP9-mediated cleavage of collagen fibres releases mature TGF-β from the latency associated peptide (LAP) and TGF-β–binding protein (LTBP) which are responsible for sequestering the ligand in the ECM (Taipale et al. 1994; Yu and Stamenkovic 2000; Dallas et al. 2002). In addition to MMPs, serine proteases can also release TGF-β from the ECM, so it is feasible that HTRA1 activity may affect signalling pathways.

7.3.2 Regulation of TGF-β signalling by HTRA1

The TGF-β signalling pathway has many roles during development, and in adult tissues. In addition to regulating cell function, proliferation, differentiation, and migration (Massague 1990), TGF-β signalling is also involved in modulating inflammation, immune homeostasis and wound repair (Wan and Flavell 2007). The TGF-β superfamily includes TGF-βs, bone mophogenic proteins (BMPs) and growth differentiation factors (GDFs). Members of each of these families of ligands have been found to interact with HTRA1 intracellularly and extracellularly, resulting in inhibition of TGF-β signalling temporally and spatially (Oka et al. 2004; Shiga et al. 2011). GDF15 was identified as an interactor of HTRA1 in this study, although further experiments were not performed. However, HTRA1 appears to be an important antagonist of TFG-β signalling, as shown when the activity of the protease is reduced in CARASIL (Hara et al. 2009). Protease activity is important to the regulation of TGF-β by HTRA1 (Oka et al. 2004; Hara et al. 2009; Shiga et al. 2011). Reduced HTRA1 activity leads to uncontrolled TGF-β signalling and thickening of cerebral small vessels by deposition of fibronectin (Hara et al. 2009).

The proTGF-β proprotein is processed in the trans-Golgi network by proprotein convertases such as furin, to generate mature TGF-β and a latency-associated peptide (LAP). Dimers of TGF-β form a non-covalent complex with LAP, which then binds to LTBP (Miyazono et al. 1991). This complex is secreted from the cell, where it becomes anchored to the ECM. Once sequestered in the ECM, mature TGF-β can be released into the extracellular space by the action of MMPs, serine proteases and acidic microenvironments (Annes et al. 2003). As hypothesised earlier, HTRA1 may be involved in the release of TGF-β from the ECM, activating signalling in this pathway.

Conversely, recent work by Shiga et al. (2011) has shown that HTRA1 directly cleaves the pro-domain of proTGF-β1 in the endoplasmic reticulum (ER). This results in degradation of the processed TGF-β1 product by the ER-associated degradation (ERAD) system, reducing the amount of mature TGF-β1. This novel mechanism of regulating TGF-β1 may be specific to the tissues affected by CARASIL, which include human cerebral small vessels, but may also have

implications in AMD where HTRA1 appears to be up-regulated, particularly in carriers of a risk genotype on chromosome 10q26.

The contribution of HTRA1 to dysregulation of TGF-β signalling becomes more complex with the consideration of thrombospondin-1 and CTGF, two substrates for HTRA1 identified in this study. Thrombospondin-1 binds the growth factor in its active and latent forms, and also activates TGF-β signalling (Schultz-Cherry and Murphy-Ullrich 1993). CTGF is a downstream mediator of the signalling pathway. Hypothetically, increased amounts of HTRA1 may reduce the amount of mature TGF-β secreted to the extracellular space. Cleavage of thrombospondin-1 may independently reduce activation of the pathway further. Inhibiting TGF-β signalling has been implicated in increased vascular and neural cell apoptosis in the mouse retina, resulting in decreased retinal function (Walshe et al. 2009). Conversely, minimising TGF-β has also been suggested to be beneficial in reducing senescence-associated changes (such as the expression of *CTGF* and fibronectin) in human RPE, such as is seen in early AMD (Yu et al. 2009). HTRA1 may also be responsible for increased release of mature TGF-β from the ECM by degrading ECM components, including thrombospondin-1, fibronectin and decorin (Canfield et al. 2007) thus activating the pathway. CTGF cleavage may result in the formation of an active fragment which increases fibrosis as a result of TGF-β signalling.

Without knowing the consequences of HTRA1-mediated cleavage upon protein function, it is difficult to speculate how TGF-β signalling may be affected. However, several components of the HTRA1 interactome may influence TGF-β signalling positively or negatively in a complicated loop. This is likely to affect processes including inflammation, ECM deposition and photoreceptor survival, and may contribute towards AMD pathogenesis.

7.3.3 Alterations in VEGF signalling by HTRA1

Wet AMD is a severe form of AMD, in which neovascularisation occurs from the choroid in the sub-macular region. The new blood vessels are fragile and prone to breakage. This can lead to leading to bleeding in the sub-retinal space, causing RPE and photoreceptor cell death and irreversible loss of central vision and fibrovascular

scarring. Under normal conditions, the choroidal vasculature is maintained by VEGF, which stimulates angiogenesis, and PEDF, which suppresses angiogenesis. Neovascularisation inwards from the choroid is thought to occur as a result of imbalances of these growth factors (Witmer et al. 2003).

Normally, RPE cells constitutively express VEGF from the basal side, towards the choroid. PEDF is expressed in the opposite direction, towards the photoreceptors (Maminishkis et al. 2006). This maintains the choroidal vasculature and the avascular nature of the inner retina. For unknown reasons - possibly as a consequence of RPE dysfunction - this balance appears to change with age and in AMD.

In wet AMD cases, VEGF expression is increased and PEDF expression is suppressed (Kvanta et al. 1996; Bhutto et al. 2006). This is also observed in experimental CNV induced by photocoagulation, when neovascularisation occurs for several days following treatment (Renno et al. 2002). However, once the RPE cells repopulate the surface of the lesion (within a few weeks), PEDF expression increases and VEGF expression decreases. This results in resolution of the new vessels (Miller et al. 1990). When RPE cells are killed by injection of sodium iodate at the same time as photocoagulation, no new vessels form. If sodium iodate is used to kill the RPE cells 4 days later, the new vessels continue to grow rather than regressing (Yamagishi et al. 1988). Thus, RPE cells obviously play a key role in regulating vascularisation in the choroid.

The significant contribution of VEGF to wet AMD has been shown by the success of treatment with anti-VEGF agents (Boyer et al. 2007; Kaiser et al. 2007). In addition to suppressing CNV, anti-VEGF therapy may also directly counteract the VEGF-mediated loss of tight junction integrity on the apical surface of RPE in confluent culture (Ablonczy and Crosson 2007). Anti-VEGF agents such as Lucentis and Avastin not only influence CNV, but also RPE cell integrity.

However, regulation of pro- and anti-angiogenic growth factors involves not only the expression of these factors by the RPE and response by endothelial cells, but also the ECM (Folkman and Shing 1992). Proteins and proteoglycans of the ECM, and biologically active fragments of these components generated by proteolysis, can affect angiogenesis directly (Davis et al. 2000). Sequestered angiogenic factors are

also released from the matrix by proteolysis (Taipale and Keski-Oja 1997; Iozzo and San Antonio 2001), leading to rapid and local signalling cascades. Several of the interactors of HTRA1 in the ECM that were identified in this study have been shown to influence angiogenesis. For example, soluble fibronectin up-regulates VEGF in RPE cells, which can promote angiogenesis (Mousa et al. 1999). Fragments of osteonectin can stimulate angiogenesis (Bornstein and Sage 2002), and have previously been implicated in VEGF-induced CNV (Nozaki et al. 2006b). CTGF has been shown to co-localise with TGF-β and VEGF to CNV membranes in AMD eyes (Watanabe et al. 2005), and to promote angiogenesis (He et al. 2003). Thrombospondin-1 appears to directly bind to and inhibit VEGF, and competes with VEGF for binding to heparan sulphate on endothelial cell surfaces to inhibit angiogenesis (Gupta et al. 1999). Thrombospondin-1 also appears to have pro-angiogenic activity in the sub-retinal space, based on evidence from an *in vitro* study using RPE cells (Mousa et al. 1999). This contradicts a predominantly anti-angiogenic role for thrombospondin-1 in other tissues (Good et al. 1990).

In this study, HTRA1 cleaved thrombospondin-1 *in vitro*. Thrombospondin-1 contains both pro- and anti-angiogenic domains (Good et al. 1990; Taraboletti et al. 1990; Taraboletti et al. 2000); differential cleavage may explain these contradictory roles. Further work is required to determine the consequences of this upon the activity of thrombospondin-1 in relation to angiogenesis. However, it is plausible that cleavage of thrombospondin-1 in Bruch's membrane may release the pro-angiogenic fragment of the protein, and/or release sequestered VEGF. This is likely to disrupt the balance of angiogenic signalling at the interface between the RPE and choroid, and may contribute to CNV. Similar theories may be proposed for other substrates of HTRA1 in the ECM that have been implicated in angiogenesis. In humans, the chromosome 10q26 risk haplotype is associated with increased susceptibility to both wet and dry forms of AMD (Cameron et al. 2007). However, mouse models over-expressing HTRA1 in the RPE may suffer from more severe CNV induced by laser injury (personal communications, Dr. Yingbin Fu). This is consistent with the protease exacerbating wet AMD in some cases.

7.3.4 Activation of the alternative complement pathway by HTRA1

There is overwhelming evidence that the alternative complement pathway is involved in the pathogenesis of AMD. This includes genetic association with variants in *CFH, C2/CFB, C3* and *FI* (Edwards et al. 2005; Haines et al. 2005; Klein et al. 2005; Gold et al. 2006; Yates et al. 2007; Fagerness et al. 2009). Proteomic studies have identified complement proteins in drusen, the characteristic hallmark of AMD (Hageman et al. 200; Crabb et al. 2002; Johnson et al. 2002), and more recently, systemic activation of complement has been reported in the plasma of AMD cases relative to controls (Scholl et al. 2008; Reynolds et al. 2009; Hecker et al. 2010). In this study, an intronic variant in *CFD* – the central activator of the alternative complement pathway – was associated with increased susceptibility to AMD. Additionally, plasma CFD concentrations were significantly higher in AMD cases than controls. This is consistent with chronic activation of complement contributing to AMD pathogenesis.

In this study, HTRA1 was found to specifically cleave the activation peptide of proCFD. The specificity of cleavage was somewhat surprising, given the previously reported role for HtrA proteins in degrading mis-folded proteins (Clausen et al. 2002). However, consistent with this dual role, bacterial HtrA family members are involved in pro-peptide processing and in maturation of a native host protein during secretion, in addition to degradation of misfolded proteins (Poquet et al. 2000).

The action of HTRA1 upon proCFD resulted in the activation of the alternative complement pathway *in vitro* assays performed using CFD-depleted human serum. Conversely, in sera from CARASIL individuals with reduced HTRA1 activity, the alternative complement pathway was less active than in normal sera. This is an exciting discovery, given that the enzyme responsible for the conversion of the inactive zymogen proCFD to the mature CFD which circulates in the blood in humans is unknown (Fearon et al. 1974; Lesavre and Müller-Eberhard 1978; Yamauchi et al. 1994). Furthermore, this is the first report of a link between a major genetic risk factor for AMD (of largely unknown function) and alternative complement pathway activation.

Can clues regarding the role of HTRA1 in activating CFD, and hence the alternative complement pathway, be gleaned from other pathological conditions? *HTRA1* is highly expressed in the placenta, where it is proposed to be involved in extensive tissue remodelling (De Luca et al. 2003; De Luca et al. 2004). Complement pathways are activated during normal pregnancy (Abramson 1992). Excessive activation of the alternative pathway has been associated with complications of pregnancy. These include spontaneous abortion in mice with high levels of adipsin/Cfd (Takeshita et al. 2010). In humans, elevated levels of Bb, produced by CFD-mediated cleavage of C3b-bound factor B, have been found in pre-eclampsia (Lynch et al. 2008) and pre-term labour (Vaisbuch et al. 2009). Excessive activation of the alternative complement pathway can also lead to pregnancy-associated atypical hemolytic uremic syndrome (Fakhouri et al. 2010).

Of these conditions, over-expression of *HTRA1* has previously been implicated in pre-eclampsia (Ajayi et al. 2008; Lorenzi et al. 2009). Interestingly, risk variants in complement regulatory genes, including MCP and CFI, have recently been shown to predispose women to the condition (Salmon et al. 2011). Other known risk factors for pre-eclampsia include older maternal age, obesity, oxidative stress and smoking. Thus, there are striking parallels between risk factors for pre-eclampsia and AMD, both conditions in which the alternative pathway appears to be pathologically activated and in which HTRA1 concentrations are elevated. Given that the interaction between HTRA1 and CFD was identified in yeast two-hybrid screening performed in a placental cDNA library, it would be fascinating to test for a genetic association between the chromosome 10q26 risk haplotype and pre-eclampsia; such investigations have not been reported to date.

7.4 Future work

It is unclear whether genetic variants in *HTRA1* influence risk for AMD, or whether the genetic association with AMD on chromosome 10q26 can be attributed to variants in the gene encoding the largely uncharacterized ARMS2 protein. In addition to showing that HTRA1 is elevated in the plasma of individuals carrying the risk haplotype at this locus, this study also implicates HTRA1 in a variety of

processes which are dysregulated in AMD pathogenesis. Perhaps the most intriguing finding of the study is that HTRA1 is capable of activating proCFD *in vitro*.

Although alternative complement pathway dysregulation plays a key role in the pathogenesis of AMD, and other diseases, there is still much to discover about the regulation and activation of the pathway. This is of particular importance at sites such as the RPE/choroid and retina, which are subject to attack in AMD, but also the source of systemic activation in the human body.

A key issue is the identity of the enzyme responsible for the activation of the proCFD zymogen into the mature CFD which circulates in the blood. Several serine proteases can convert the propeptide into mature CFD *in vitro* when present in catalytic excess (Fearon et al. 1974; Yamauchi et al. 1994). These proteases, including thrombin and trypsin, are not thought to be physiologically responsible (Takahashi et al. 2010). Recent work by Takahashi et al. has suggested that the mannose-binding lectin-associated serine protease-1 (Masp1), a component of the lectin pathway, is responsible for activating CFD in mice. However, in humans, *MASP1* expression does not correlate with the major sites of *CFD* expression (White et al. 1992). It is possible that this is a fundamental difference between mouse and human complement pathways. Indeed, the alternative complement pathway of mice and humans is known to differ (Holers et al. 1992). CFD itself shares only 72% identity between mouse and human, and the activation peptide for the two species differs by one amino acid. Mouse CFD is heavily glycosylated and this appears essential for activity (Rosen et al 1989), whilst human CFD is not modified in this way. These differences may alter substrate recognition by various proteases. Alternatively, it may suggest that several proteases are responsible for activating proCFD in a variety of contexts. This is supported by the observation that one of the CARASIL patients (CARASIL2) has a premature stop codon in *HTRA1* (R370X), resulting in nonsense mediated decay and absence of the protein in fibroblasts (Hara et al. 2009). This individual shows 15% of the normal level of alternative complement pathway-specific red blood cell lysis. Therefore, some active CFD is present in their serum. This may represent proCFD that escapes activation by HTRA1 during maturation and secretion, and is activated by MASP1 in the plasma. This could be addressed using mass spectrometry to quantitate proCFD in CARASIL

sera, relative to normal sera. This was not possible using Western blotting due to the difficulty of resolving the small shift in molecular weight resulting from activation of the 5 amino acid activation peptide. Mass spectrometry could also be utilised to identify the high molecular weight complex containing factor B that is detected in CARASIL sera following addition of CVF. These two pieces of data would provide powerful evidence that HTRA1 is involved in the activation of CFD in humans. The remaining alternative complement components should also be measured in these samples to confirm that there is no deficiency of C3 or factor B or excess of inhibiting factors (CFH, CFI). Normal levels of MASP1 should also be confirmed. It is worth noting that variants in *MASP1* have not been associated with AMD (Ennis et al. 2008)

In addition to the potential impact upon the alternative complement pathway, investigation of HTRA1-mediated changes in Bruch's membrane remodelling, drusen formation, TGF-β signalling and angiogenesis should be performed. Several of the other interactors of HTRA1 that were identified in this study – for example, thrombospondin-1 and connective tissue growth factor – may have relevance to AMD pathogenesis, and are suitable targets for further investigation. It would be useful to study protein interactions and co-localisation in human eyes (and placental tissue), although these are understandably difficult to obtain. Cell culture systems utilising siRNA knock-down of HTRA1 and transfection to over-express the protease could be used to investigate the effect of protease activity upon signalling. However, it seems likely that the complex layered structure of the retina, specifically the interplay between the choroid, Bruch's membrane and RPE, may be important in elucidating the whole picture. A recent report has shown that stem cells can differentiate to form early retinal structures *in vitro* (Eiraku et al. 2011). However, such *in vitro* organogenesis not easily achieved, and has yet to be developed for human eyes. Rather, valuable information may be obtained from mice in which HTRA1 is absent or over-expressed. Although such animals have yet to be reported, they are available (personal communications, Dr. Elod Kortvely, Dr. Ulrich Luhmann).

A specific inhibitor of HTRA1 would be a useful tool for investigating this protease, both in cell-culture and in animal models. This may also have therapeutic

potential in AMD in the future, although there are clear risks associated with reduced HTRA1 activity, as observed in CARASIL. The potential for partial inhibition of the specific cleavage of proCFD by HTRA1 may provide a better therapeutic target, with fewer "off-target" effects than inhibition of the either HTRA1 or activated CFD. The therapeutic potential of inhibiting CFD is already being explored in clinical trials.

The data presented in this study strongly suggest that HTRA1 plays a role in AMD pathogenesis, expanding considerably upon the roles of this protease in AMD. However, these data do not exclude a role for ARMS2 in disease, as HTRA1 may be up-regulated by the risk haplotype that either results in loss of ARMS2 protein, and/or contains the A69S coding change in ARMS2 (Yang et al. 2010). The current confusion regarding the effect of the indel upon *ARMS2* expression complicates this issue. If the indel does result in loss of ARMS2 protein (Fritsche et al. 2008; Zang et al 2010), some 40% of individuals of Caucasian ancestry will have only half the normal level of ARMS2 protein. Individuals who are homozygous for the indel (approximately 2-5% of Caucasians) will have no detectable ARMS2 (Allikmets and Dean 2008). Further confusing the potential impact of a deficiency of ARMS2 in relation to AMD risk is the observation that another variant (R38X) in *ARMS2,* which should also lead to nonsense-mediated decay of the transcript, occurs on a haplotype which is considered neutral or weakly protective for the disease (Allikmets and Dean 2008). However, if the indel does not result in loss of ARMS2 as has recently been suggested (Wang et al. 2010b), then attention must be given to the functional effect of the A69S variant in addition to the consequences of *HTRA1* up-regulation. Although the role of ARMS2 remains to be clarified, the multi-functional serine protease HTRA1 seems likely to affect the balance of BM remodelling, angiogenic signalling and inflammation, and to contribute to the pathogenesis of AMD.

Bibliography

Ablonczy Z, Crosson CE (2007) VEGF modulation of retinal pigment epithelium resistance. Experimental Eye Research 85:762-771

Abraham DJ, Shiwen X, Black CM, Sa S, Xu Y, Leask A (2000) Tumor Necrosis Factor alpha Suppresses the Induction of Connective Tissue Growth Factor by Transforming Growth Factor-beta in Normal and Scleroderma Fibroblasts. Journal of Biological Chemistry 275:15220-15225

Abramson S, Buyon, JP. (1992) Activation of the complement pathway: comparison of normal pregnancy, preeclampsia, and systemic lupus erythematosus during pregnancy. Am J Reprod Immunol 28:183-187.

Age-Related Eye Disease Study Research G (2001) A Randomized, Placebo-Controlled, Clinical Trial of High-Dose Supplementation With Vitamins C and E, Beta Carotene, and Zinc for Age-Related Macular Degeneration and Vision Loss: AREDS Report No. 8. Arch Ophthalmol 119:1417-1436

Aisenbrey S, Zhang M, Bacher D, Yee J, Brunken WJ, Hunter DD (2006) Retinal Pigment Epithelial Cells Synthesize Laminins, Including Laminin 5, and Adhere to Them through alpha3- and alpha6-Containing Integrins. Investigative Ophthalmology & Visual Science 47:5537-5544

Ajayi F, Kongoasa N, Gaffey T, Asmann YW, Watson WJ, Baldi A, Lala P, Shridhar V, Brost B, Chien J (2008) Elevated expression of serine protease HtrA1 in preeclampsia and its role in trophoblast cell migration and invasion. American Journal of Obstetrics and Gynecology 199:557.e551-557.e510

Allikmets R, Dean M (2008) Bringing age-related macular degeneration into focus. Nat Genet 40:820-821

Altman DG (1980) Statistics and ethics in medical research: III How large a sample? British Medical Journal 281:1336-1338

Ambati J, Anand A, Fernandez S, Sakurai E, Lynn BC, Kuziel WA, Rollins BJ, Ambati BK (2003) An animal model of age-related macular degeneration in senescent Ccl-2- or Ccr-2-deficient mice. Nat Med 9:1390-1397

An E, Lu X, Flippin J, Devaney JM, Halligan B, Hoffman E, Csaky K, Hathout Y (2006) Secreted Proteome Profiling in Human RPE Cell Cultures Derived from Donors with Age Related Macular Degeneration and Age Matched Healthy Donors. Journal of Proteome Research 5:2599-2610

An E, Sen S, Park SK, Gordish-Dressman H, Hathout Y (2010) Identification of novel substrates for the serine protease HTRA1 in the human RPE secretome. Investigative ophthalmology & visual science 51:3379-3386

Anderson DH, Mullins RF, Hageman GS, Johnson LV (2002) A role for local inflammation in the formation of drusen in the aging eye. American Journal of Ophthalmology 134:411-431

Anderson DH, Radeke MJ, Gallo NB, Chapin EA, Johnson PT, Curletti CR, Hancox LS, Hu J, Ebright JN, Malek G, Hauser MA, Bowes Rickman C, Bok D, Hageman GS, Johnson LV (2010) The pivotal role of the complement system in aging and age-related macular degeneration: Hypothesis re-visited. Progress in Retinal and Eye Research 29:95-112

Annes JP, Munger JS, Rifkin DB (2003) Making sense of latent TGFβ activation. Journal of Cell Science 116:217-224

Apte RS, Richter J, Herndon J, Ferguson TA (2006) Macrophages Inhibit Neovascularization in a Murine Model of Age-Related Macular Degeneration. PLoS Med 3:e310

Argraves WS, Dickerson K, Burgess WH, Ruoslahti E (1989) Fibulin, a novel protein that interacts with the fibronectin receptor [beta] subunit cytoplasmic domain. Cell 58:623-629

Aspberg A, Adam S, Kostka G, Timpl R, Heinegård D (1999) Fibulin-1 Is a Ligand for the C-type Lectin Domains of Aggrecan and Versican. Journal of Biological Chemistry 274:20444-20449

Auge N, Maupas-Schwalm F, Elbaz M, Thiers J-C, Waysbort A, Itohara S, Krell H-W, Salvayre R, Negre-Salvayre A (2004) Role for Matrix Metalloproteinase-2 in Oxidized Low-Density Lipoprotein-Induced Activation of the Sphingomyelin/Ceramide Pathway and Smooth Muscle Cell Proliferation. Circulation 110:571-578

Bakay M, Zhao P, Chen J, Hoffman EP (2002) A web-accessible complete transcriptome of normal human and DMD muscle. Neuromuscular Disorders 12:S125-S141

Baldi A, De Luca A, Morini M, Battista T, Felsani A, Baldi F, Catricalà C, Amantea A, Noonan D, Albini A, Natali P, Lombardi D, MG. P (2002) The HtrA1 serine protease is down-regulated during human melanoma progression and represses growth of metastatic melanoma cells. Oncogene 21:6684-6688.

Baldi A, Mottolese M, Vincenzi B, Campioni M, Mellone P, Di Marino M, di Crescenzo VG, Visca P, Menegozzo S, Spugnini EP, Citro G, Ceribelli A, Mirri A, Chien J, Shridhar V, Ehrmann M, Santini M, Facciolo F (2008) The serine protease HtrA1 is a novel prognostic factor for human mesothelioma. Pharmacogenomics 9:1069-1077

Barnum SR, Niemann MA, Kearney JF, Volanakis JE (1984) Quantitation of complement factor D in human serum by a solid-phase radioimmunoassay. Journal of Immunological Methods 67:303-309

Barnum SR, Volanakis JE (1985) In vitro biosynthesis of complement protein D by U937 cells. The Journal of Immunology 134:1799-1803

Barron MJ, Johnson MA, Andrews RM, Clarke MP, Griffiths PG, Bristow E, He L-P, Durham S, Turnbull DM (2001) Mitochondrial Abnormalities in Ageing Macular Photoreceptors. Investigative Ophthalmology & Visual Science 42:3016-3022

Beatty S, Koh H-H, Phil M, Henson D, Boulton M (2000) The Role of Oxidative Stress in the Pathogenesis of Age-Related Macular Degeneration. Survey of Ophthalmology 45:115-134

Beddy D, Mulsow J, Watson RWG, Fitzpatrick JM, O'Connell PR (2006) Expression and regulation of connective tissue growth factor by transforming growth factor β and tumour necrosis factor α in fibroblasts isolated from strictures in patients with Crohn's disease. British Journal of Surgery 93:1290-1296

Bein K, Simons M (2000) Thrombospondin Type 1 Repeats Interact with Matrix Metalloproteinase 2. Journal of Biological Chemistry 275:32167-32173

Bhutto IA, McLeod DS, Hasegawa T, Kim SY, Merges C, Tong P, Lutty GA (2006) Pigment epithelium-derived factor (PEDF) and vascular endothelial growth factor (VEGF) in aged human choroid and eyes with age-related macular degeneration. Experimental Eye Research 82:99-110

Bhutto Ia, Uno K, Merges C, Zhang L, McLeod DS, Lutty Ga (2008) Reduction of endogenous angiogenesis inhibitors in Bruch's membrane of the submacular region in eyes with age-related macular degeneration. Archives of ophthalmology 126:670-678

Biesma DH, Hannema AJ, Velzen-blad HV, Mulder L, Zwieten RV, Kluijt I, Roos D (2001) A family with complement factor D deficiency. Journal of Clinical Investigation 108:233-240

Bird A, Bressler N, Bressler S, Chisholm I, Coscas G, Davis, MD., de Jong, PT., Klaver, CC., Klein, BE., Klein, R., et al. (1995) An international classification and grading system for age-related maculopathy and age-related macular degeneration. The International ARM Epidemiological Study Group. Surv Ophthalmol 39:367-374.

Blankenberg S, Rupprecht HJ, Poirier O, Bickel C, Smieja M, Hafner G, Meyer J, Cambien F, Tiret L, for the AtheroGene I (2003) Plasma Concentrations and Genetic Variation of Matrix Metalloproteinase 9 and Prognosis of Patients With Cardiovascular Disease. Circulation 107:1579-1585

Booij J, van Soest S, Swagemakers S, Essing A, Verkerk A, van der Spek P, Gorgels T, Bergen A (2009) Functional annotation of the human retinal pigment epithelium transcriptome. BMC Genomics 10:164

Booij JC, Baas DC, Beisekeeva J, Gorgels TGMF, Bergen AAB (2010) The dynamic nature of Bruch's membrane. Progress in Retinal and Eye Research 29:1-18

Bora PS, Sohn J-H, Cruz JMC, Jha P, Nishihori H, Wang Y, Kaliappan S, Kaplan HJ, Bora NS (2005) Role of Complement and Complement Membrane Attack Complex in Laser-Induced Choroidal Neovascularization. The Journal of Immunology 174:491-497

Bornstein P (2001) Thrombospondins as matricellular modulators of cell function. The Journal of Clinical Investigation 107:929-934

Bornstein P, Sage EH (2002) Matricellular proteins: extracellular modulators of cell function. Current Opinion in Cell Biology 14:608-616

Boyer DS, Antoszyk AN, Awh CC, Bhisitkul RB, Shapiro H, Acharya NR (2007) Subgroup Analysis of the MARINA Study of Ranibizumab in Neovascular Age-Related Macular Degeneration. Ophthalmology 114:246-252

Brekken RA, Sage EH (2001) SPARC, a matricellular protein: at the crossroads of cell-matrix communication: [Matrix Biology (2000) 569-580]. Matrix Biology 19:815-827

Brigstock DR, Steffen CL, Kim GY, Vegunta RK, Diehl JR, Harding PA (1997) Purification and Characterization of Novel Heparin-binding Growth Factors in Uterine Secretory Fluids. Journal of Biological Chemistry 272:20275-20282

Cameron DJ, Yang Z, Gibbs D, Chen H, Kaminoh Y, Jorgensen A, Zeng J, Luo L, Brinton E, Brinton G, Brand JM, Bernstein PS, Zabriskie NA, Tang S, Constantine R, Tong Z, Zhang K (2007) HTRA1 Variant Confers Similar Risks to Geographic Atrophy and Neovascular Age-related Macular Degeneration. Cell Cycle 6:1122-1125

Campioni M, Severino A, Manente L, De Luca A, La Porta R, Vitiello A, Fiore P, Toldo S, Spugnini E, Paggi M, A. B (2011) Identification of protein-protein interactions of human HtrA1. Front Biosci (Elite Ed) 3:1493-1499.

Canfield aE, Hadfield KD, Rock CF, Wylie EC, Wilkinson FL (2007) HtrA1: a novel regulator of physiological and pathological matrix mineralization? Biochemical Society transactions 35:669-671
Canter JA, Olson LM, Spencer K, Schnetz-Boutaud N, Anderson B, Hauser MA, Schmidt S, Postel EA, Agarwal A, Pericak-Vance MA, Sternberg P, Jr., Haines JL (2008) Mitochondrial DNA Polymorphism A4917G Is Independently Associated with Age-Related Macular Degeneration. PLoS ONE 3:e2091
Carelli V, Ross-Cisneros FN, Sadun AA (2004) Mitochondrial dysfunction as a cause of optic neuropathies. Progress in Retinal and Eye Research 23:53-89
Carroll MV, Lack N, Sim E, Krarup A, Sim RB (2009) Multiple routes of complement activation by Mycobacterium bovis BCG. Molecular immunology 46:3367-3378
Carron JA, Hiscott P, Hagan S, Sheridan CM, Magee R, Gallagher JA (2000) Cultured human retinal pigment epithelial cells differentially express thrombospondin-1, -2, -3, and -4. The International Journal of Biochemistry & Cell Biology 32:1137-1142
CATT (2011) Ranibizumab and Bevacizumab for Neovascular Age-Related Macular Degeneration. New England Journal of Medicine 364:1897-1908
Chamberland A, Wang E, Jones AR, Collins-Racie LA, LaVallie ER, Huang Y, Liu L, Morris EA, Flannery CR, Yang Z (2009) Identification of a Novel HtrA1-susceptible Cleavage Site in Human Aggrecan. Journal of Biological Chemistry 284:27352-27359
Chambers RC, Leoni P, Blanc-Brude OP, Wembridge DE, Laurent GJ (2000) Thrombin Is a Potent Inducer of Connective Tissue Growth Factor Production via Proteolytic Activation of Protease-activated Receptor-1. Journal of Biological Chemistry 275:35584-35591
Chan C, Ross R, Shen D, Ding X, Majumdar Z, Bojanowski C, Zhou M, Salem NJ, Bonner R, J. T (2008) Ccl2/Cx3cr1-deficient mice: an animal model for age-related macular degeneration. Ophthalmic Res 40:124-128.
Chan C, Shen D, Zhou M, Ross R, Ding X, Zhang K, Green W, Tuo J (2007) Human HtrA1 in the archived eyes with age-related macular degeneration. Trans Am Ophthalmol Soc 105:92-98
Chau KY, Sivaprasad S, Patel N, Donaldson TA, Luthert PJ, Chong NV (2007) Plasma levels of matrix metalloproteinase-2 and -9 (MMP-2 and MMP-9) in age-related macular degeneration. Eye 22:855-859
Chen L, Yang P, Kijlstra A (2002) Distribution, markers, and functions of retinal microglia. Ocul Immunol Inflamm 10:27-39.
Chen W, Stambolian D, Edwards AO, Branham KE, Othman M, Jakobsdottir J, Tosakulwong N, et al. (2010) Genetic variants near TIMP3 and high-density lipoprotein-associated loci influence susceptibility to age-related macular degeneration. Proceedings of the National Academy of Sciences 107:7401-7406
Chen Y, Zeng J, Zhao C, Wang K, Trood E, Buehler J, Weed M, Kasuga D, Bernstein PS, Hughes G, Fu V, Chin J, Lee C, Crocker M, Bedell M, Salasar F, Yang Z, Goldbaum M, Ferreyra H, Freeman WR, Kozak I, Zhang K (2011) Assessing Susceptibility to Age-Related Macular Degeneration With Genetic Markers and Environmental Factors. Arch Ophthalmol 129:344-351
Chien J, Aletti G, Baldi A, Catalano V, Muretto P, Keeney GL, Kalli KR, Staub J, Ehrmann M, Cliby WA, Lee YK, Bible KC, Hartmann LC, Kaufmann SH,

Shridhar V (2006) Serine protease HtrA1 modulates chemotherapy-induced cytotoxicity. 116
Chien J, He X, Shridhar V (2009a) Identification of tubulins as substrates of serine protease HtrA1 by mixture-based oriented peptide library screening. Journal of Cellular Biochemistry 107:253-263
Chien J, Ota T, Aletti G, Shridhar R, Boccellino M, Quagliuolo L, Baldi A, Shridhar V (2009b) Serine Protease HtrA1 Associates with Microtubules and Inhibits Cell Migration. Mol Cell Biol 29:4177-4187
Chien J, Staub J, Hu S-I, Erickson-Johnson MR, Couch FJ, Smith DI, Crowl RM, Kaufmann SH, Shridhar V (2004) A candidate tumor suppressor HtrA1 is downregulated in ovarian cancer. Oncogene 23:1636-1644
Cho E, Hung S, Willett WC, Spiegelman D, Rimm EB, Seddon JM, Colditz GA, Hankinson SE (2001) Prospective study of dietary fat and the risk of age-related macular degeneration. The American Journal of Clinical Nutrition 73:209-218
Cho Y, Cao X, Shen D, Tuo J, Parver LM, Rickles FR, Chan C-C (2011) Evidence for enhanced tissue factor expression in age-related macular degeneration. Lab Invest 91:519-526
Chong NHV, Keonin J, Luthert PJ, Frennesson CI, Weingeist DM, Wolf RL, Mullins RF, Hageman GS (2005) Decreased Thickness and Integrity of the Macular Elastic Layer of Bruch's Membrane Correspond to the Distribution of Lesions Associated with Age-Related Macular Degeneration. The American Journal of Pathology 166:241-251
Chowers I, Liu D, Farkas RH, Gunatilaka TL, Hackam AS, Bernstein SL, Campochiaro PA, Parmigiani G, Zack DJ (2003) Gene expression variation in the adult human retina. Human Molecular Genetics 12:2881-2893
Chowers I, Meir T, Lederman M, Goldenberg-Cohen N, Cohen Y, Banin E, Averbukh E, Hemo I, A P, R A-S, O W, Hoh J, Zack D, Galbinur T (2008) Sequence variants in HTRA1 and LOC387715/ARMS2 and phenotype and response to photodynamic therapy in neovascular age-related macular degeneration in populations from Israel. Mol Vis 14::2263-2271.
Christen W, Glynn R, Manson J, Ajani U, Buring J (1996) A prospective study of cigarette smoking and risk of age-related macular degeneration in men. JAMA 276:1147-1151
Churchill AJ, Carter JG, Lovell HC, Ramsden C, Turner SJ, Yeung A, Escardo J, Atan D (2006) VEGF polymorphisms are associated with neovascular age-related macular degeneration. Human Molecular Genetics 15:2955-2961
Clausen T, Southan C, Ehrmann M (2002) The HtrA Family of ProteasesImplications for Protein Composition and Cell Fate. Molecular Cell 10:443-455
Coffey P, Gias C, McDermott C, Lundh P, Pickering M, Sethi C, Bird A, Fitzke F, Maass A, Chen L, Holder G, Luthert P, Salt T, Moss S, Greenwood J (2007) Complement factor H deficiency in aged mice causes retinal abnormalities and visual dysfunction. Proc Natl Acad Sci U S A 104:16651–16656
Coleman HR, Chan C-C, Ferris Iii FL, Chew EY (2008) Age-related macular degeneration. The Lancet 372:1835-1845
Combadière C, Feumi C, Raoul W, Keller N, Rodéro M, Pézard A, Lavalette S, Houssier M, Jonet L, Picard E, Debré P, Sirinyan M, Deterre P, Ferroukhi T, Cohen S-Y, Chauvaud D, Jeanny J-C, Chemtob S, Behar-Cohen F, Sennlaub F

(2007) CX3CR1-dependent subretinal microglia cell accumulation is associated with cardinal features of age-related macular degeneration. The Journal of Clinical Investigation 117:2920-2928
Conley YP, Thalamuthu A, Jakobsdottir J, Weeks DE, Mah T, Ferrell RE, Gorin MB (2005) Candidate gene analysis suggests a role for fatty acid biosynthesis and regulation of the complement system in the etiology of age-related maculopathy. Human Molecular Genetics 14:1991-2002
Cook KS, Groves DL, Min HY, Spiegelman BM (1985) A developmentally regulated mRNA from 3T3 adipocytes encodes a novel serine protease homologue. Proceedings of the National Academy of Sciences 82:6480-6484
Crabb JW, Miyagi M, Gu X, Shadrach K, West KA, Sakaguchi H, Kamei M, Hasan A, Yan L, Rayborn ME, Salomon RG, Hollyfield JG (2002) Drusen proteome analysis: An approach to the etiology of age-related macular degeneration. Proceedings of the National Academy of Sciences 99:14682-14687
Cruickshanks KJ, Hamman RF, Klein R, Nondahl DM, Shetterly SM (1997) The Prevalence of Age-Related Maculopathy by Geographic Region and Ethnicity: The Colorado-Wisconsin Study of Age-Related Maculopathy. Arch Ophthalmol 115:242-250
Curcio CA, Millican CL (1999) Basal Linear Deposit and Large Drusen Are Specific for Early Age-Related Maculopathy. Arch Ophthalmol 117:329-339
Dallas SL, Rosser JL, Mundy GR, Bonewald LF (2002) Proteolysis of Latent Transforming Growth Factor-Î² (TGF-Î²)-binding Protein-1 by Osteoclasts. Journal of Biological Chemistry 277:21352-21360
Dastgheib K, Green WR (1994) Granulomatous Reaction to Bruch's Membrane in Age-Related Macular Degeneration. Arch Ophthalmol 112:813-818
Davis GE, Bayless KJ, Davis MJ, Meininger GA (2000) Regulation of Tissue Injury Responses by the Exposure of Matricryptic Sites within Extracellular Matrix Molecules. The American Journal of Pathology 156:1489-1498
de Jong PTVM (2006) Age-Related Macular Degeneration. New England Journal of Medicine 355:1474-1485
De Luca A, De Falco M, Fedele V, Cobellis L, Mastrogiacomo A, Laforgia V, Tuduce IL, Campioni M, Giraldi D, Paggi MG, Baldi A (2004) The serine protease HtrA1 is upregulated in the human placenta during pregnancy. The journal of histochemistry and cytochemistry : official journal of the Histochemistry Society 52:885-892
De Luca A, De Falco M, Severino A, Campioni M, Santini D, Baldi F, Paggi MG, Baldi A (2003) Distribution of the Serine Protease HtrA1 in Normal Human Tissues. Journal of Histochemistry & Cytochemistry 51:1279-1284
Del Priore LV, Tezel TH (1998) Reattachment Rate of Human Retinal Pigment Epithelium to Layers of Human Bruch's Membrane. Arch Ophthalmol 116:335-341
den Hollander AI, Koenekoop RK, Mohamed MD, Arts HH, Boldt K, Towns KV, Sedmak T, et al. (2007) Mutations in LCA5, encoding the ciliary protein lebercilin, cause Leber congenital amaurosis. Nat Genet 39:889-895
Dewan A, Liu M, Hartman S, Zhang SS-M, Liu DTL, Zhao C, Tam POS, Chan WM, Lam DSC, Snyder M, Barnstable C, Pang CP, Hoh J (2006) HTRA1 promoter polymorphism in wet age-related macular degeneration. Science (New York, NY) 314:989-992

Ding X, Patel M, Chan C-C (2009) Molecular pathology of age-related macular degeneration. Progress in Retinal and Eye Research 28:1-18
Edwards AO, Chen D, Fridley BL, James KM, Wu Y, Abecasis G, Swaroop A, Othman M, Branham K, Iyengar SK, Sivakumaran TA, Klein R, Klein BEK, Tosakulwong N (2008) Toll-like Receptor Polymorphisms and Age-Related Macular Degeneration. Investigative Ophthalmology & Visual Science 49:1652-1659
Edwards AO, Ritter R, Abel KJ, Manning A, Panhuysen C, Farrer La (2005) Complement factor H polymorphism and age-related macular degeneration. Science (New York, NY) 308:421-424
Eiraku M, Takata N, Ishibashi H, Kawada M, Sakakura E, Okuda S, Sekiguchi K, Adachi T, Sasai Y (2011) Self-organizing optic-cup morphogenesis in three-dimensional culture. Nature 472:51-56
Ennis S, Gibson J, Cree AJ, Collins A, Lotery AJ (2009) Support for the involvement of complement factor I in age-related macular degeneration. Eur J Hum Genet 18:15-16
Ennis S, Jomary C, Mullins R, Cree A, Chen X, MacLeod A, Jones S, Collins A, Stone E, Lotery A (2008) Association between the SERPING1 gene and age-related macular degeneration: a two-stage case-control study. The Lancet 372:1828-1834
Espinosa-Heidmann DG, Suner IJ, Catanuto P, Hernandez EP, Marin-Castano ME, Cousins SW (2006) Cigarette Smoke-Related Oxidants and the Development of Sub-RPE Deposits in an Experimental Animal Model of Dry AMD. Investigative Ophthalmology & Visual Science 47:729-737
Espinosa-Heidmann DG, Suner IJ, Hernandez EP, Monroy D, Csaky KG, Cousins SW (2003) Macrophage Depletion Diminishes Lesion Size and Severity in Experimental Choroidal Neovascularization. Investigative Ophthalmology & Visual Science 44:3586-3592
Evans JR, Fletcher AE, Wormald RPL (2004) Age-related macular degeneration causing visual impairment in people 75 years or older in Britain: An add-on study to the Medical Research Council Trial of Assessment and Management of Older People in the Community. Ophthalmology 111:513-517
Fagerness Ja, Maller JB, Neale BM, Reynolds RC, Daly MJ, Seddon JM (2009) Variation near complement factor I is associated with risk of advanced AMD. European journal of human genetics : EJHG 17:100-104
Fakhouri F, Roumenina L, Provot F, Sallée, Marion, Caillard S, Couzi L, Essig M, Ribes D, Dragon-Durey M-A, Bridoux F, Rondeau E, Frémeaux-Bacchi V (2010) Pregnancy-Associated Hemolytic Uremic Syndrome Revisited in the Era of Complement Gene Mutations. Journal of the American Society of Nephrology 21:859-867
Fanciulli M, Petretto E, Aitman TJ (2010) Gene copy number variation and common human disease. Clinical Genetics 77:201-213
Fantuzzi G (2005) Adipose tissue, adipokines, and inflammation. Journal of Allergy and Clinical Immunology 115:911-919
Fearon D, Austen K, Ruddy S (1974) Properdin factor D: characterization of its active site and isolation of the precursor form. J Exp Med 139:355-366.

Feeney-Burns L, Hilderbrand ES, Eldridge S (1984) Aging human RPE: morphometric analysis of macular, equatorial, and peripheral cells. Investigative Ophthalmology & Visual Science 25:195-200
Feher J, Kovacs I, Artico M, Cavallotti C, Papale A, Balacco Gabrieli C (2006) Mitochondrial alterations of retinal pigment epithelium in age-related macular degeneration. Neurobiology of Aging 27:983-993
Finckenberg P, Inkinen K, Ahonen J, Merasto S, Louhelainen M, Vapaatalo H, Müller D, Ganten D, Luft F, Mervaala E (2003) Angiotensin II Induces Connective Tissue Growth Factor Gene Expression via Calcineurin-Dependent Pathways. The American Journal of Pathology 163:355-366
Fine SL, Berger JW, Maguire MG, Ho AC (2000) Age-Related Macular Degeneration. New England Journal of Medicine 342:483-492
Finn J, Mathieson P (1993) Molecular analysis of C3 allotypes in patients with nephritic factor. Clin Exp Immunol 91 410-414.
Fiotti N, Pedio M, Parodi MB, Altamura N, Uxa L, Guarnieri G, Giansante C, Ravalico G (2005) MMP-9 microsatellite polymorphism and susceptibility to exudative form of age-related macular degeneration. Genetics in Medicine 7:272-277 210.1097/1001.GIM.0000159903.0000169597.0000159973
Fisher SA, Abecasis GR, Yashar BM, Zareparsi S, Swaroop A, Iyengar SK, Klein BEK, Klein R, Lee KE, Majewski J, Schultz DW, Klein ML, Seddon JM, Santangelo SL, Weeks DE, Conley YP, Mah TS, Schmidt S, Haines JL, Pericak-Vance MA, Gorin MB, Schulz HL, Pardi F, Lewis CM, Weber BHF (2005) Meta-analysis of genome scans of age-related macular degeneration. Human Molecular Genetics 14:2257-2264
Fisher SA, Rivera A, Fritsche LG, Keilhauer CN, Lichtner P, Meitinger T, Rudolph G, Weber BHF (2007) Case–control genetic association study of fibulin-6 (FBLN6 or HMCN1) variants in age-related macular degeneration (AMD). Human Mutation 28:406-413
Folkman J, Shing Y (1992) Angiogenesis. Journal of Biological Chemistry 267:10931-10934
Forneris F, Ricklin D, Wu J, Tzekou A, Wallace RS, Lambris JD, Gros P (2010) Structures of C3b in Complex with Factors B and D Give Insight into Complement Convertase Formation. Science 330:1816-1820
Forrester JV (2003) Macrophages eyed in macular degeneration. Nat Med 9:1350-1351
Francis PJ, Appukuttan B, Simmons E, Landauer N, Stoddard J, Hamon S, Ott J, Ferguson B, Klein M, Stout JT, Neuringer M (2008) Rhesus monkeys and humans share common susceptibility genes for age-related macular disease. Human Molecular Genetics 17:2673-2680
Frank RN, Amin RH, Puklin JE (1999) Antioxidant enzymes in the macular retinal pigment epithelium of eyes with neovascular age-related macular degeneration. American Journal of Ophthalmology 127:694-709
Frazier K, Williams S, Kothapalli D, Klapper H, Grotendorst G (1996) Stimulation of fibroblast cell growth, matrix production, and granulation tissue formation by connective tissue growth factor. J Invest Dermatol 107:404-411.
Friedman D, O'Colmain B, Muñoz B, Tomany S, McCarty C, de Jong P, Nemesure B, Mitchell P, Kempen J, Group. EDPR (2004) Prevalence of Age-Related Macular Degeneration in the United States. Arch Ophthalmol 122:564-572

Friedrich U, Myers CA, Fritsche LG, Milenkovich A, Wolf A, Corbo JC, Weber BHF (2011) Risk- and non-risk-associated variants at the 10q26 AMD locus influence ARMS2 mRNA expression but exclude pathogenic effects due to protein deficiency. Human Molecular Genetics 20:1387-1399

Fritsche LG, Loenhardt T, Janssen A, Fisher SA, Rivera A, Keilhauer CN, Weber BHF (2008) Age-related macular degeneration is associated with an unstable ARMS2 (LOC387715) mRNA. Nat Genet 40:892-896

Fujihara M, Nagai N, Sussan TE, Biswal S, Handa JT (2008) Chronic Cigarette Smoke Causes Oxidative Damage and Apoptosis to Retinal Pigmented Epithelial Cells in Mice. PLoS ONE 3:e3119

Fukutake T, Hirayama K (1995) Familial Young-Adult-Onset Arteriosclerotic Leukoencephalopathy with Alopecia and Lumbago without Arterial Hypertension. Eur Neurol 35:69-79

Gilicze A, Kohalmi B, Pocza P, Keszei M, Jaeger J, Gorbe E, Papp Z, Toth S, Falus A, Wiener Z (2007) HtrA1 is a novel mast cell serine protease of mice and men. Molecular immunology 44:2961-2968

Gloeckner CJ, Boldt K, Schumacher A, Roepman R, Ueffing M (2007) A novel tandem affinity purification strategy for the efficient isolation and characterisation of native protein complexes. PROTEOMICS 7:4228-4234

Gold B, Merriam JE, Zernant J, Hancox LS, Taiber AJ, Gehrs K, Cramer K, Neel J, Bergeron J, Barile GR, Smith RT, Hageman GS, Dean M, Allikmets R (2006) Variation in factor B (BF) and complement component 2 (C2) genes is associated with age-related macular degeneration. Nature genetics 38:458-462

Goldblum SE, Ding X, Funk SE, Sage EH (1994) SPARC (secreted protein acidic and rich in cysteine) regulates endothelial cell shape and barrier function. Proceedings of the National Academy of Sciences 91:3448-3452

Good DJ, Polverini PJ, Rastinejad F, Le Beau MM, Lemons RS, Frazier WA, Bouck NP (1990) A tumor suppressor-dependent inhibitor of angiogenesis is immunologically and functionally indistinguishable from a fragment of thrombospondin. Proceedings of the National Academy of Sciences 87:6624-6628

Gotoh N, Yamada R, Hiratani H, Renault V, Kuroiwa S, Monet M, Toyoda S, Chida S, Mandai M, Otani A, Yoshimura N, Matsuda F (2006) No association between complement factor H gene polymorphism and exudative age-related macular degeneration in Japanese. Human Genetics 120:139-143

Götze O, Müller-Eberhard H (1971) The c3-activator system: an alternate pathway of complement activation. J Exp Med 134:90-108

Goverdhan SV, Howell MW, Mullins RF, Osmond C, Hodgkins PR, Self J, Avery K, Lotery AJ (2005) Association of HLA Class I and Class II Polymorphisms with Age-Related Macular Degeneration. Investigative Ophthalmology & Visual Science 46:1726-1734

Grau S, Baldi A, Bussani R, Tian X, Stefanescu R, Przybylski M, Richards P, Jones SA, Shridhar V, Clausen T, Ehrmann M (2005) Implications of the serine protease HtrA1 in amyloid precursor protein processing. Proceedings of the National Academy of Sciences of the United States of America 102:6021-6026

Grau S, Richards PJ, Kerr B, Hughes C, Caterson B, Williams AS, Junker U, Jones Sa, Clausen T, Ehrmann M (2006) The role of human HtrA1 in arthritic disease. The Journal of biological chemistry 281:6124-6129

Graves D, Jiang Y (1995) Chemokines, a Family of Chemotactic Cytokines. Critical Reviews in Oral Biology & Medicine 6:109-118
Gray CW, Ward RV, Karran E, Turconi S, Rowles a, Viglienghi D, Southan C, Barton a, Fantom KG, West a, Savopoulos J, Hassan NJ, Clinkenbeard H, Hanning C, Amegadzie B, Davis JB, Dingwall C, Livi GP, Creasy CL (2000) Characterization of human HtrA2, a novel serine protease involved in the mammalian cellular stress response. European journal of biochemistry / FEBS 267:5699-5710
Green W (1999) Histopathology of age-related macular degeneration. Mol Vis 5:27
Green WR, Enger C (1993) Age-related macular degeneration histopathologic studies. The 1992 Lorenz E. Zimmerman Lecture. Ophthalmology 100:1519-1535
Grossniklaus HE, Ling JX, Wallace TM, Dithmar S, Lawson DH, Cohen C, Elner VM, Elner SG, Sternberg PJ (2002) Macrophage and retinal pigment epithelium expression of angiogenic cytokines in choroidal neovascularization. Mol Vis 8:119-126
Grotendorst GR (1997) Connective tissue growth factor: a mediator of TGF-[beta] action on fibroblasts. Cytokine & Growth Factor Reviews 8:171-179
Gugliucci A, Mehlhaff K, Kinugasa E, Ogata H, Hermo R, Schulze J, Kimura S (2007) Paraoxonase-1 concentrations in end-stage renal disease patients increase after hemodialysis: Correlation with low molecular AGE adduct clearance. Clinica Chimica Acta 377:213-220
Guo L, Hussain AA, Limb GA, Marshall J (1999) Age-Dependent Variation in Metalloproteinase Activity of Isolated Human Bruchâ€™s Membrane and Choroid. Investigative Ophthalmology & Visual Science 40:2676-2682
Gupta K, Gupta P, Wild R, Ramakrishnan S, Hebbel R (1999) Binding and displacement of vascular endothelial growth factor (VEGF) by thrombospondin: Effect on human microvascular endothelial cell proliferation and angiogenesis. Angiogenesis 3:147-158
Gupta N, Brown KE, Milam AH (2003) Activated microglia in human retinitis pigmentosa, late-onset retinal degeneration, and age-related macular degeneration. Experimental Eye Research 76:463-471
Hadfield KD, Rock CF, Inkson CA, Dallas SL, Sudre L, Wallis GA, Boot-handford RP, Canfield AE (2008) HtrA1 Inhibits Mineral Deposition by Osteoblasts. Journal of Biological Chemistry 283:5928-5938
Hageman GS, Anderson DH, Johnson LV, Hancox LS, Taiber AJ, Hardisty LI, Hageman JL, et al. (2005) A common haplotype in the complement regulatory gene factor H (HF1/CFH) predisposes individuals to age-related macular degeneration. Proceedings of the National Academy of Sciences of the United States of America 102:7227-7232
Hageman GS, Luthert PJ, Victor Chong NH, Johnson LV, Anderson DH, Mullins RF (2001) An Integrated Hypothesis That Considers Drusen as Biomarkers of Immune-Mediated Processes at the RPE-Bruch's Membrane Interface in Aging and Age-Related Macular Degeneration. Progress in Retinal and Eye Research 20:705-732
Hahn P, Milam AH, Dunaief JL (2003) Maculas Affected by Age-Related Macular Degeneration Contain Increased Chelatable Iron in the Retinal Pigment Epithelium and Bruch's Membrane. Arch Ophthalmol 121:1099-1105

Haines J, Hauser M, Schmidt S, Scott W, Olson L, Gallins P, Spencer K, Kwan S, Noureddine M, Gilbert J, Schnetz-Boutaud N, Agarwal A, Postel E, Pericak-Vance M (2005) Complement Factor H Variant Increases the Risk of Age-Related Macular Degeneration. Science 308:419-421

Haines JL, Schnetz-Boutaud N, Schmidt S, Scott WK, Agarwal A, Postel EA, Olson L, Kenealy SJ, Hauser M, Gilbert JR, Pericak-Vance MA (2006) Functional Candidate Genes in Age-Related Macular Degeneration: Significant Association with VEGF, VLDLR, and LRP6. Investigative Ophthalmology & Visual Science 47:329-335

Hakobyan S, Harris CL, Tortajada A, Goicochea de Jorge E, Garcia-Layana A, Fernandez-Robredo P, Rodriguez de Cordoba S, Morgan BP (2008) Measurement of Factor H Variants in Plasma Using Variant-Specific Monoclonal Antibodies: Application to Assessing Risk of Age-Related Macular Degeneration. Investigative Ophthalmology & Visual Science 49:1983-1990

Handwerger S (1991) CLINICAL COUNTERPOINT: The Physiology of Placental Lactogen in Human Pregnancy. Endocrine Reviews 12:329-336

Hara K, Shiga A, Fukutake T, Nozaki H, Miyashita A, Yokoseki A, Kawata H, et al. (2009) Association of HTRA1 Mutations and Familial Ischemic Cerebral Small-Vessel Disease. New England Journal of Medicine 360:1729-1739

Hauck SM, Gloeckner CJ, Harley ME, Schoeffmann S, Boldt K, Ekstrom PAR, Ueffing M (2008) Identification of Paracrine Neuroprotective Candidate Proteins by a Functional Assay-driven Proteomics Approach. Molecular & Cellular Proteomics 7:1349-1361

He S, Incardona F, Jin M, Ryan S, Hinton D (2006) Thrombospondin-1 expression in RPE and choroidal neovascular membranes. Yan Ke Xue Bao 22:265-274.

He S, Jin ML, Worpel V, Hinton DR (2003) A role for connective tissue growth factor in the pathogenesis of choroidal neovascularization. Archives of ophthalmology 121:1283-1288

Hecker La, Edwards AO, Ryu E, Tosakulwong N, Baratz KH, Brown WL, {{Charbel Issa}} P, Scholl HP, Pollok-Kopp B, Schmid-Kubista KE, Bailey KR, Oppermann M (2010) Genetic control of the alternative pathway of complement in humans and age-related macular degeneration. Human molecular genetics 19:209-215

Herbert AP, Deakin JA, Schmidt CQ, Blaum BS, Egan C, Ferreira VP, Pangburn MK, Lyon M, Uhrin D, Barlow PN (2007) Structure Shows That a Glycosaminoglycan and Protein Recognition Site in Factor H Is Perturbed by Age-related Macular Degeneration-linked Single Nucleotide Polymorphism. Journal of Biological Chemistry 282:18960-18968

Heurich M, Martínez-Barricarte R, Francis NJ, Roberts DL, Rodríguez de Córdoba S, Morgan BP, Harris CL (2011) Common polymorphisms in C3, factor B, and factor H collaborate to determine systemic complement activity and disease risk. Proceedings of the National Academy of Sciences 108:8761-8766

Hewitt AT, Nakazawa K, Newsome DA (1989) Analysis of newly synthesized Bruch's membrane proteoglycans. Investigative Ophthalmology & Visual Science 30:478-486

Hiemstra PS, Langeler E, Compier B, Keepers Y, Leijh PC, van den Barselaar MT, Overbosch D, Daha MR (1989) Complete and partial deficiencies of complement factor D in a Dutch family. The Journal of Clinical Investigation 84:1957-1961

Hiscott P, Paraoan L, Choudhary A, Ordonez JL, Al-Khaier A, Armstrong DJ (2006) Thrombospondin 1, thrombospondin 2 and the eye. Progress in Retinal and Eye Research 25:1-18
Ho L, van Leeuwen R, Witteman JCM, van Duijn CM, Uitterlinden AG, Hofman A, de Jong PTVM, Vingerling JR, Klaver CCW (2011) Reducing the Genetic Risk of Age-Related Macular Degeneration With Dietary Antioxidants, Zinc, and {omega}-3 Fatty Acids: The Rotterdam Study. Arch Ophthalmol 129:758-766
Holers M, Kinoshita T, Molina H (1992) The evolution of mouse and human complement C3-binding proteins: divergence of form but conservation of function. Immunology Today 13:231-236
Hollyfield JG, Bonilha VL, Rayborn ME, Yang X, Shadrach KG, Lu L, Ufret RL, Salomon RG, Perez VL (2008) Oxidative damage-induced inflammation initiates age-related macular degeneration. Nature medicine 14:194-198
Holz FG, Sheraidah G, Pauleikhoff D, Bird AC (1994) Analysis of Lipid Deposits Extracted From Human Macular and Peripheral Bruch's Membrane. Arch Ophthalmol 112:402-406
Hotamisligil GS, Arner P, Caro JF, Atkinson RL, Spiegelman BM (1995) Increased adipose tissue expression of tumor necrosis factor-alpha in human obesity and insulin resistance. The Journal of Clinical Investigation 95:2409-2415
Hu SI, Carozza M, Klein M, Nantermet P, Luk D, Crowl RM (1998) Human HtrA, an evolutionarily conserved serine protease identified as a differentially expressed gene product in osteoarthritic cartilage. The Journal of biological chemistry 273:34406-34412
Huang J-D, Presley JB, Chimento MF, Curcio CA, Johnson M (2007) Age-related changes in human macular Bruch's membrane as seen by quick-freeze/deep-etch. Experimental Eye Research 85:202-218
Hughes AE, Orr N, Esfandiary H, Diaz-Torres M, Goodship T, Chakravarthy U (2006) A common CFH haplotype, with deletion of CFHR1 and CFHR3, is associated with lower risk of age-related macular degeneration. Nature genetics 38:1173-1177
Hughes AE, Orr N, Patterson C, Esfandiary H, Hogg R, McConnell V, Silvestri G, Chakravarthy U (2007) Neovascular Age-Related Macular Degeneration Risk Based on CFH, LOC387715/HTRA1, and Smoking. PLoS Med 4:e355
Hung AY, Sheng M (2002) PDZ domains: structural modules for protein complex assembly. The Journal of biological chemistry 277:5699-5702
Iafrate AJ, Feuk L, Rivera MN, Listewnik ML, Donahoe PK, Qi Y, Scherer SW, Lee C (2004) Detection of large-scale variation in the human genome. Nat Genet 36:949-951
Igarashi A, Okochi H, Bradham DM, Grotendorst GR (1993) Regulation of connective tissue growth factor gene expression in human skin fibroblasts and during wound repair. Mol Biol Cell 4:637-645
Inatani M, Tanihara H (2002) Proteoglycans in retina. Progress in Retinal and Eye Research 21:429-447
Iozzo RV, San Antonio JD (2001) Heparan sulfate proteoglycans: heavy hitters in the angiogenesis arena. The Journal of Clinical Investigation 108:349-355
Ishida O, Oku H, Ikeda T., Nishimura M., Kawagoe K., K. N (2003) Is Chlamydia pneumoniae infection a risk factor for age related macular degeneration? British Journal of Ophthalmology 87:523–524

Iyengar SK, Song D, Klein BEK, Klein R, Schick JH, Humphrey J, Millard C, Liptak R, Russo K, Jun G, Lee KE, Fijal B, Elston RC (2004) Dissection of Genomewide-Scan Data in Extended Families Reveals a Major Locus and Oligogenic Susceptibility for Age-Related Macular Degeneration. The American Journal of Human Genetics 74:20-39

Jakobsdottir J, Conley YP, Weeks DE, Mah TS, Ferrell RE, Gorin MB (2005) Susceptibility Genes for Age-Related Maculopathy on Chromosome 10q26. The American Journal of Human Genetics 77:389-407

Jakobsson M, Scholz SW, Scheet P, Gibbs JR, VanLiere JM, Fung H-C, Szpiech ZA, Degnan JH, Wang K, Guerreiro R, Bras JM, Schymick JC, Hernandez DG, Traynor BJ, Simon-Sanchez J, Matarin M, Britton A, van de Leemput J, Rafferty I, Bucan M, Cann HM, Hardy JA, Rosenberg NA, Singleton AB (2008) Genotype, haplotype and copy-number variation in worldwide human populations. Nature 451:998-1003

Jing H, Macon KJ, Moore D, DeLucas LJ, Volanakis JE, Narayana SV (1999) Structural basis of profactor D activation: from a highly flexible zymogen to a novel self-inhibited serine protease, complement factor D. The EMBO journal 18:804-814

Johnson LV, Leitner WP, Rivest AJ, Staples MK, Radeke MJ, Anderson DH (2002) The Alzheimer's Aβ-peptide is deposited at sites of complement activation in pathologic deposits associated with aging and age-related macular degeneration. Proceedings of the National Academy of Sciences 99:11830-11835

Johnson LV, Ozaki S, Staples MK, Erickson PA, Anderson DH (2000) A Potential Role for Immune Complex Pathogenesis in Drusen Formation. Experimental Eye Research 70:441-449

Kaiser PK, Brown DM, Zhang K, Hudson HL, Holz FG, Shapiro H, Schneider S, Acharya NR (2007) Ranibizumab for Predominantly Classic Neovascular Age-related Macular Degeneration: Subgroup Analysis of First-year ANCHOR Results. American Journal of Ophthalmology 144:850-857.e854

Kalayoglu MV, Galvan C, Mahdi OS, Byrne GI, Mansour S (2003) Serological Association Between Chlamydia pneumoniae Infection and Age-Related Macular Degeneration. Arch Ophthalmol 121:478-482

Kamei M, Hollyfield JG (1999) TIMP-3 in Bruchs Membrane: Changes during Aging and in Age-Related Macular Degeneration. Investigative Ophthalmology & Visual Science 40:2367-2375

Kanda A, Chen W, Othman M, Branham KEH, Brooks M, Khanna R, He S, Lyons R, Abecasis GR, Swaroop A (2007) A variant of mitochondrial protein LOC387715/ARMS2, not HTRA1, is strongly associated with age-related macular degeneration. Proceedings of the National Academy of Sciences of the United States of America 104:16227-16232

Kanda A, Stambolian D, Chen W, Curcio C, Abecasis G, Swaroop A (2010) Age-related macular degeneration-associated variants at chromosome 10q26 do not significantly alter ARMS2 and HTRA1 transcript levels in the human retina. Mol Vis 16:1317-1323.

Kenealy S, Schmidt S, Agarwal A, Postel E, De La Paz M, Pericak-Vance M, Haines J (2004) Linkage analysis for age-related macular degeneration supports a gene on chromosome 10q26. Mol Vis 10:57-61.

Killingsworth MC, Sarks JP, Sarks SH (1990) Macrophages related to Bruch's membrane in age-related macular degeneration. Eye (London, England) 4 (Pt 4):613-621
Kim DD, Song W-C (2006) Membrane complement regulatory proteins. Clinical Immunology 118:127-136
Kim S, Narayana SVL, Volanakis JE (1994) Mutational Analysis of the Substrate Binding Site of Human Complement Factor D. Biochemistry 33:14393-14399
Klaver CCW, Wolfs RCW, Assink JJM, van Duijn CM, Hofman A, de Jong PTVM (1998) Genetic Risk of Age-related Maculopathy: Population-Based Familial Aggregation Study. Arch Ophthalmol 116:1646-1651
Klein ML, Ferris Iii FL, Francis PJ, Lindblad AS, Chew EY, Hamon SC, Ott J (2010) Progression of Geographic Atrophy and Genotype in Age-Related Macular Degeneration. Ophthalmology 117:1554-1559.e1551
Klein R, Klein B, Jensen S, Meuer S (1997) The five-year incidence and progression of age-related maculopathy: the Beaver Dam Eye Study. Ophthalmology 104:7-21
Klein R, Klein B, Linton K (1992) Prevalence of age-related maculopathy. The Beaver Dam Eye Study. Ophthalmology 99:933-943
Klein R, Klein BEK, Knudtson MD, Wong TY, Cotch MF, Liu K, Burke G, Saad MF, Jacobs JDR (2006) Prevalence of Age-Related Macular Degeneration in 4 Racial/Ethnic Groups in the Multi-ethnic Study of Atherosclerosis. Ophthalmology 113:373-380
Klein R, Klein BEK, Tomany SC, Meuer SM, Huang G-H (2002) Ten-year incidence and progression of age-related maculopathy: The Beaver Dam eye study. Ophthalmology 109:1767-1779
Klein R, Peto T, Bird A, Vannewkirk MR (2004) The epidemiology of age-related macular degeneration. American Journal of Ophthalmology 137:486-495
Klein RJ, Zeiss C, Chew EY, Tsai J-Y, Sackler RS, Haynes C, Henning AK, SanGiovanni JP, Mane SM, Mayne ST, Bracken MB, Ferris FL, Ott J, Barnstable C, Hoh J (2005) Complement Factor H Polymorphism in Age-Related Macular Degeneration. Science 308:385-389
Koliopanos A, Friess H, di Mola FF, Tang W-H, Kubulus D, Brigstock D, Zimmermann A, Büchler MW (2002) Connective Tissue Growth Factor Gene Expression Alters Tumor Progression in Esophageal Cancer. World Journal of Surgery 26:420-427
Kondo N, Bessho H, Honda S, Negi A (2010) Additional evidence to support the role of a common variant near the complement factor I gene in susceptibility to age-related macular degeneration. Eur J Hum Genet 18:634-635
Kortvely E, Hauck SM, Duetsch G, Gloeckner CJ, Kremmer E, Alge-Priglinger CS, Deeg CA, Ueffing M (2010) ARMS2 Is a Constituent of the Extracellular Matrix Providing a Link between Familial and Sporadic Age-Related Macular Degenerations. Investigative Ophthalmology & Visual Science 51:79-88
Kralovicova J, Vorechovsky I (2009) SERPING1 rs2511988 and age-related macular degeneration. The Lancet 373:461-462
Krojer T, Pangerl K, Kurt J, Sawa J, Stingl C, Mechtler K, Huber R, Ehrmann M, Clausen T (2008) Interplay of PDZ and protease domain of DegP ensures efficient elimination of misfolded proteins. Proceedings of the National Academy of Sciences 105:7702-7707

Kuiper EJ, de Smet MD, van Meurs JC, Tan HS, Tanck MWT, Oliver N, van Nieuwenhoven FA, Goldschmeding R, Schlingemann RO (2006) Association of Connective Tissue Growth Factor With Fibrosis in Vitreoretinal Disorders in the Human Eye. Arch Ophthalmol 124:1457-1462

Kumar JK, Tabor S, Richardson CC (2004) Proteomic analysis of thioredoxin-targeted proteins in Escherichia coli. Proceedings of the National Academy of Sciences of the United States of America 101:3759-3764

Kurz T, Terman A, Brunk UT (2007) Autophagy, ageing and apoptosis: The role of oxidative stress and lysosomal iron. Archives of Biochemistry and Biophysics 462:220-230

Kvanta A, Algvere PV, Berglin L, Seregard S (1996) Subfoveal fibrovascular membranes in age-related macular degeneration express vascular endothelial growth factor. Investigative Ophthalmology & Visual Science 37:1929-1934

Labat-Robert J (2002) Fibronectin in malignancy: Effect of aging. Seminars in Cancer Biology 12:187-195

Labat-Robert J, Potazman JP, Derouette JC, Robert L (1981) Age-dependent increase of human plasma fibronectin. Cell Biology International Reports 5:969-973

Lambert V, Munaut C, Jost M, Noël A, Werb Z, Foidart J-M, Rakic J-M (2002) Matrix Metalloproteinase-9 Contributes to Choroidal Neovascularization. The American Journal of Pathology 161:1247-1253

Lambert V, Wielockx B, Munaut C, Galopin C, Jost M, Itoh T, Werb Z, Baker A, Libert C, Krell H-W, Foidart J-M, NoÃ«l As, Rakic J-M (2003) MMP-2 and MMP-9 synergize in promoting choroidal neovascularization. The FASEB Journal

Langmann T (2007) Microglia activation in retinal degeneration. Journal of Leukocyte Biology 81:1345-1351

Launay S, Maubert E, Lebeurrier N, Tennstaedt A, Campioni M, Docagne F, Gabriel C, Dauphinot L, Potier MC, Ehrmann M, Baldi A, Vivien D (2008) HtrA1-dependent proteolysis of TGF-[beta] controls both neuronal maturation and developmental survival. Cell Death Differ 15:1408-1416

Lee N, Saeed A (2007) Microarrays: an overview. Methods Mol Biol 353:265-300.

Lengyel I, Flinn JM, Peto T, Linkous DH, Cano K, Bird AC, Lanzirotti A, Frederickson CJ, van Kuijk FJGM (2007) High concentration of zinc in sub-retinal pigment epithelial deposits. Experimental Eye Research 84:772-780

Lesavre P, Müller-Eberhard H (1978) Mechanism of action of factor D of the alternative complement pathway. J Exp Med 148:1498–1509.

Leu ST, Batni S, Radeke MJ, Johnson LV, Anderson DH, Clegg DO (2002) Drusen are Cold Spots for Proteolysis: Expression of Matrix Metalloproteinases and Their Tissue Inhibitor Proteins in Age-related Macular Degeneration. Experimental Eye Research 74:141-154

Levy M, Halbwachs-Mecarelli L, Gubler M, Kohout G, Bensenouci A, Niaudet P, Hauptmann G, P. L (1986) H deficiency in two brothers with atypical dense intramembranous deposit disease. Kidney Int 30:949-956.

Li M, Atmaca-Sonmez P, Othman M, Branham KEH, Khanna R, Wade MS, Li Y, Liang L, Zareparsi S, Swaroop A, Abecasis GR (2006) CFH haplotypes without the Y402H coding variant show strong association with susceptibility to age-related macular degeneration. Nat Genet 38:1049-1054

Li Y-J, Oliveira SA, Xu P, Martin ER, Stenger JE, Scherzer CR, Hauser MA, et al. (2003) Glutathione S-transferase omega-1 modifies age-at-onset of Alzheimer disease and Parkinson disease. Human Molecular Genetics 12:3259-3267
Liang F-Q, Godley BF (2003) Oxidative stress-induced mitochondrial DNA damage in human retinal pigment epithelial cells: a possible mechanism for RPE aging and age-related macular degeneration. Experimental Eye Research 76:397-403
Lin MT, Beal MF (2006) Mitochondrial dysfunction and oxidative stress in neurodegenerative diseases. Nature 443:787-795
Lokki M, Koskimies S (1991) Allelic differences in hemolytic activity and protein concentration of BF molecules are found in association with particular HLA haplotypes. Immunogenetics 34:242-246.
Lopez P, Grossniklaus, HE., Lambert, HM., Aaberg, TM., Capone, A Jr., Sternberg, P Jr., L'Hernault, N. (1991) Pathologic features of surgically excised subretinal neovascular membranes in age-related macular degeneration. Am J Ophthalmol 112:647-656
Lopez P, Lambert H, Grossniklaus H, Sternberg PJ (1993) Well-defined subfoveal choroidal neovascular membranes in age-related macular degeneration. Ophthalmology 100:415-422.
Lorenzi T, Marzioni D, Giannubilo S, Quaranta A, Crescimanno C, De Luca A, Baldi A, Todros T, Tranquilli AL, Castellucci M (2009) Expression Patterns of Two Serine Protease HtrA1 Forms in Human Placentas Complicated by Preeclampsia with and without Intrauterine Growth Restriction. Placenta 30:35-40
Luhmann UFO, Robbie S, Munro PMG, Barker SE, Duran Y, Luong V, Fitzke FW, Bainbridge JWB, Ali RR, MacLaren RE (2009) The Drusenlike Phenotype in Aging Ccl2-Knockout Mice Is Caused by an Accelerated Accumulation of Swollen Autofluorescent Subretinal Macrophages. Investigative Ophthalmology & Visual Science 50:5934-5943
Ly DH, Lockhart DJ, Lerner RA, Schultz PG (2000) Mitotic Misregulation and Human Aging. Science 287:2486-2492
Lynch AM, Murphy JR, Byers T, Gibbs RS, Neville MC, Giclas PC, Salmon JE, Holers VM (2008) Alternative complement pathway activation fragment Bb in early pregnancy as a predictor of preeclampsia. American Journal of Obstetrics and Gynecology 198:385.e381-385.e389
Magnusson KP, Duan S, Sigurdsson H, Petursson H, Yang Z, Zhao Y, Bernstein PS, Ge J, Jonasson F, Stefansson E, Helgadottir G, Zabriskie NA, Jonsson T, Björnsson A, Thorlacius T, Jonsson PV, Thorleifsson G, Kong A, Stefansson H, Zhang K, Stefansson K, Gulcher JR (2005) CFH Y402H Confers Similar Risk of Soft Drusen and Both Forms of Advanced AMD. PLoS Med 3:e5
Majewski J, Schultz DW, Weleber RG, Schain MB, Edwards AO, Matise TC, Acott TS, Ott J, Klein ML (2003) Age-Related Macular Degeneration--a Genome Scan in Extended Families. The American Journal of Human Genetics 73:540-550
Maller J, George S, Purcell S, Fagerness J, Altshuler D, Daly MJ, Seddon JM (2006) Common variation in three genes, including a noncoding variant in CFH, strongly influences risk of age-related macular degeneration. Nat Genet 38:1055-1059
Maminishkis A, Chen S, Jalickee S, Banzon T, Shi G, Wang FE, Ehalt T, Hammer JA, Miller SS (2006) Confluent Monolayers of Cultured Human Fetal Retinal Pigment Epithelium Exhibit Morphology and Physiology of Native Tissue. Investigative Ophthalmology & Visual Science 47:3612-3624

Mantovani A, Sica A, Sozzani S, Allavena P, Vecchi A, Locati M (2004) The chemokine system in diverse forms of macrophage activation and polarization. Trends in Immunology 25:677-686
Mares-Perlman JA, Brady WE, Klein R, VandenLangenberg GM, Klein BEK, Palta M (1995) Dietary Fat and Age-Related Maculopathy. Arch Ophthalmol 113:743-748
Marshall GE, Konstas AG, Reid GG, Edwards JG, Lee WR (1992) Type IV collagen and laminin in Bruch's membrane and basal linear deposit in the human macula. Br J Ophthalmol 76:607–614
Marshall GE, Konstas AGP, Reid GG, Edwards JG, Lee WR (1994) Collagens in the aged human macula. Graefe's Archive for Clinical and Experimental Ophthalmology 232:133-140
Massague J (1990) The Transforming Growth Factor-beta Family. Annual Review of Cell Biology 6:597-641
Mathis D, Shoelson SE (2011) Immunometabolism: an emerging frontier. Nat Rev Immunol 11:81-83
Mathivanan S, Ahmed M, Ahn NG, Alexandre H, Amanchy R, Andrews PC, Bader JS, et al. (2008) Human Proteinpedia enables sharing of human protein data. Nat Biotech 26:164-167
Matsuda S, Gomi F, Oshima Y, Tohyama M, Tano Y (2005) Vascular Endothelial Growth Factor Reduced and Connective Tissue Growth Factor Induced by Triamcinolone in ARPE19 Cells under Oxidative Stress. Investigative Ophthalmology & Visual Science 46:1062-1068
Matsushita M, Thiel S, Jensenius JC, Terai I, Fujita T (2000) Proteolytic Activities of Two Types of Mannose-Binding Lectin-Associated Serine Protease. The Journal of Immunology 165:2637-2642
McIlwain JT (1996) An Introduction to the Biology of Vision. Cambridge University Press.
Meri S, Pangburn MK (1994) Regulation of Alternative Pathway Complement Activation by Glycosaminoglycans: Specificity of the Polyanion Binding Site on Factor H. Biochemical and Biophysical Research Communications 198:52-59
Miller H, Miller B, Ishibashi T, Ryan SJ (1990) Pathogenesis of laser-induced choroidal subretinal neovascularization. Investigative Ophthalmology & Visual Science 31:899-908
Miyajima-Uchida H, Hayashi H, Beppu R, Kuroki M, Fukami M, Arakawa F, Tomita Y, Kuroki M, Oshima K (2000) Production and Accumulation of Thrombospondin-1 in Human Retinal Pigment Epithelial Cells. Investigative Ophthalmology & Visual Science 41:561-567
Miyazono K, Olofsson A, Colosetti P, Heldin C (1991) A role of the latent TGF-beta 1-binding protein in the assembly and secretion of TGF-beta 1. EMBO J 10:1091-1101.
Montes T, Goicoechea de Jorge E, Ramos R, Gomà M, Pujol O, Sánchez-Corral P, Rodríguez de Córdoba S (2008) Genetic deficiency of complement factor H in a patient with age-related macular degeneration and membranoproliferative glomerulonephritis. Molecular Immunology 45:2897-2904
Montes T, Tortajada A, Morgan BP, Rodríguez de Córdoba S, Harris CL (2009) Functional basis of protection against age-related macular degeneration conferred

by a common polymorphism in complement factor B. Proceedings of the National Academy of Sciences 106:4366-4371
Morgan B, Gasque P (1997) Extrahepatic complement biosynthesis: where, when and why? . Clin Exp Immunol 107:1-7.
Mousa SA, Lorelli W, Campochiaro PA (1999) Role of hypoxia and extracellular matrix-integrin binding in the modulation of angiogenic growth factors secretion by retinal pigmented epithelial cells. Journal of Cellular Biochemistry 74:135-143
Müller-Eberhard H, Götze O (1972) C3 proactivator convertase and its mode of action. J Exp Med 135:1003-1008.
Mullins R, Aptsiauri N, Hageman G (2001) Structure and composition of drusen associated with glomerulonephritis: implications for the role of complement activation in drusen biogenesis. Eye (Lond) 15:390-395.
Mullins RF, Russell SR, Anderson DH, Hageman GS (2000) Drusen associated with aging and age-related macular degeneration contain proteins common to extracellular deposits associated with atherosclerosis, elastosis, amyloidosis, and dense deposit disease. The FASEB Journal 14:835-846
Murphy-Ullrich JE, Schultz-Cherry S, Hook M (1992) Transforming growth factor-beta complexes with thrombospondin. Mol Biol Cell 3:181-188
Murphy M, Godson C, Cannon S, Kato S, Mackenzie HS, Martin F, Brady HR (1999) Suppression Subtractive Hybridization Identifies High Glucose Levels as a Stimulus for Expression of Connective Tissue Growth Factor and Other Genes in Human Mesangial Cells. Journal of Biological Chemistry 274:5830-5834
Murwantoko, Yano M, Ueta Y, Murasaki A, Kanda H, Oka C, Kawaichi M (2004) Binding of proteins to the PDZ domain regulates proteolytic activity of HtrA1 serine protease. The Biochemical journal 381:895-904
Nagai N, Klimava A, Lee W-H, Izumi-Nagai K, Handa JT (2009) CTGF Is Increased in Basal Deposits and Regulates Matrix Production through the ERK (p42/p44mapk) MAPK and the p38 MAPK Signaling Pathways. Investigative Ophthalmology & Visual Science 50:1903-1910
Nan R, Gor J, Lengyel I, Perkins SJ (2008) Uncontrolled Zinc- and Copper-Induced Oligomerisation of the Human Complement Regulator Factor H and Its Possible Implications for Function and Disease. Journal of Molecular Biology 384:1341-1352
Narayanan AS, Page RC (1983) Biosynthesis and regulation of type V collagen in diploid human fibroblasts. Journal of Biological Chemistry 258:11694-11699
Nicosia RF, Tuszynski GP (1994) Matrix-bound thrombospondin promotes angiogenesis in vitro. The Journal of Cell Biology 124:183-193
Nie G-Y, Hampton A, Li Y, Findlay JK, Salamonsen LA (2003) Identification and cloning of two isoforms of human high-temperature requirement factor A3 (HtrA3), characterization of its genomic structure and comparison of its tissue distribution with HtrA1 and HtrA2. Biochem J 371:39-48
Nozaki M, Raisler BJ, Sakurai E, Sarma JV, Barnum SR, Lambris JD, Chen Y, Zhang K, Ambati BK, Baffi JZ, Ambati J (2006a) Drusen complement components C3a and C5a promote choroidal neovascularization. Proceedings of the National Academy of Sciences of the United States of America 103:2328-2333
Nozaki M, Sakurai E, Raisler BJ, Baffi JZ, Witta J, Ogura Y, Brekken RA, Sage EH, Ambati BK, Ambati J (2006b) Loss of SPARC-mediated VEGFR-1 suppression

after injury reveals a novel antiangiogenic activity of VEGF-A. The Journal of Clinical Investigation 116:422-429
Oemar BS, Luscher TF (1997) Connective Tissue Growth Factor : Friend or Foe? Arterioscler Thromb Vasc Biol 17:1483-1489
Oka C, Tsujimoto R, Kajikawa M, Koshiba-Takeuchi K, Ina J, Yano M, Tsuchiya A, Ueta Y, Soma A, Kanda H, Matsumoto M, Kawaichi M (2004) HtrA1 serine protease inhibits signaling mediated by Tgfbeta family proteins. Development (Cambridge, England) 131:1041-1053
Østerud B, Eskeland T (1982) The mandatory role of complement in the endotoxin-induced synthesis of tissue thromboplastin in blood monocytes. FEBS Letters 149:75-79
Ozturk A, Desai PP, Minster RL, DeKosky ST, Kamboh MI (2005) Three SNPs in the GSTO1, GSTO2 and PRSS11 genes on chromosome 10 are not associated with age-at-onset of Alzheimer's disease. Neurobiology of Aging 26:1161-1165
Pangburn MK, Pangburn KLW, Koistinen V, Meri S, Sharma AK (2000) Molecular Mechanisms of Target Recognition in an Innate Immune System: Interactions Among Factor H, C3b, and Target in the Alternative Pathway of Human Complement ,2. The Journal of Immunology 164:4742-4751
Pascual M, Steiger G, Estreicher J, Macon K, Volanakis JE, Schifferli JA (1988) Metabolism of complement factor D in renal failure. Kidney International 34:529-536
Pauleikhoff D, Zuels S, Sheraidah GS, Marshall J, Wessing A, Bird AC (1992) Correlation between biochemical composition and fluorescein binding of deposits in Bruch’s membrane. . Ophthalmology 99:1548-1553
Penfold P, Killingsworth M, Sarks S (1985) Senile macular degeneration: the involvement of immunocompetent cells. Graefes Arch Clin Exp Ophthalmol 223:69-76.
Penfold PL, Madigan MC, Gillies MC, Provis JM (2001) Immunological and Aetiological Aspects of Macular Degeneration. Progress in Retinal and Eye Research 20:385-414
Pickering MC, Cook HT, Warren J, Bygrave AE, Moss J, Walport MJ, Botto M (2002) Uncontrolled C3 activation causes membranoproliferative glomerulonephritis in mice deficient in complement factor H. Nat Genet 31:424-428
Poquet I, Saint V, Seznec E, Simoes N, Bolotin A, Gruss A (2000) HtrA is the unique surface housekeeping protease in Lactococcus lactis and is required for natural protein processing. Molecular Microbiology 35:1042-1051
Prosser BE, Johnson S, Roversi P, Herbert AP, Blaum BS, Tyrrell J, Jowitt TA, Clark SJ, Tarelli E, Uhrín D, Barlow PN, Sim RB, Day AJ, Lea SM (2007) Structural basis for complement factor H-linked age-related macular degeneration. The Journal of Experimental Medicine 204:2277-2283
Puig O, Caspary F, Rigaut G, Rutz B, Bouveret E, Bragado-Nilsson E, Wilm M, Séraphin B (2001) The Tandem Affinity Purification (TAP) Method: A General Procedure of Protein Complex Purification. Methods 24:218-229
Ramrattan RS, van der Schaft TL, Mooy CM, de Bruijn WC, Mulder PG, de Jong PT (1994) Morphometric analysis of Bruch's membrane, the choriocapillaris, and the choroid in aging. Investigative Ophthalmology & Visual Science 35:2857-2864

Rattner A, Smallwood PM, Nathans J (2000) Identification and Characterization of All-trans-retinol Dehydrogenase from Photoreceptor Outer Segments, the Visual Cycle Enzyme That Reduces All-trans-retinal to All-trans-retinol. Journal of Biological Chemistry 275:11034-11043

Raychaudhuri S, Ripke S, Li M, Neale BM, Fagerness J, Reynolds R, Sobrin L, Swaroop A, Abecasis G, Seddon JM, Daly MJ (2010) Associations of CFHR1-CFHR3 deletion and a CFH SNP to age-related macular degeneration are not independent. Nat Genet 42:553-555

Renno RZ, Youssri AI, Michaud N, Gragoudas ES, Miller JW (2002) Expression of Pigment Epitheliumâ€"Derived Factor in Experimental Choroidal Neovascularization. Investigative Ophthalmology & Visual Science 43:1574-1580

Reynolds R, Hartnett ME, Atkinson JP, Giclas PC, Rosner B, Seddon JM (2009) Plasma complement components and activation fragments: associations with age-related macular degeneration genotypes and phenotypes. Investigative ophthalmology & visual science 50:5818-5827

Riley-Vargas RC, Gill DB, Kemper C, Liszewski MK, Atkinson JP (2004) CD46: expanding beyond complement regulation. Trends in Immunology 25:496-503

Rivera A, Fisher SA, Fritsche LG, Keilhauer CN, Lichtner P, Meitinger T, Weber BHF (2005) Hypothetical LOC387715 is a second major susceptibility gene for age-related macular degeneration, contributing independently of complement factor H to disease risk. Human Molecular Genetics 14:3227-3236

Robman L, Mahdi O, McCarty C, Dimitrov P, Tikellis G, McNeil J, Byrne G, Taylor H, Guymer R (2005) Exposure to Chlamydia pneumoniae Infection and Progression of Age-related Macular Degeneration. American Journal of Epidemiology 161:1013-1019

Rodriguez-Manzaneque JC, Lane TF, Ortega MAn, Hynes RO, Lawler J, Iruela-Arispe ML (2001) Thrombospondin-1 suppresses spontaneous tumor growth and inhibits activation of matrix metalloproteinase-9 and mobilization of vascular endothelial growth factor. Proceedings of the National Academy of Sciences 98:12485-12490

Rodríguez de Córdoba S, Esparza-Gordillo J, Goicoechea de Jorge E, Lopez-Trascasa M, Sánchez-Corral P (2004) The human complement factor H: functional roles, genetic variations and disease associations. Molecular Immunology 41:355-367

Rohrer B, Guo Y, Kunchithapautham K, Gilkeson GS (2007) Eliminating complement factor D reduces photoreceptor susceptibility to light-induced damage. Investigative ophthalmology & visual science 48:5282-5289

Ross RJ, Zhou M, Shen D, Fariss RN, Ding X, Bojanowski CM, Tuo J, Chan C-C (2008) Immunological protein expression profile in Ccl2/Cx3cr1 deficient mice with lesions similar to age-related macular degeneration. Experimental Eye Research 86:675-683

Ruiz-Ortega M, Rupérez M, Esteban V, Rodriguez-Vita J, Sánchez-López E, Carvajal G, Egido J (2006) Angiotensin II: a key factor in the inflammatory and fibrotic response in kidney diseases. Nephrology Dialysis Transplantation 21:16-20

Runyon ST, Zhang Y, Appleton BA, Sazinsky SL, Wu P, Pan B, Wiesmann C, Skelton NJ, Sidhu SS (2007) Structural and functional analysis of the PDZ domains of human HtrA1 and HtrA3. Protein Science 16:2454-2471

Russell SR, Mullins RF, Schneider BL, Hageman GS (2000) Location, substructure, and composition of basal laminar drusen compared with drusen associated with aging and age-related macular degeneration. American Journal of Ophthalmology 129:205-214

Sakurai E, Anand A, Ambati BK, van Rooijen N, Ambati J (2003) Macrophage Depletion Inhibits Experimental Choroidal Neovascularization. Investigative Ophthalmology & Visual Science 44:3578-3585

Salmon JE, Heuser C, Triebwasser M, Liszewski MK, Kavanagh D, Roumenina L, Branch DW, Goodship T, Fremeaux-Bacchi V, Atkinson JP (2011) Mutations in Complement Regulatory Proteins Predispose to Preeclampsia: A Genetic Analysis of the PROMISSE Cohort. PLoS Med 8:e1001013

Sarks S, Cherepanoff S, Killingsworth M, Sarks J (2007) Relationship of Basal Laminar Deposit and Membranous Debris to the Clinical Presentation of Early Age-Related Macular Degeneration. Investigative Ophthalmology & Visual Science 48:968-977

Schmid-Kubista KE, Tosakulwong N, Wu Y, Ryu E, Hecker LA, Baratz KH, Brown WL, Edwards AO (2009) Contribution of Copy Number Variation in the Regulation of Complement Activation Locus to Development of Age-Related Macular Degeneration. Investigative Ophthalmology & Visual Science 50:5070-5079

Schmidt S, Hauser MA, Scott WK, Postel EA, Agarwal A, Gallins P, Wong F, Chen YS, Spencer K, Schnetz-Boutaud N, Haines JL, Pericak-Vance MA (2006) Cigarette Smoking Strongly Modifies the Association of LOC387715 and Age-Related Macular Degeneration. The American Journal of Human Genetics 78:852-864

Scholl HPN, Fleckenstein M, Fritsche LG, Schmitz-Valckenberg S, Göbel A, Adrion C, Herold C, Keilhauer CN, Mackensen F, Mößner A, Pauleikhoff D, Weinberger AWA, Mansmann U, Holz FG, Becker T, Weber BHF (2009) CFH, C3 and ARMS2 Are Significant Risk Loci for Susceptibility but Not for Disease Progression of Geographic Atrophy Due to AMD. PLoS ONE 4:e7418

Scholl HPN, Issa PC, Walier M, Janzer S, Pollok-kopp B, Fritsche LG, Chong NV, Fimmers R, Wienker T, G F, Weber BHF, Oppermann M (2008) Systemic Complement Activation in Age-Related Macular Degeneration. Complement 3:1-7

Schreiber R, Müller-Eberhard H (1978) Assembly of the cytolytic alternative pathway of complement from 11 isolated plasma proteins. J Exp Med 148:1722-1727.

Schultz-Cherry S, Murphy-Ullrich JE (1993) Thrombospondin causes activation of latent transforming growth factor-beta secreted by endothelial cells by a novel mechanism. The Journal of Cell Biology 122:923-932

Schultz DW, Klein ML, Humpert AJ, Luzier CW, Persun V, Schain M, Mahan A, Runckel C, Cassera M, Vittal V, Doyle TM, Martin TM, Weleber RG, Francis PJ, Acott TS (2003) Analysis of the ARMD1 locus: evidence that a mutation in HEMICENTIN-1 is associated with age-related macular degeneration in a large family. Human Molecular Genetics 12:3315-3323

Schwesinger C, Yee C, Rohan RM, Joussen AM, Fernandez A, Meyer TN, Poulaki V, Ma JJK, Redmond TM, Liu S, Adamis AP, D'Amato RJ (2001) Intrachoroidal Neovascularization in Transgenic Mice Overexpressing Vascular Endothelial

Growth Factor in the Retinal Pigment Epithelium. The American Journal of Pathology 158:1161-1172
Sciarra J, Kaplan S, Grumbach M (1963) LOCALIZATION OF ANTI-HUMAN GROWTH HORMONE SERUM WITHIN THE HUMAN PLACENTA: EVIDENCE FOR A HUMAN CHORIONIC 'GROWTH HORMONE-PROLACTIN'. Nature 199:1005-1006.
Seddon J, Ajani U, Sperduto R, Hiller R, Blair N, Burton T, Farber M, Gragoudas E, Haller J, Miller D, al. e (1994) Dietary carotenoids, vitamins A, C, and E, and advanced age-related macular degeneration. Eye Disease Case-Control Study Group. JAMA 272:1413-1420
Seddon J, Cote J, Davis N, Rosner B (2003a) Progression of age-related macular degeneration: association with body mass index, waist circumference, and waist-hip ratio. Arch Ophthalmol 121:785-792.
Seddon J, Willett W, Speizer F, SE. H (1996) A prospective study of cigarette smoking and age-related macular degeneration in women. . JAMA 276:1141-1146
Seddon JM, Cote J, Davis N, Rosner B (2003b) Progression of Age-Related Macular Degeneration: Association With Body Mass Index, Waist Circumference, and Waist-Hip Ratio. Arch Ophthalmol 121:785-792
Seddon JM, Cote J, Rosner B (2003c) Progression of Age-Related Macular Degeneration: Association With Dietary Fat, Transunsaturated Fat, Nuts, and Fish Intake. Arch Ophthalmol 121:1728-1737
Seddon JM, Gensler G, Klein ML, Milton RC (2006a) C-reactive protein and homocysteine are associated with dietary and behavioral risk factors for age-related macular degeneration. Nutrition 22:441-443
Seddon JM, Gensler G, Rosner B (2010) C-Reactive Protein and CFH, ARMS2/HTRA1 Gene Variants Are Independently Associated with Risk of Macular Degeneration. Ophthalmology 117:1560-1566
Seddon JM, Reynolds R, Maller J, Fagerness JA, Daly MJ, Rosner B (2009) Prediction Model for Prevalence and Incidence of Advanced Age-Related Macular Degeneration Based on Genetic, Demographic, and Environmental Variables. Investigative Ophthalmology & Visual Science 50:2044-2053
Seddon JM, Rosner B, Sperduto RD, Yannuzzi L, Haller JA, Blair NP, Willett W (2001) Dietary Fat and Risk for Advanced Age-Related Macular Degeneration. Arch Ophthalmol 119:1191-1199
Seddon JM, Santangelo SL, Book K, Chong S, Cote J (2003d) A Genomewide Scan for Age-Related Macular Degeneration Provides Evidence for Linkage to Several Chromosomal Regions. The American Journal of Human Genetics 73:780-790
Seddon JM, Sharma S, Adelman RA (2006b) Evaluation of the Clinical Age-Related Maculopathy Staging System. Ophthalmology 113:260-266
Seher A, Nickel J, Mueller T, Kneitz S, Gebhardt S, ter Vehn T, Schlunck G, Sebald W (2011) Gene expression profiling of connective tissue growth factor (CTGF) stimulated primary human tenon fibroblasts reveals an inflammatory and wound healing response in vitro. Mol Vis 17:53-62.
Sheridan CM, Magee RM, Hiscott PS, Hagan S, Wong DH, McGalliard JN, Grierson I (2002) The role of matricellular proteins thrombospondin-1 and osteonectin during RPE cell migration in proliferative vitreoretinopathy. Current Eye Research 25:279-285

Shiga A, Nozaki H, Yokoseki A, Nihonmatsu M, Kawata H, Kato T, Koyama A, Arima K, Ikeda M, Katada S, Toyoshima Y, Takahashi H, Tanaka A, Nakano I, Ikeuchi T, Nishizawa M, Onodera O (2011) Cerebral small-vessel disease protein HTRA1 controls the amount of TGF-B1 via cleavage of proTGF-B1. Human Molecular Genetics 20:1800-1810.

Shimo T, Nakanishi T, Nishida T, Asano M, Kanyama M, Kuboki T, Tamatani T, Tezuka K, Takemura M, Matsumura T, Takigawa M (1999) Connective Tissue Growth Factor Induces the Proliferation, Migration, and Tube Formation of Vascular Endothelial Cells In Vitro, and Angiogenesis In Vivo. Journal of Biochemistry 126:137-145

Singh KK, Krawczak M, Dawson WW, Schmidtke J (2009) Association of HTRA1 and ARMS2 gene variation with drusen formation in rhesus macaques. Experimental Eye Research 88:479-482

Sobrin L, Reynolds R, Yu Y, Fagerness J, Leveziel N, Bernstein PS, Souied EH, Daly MJ, Seddon JM (2011) ARMS2/HTRA1 Locus Can Confer Differential Susceptibility to the Advanced Subtypes of Age-Related Macular Degeneration. American Journal of Ophthalmology 151:345-352.e343

Sommer A, Tielsch JM, Katz J, Quigley HA, Gottsch JD, Javitt JC, Martone JF, Royall RM, Witt KA, Ezrine S (1991) Racial Differences in the Cause-Specific Prevalence of Blindness in East Baltimore. New England Journal of Medicine 325:1412-1417

Sparrow JR, Boulton M (2005) RPE lipofuscin and its role in retinal pathobiology. Experimental Eye Research 80:595-606

Spraul CW, Lang GE, Grossniklaus HE, Lang GK (1999) Histologic and Morphometric Analysis of the Choroid, Bruch's Membrane, and Retinal Pigment Epithelium in Postmortem Eyes With Age-Related Macular Degeneration and Histologic Examination of Surgically Excised Choroidal Neovascular Membranes. Survey of Ophthalmology 44:S10-S32

Sprong T, Roos D, Weemaes C, Neeleman C, Geesing CLM, Mollnes TE, van Deuren M (2006) Deficient alternative complement pathway activation due to factor D deficiency by 2 novel mutations in the complement factor D gene in a family with meningococcal infections. Blood 107:4865-4870

Stone EM, Braun Ta, Russell SR, Kuehn MH, Lotery AJ, Moore Pa, Eastman CG, Casavant TL, Sheffield VC (2004) Missense variations in the fibulin 5 gene and age-related macular degeneration. The New England journal of medicine 351:346-353

Stone EM, Lotery AJ, Munier FL, Heon E, Piguet B, Guymer RH, Vandenburgh K, Cousin P, Nishimura D, Swiderski RE, Silvestri G, Mackey DA, Hageman GS, Bird AC, Sheffield VC, Schorderet DF (1999) A single EFEMP1 mutation associated with both Malattia Leventinese and Doyne honeycomb retinal dystrophy. Nat Genet 22:199-202

Strauss O (2005) The Retinal Pigment Epithelium in Visual Function. Physiological Reviews 85:845-881

Surveyor GA, Wilson AK, Brigstock DR (1998) Localization of Connective Tissue Growth Factor during the Period of Embryo Implantation in the Mouse. Biology of Reproduction 59:1207-1213

Taipale J, Keski-Oja J (1997) Growth factors in the extracellular matrix. The FASEB Journal 11:51-59

Taipale J, Miyazono K, Heldin CH, Keski-Oja J (1994) Latent transforming growth factor-beta 1 associates to fibroblast extracellular matrix via latent TGF-beta binding protein. The Journal of Cell Biology 124:171-181
Takahashi M, Ishida Y, Iwaki D, Kanno K, Suzuki T, Endo Y, Homma Y, Fujita T (2010) Essential role of mannose-binding lectin-associated serine protease-1 in activation of the complement factor D. The Journal of experimental medicine 207:29-37
Takeshita A, Kondo T, Okada T, Kusakabe KT (2010) Elevation of Adipsin, a Complement Activating Factor, in the Mouse Placenta During Spontaneous Abortion. The Journal of Reproduction and Development 56:508-514
Taraboletti G, Morbidelli L, Donnini S, Parenti A, Granger HJ, Giavazzi R, Ziche M (2000) The heparin binding 25 kDa fragment of thrombospondin-1 promotes angiogenesis and modulates gelatinase and TIMP-2 production in endothelial cells. The FASEB Journal 14:1674-1676
Taraboletti G, Roberts D, Liotta LA, Giavazzi R (1990) Platelet thrombospondin modulates endothelial cell adhesion, motility, and growth: a potential angiogenesis regulatory factor. The Journal of Cell Biology 111:765-772
Tate DJ, Miceli MV, Newsome DA (1995) Phagocytosis and H2O2 induce catalase and metallothionein gene expression in human retinal pigment epithelial cells. Investigative Ophthalmology & Visual Science 36:1271-1279
ten Dijke P, Arthur HM (2007) Extracellular control of TGF[beta] signalling in vascular development and disease. Nat Rev Mol Cell Biol 8:857-869
Terai I, Kobayashi K, Matsushita M, Fujita T (1997) Human serum mannose-binding lectin (MBL)-associated serine protease-1 (MASP-1): determination of levels in body fluids and identification of two forms in serum. Clin Exp Immunol 110:317-323.
Termine JD, Kleinman HK, Whitson SW, Conn KM, McGarvey ML, Martin GR (1981) Osteonectin, a bone-specific protein linking mineral to collagen. Cell 26:99-105
The Eye Diseases Prevalence Research G (2004) Prevalence of Age-Related Macular Degeneration in the United States. Arch Ophthalmol 122:564-572
Thurman JM, Renner B, Kunchithapautham K, Ferreira VP, Pangburn MK, Ablonczy Z, Tomlinson S, Holers VM, Rohrer Br (2009) Oxidative Stress Renders Retinal Pigment Epithelial Cells Susceptible to Complement-mediated Injury. Journal of Biological Chemistry 284:16939-16947
Tomany SC, Wang JJ, van Leeuwen R, Klein R, Mitchell P, Vingerling JR, Klein BEK, Smith W, de Jong PTVM (2004) Risk factors for incident age-related macular degeneration: Pooled findings from 3 continents. Ophthalmology 111:1280-1287
Tortajada An, Montes T, MartÄ±Ì□nez-Barricarte Rn, Morgan BP, Harris CL, de CÃ³rdoba SRg (2009) The disease-protective complement factor H allotypic variant Ile62 shows increased binding affinity for C3b and enhanced cofactor activity. Human Molecular Genetics 18:3452-3461
Truebestein L, Tennstaedt A, MÃ¶nig T, Krojer T, Canellas F, Kaiser M, Clausen T, Ehrmann M (2011) Substrate-induced remodeling of the active site regulates human HTRA1 activity. Nat Struct Mol Biol 18:386-388
Tuo J, Bojanowski CM, Zhou M, Shen D, Ross RJ, Rosenberg KI, Cameron DJ, Yin C, Kowalak JA, Zhuang Z, Zhang K, Chan C-C (2007) Murine Ccl2/Cx3cr1

Deficiency Results in Retinal Lesions Mimicking Human Age-Related Macular Degeneration. Investigative Ophthalmology & Visual Science 48:3827-3836
Tuo J, Smith BC, Bojanowski CM, Meleth AD, Gery I, Csaky KG, Chew EY, Chan C-C (2004) The involvement of sequence variation and expression of CX3CR1 in the pathogenesis of age-related macular degeneration. The FASEB Journal
Uno K, Bhutto Ia, McLeod DS, Merges C, Lutty Ga (2006) Impaired expression of thrombospondin-1 in eyes with age related macular degeneration. The British journal of ophthalmology 90:48-54
Vaisbuch E, Romero R, Erez O, Mazaki-Tovi S, Pedro KJ, Soto E, Gotsch F, Dong Z, Chaiworapongsa T, Kim SK, Mittal P, Pacora P, Yeo L, Hassan SS (2009) Fragment Bb in amniotic fluid: evidence for complement activation by the alternative pathway in women with intra-amniotic infection/inflammation. Journal of Maternal-Fetal and Neonatal Medicine 22:905-916
van der Schaft TL, Mooy CM, de Bruijn WC, Oron FG, Mulder PG, de Jong PT (1992) Histologic features of the early stages of age-related macular degeneration. A statistical analysis. Ophthalmology 99:278-286
van Soest S, de Wit GM, Essing AH, ten Brink JB, Kamphuis W, de Jong PT, Bergen AA (2007) Comparison of human retinal pigment epithelium gene expression in macula and periphery highlights potential topographic differences in Bruch's membrane. Mol Vis 13:1608 - 1617
VanNewkirk MR, Nanjan MB, Wang JJ, Mitchell P, Taylor HR, McCarty CA (2000) The prevalence of age-related maculopathy : The visual impairment project. Ophthalmology 107:1593-1600
Vaziri-Sani F, Hellwage J, Zipfel PF, Sjöholm AG, Iancu R, Karpman D (2005) Factor H binds to washed human platelets. Journal of Thrombosis and Haemostasis 3:154-162
Vierkotten S, Muether PS, Fauser S (2011) Overexpression of HTRA1 Leads to Ultrastructural Changes in the Elastic Layer of Bruch's Membrane via Cleavage of Extracellular Matrix Components. PLoS ONE 6:e22959
Vogt W, Dieminger L, Lynen R, Schmidt G (1974) Alternative pathway for the activation of complement in human serum. Formation and composition of the complex with cobra venom factor that cleaves the third component of complement. Hoppe Seylers Z Physiol Chem 55:171-183.
Volanakis JE, Narayana SVL (1996) Complement factor D, a novel serine protease. Protein Science 5:553-564
Wallace DC (2005) A MITOCHONDRIAL PARADIGM OF METABOLIC AND DEGENERATIVE DISEASES, AGING, AND CANCER: A Dawn for Evolutionary Medicine. Annual Review of Genetics 39:359-407
Walport MJ (2001) Complement. New England Journal of Medicine 344:1058-1066
Walshe TE, Saint-Geniez M, Maharaj ASR, Sekiyama E, Maldonado AE, D'Amore PA (2009) TGF-β Is Required for Vascular Barrier Function, Endothelial Survival and Homeostasis of the Adult Microvasculature. PLoS ONE 4:e5149
Wan YY, Flavell RA (2007) 'Yin–Yang' functions of transforming growth factor-β and T regulatory cells in immune regulation. Immunological Reviews 220:199-213
Wang G, Scott WK, Haines JL, Pericak-Vance MA (2010a) Genotype at Polymorphism rs11200638 and HTRA1 Expression Level. Arch Ophthalmol 128:1491-1493

Wang G, Spencer K, Scott W, Whitehead P, Court B, Ayala-Haedo J, Mayo P, Schwartz S, Kovach J, Gallins P, Polk M, Agarwal A, Postel E, Haines J, Pericak-Vance M (2010b) Analysis of the indel at the ARMS2 3′UTR in age-related macular degeneration. Human Genetics 127:595-602

Wang J, Ohno-Matsui K, Yoshida T, Kojima A, Shimada N, Nakahama K-i, Safranova O, Iwata N, Saido TC, Mochizuki M, Morita I (2008) Altered Function of Factor I Caused by Amyloid β: Implication for Pathogenesis of Age-Related Macular Degeneration from Drusen. The Journal of Immunology 181:712-720

Wang Z, Rolish ME, Yeo G, Tung V, Mawson M, Burge CB (2004) Systematic Identification and Analysis of Exonic Splicing Silencers. Cell 119:831-845

Warburton S, Southwick K, Hardman R, Secrest A, Grow R, Xin H, Woolley A, Burton G, Thulin C (2005) Examining the proteins of functional retinal lipofuscin using proteomic analysis as a guide for understanding its origin. Mol Vis 11:1122-1134.

Watanabe D, Takagi H, Suzuma K, Oh H, Ohashi H, Y. H (2005) Expression of connective tissue growth factor and its potential role in choroidal neovascularization. Retina 25:911-918.

Weber BHF, Vogt G, Pruett RC, Stohr H, Felbor U (1994) Mutations in the tissue inhibitor of metalloproteinases-3 (TIMP3) in patients with Sorsby's fundus dystrophy. Nat Genet 8:352-356

Weeks DE, Conley YP, Tsai H-J, Mah TS, Schmidt S, Postel EA, Agarwal A, Haines JL, Pericak-Vance MA, Rosenfeld PJ, Paul TO, Eller AW, Morse LS, Dailey JP, Ferrell RE, Gorin MB (2004) Age-Related Maculopathy: A Genomewide Scan with Continued Evidence of Susceptibility Loci within the 1q31, 10q26, and 17q25 Regions. The American Journal of Human Genetics 75:174-189

Weiss LA, Pan L, Abney M, Ober C (2006) The sex-specific genetic architecture of quantitative traits in humans. Nat Genet 38:218-222

Weyer C, Yudkin JS, Stehouwer CDA, Schalkwijk CG, Pratley RE, Tataranni PA (2002) Humoral markers of inflammation and endothelial dysfunction in relation to adiposity and in vivo insulin action in Pima Indians. Atherosclerosis 161:233-242

Whaley K (1980) Biosynthesis of the complement components and the regulatory proteins of the alternative complement pathway by human peripheral blood monocytes. J Exp Med 151:501-516.

White RT, Damm D, Hancock N, Rosen BS, Lowell BB, Usher P, Flier JS, Spiegelman BM (1992) Human adipsin is identical to complement factor D and is expressed at high levels in adipose tissue. Journal of Biological Chemistry 267:9210-9213

Witmer AN, Vrensen GFJM, Van Noorden CJF, Schlingemann RO (2003) Vascular endothelial growth factors and angiogenesis in eye disease. Progress in Retinal and Eye Research 22:1-29

WTCCC (2007) Genome-wide association study of 14,000 cases of seven common diseases and 3,000 shared controls. Nature 447:661-678

Xu H, Chen M, Manivannan A, Lois N, Forrester JV (2008) Age-dependent accumulation of lipofuscin in perivascular and subretinal microglia in experimental mice. Aging Cell 7:58-68

Xu Y, Narayana SVL, Volanakis JE (2001) Structural biology of the alternative pathway convertase. Immunological Reviews 180:123-135

Yamada Y, Ishibashi K, Ishibashi K, Bhutto IA, Tian J, Lutty GA, Handa JT (2006) The expression of advanced glycation endproduct receptors in rpe cells associated with basal deposits in human maculas. Experimental Eye Research 82:840-848
Yamagishi K, Ohkuma H, Itagaki T, Katoh N, Takahashi K, Uyama M (1988) Implication of retinal pigment epithelium on experimental subretinal neovascularization in the developmental stage. Nippon Ganka Gakkai Zasshi 92:1629–1636.
Yamauchi Y, Stevens JW, Macon KJ, Volanakis JE (1994) Recombinant and native zymogen forms of human complement factor D. Journal of immunology (Baltimore, Md : 1950) 152:3645-3653
Yang M, Huang H, Li J, Huang W, Wang H (2007) Connective tissue growth factor increases matrix metalloproteinase-2 and suppresses tissue inhibitor of matrix metalloproteinase-2 production by cultured renal interstitial fibroblasts. Wound Repair and Regeneration 15:817-824
Yang Z, Camp NJ, Sun H, Tong Z, Gibbs D, Cameron DJ, Chen H, Zhao Y, Pearson E, Li X, Chien J, Dewan A, Harmon J, Bernstein PS, Shridhar V, Zabriskie Na, Hoh J, Howes K, Zhang K (2006) A variant of the HTRA1 gene increases susceptibility to age-related macular degeneration. Science (New York, NY) 314:992-993
Yang Z, Tong Z, Chen Y, Zeng J, Lu F, Sun X, Zhao C, et al. (2010) Genetic and Functional Dissection of HTRA1 and LOC387715 in Age-Related Macular Degeneration. PLoS Genet 6:e1000836
Yasuma T, Nakamura M, Nishiguchi K, Kikuchi M, Kaneko H, Niwa T, Hamajima N, Terasaki H (2010) Elevated C-reactive protein levels and ARMS2/HTRA1 gene variants in subjects without age-related macular degeneration. Mol Vis 16:2923-2930.
Yates JRW, Sepp T, Matharu BK, Khan JC, Thurlby DA, Shahid H, Clayton DG, Hayward C, Morgan J, Wright AF, Armbrecht AM, Dhillon B, Deary IJ, Redmond E, Bird AC, Moore AT (2007) Complement C3 Variant and the Risk of Age-Related Macular Degeneration. New England Journal of Medicine 357:553-561
Yu AL, Lorenz RL, Haritoglou C, Kampik A, Welge-Lussen U (2009) Biological effects of native and oxidized low-density lipoproteins in cultured human retinal pigment epithelial cells. Experimental Eye Research 88:495-503
Yu Q, Stamenkovic I (2000) Cell surface-localized matrix metalloproteinase-9 proteolytically activates TGF-beta and promotes tumor invasion and angiogenesis. Genes & Development 14:163-176
Yu Y, Bhangale TR, Fagerness J, Ripke S, Thorleifsson G, Tan PL, Souied EH, et al. (2011) Common variants near FRK/COL10A1 and VEGFA are associated with advanced age-related macular degeneration. Human Molecular Genetics
Yuan X, Gu X, Crabb JS, Yue X, Shadrach K, Hollyfield JG, Crabb JW (2010) Quantitative Proteomics: Comparison of the Macular Bruch Membrane/Choroid Complex from Age-related Macular Degeneration and Normal Eyes. Molecular & Cellular Proteomics 9:1031-1046
Yudkin JS, Stehouwer CDA, Emeis JJ, Coppack SW (1999) C-Reactive Protein in Healthy Subjects: Associations With Obesity, Insulin Resistance, and Endothelial Dysfunction : A Potential Role for Cytokines Originating From Adipose Tissue? Arterioscler Thromb Vasc Biol 19:972-978

Zamiri P, Masli S, Kitaichi N, Taylor AW, Streilein JW (2005) Thrombospondin Plays a Vital Role in the Immune Privilege of the Eye. Investigative Ophthalmology & Visual Science 46:908-919

Zareparsi S, Branham KEH, Li M, Shah S, Klein RJ, Ott J, Hoh J, Abecasis GR, Swaroop A (2005a) Strong Association of the Y402H Variant in Complement Factor H at 1q32 with Susceptibility to Age-Related Macular Degeneration. The American Journal of Human Genetics 77:149-153

Zareparsi S, Buraczynska M, Branham KEH, Shah S, Eng D, Li M, Pawar H, Yashar BM, Moroi SE, Lichter PR, Petty HR, Richards JE, Abecasis GaR, Elner VM, Swaroop A (2005b) Toll-like receptor 4 variant D299G is associated with susceptibility to age-related macular degeneration. Human Molecular Genetics 14:1449-1455

Zeiss CJ (2010) REVIEW PAPER: Animals as Models of Age-Related Macular Degeneration. Veterinary Pathology Online 47:396-413

Zeng J, Chen Y, Tong Z, Zhou X, Zhao C, Wang K, Hughes G, Kasuga D, Bedell M, Lee C, Ferreyra H, Kozak I, Haw W, Guan J, Shaw R, Stevenson W, Weishaar P, Nelson M, Tang L, Zhang K (2010) Lack of association of CFD polymorphisms with advanced age-related macular degeneration. Mol Vis 16:2273-2278.

Zhou J, Jang YP, Kim SR, Sparrow JR (2006) Complement activation by photooxidation products of A2E, a lipofuscin constituent of the retinal pigment epithelium. Proceedings of the National Academy of Sciences 103:16182-16187

Zumbrunn J, Trueb B (1996) Primary structure of a putative serine protease specific for IGF-binding proteins. FEBS Letters 398:187-192

Zurawa-Janicka D, Kobiela J, Stefaniak T, Wozniak A, Narkiewicz J, Wozniak M, Limon J, Lipinska B (2008) Changes in expression of serine proteases HtrA1 and HtrA2 during estrogen-induced oxidative stress and nephrocarcinogenesis in male Syrian hamster. Acta Biochim Pol 55:9-19.